Optimisation of Fixation Methods for Vancouver Type B2 and B3 Periprosthetic Femoral Fracture Treatment

Lee William Etchels

Submitted in accordance with the requirements for the degree of Doctor of Philosophy

The University of Leeds
School of Mechanical Engineering

October, 2014

The candidate confirms that the work submitted is his own and that appropriate credit has been given where reference has been made to the work of others.

Acknowledgements

I would like to thank Ruth Wilcox and Alison Jones for all their support and advice over the years, as well as for reading through this thesis far more times than could ever be fair and, quite frankly, for having enough of a sense of humour to put up with me. Eleftherios Tsiridis for all the phone calls and conversations that made the transition into a biomedical project easier and made the clinical importance much clearer, and also for being utterly tireless during the experimental testing phases. Zhongmin Jin for his help and feedback on all my abstracts and reports, Simon Graham for his help setting up and testing our specimens and Jon and Mehran for all their help over the years, from modelling advice to experimental help, feedback on abstracts, suggestions on interpreting results and just generally for keeping me sane. I'd like to thank the technicians, IT support and admin staff at the University of Leeds Engineering department for fixing every problem that I could invent and everyone at the Institute of Medical and Biological Engineering for making it an interesting and enjoyable place to work.

Finally I'd like to thanks everyone who made getting through thesis submission possible. From cooked lunches and cakes to encouraging texts, dances, hugs and the occasional much needed drink, it made an unbelievable difference when I was sat late in the office having to turn the motion sensitive lights back on every 20 minutes.

This work is supported by British Orthopaedic Association (BOA) through the Latta Fellowship. In addition, it was partially funded through WELMEC, a Centre of Excellence in Medical Engineering funded by the Wellcome Trust and EPSRC, under grant number WT 088908/Z/09/Z and additionally supported by the NIHR (National Institute for Health Research) as part of a collaboration with the LMBRU (Leeds Musculoskeletal Biomedical Research Unit). Surgical components for the experimental testing were provided by Stryker (Stryker UK Limited, Berkshire).

Abstract

Periprosthetic femoral fractures (PFF) are a complication associated with total hip arthroplasty patients that can be both traumatic and challenging to treat. With the increasing age of the population and increasing prevalence of hip replacement surgery periprosthetic femoral fractures are expected to occur more frequently in the future. The most common type of PFF is the Vancouver Type B fracture that occurs near the tip of the original prosthesis. These fractures can be complicated further by loosening of the primary femoral stem (Type B2 fractures) and poor bone stock (Type B3 fractures). Clinical failures and unclear optimal treatment recommendations for many fractures suggest that further investigation is required.

This study mechanically tested experimental specimens representing the cemented long stem revision treatment of a Type B2 PFF at a range of loading orientations to evaluate their biomechanical response. From these specimens the axial stiffness, medial axial strain, distal lateral axial strain, and relative fracture movement were recorded under semi-physiological loading. These experimental results were also used to validate computational, finite element (FE), models of long stem PFF treatment. The computational models were shown to achieve reasonable agreement with the experimental data, such that they could be used to investigate a wider range of clinical scenarios. The FE models were then used to compare the relative effects of different cement mantle geometries, fracture location, fracture bridging distance, fracture angle, revision femoral stem length and osteoporosis.

The specific location and angle of the fracture appeared to have an effect on the bending response of the femur and the optimal treatment. Long stem revision treatment however seemed to be suitable for achieving stability around an unstable fracture and it may be possible to counter-act the increased risk of fixation failure in osteoporotic patients by selecting a longer bridging distance.

Table of Contents

List of Tables

List of Figures

Abbreviations

ABC	-	Adjusted boundary conditions
ANOVA	-	Analysis of variance
BW	-	Body weight
CAD	-	Computer aided design
CoM	-	Centre of mass
CTR	-	Cortical thickness ratio
DIC	-	Digital image correlation
DSA	-	Distal surface area
FBD	-	Fracture bridging distance
FD	-	Femoral diameter
FE	-	Finite element
FEA	-	Finite element analysis
LM	-	Lateromedial
LVDT	-	Linear variable differential transformer
MFBD	-	Minimum fracture bridging distance
ML	-	Mediolateral
OP	-	Osteoporotic
ORIF	-	Open reduction and internal fixation
PFF	-	Periprosthetic femoral fracture
PMMA	-	Polymethylmethacrylate
SD	-	Standard deviation
SG	-	Strain gauge
THA	-	Total hip arthroplasty
TKR	-	Total knee replacement

1. Introduction and Project Overview

1.1 Introduction

Eighty-six thousand hip replacement surgeries were recorded in England and Wales by the National Joint Registry in 2012 [1]. With factors such as the increasing age of the population this is expected to rise [2, 3]. Periprosthetic femoral fracture is a complication involving fracture around a pre-existing femoral hip prosthesis. Although periprosthetic femoral fractures (PFF) only occur in a small percentage of cases, 0.1 - 6% as reported by Lever et al [4], this still results in a large number of affected patients.

With surgery around an existing hip prosthesis stem, selecting fracture fixation methods can be difficult and clinical failures of treatment constructs have been reported [5-8]. This is due, in part, to the necessity to work around the original structure, the likelihood of reduced available bone stock from previous surgeries and possibly the co-morbidities which required the original total hip arthroplasty [2, 9, 10]. The complexity of the surgery is amplified when the existing stem has become loose. With a loose stem the surgeon must both revise the original hip replacement and stabilise the periprosthetic femoral fracture [11].

Comparing the suitability of different fracture fixation methods using experiments on cadaveric femurs is extremely difficult. This is due, in part, to the large variations in geometry and material properties between samples [12] as well as the difficulty in obtaining, storing, preparing and testing human tissue. This inter-specimen variation requires large sample sizes to obtain statistically significant results [13], and this is often infeasible because of the difficulty of obtaining the samples. As an alternative, synthetic femurs can be used which have extremely consistent geometries and material properties [14], allowing for the comparative benchmarking of different fracture fixation methods [10]. Synthetic femurs, however, usually represent relatively strong, healthy bone, compared to the range of material properties and cortical thicknesses found across the human population [15], which is not typical of PFF cases. They do not therefore allow consideration of how the fracture fixation methods will perform across the range of human femurs.

Finite element analysis (FEA) provides a potential alternative approach to the analysis of periprosthetic fracture fixation. Experimental data from tests on synthetic femurs can be used to calibrate and validate FEA models. The models can then be modified relatively quickly and easily to investigate a much wider range of relevant clinical situations [16].

The most commonly occurring PFFs are Vancouver Type B fractures at the distal end of the stem [13, 17]. In many cases these are combined with a loose femoral component [4]. One of the most common treatment methods used currently is a long stem revision with or without supporting structure. A long stem may have a significant effect on the biomechanics, stresses and failure patterns of a fractured femur. The aim of this research is therefore to investigate the optimal treatment methods for these clinical situations. The combination of computational modelling and experimental testing of synthetic specimens will be used to categorise the mechanics of a current treatment system. Modifications to the treatment setup and varying patient and clinical conditions will then be investigated. From this treatment recommendations can then be made based on the effects of fracture type, location, stem condition and bone quality/geometry.

1.2 Research Aims and Objectives

1.2.1 Research Aim

To evaluate the fixation methods for repairing Vancouver Type B2 and B3 periprosthetic femoral fractures, and make recommendations for their improvement where necessary, using computational modelling methods validated with experimental data.

1.2.2 Objectives

- Mechanically test experimental specimens, using synthetic femurs, that represent a long stem revision treated PFF.
- Record and evaluate the experimental results in terms of stiffness, strain and fracture movement.

- Create a computational model to simulate a long stem with a fracture to match the experimental specimens.
- Verify the computational model.
- Validate the computational model using the experimental data.
- Conduct sensitivity testing on the long stem FE model to evaluate the relative effects of different modelling techniques on the results.
- Use the results of the experimental and computational testing to recommend possible improvements to the pre-clinical testing of potential PFF treatments.
- Use the FE models to consider the effect of different cement mantle thicknesses and distributions.
- Use the FE models to consider the effect of fracture location.
- Use the FE models to consider the effect of fracture bridging distance.
- Use the FE models to consider the effect of fracture angle.
- Use the FE models to consider the effect of stem length.
- Use the FE models to consider the effect of osteoporosis.
- Use the results from these comparisons to recommend possible improvements to the way Vancouver Type B fractures are treated clinically.

1.3 Project Overview

The research that makes up this thesis was a part of a larger project on the topic of periprosthetic femoral fractures. This study focussed on representing long revision stem treatment of a fracture, which is predominantly used for Type B2 and B3 fractures. Concurrent studies by Mak [16], Mak et al. [18], Moazen et al. [13, 19-24] and Graham et al. [8] focussed more on the use of plated fixation, without stem revision, which is predominantly used for Type B1 fractures.

The development of the computational models for this project and the concurrent studies occurred in parallel. Modelling techniques were developed and tested across computational models for both plated and long revision stem treatments. This resulted in areas of the modelling in which a generic modelling approach was used across all studies. The purpose of this was to develop modelling techniques that were sufficiently

representative to be applicable to a range of cases. A less realistic calibration of the models to the treatment specific experimental results, which would have provided better numerical agreement between the two, was therefore avoided where possible. The boundary conditions, load application methods and interface properties were areas of the model where agreement was investigated, comparing against experimental data, for both long revision stem and plated treatment models.

1.4 Thesis Structure

In terms of the structure of the thesis, Chapter 2 will discuss the current state of the literature relating to periprosthetic femoral fractures, their treatment and the evaluation of their treatment. It will also include relevant background information upon which this study has relied. Chapter 3 will discuss the experimental methodology used to test long stem revision PFF models and the results gathered from these experiments. Chapter 4 will describe the development of a computational model to replicate these experimental results, discuss the agreement between the two and consider the applicability of the FE model for further testing. Chapter 5 investigates the effect of changing the fracture configuration of this validated FE model. The effect of different fracture heights and fracture angles will be presented and discussed. Chapter 6 introduces a second, longer revision stem geometry to the model as well as an altered, osteoporotic geometry for the femur. These results of these models are compared against the results of the original case to consider the effect of treating a more distal fracture, of treating a fracture with a longer stem and of treating fractures at different angles on two different bone quality scenarios. Chapter 7 will then offer a final discussion of the results of this project and describe how this fits within, and extends, the current research on the subject of periprosthetic femoral fractures.

2. Literature Review and Background Information

2.1 Periprosthetic Femoral Fracture

2.1.1 Introduction

This section of the literature review is concerned with the definition and clinical background of periprosthetic femoral fractures. It will detail typical reasons for the pre-existing total hip arthroplasty surgery that the patient would have experienced and the surgical implants involved. It will then consider the range of different causes for a PFF, the possible types of PFF that can be seen clinically, the range of treatment options currently in use by surgeons and some of the issues that still persist with these treatments.

2.1.2 Total Hip Arthroplasty

Total hip arthroplasty involves replacing the femoral head and acetabulum with manufactured components. A femoral hip prosthesis, or stem, is inserted into the proximal end of the femur and an acetabular cup is inserted into the acetabulum, providing the surface that it will articulate against on the hip bone.

There are several reasons that a THA procedure would be considered. Osteoarthritis is one of the main indications [25], as is fractures of the acetabulum or femoral head/neck and, as these conditions are more likely to affect elderly patients, this is where the majority of hip replacements are performed [4].

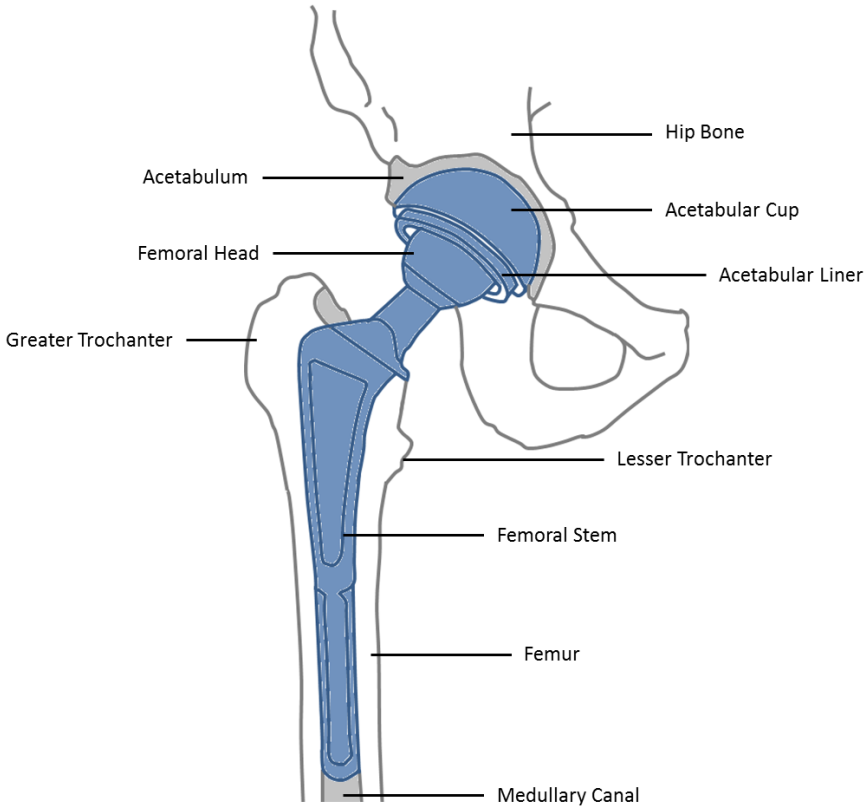

Figure 2.1 The femoral hip prosthesis and acetabular component.

Femoral hip prostheses (Figure 2.1) can be fixed into the femur in one of two ways. The stem can be cemented in place into the medullary canal or, for cementless stems, it can be press-fitted.

A variety of surface finishes have been used for stems which can be simply categorised as rough or smooth. With a smooth surface finish the stem is expected to subside and the design allows for expected compressive loading to continue as this happens. It is recommended that the stem be inserted while the cement is in its doughy state as it makes it easier for the surgeon to position. The rough surface on the other hand is designed to integrate with the cement mantle for stability and therefore the stem is inserted while the cement is less viscous to promote a strong interface [25]. Briant-Evans et al [17] reported an average subsidence of 1.0mm (range 0-3.2) after three years with cemented revision polished tapered stems. Gie et al. [26] reported similar values when measuring both the stem into cement subsidence and the cement into bone subsidence. They found that subsidence was predominantly due to subsidence of the stem into the cement, with most patients experiencing no measurable subsidence of the cement into the bone.

For press-fitted stems the surface can often be roughened or treated to allow and induce the bone to grow into the stem-bone interface and improve the stability of the prosthesis [27, 28].

2.1.3 Definition and Epidemiology of PFF

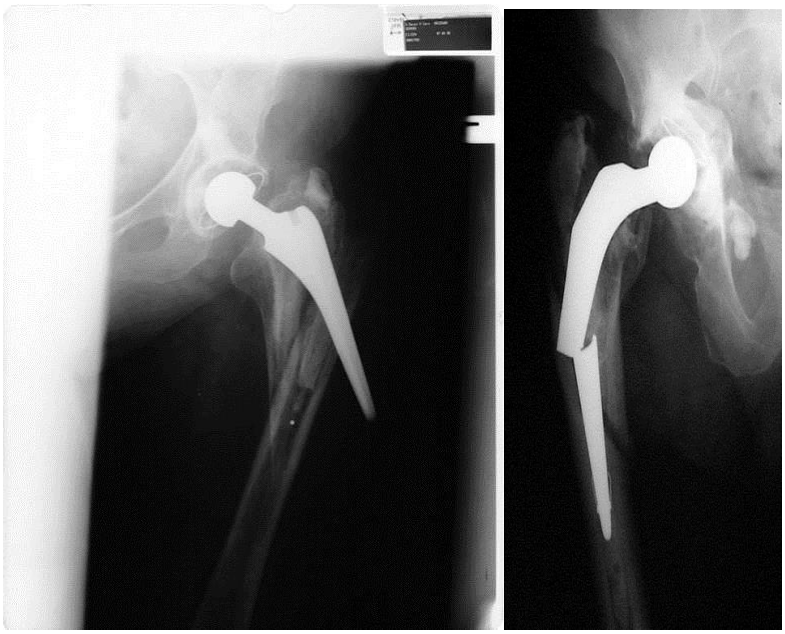

Figure 2.2 Example radiographs of periprosthetic femoral fractures.

A periprosthetic femoral fracture is a fracture of the femur bone that occurs around a hip prosthesis stem that exists from a previous surgical procedure [29]. Examples of two clinical PFF are given in Figure 2.2. It has the additional complications over a conventional femoral fracture of having to apply fracture fixation around the existing components. There is also the potential for a loose stem, which may require treatment. Beals et al. [30] recorded the pre-PFF state of the cement-to-stem interface for 56 cemented THA cases that later experienced a fracture. Forty-five percent of the cases had a radiologically loose cement-to-stem interface before the fracture occurred. Corten et al. [31] performed intraoperative stem stability tests on 45 PFF cases where the stem appeared stable in pre-operative radiographs. They found that 20% of the stems were loose, despite this not being evident in the radiographs. There is also the likelihood of osteoporosis, and therefore weakened bone and reduced bone stock, and other comorbidities due to the typically elderly

patients [30]. The fractures can be cortical perforations, cracks, fractures, displaced fractures or comminuted fractures [32].

There are many different causes of periprosthetic femoral fractures, and conditions that increase the likelihood of it occurring, described in the literature. Adolphson et al. [33] described a series of 32 PFF cases. Of these 32 cases, 63% were due to minor trauma, 6% were due to major trauma, 6% were described as spontaneous and 25% occurred perioperatively. Beals et al. [30] reported the causes for 82 periprosthetic femoral fractures, with 84% due to minor trauma, 8% described as spontaneous and 8% due to major trauma. Out of 75 PFF cases Cooke et al. [34] listed 8% as resulting from major trauma, 9% due to a cortical defect, 4% due to a tumour, 3% due to polyethylene granuloma and 4% due to infection. The causes for the remaining 72% of cases were not given.

In order to provide surgeons with an algorithm for the treatment of different types of periprosthetic femoral fracture many classification methods have been developed, including systems by Johansson et al. [35], Kavanagh [36], Mallory et al. [37], Schwartz et al. [38], Stuchin [39], Roffman and Mendez [40] and the Vancouver group [41]. Initially, several classifications focused on the location of the fracture, Roffman and Mendez were the first to consider the stability of the implant and following from this the Vancouver group identified the three key factors in defining a PFF as the fracture location, implant stability and quality of the surrounding bone [2] This has also been expanded further to account for when they are discovered by Masri et al [32].

In the Vancouver system, Type A fractures are proximal metaphyseal, Type B fractures are in the diaphysis but not distal enough to prevent long-stem revision from bridging the fracture gap and Type C fractures are distal to the longest revision stem and can be in the distal metaphysis. Type A fractures can then be subdivided into Type A_G, fractures of the greater trochanter, and Type A_L, fractures of the lesser trochanter. In addition Type B fractures are divided into Type B1 where the implant is stable, Type B2 where the femoral hip prosthesis has become loose and Type B3 where the stem is loose and the bone quality is also poor [41]. The six different classifications of PFF are illustrated in Figure 2.3.

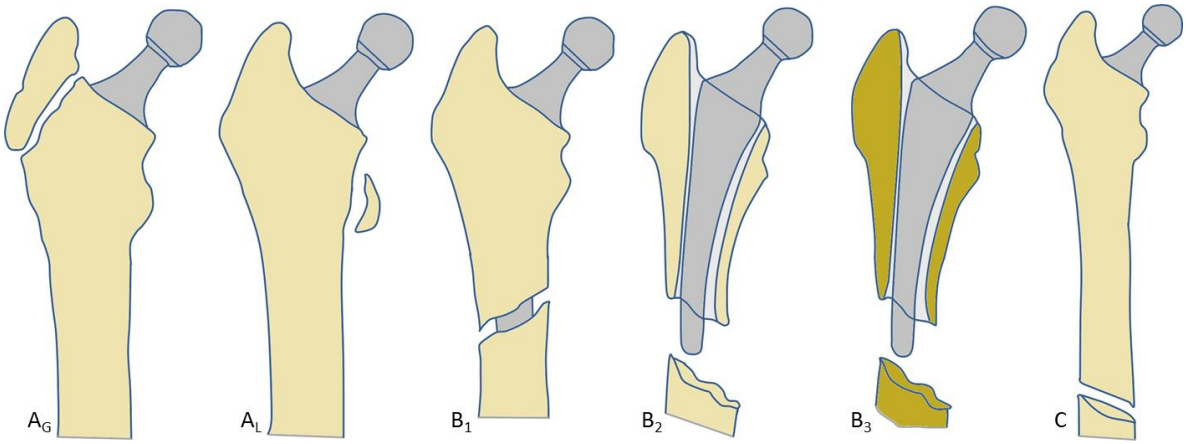

Figure 2.3 The six different classifications of PFF under the Vancouver classification system.

Due to the fact that it is generally considered reproducible and easy to use, the Vancouver classification has become the most commonly used system at the moment, however there are still areas which require improvement. Most remaining controversy regarding the suggested treatment methods is in relation to Type B fractures [32] and the fact that several reports have shown failure of fracture fixation devices [13, 42, 43] suggests that the recommended fixation methods were not sufficient for the situation.

2.1.4 Clinical Management of PFF

The treatment recommendations from the Vancouver classification system are given in Table 2.1. A displaced fracture refers to a case where parts of the bone and/or fracture must be returned to their original position and alignment. An undisplaced fracture is one that left the bone in its original anatomical position. Open reduction and internal fixation (ORIF) is the process of surgical fixation of the fracture using a plate or strut based treatment fitted to, or very close to, the external surface of the bone. An allograft strut is a bone graft transplant used to provide additional structural support and improve bone stock. A long stem revision treatment replaces the original femoral stem with a longer stem. This longer stem extends past the fracture site, typically by at least two femoral diameters [44, 45], and provides stability to the fracture site from within. A tumour prosthesis is one typically designed for returning function to a limb after the removal of bone tumours [46, 47]. They are therefore designed to provide support in cases with extensive areas of bone loss.

Table 2.1 Treatment algorithm for the Vancouver classification system of periprosthetic femoral fracture from Masri et al. [32].

<table>
<tr><td colspan="6">Vancouver Type</td></tr>
<tr><td colspan="2">A</td><td colspan="3">B</td><td>C</td></tr>
<tr><td>A_L</td><td>A_G</td><td>B1, Well Fixed Stem</td><td colspan="2">B2, Loose Stem</td><td>Ignore implant, fix fracture, if necessary address implant after fracture healed.</td></tr>
<tr><td>Lesser trochanter, symptomatic treatment only if displaced. Intervene only if substantial segment medial cortex attached.</td><td>Greater trochanter, symptomatic treatment with crutches and limit abduction. Intervene only if displaced to avoid pain, weakness, limp, or instability.</td><td>Open reduction and internal fixation (ORIF) with cerclage and struts and plate.</td><td>B2, Good Bone Stock</td><td>B3, Poor Bone Stock</td><td></td></tr>
<tr><td></td><td></td><td></td><td>Revision with long stem – cemented or cementless.</td><td>Revision and augmentation of bone stock with allograft in physiologically young or tumour prosthesis in elderly patients</td><td></td></tr>
</table>

The Vancouver classification system suggests that all B1 fractures can be treated with open reduction and internal fixation. Several studies, however, have highlighted that certain clinical scenarios may require different treatment [7, 19, 48-52].

Springer et al. [48] commented that they used revision with a long stem for B1 cases when “the surgeon believed that the advantages of intramedullary fracture fixation that were gained by revision to a long-stemmed implant outweighed the disadvantages of removal of the prosthesis”. Buttaro et al. [7] experienced a high failure rate when treating B1 fractures using locking compression plates, commenting that they would therefore consider long stem revision for patients with a well-fixed stem. In particular they highlighted short oblique or transverse fractures as particularly unstable.

Venu et al. [49] recorded the results of 13 PFF treatments using the Dall-Miles cable and plate fixation method. They recommended that this type of plated fixation was not suitable for cases where the original stem had a varus angulation of more than 6°. Tadross et al. [50] made a similar recommendation that periprosthetic femoral fractures around a stem in varus alignment might be more suitably treated with a long-revision stem. Lewallen and Berry [51] suggested that long stem revision may be required for B1 fractures in patients with problems relating to the position of the stem. Additionally, they

recommended revision for problems with the implant bearing surface or in patients with a first-generation implant.

Moazen et al. [19] compared B1 and B2 fixation methods using computational modelling. They reported that a single locking plate may struggle to provide adequate fracture stability in cases with a fracture gap or a comminuted fracture. They found that stresses in the plated fixation were also extremely sensitive to the degree of weight-bearing, suggesting that higher loads representative of early, full weight-bearing (intentional or otherwise) could lead to plate failure. The long stem revision treatment of the same fracture scenario provided lower maximum implant stresses and a more even cortical strain distribution, suggesting it may be a more suitable treatment for difficult to reduce fractures. Oh et al. [52] specifically investigated the effect of fracture gap and fracture width (as in how far the fracture propagates through the width of the femur). They also found that the plate stresses were extremely dependent on the level of fracture reduction, with fracture gaps creating an increased risk of fixation failure.

The recommendation for type B2 fractures is a long stem revision. This suggestion is generally well supported by the literature due to the fact that the loose stem requires revision and long revision stems, when used appropriately, can provide good fracture stability. Springer et al. [48] achieved improved clinical results from uncemented, extensively porous-coated long stems compared against cemented stems or uncemented, proximally porous-coated stems. They continued to use cemented long revision stems for older patients with poor bone and an easily reduced fracture however.

There appears to be less concern in the literature regarding fracture configuration, either in terms of fracture type or fracture comminution, when treating B2 fractures. This may be due to the intramedullary mode of fracture fixation provided by long stem revision, which may be less sensitive to these factors than plated fixation. Issues with stem loosening [48, 53, 54], infection [48, 55] and non-union [44, 56, 57] persist, however. Proximal stress shielding is also a concern [58, 59]. It may therefore be possible to improve the clinical outcomes from long stem revision treatments through careful selection of stem design. The clinical and biomechanical evidence necessary to do this is not currently available however.

B3 fractures had a wider range of recommended treatments that may suggest that further subdivision, and therefore greater detail, is required in the treatment algorithm. The Vancouver classification system recommends one of two different treatments, either stem

revision with an allograft strut in physiologically young patients or a tumour prosthesis in elderly patients. This division suggests two different treatment aims, for young patients the femur is supported with a bone graft in an attempt to improve the available bone stock. In an elderly patient the focus of the treatment recommendation is to regain function within the poor bone stock. This may suggest that type B3 fractures could be subdivided further, according to the expected activity level of the patient and the likelihood that the poor bone stock could be surgically improved. This may not significantly impact the treatment of B3 fractures, as both of these cases are considered in the treatment recommendation; however it could separate these cases when reported in follow up studies and enable a more relevant analysis of clinical results.

The available literature generally recommends that relatively simple B3 cases, with fractures that could be anatomically reduced, can be treated with a long cemented stem with an allograft strut [6, 19, 48, 60]. The long cemented stem provides stability and support without generating the high intra-operative hoop stresses that come from inserting press-fit stems. As the stem does not require a tight fit against the cortical bone for fixation a cemented stem does not require the same level of reaming, which can reduce the already poor bone stock. The allograft strut is then used to provide additional support and improve bone stock. In cases where the proximal bone stock is sufficiently poor that it needs to be protected from load bearing stems that achieve distal fixation are recommended. For cases with greater levels of bone loss, other stem designs are recommended, including proximal femoral replacements, allograft-prosthesis composites or tumour prostheses [48, 60].

2.1.5 Discussion

The Vancouver classification system does offer useful guidance to surgeons faced with periprosthetic femoral fractures. Classification systems provide a way for the treatment options to be divided between different clinical scenarios based on the most important biomechanical and biological factors. They also provide an efficient method for combining the expertise and experience of a large number of clinicians and clinics. This is important when, individually, these clinicians may not have treated enough patients to distinguish between patient variability and identify optimal treatments.

It is important, however, to continue to develop these treatment algorithms in order to provide up to date guidelines. The Vancouver classification and treatment algorithm was originally proposed in 1995 [41] and despite the wide range of clinical and biomechanical studies performed since it has remained relatively constant. Corten et al. proposed an extension of the Vancouver classification in 2009 [31] in response to their clinical experiences (Table 2.2).

Table 2.2 Modified treatment algorithm, based on the Vancouver classification, used by Corten et al. [31].

<table>
<tr><th colspan="4">Vancouver Type</th></tr>
<tr><th colspan="3">B</th><th>C</th></tr>
<tr><td>B1, Radiologically Well-Fixed Stem</td><td colspan="2">B2, Loose Stem</td><td>If more than two femoral diameters distal to the stem tip, with room for four proximal bi-cortical screws, use distal locking plate. Otherwise treat as B1.</td></tr>
<tr><td>Intraoperative stem stability check. If stable use ORIF, if not treat as B2. After ORIF, if medial cortex not restored supplement with anterior strut or plate.</td><td>B2, Good Bone Stock</td><td>B3, Poor Bone Stock</td><td></td></tr>
<tr><td></td><td>Revision with cementless modular revision stem, with or without plate or strut.</td><td>Revision with cementless modular revision stem, with or without plate or strut.</td><td></td></tr>
</table>

This extension focussed on the addition of an intraoperative stem stability test to better differentiate cases between Vancouver type B1 and B2. They also included, when using ORIF treatments, an intraoperative evaluation of the medial fracture reduction. If load transfer through the medial cortex was not restored the addition of an anterior strut or plate was recommended. The recommendation for long stem revision for type B2 and B3 fractures was modified to specifically recommend a cementless modular revision stem, with or without a plate or strut.

A specific recommendation was made for what constituted a type C fracture. Previously the definition of a type C fracture was vague in that it was a fracture unsuitable for long stem revision treatment. Biomechanical evidence had not been provided to define at what point a fracture could no longer be treated with a long revision stem. The suitability of long stem PFF treatments will also depend on other factors such as the type of stem,

fracture configuration, bone quality and condition of the original stem. Corten et al. [31] recommended that fractures less than two femoral diameters below the stem, or where there was not room for four bi-cortical screws proximal to the fracture, should be treated in the same manner as a B1 fracture, with ORIF. They specified that fractures beyond this should be treated with a distal locking plate. Although this is an important step in defining the difference between a type B1 and a type C fracture, and the recommendations appear sensible based on our current knowledge of PFF treatments, no biomechanical justification for these specific guidelines was presented. A stress riser effect between the plate and stem would be a potential concern that would need to be carefully addressed.

The algorithm presented by Corten et al. [31] improves upon several of the deficiencies with the original Vancouver system. It reduces the likelihood of misdiagnosing, and therefore mistreating, a B2 fracture as a B1 fracture. It provides a recommendation for additional fixation around fractures that could not be well reduced during surgery, which accounts for some of the concerns raised by Moazen et al. [19] and Oh et al. [52]. It also provides specific treatment recommendations for fractures distal to the tip of the stem, which attempt to take the existence of the original implant into account.

In the updated treatment algorithm there are several factors, which may affect the likelihood of successful treatment, that have yet to be included. The same treatment recommendation is made for type B2 and B3 fractures, which fails to take into account the effect that reduced bone quality may have on fixation. A modular stem is recommended for both of these fracture types, which may allow for a degree of optimisation of the treatment, however the variation of bone quality that can be experienced in these cases is extremely wide [12]. Removal of a well-fixed femoral stem can be an extremely traumatic procedure and as such would not be suitable for many patients. An alternative treatment recommendation for a patient with poor bone quality, who doesn't have evidence of stem loosening, that doesn't involve stem revision might also be relevant to some cases.

The treatment algorithm does not take into account the configuration of the fracture, either in terms of the type (transverse, oblique or spiral), angle or degree of comminution. The algorithm recommends considering the fracture reduction achieved during ORIF and providing additional fixation if a medial fracture gap or comminution is present. The intraoperative fracture reduction that can be achieved may not be something that the surgeon could estimate before surgery, hence why providing additional support after plating

is relevant. The degree of comminution can be evaluated before plating, however, which provides the opportunity to select an alternate treatment, such as long stem revision, before committing to ORIF. Finally, there are many different plating options, and plate application options, available to a surgeon. Using a treatment algorithm to bring together the results of a large number of PFF treatments using plated fixation might enable more specific plating recommendations to be made. These could consist of the recommendation of a particular plating technique or the identification of which scenarios are best suited to each plating option.

There may be opportunities to extend the Vancouver classification further in order to account for more patient-specific factors such as the fracture configuration, initial stem position, patient weight and activity level and more detailed measures for bone quality and geometry. For factors such as these to be included in a treatment algorithm, however, there needs to be robust biomechanical or clinical evidence describing the effects that they will have on the success of the treatment.

The success of a PFF clinical operation is generally defined by the restoration of function without pain. Beals et al. [30] described clinical failure as “a loose prosthesis, painful or not, or a nonunion, sepsis, new fracture, severe deformity, or severe shortening.” These factors may be dependent on the patient and aims of the surgery however, for example a degree of pain might be tolerated if it restores function or results in an overall improvement to quality of life. Some of these factors can be related from clinical aims to biomechanical testing outcomes. For example, the likelihood of stem loosening, stem migration or re-fracture could be evaluated, depending on the testing methodology. Evaluating the likelihood of pain, fracture healing or infection, however, would likely rely on patient specific biological processes that would be difficult or impossible to simulate outside the human body. Patient follow up, and the statistical analysis of this data, therefore remains an important part of improving periprosthetic femoral fracture treatments.

2.2 In Vivo Mechanical Environment

2.2.1 Introduction

This section of the literature review will focus on the in vivo scenario that surrounds a periprosthetic femoral fracture and the treatment constructs used to stabilise them. It will describe the surrounding anatomy of the musculoskeletal system, the range of motion of this system, the loading that is applied to the femur during a range of activities and the constraining effect of the human body against deformations from this loading. It will also investigate the distribution and material properties of the various biological tissues involved, from the cortical and cancellous bone that makes up the femur to the muscles and ligaments that hold it in place.

2.2.2 Anatomy

The anatomical planes used to describe the human body are given in Figure 2.4. The mediolateral plane can also be referred to as the frontal plane or coronal plane, the anteroposterior plane can also be referred to as the sagittal plane or the lateral plane and the transverse plane can also be referred to as the axial plane. Anterior and posterior refer to the front and back of the body respectively and medial and lateral refer to towards the midline and away from the midline of the body. Proximal refers to a location towards the point of attachment of an appendage to the body and distal refers to a location away from the point of attachment (Figure 2.5).

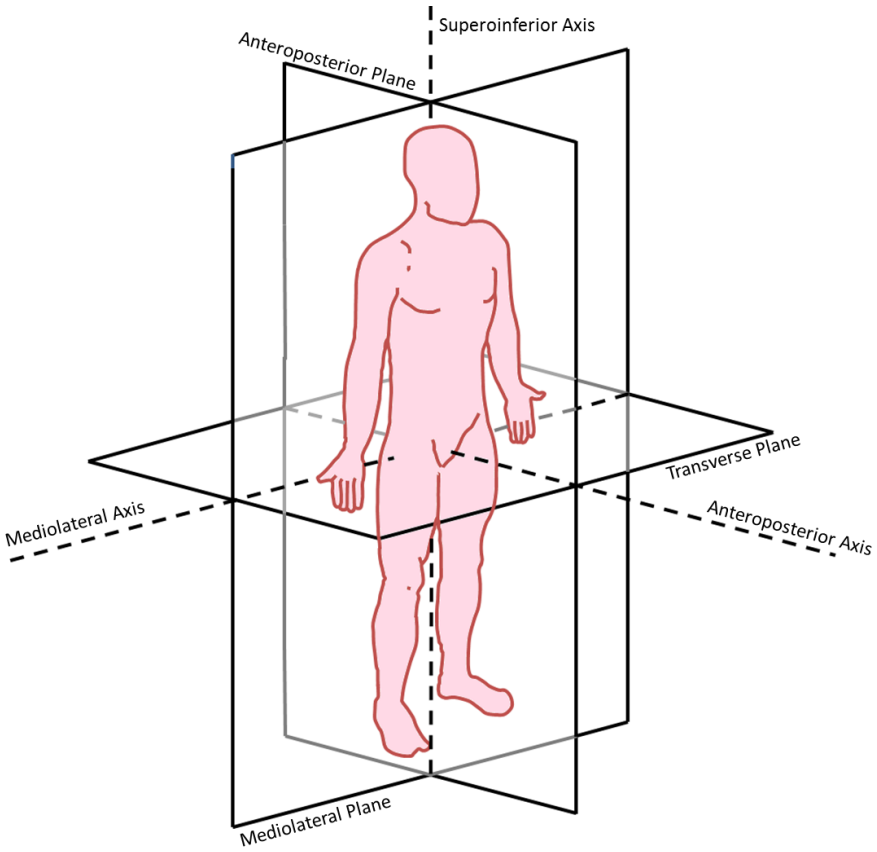

Figure 2.4 Anatomical planes of the body.

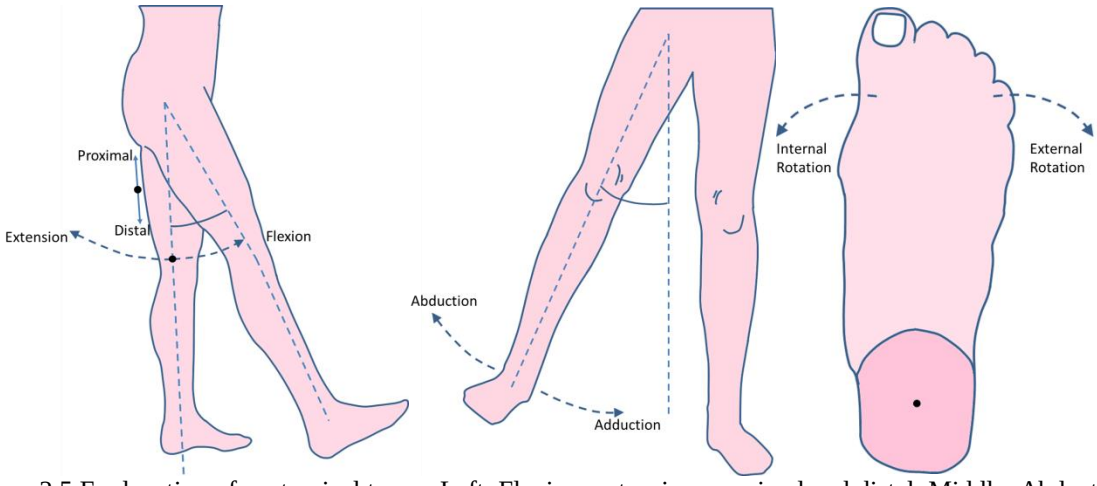

Figure 2.5 Explanation of anatomical terms. Left: Flexion, extension, proximal and distal. Middle: Abduction and adduction. Right: Internal and external rotation.

The hip joint (Figure 2.6) is a ball and socket joint where the femoral head articulates against the acetabulum of the innominate bone (hip bone). The hips support the weight of the body and any muscle forces and must do so with sufficient stability to allow

for activities such as running and stair climbing. The innominate bone is made up of three smaller bones, the ilium, ischium and pubis which meet at the epiphyseal junction. The acetabulum is then a hemispherical hollow, the anterior one-fifth of which is formed by the pubis, the superior two-fifths by the ilium and the inferior two-fifths by the ischium [61, 62].

The femoral head (Figure 2.7), which is covered in articular cartilage so that it can articulate smoothly in the similarly coated acetabulum, is shaped as just over half a sphere. The ligament at the head of the femur is attached to a small depression called the fovea. The neck joins the head to the shaft and is about 50mm long and about 125 degrees to the shaft. The greater trochanter sits on the upper lateral side of the shaft, lateral to the neck and the lesser trochanter is conical and sits medially, behind and below the neck [62]. The proximal femur and neck are formed by a shell of cortical bone filled with a less dense cancellous structure [25, 61].

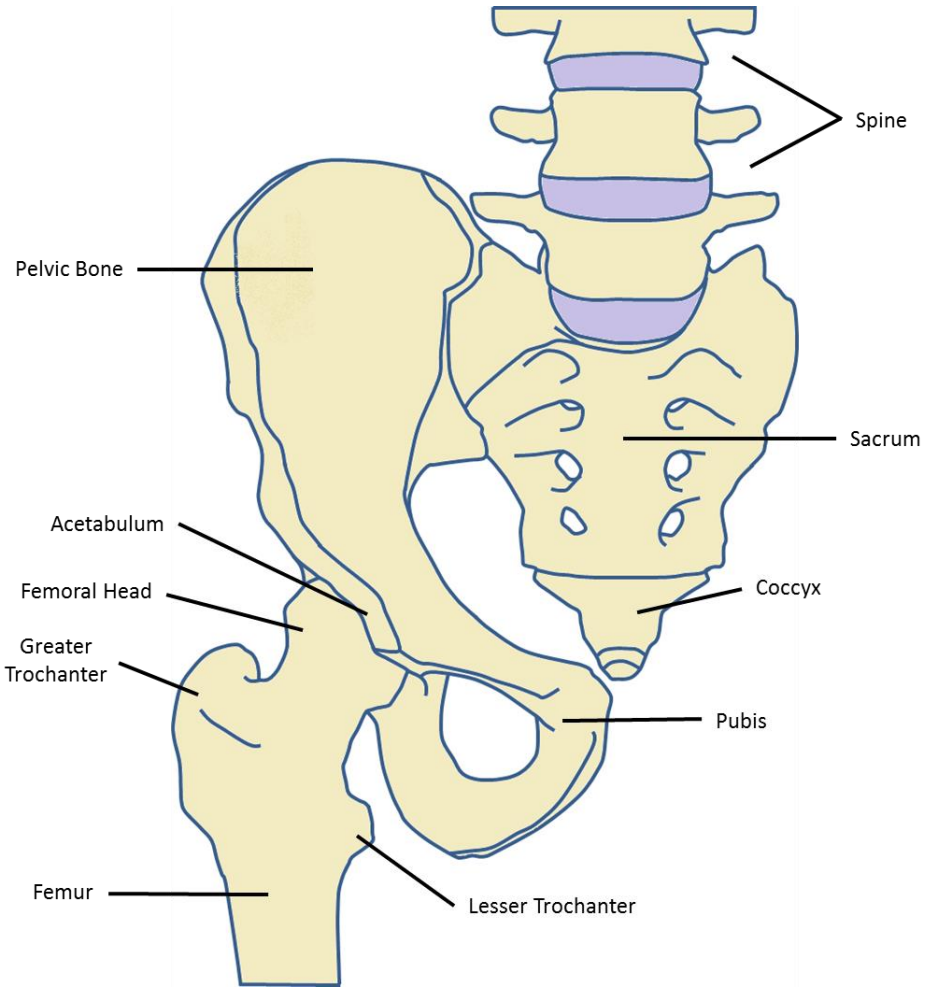

Figure 2.6 The hip joint and Surrounding Bones.

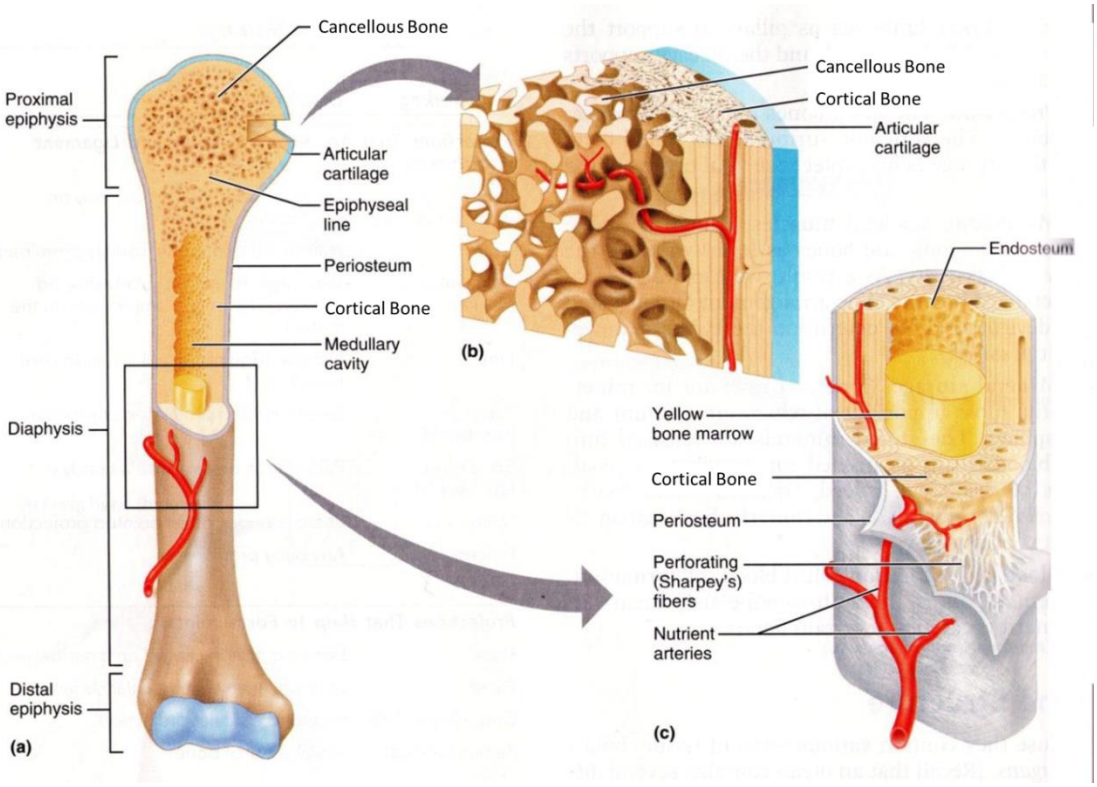

Figure 2.7 The femur and its internal structure, taken from [63].

The offset of the ball and socket joint away from the axis of the femur, due to the femoral neck, creates a joint with a large range of possible movement. Controlling and enabling this range of movement therefore requires a correspondingly large range of muscle groups [62]. There are six principle directions in which the hip joint can move and these are flexion, extension, adduction, abduction, internal rotation and external rotation (Figure 2.5). Each of these movements is controlled by different combinations of muscles. Figures 2.8 – 2.13 show the muscles acting around the hip joint to cause each of these movements.

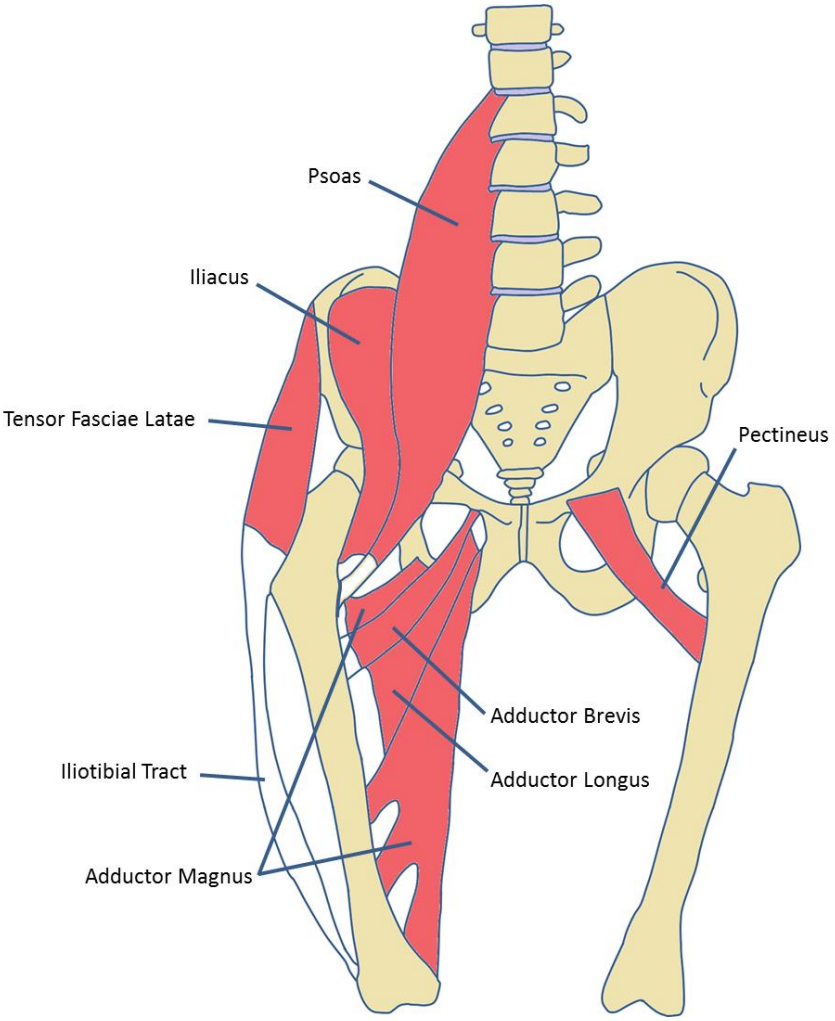

Figure 2.8 Anterior view of the muscles involved in flexion of the hip.

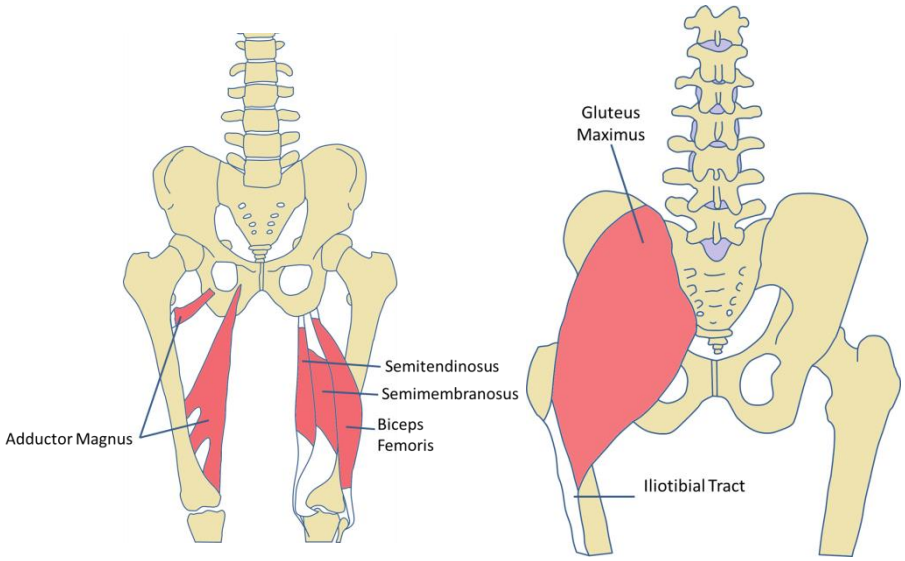

Figure 2.9 Muscles involved in extension of the hip. Left: Anterior view, Right: Posterior view.

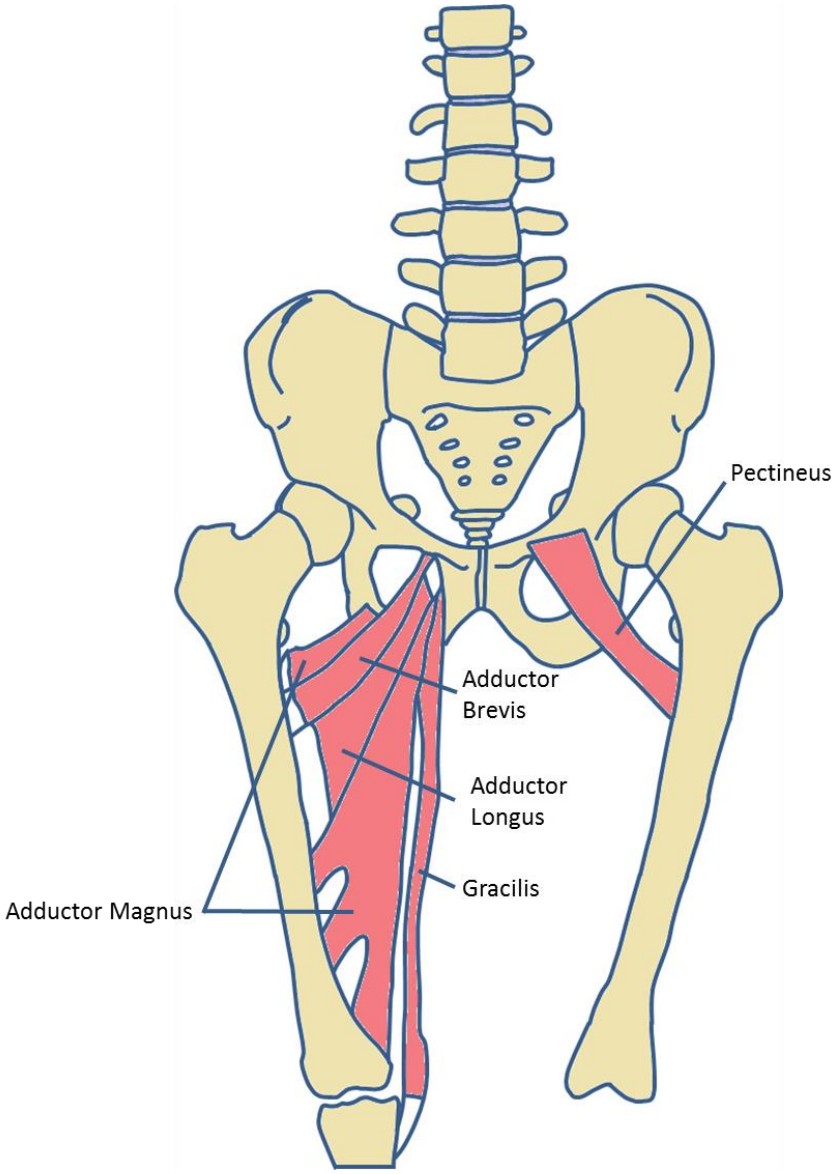

Figure 2.10 Anterior view of the muscles involved in adduction of the hip.

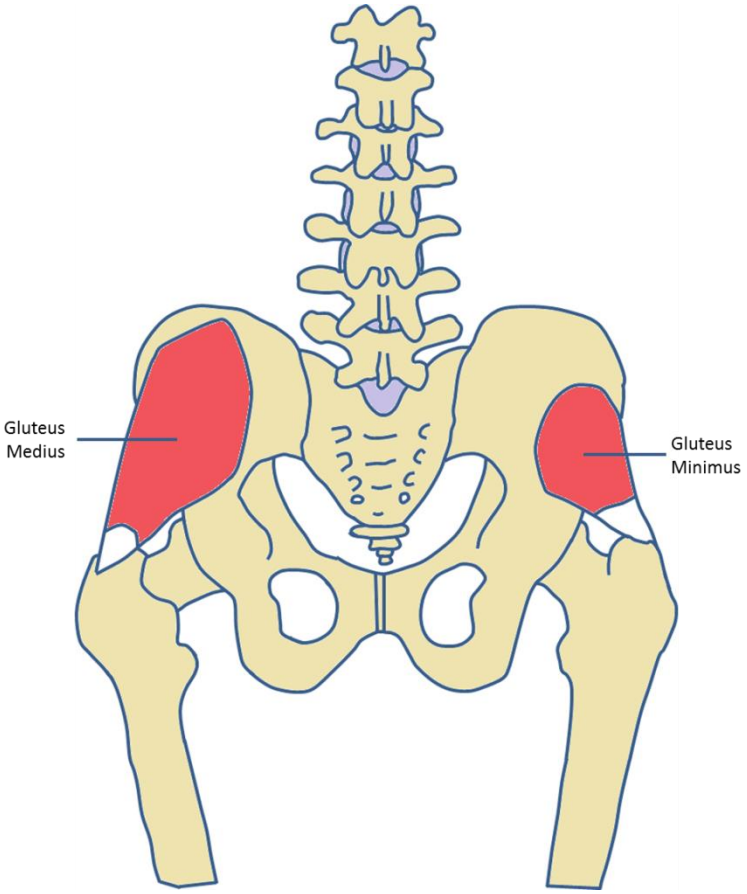

Figure 2.11 Posterior view of the muscles involved in abduction of the hip.

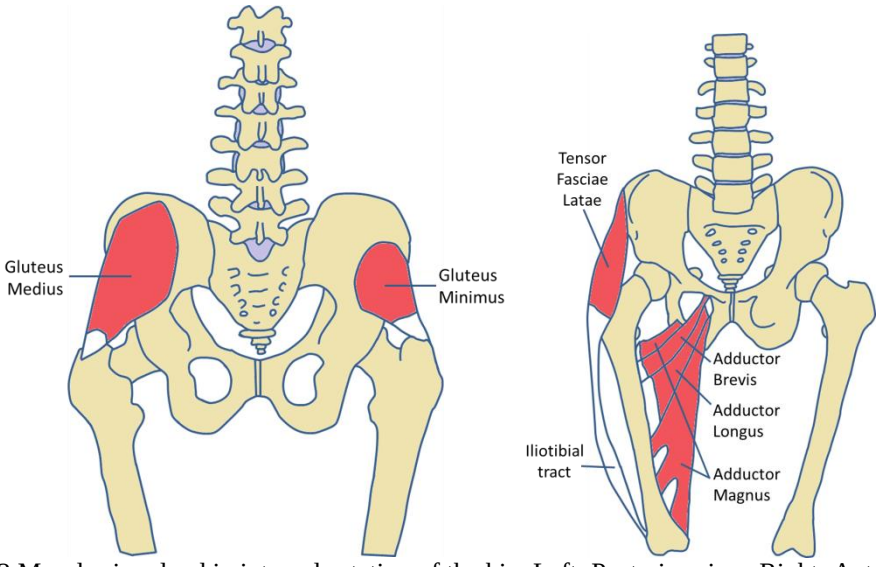

Figure 2.12 Muscles involved in internal rotation of the hip. Left: Posterior view, Right: Anterior view.

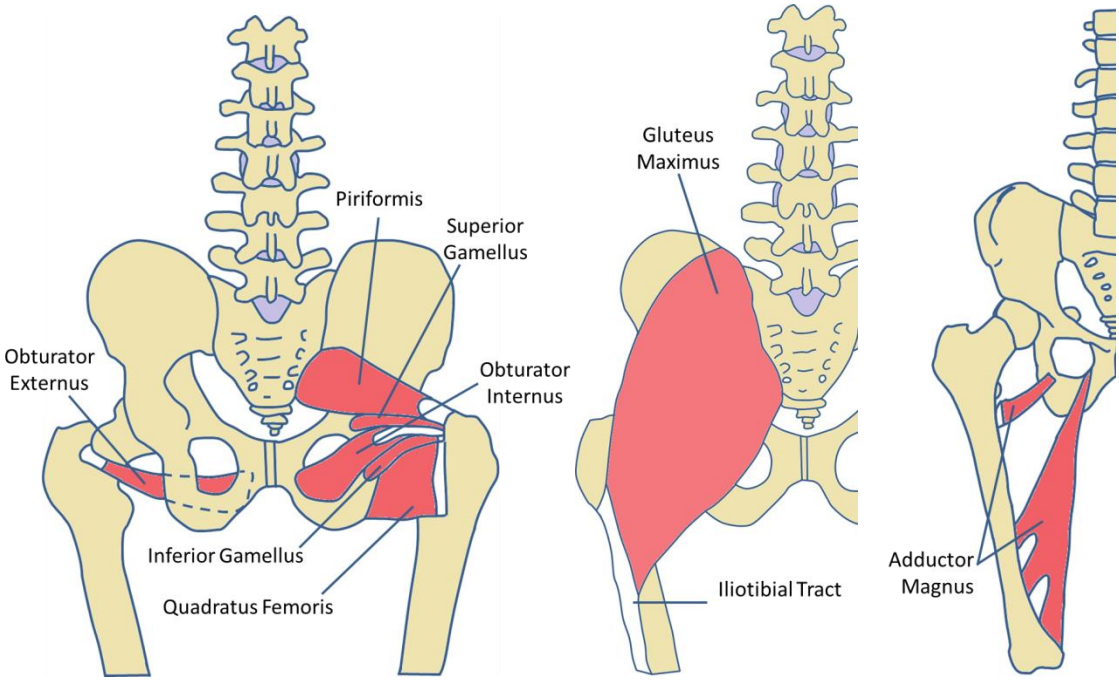

Figure 2.13 Muscles involved in external rotation of the hip. Left: Posterior view, Middle: Posterior view, Right: Anterior view.

2.2.3 Joint Kinematics and Kinetics

Various methods have been used to estimate the loading applied at the hip and femur during common, day-to-day activities. Common experimental measurements that are used in these calculations are gait data [64-66], ground reaction forces [64, 65, 67], instrumented femoral hip stems [64, 68] and in vivo bone strains [69]. Mathematical models can also be used to estimate the forces and moments at the joints, such as free body diagrams [70] and musculoskeletal models [71, 66]. A combination of experimental and mathematical modelling techniques is often used [68, 72]. An example would be entering experimental gait analysis data into a musculoskeletal model to estimate the muscle forces, and therefore joint forces, of the overall system [64]. Another example would be using numerical optimisation techniques to estimate the combination of muscle and hip contact forces required to produce measured force, displacement or strain data [65, 73].

Bergmann et al. [64] recorded force and moment data from instrumented hip replacement stems as well as corresponding gait data and ground reaction force data for a range of activities. These activities included walking, stair climb and stair descend. For their study the gait data was used as inputs for a musculoskeletal model to estimate the

muscle forces. The force data from the instrumented stem was then used to validate these results. For normal walking at 4km/h they calculated a maximum hip contact force of 2.38x body weight (BW). This was maximum force occurred 13° medially from the long axis of the femoral shaft and 31° anteriorly from the mediolateral axis. For stair climb the hip contact force of 2.51x BW occurred 13° medially from the long axis of the femoral shaft and 46° anteriorly from the mediolateral axis. Although the hip contact forces were similar, the more anterior force caused the stair climb maximum torsional moment around the long axis of the stem to be almost 50% larger than for normal walking.

Balancing on one leg resulted in a hip contact force (2.31x BW) that was similar to both normal walking and stair climb. The normal walking peak force and stair climb peak force values were due to a combination of peaks in axial force, lateral force and anterior force occurring at the same time. Although these force components were dominated by the axial component of the force both the lateral and anterior components were significant (approximately 24% and 14% of the maximum total force, respectively). When balancing on one leg, however, the relative contribution of the lateral and anterior forces to the maximum total force was much smaller (13% and 6%, respectively). This was likely due to the fact that when standing on two legs the centre of mass (CoM) of the body lies between both hips. The natural standing or walking position can allow for a medial force acting from each femur into the hip to provide stability. This would also allow the feet to be slightly further apart, providing a more stable base [74]. The medial forces from both the left and right legs would then balance. When standing on one leg however the most stable position would be one where the CoM of the body is directly over the single supporting leg. This would then generate a predominantly vertical load at the head of the femur, with no major force components in the transverse plane that could lead to falling. This is described in Figure 2.14.

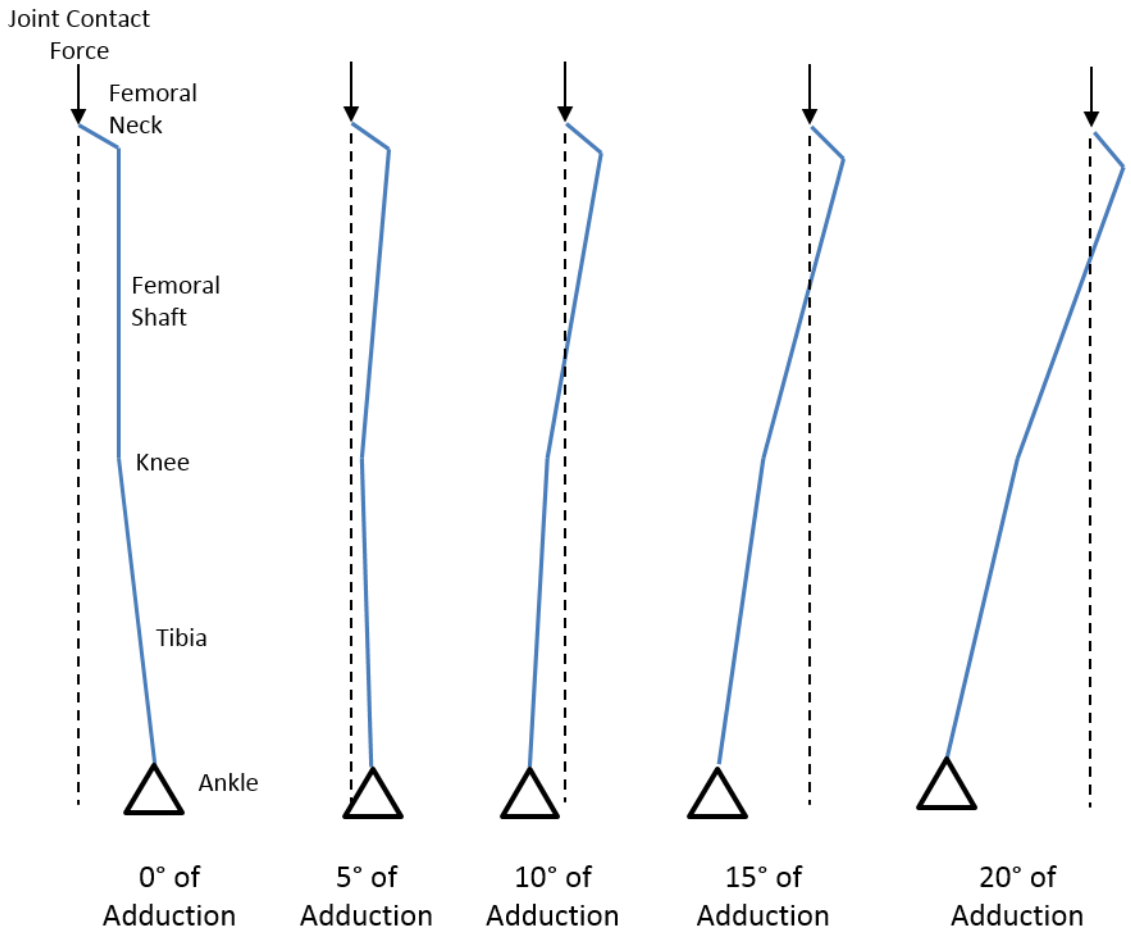

Figure 2.14 Direction of the load through the femoral head, relative to the hip, knee and ankle for five different adduction angles (calculated relative to the femoral shaft).

The direction of loading, relative to the femur and tibia, is given in a simplified form for five different adduction angles in Figure 2.14. The lengths of the femur and tibia, length of the femoral neck and angle of the femoral neck were taken from synthetic bone models used to represent a typical human skeleton (large, left, Model #3406 and #3402, Sawbones, Pacific Research Laboratories Inc., Sweden). When aligning the femur and tibia the mechanical tibiofemoral angle (angle between the tibial shaft and the line between the femoral head and knee) was set 0° to represent a natural alignment [75-77]. This corresponded to an anatomical tibiofemoral angle (angle between the shaft of the tibia and shaft of the femur) or approximately 7°, which is also reported to represent a natural alignment [75-79]. Note that the cases represented in Figure 2.14 are at the immediate onset of loading. Only an axial force is accounted for as the transverse forces would depend on how the structure initially responded to this axial force.

At 0° of adduction the load path would cause the leg to fall medially. This movement would be resisted by the hip bone, resulting in a lateral force acting on the femoral head, as recorded by Bergmann et al. [64]. This loading would be expected to cause the femur to fall into abduction. The muscle groups that would resist this would therefore be those that cause adduction, as shown in Figure 2.10.

At 5° of adduction the load path would also cause the leg to fall medially and would also cause the femur to fall into abduction. The moment arm in this case is much smaller, however, meaning that smaller muscle forces would be required to prevent this.

At 10° of adduction the load path would cause the leg to fall laterally. In two-legged stance this could be counteracted by a tensile force from the muscles and ligaments holding the femoral head into the acetabular cup. Depending on the resulting level of compression between the femoral head and acetabulum this could again lead to a lateral force acting on the femoral head. As with the 5° of adduction case the moment arm between the load and ankle is small so the muscle forces required would likely also be relatively small. At 10° of adduction the femur would attempt to fall into adduction. The muscle groups that would be expected to resist this would therefore be those that cause abduction, as shown in Figure 2.11.

At 15° and 20° of adduction the moment arm causing the leg to fall laterally and the femur to fall into adduction increases, requiring larger muscle forces to compensate.

When perfectly balanced in single-leg stance the CoM of the body would ideally be directly above the centre of the femoral head. This would reduce the adduction/abduction forces required to prevent tilting if the hip. The femoral head would also be directly above the ankle, such that there was no moment arm causing the person to topple. From Figure 2.14 this would be expected to occur at an adduction angle of between 5° and 10° and would generate an almost entirely vertical load on the femoral head. Comparing this with the results of Bergmann et al. [64] shows that they measured the maximum hip contact force during single leg stance at an angle corresponding to 7° of adduction with minimal transverse forces.

The good agreement between Figure 2.14 and the in vivo hip contact force data, even from a very simple comparison, may suggest that the balanced single leg stance may be a more simple anatomical position to represent during testing. This may be due to the reduction in moment arms and the fact that the hip contact force is focussed towards a

vertical load. Transverse components of force would be more dependent on an accurate representation of the bending and deformation of the whole structure, as they are partly due to the constraining effect of the acetabular cup. The single leg stance may therefore be a good comparison case against which the applicability of testing regimes and simulation models could be validated.

2.2.4 Properties of Human Tissues and Fixation Constructs

Accurate material properties for the bone and fixation constructs are important for any simulation or model attempting to capture the response of such a construct to loading. Biological tissues often display complex mechanical behaviour however, with tissues displaying anisotropic, time dependent properties as well as altering their size, geometry or internal configuration due to loading or other factors [80-83]. Material properties will also vary from patient to patient [84] and, often, from location to location [80, 85, 87].

Experimental testing of cortical bone sections has given a range of Young's modulus values and failure properties. A review of the literature gives longitudinal Young's modulus values for cortical bone between 9.7 – 23.5 GPa [80, 84, 87-90]. The Young's modulus of cortical bone in the transverse plane is generally reported to be lower (5.7 – 16.6 GPa [80, 84, 90]). Reilly and Burstein [84] described the behaviour of cortical bone to be transversely isotropic. The tensile yield strain has been recorded as 0.73±0.05% [87] and the ultimate tensile stress recorded between 101-128 MPa [80]. The strain hardening modulus, representing the stiffness of cortical bone during plastic deformation has been given as between 0.64-1.07 GPa [84, 87]. Shear modulus values were recorded by Reilly and Burstein [84] between 3.1-3.7 GPa. The poisons ratio for cortical bone has also been shown to vary between the longitudinal (0.29-0.51) and transverse (0.45-0.63) directions [84]. Berteau et al. [91] measured the Young's modulus of samples from children and elderly people. The Young's modulus values varied between 9.1-15.5 GPa for the children and 5.8-16.7 for the elderly group. Poisson's ratio was also measured and was shown to vary from 0.24-0.27. Abdel-Wahab et al. [92] and Johnson et al. [93] also showed that the response of cortical bone viscoelastoplastic, with the response of cortical bone to loading displaying non-linear elastic-plastic behaviour with strain hardening, creep and stress

relaxation. A relationship was also found where the recorded Young's modulus of the cortical bone increased with strain rate.

Similar testing has been performed in the literature to evaluate and characterise the mechanical response of cancellous bone. Some studies have focussed on evaluating the bulk material properties of a section of cancellous bone [94-97] and some studies have focussed on measuring the properties of individual trabecular struts [87, 89, 98, 99, 90, 97, 100]. The wide range of reported values makes it difficult to draw conclusions however the work of Rho et al. [89] may suggest that at the tissue level there is a difference between the mechanical properties of trabecular tissue and cortical tissue. Reported values for the Young's modulus of trabecular tissue range from 3.5-22.3 GPa [87, 89, 90, 97-100]. Apparent modulus values reported for sections of cancellous bone, representing the bulk behaviour of the cancellous architecture, range from 55-2988 MPa [94-97]. Brown et al. [94] recorded the apparent modulus of sections of cancellous bone taken from two different sites within the femoral head. They found a marked difference between the apparent modulus of cancellous bone from the proximal region (237 MPa) compared to the distal region (55 MPa) which suggests that there are large variations in apparent modulus within the femur. This trend occurred across 32 patients, suggesting that these regional differences in cancellous bone properties may be relatively consistent between subjects. Bayraktar et al. [87] also recorded the tensile yield strain (0.62%) and compressive yield strain (1.04%) for trabecular tissue.

The wide range of reported properties for cortical and cancellous bone suggest that pre-clinical testing of treatments and devices should attempt to consider a similarly wide range of cases. Failing to do so may not adequately represent the patient population on which those treatments and devices may be applied.

The Young's modulus values for a range of materials commonly used in, or with, surgical implants are listed in Table 2.3.

Table 2.3 Young's modulus of several materials used in surgical treatments.

Material	Young's Modulus (GPa)
Ultra High Molecular Weight PolyEthylene (UHMWPE)	0.69 [101]
PolyMethylMethAcrylate Bone Cement (PMMA)	2.5 [101]
Ti-6Al-4V Titanium Alloy	113.8 [101, 102]
316L Stainless Steel	200 [101, 102]
Cobalt Chromium Molybdenum (Co-Cr-Mo) Alloy	221 [101, 102]

2.2.5 Fracture Configurations and Fracture Healing

Periprosthetic fractures can be spiral fractures, oblique fractures (short or long) or transverse fractures. Spiral fractures often occur due to loading of the femur in torsion and oblique or transverse fractures often occur due to loading of the femur in bending [12]. Beals et al. [30] found that spiral fractures were the most common but that transverse and oblique fractures were also commonly seen around a loose, cemented, original stem.

There are two distinctly different ways that a fracture can heal depending on the type of fracture fixation selected and these are typically described as indirect and direct healing. Indirect healing is stimulated by flexible fixation, whether intentional or not, which leads to motion, in the millimetre range, across the fracture site. After the fracture occurs and the fracture ends are reduced back together a blood clot/soft connective tissue (haematoma) forms in the gap. This blood clot forms into soft callus (fibrocartilage) which, following resorption of the fractured surfaces, unites the fracture fragments. The callus calcifies into woven bone which is stronger than the soft callus but still disorganised in structure and therefore weaker than healthy bone. At this point bone remodelling begins to

convert the woven bone to cortical bone. Issues with indirect healing are that it instigates bone resorption of the fracture fragments and flexible fixation can lead to delayed or non-union [103]. Large fracture gaps can also delay the healing process [104] but may be necessary in order to avoid very small unstable gaps of high strain [105]. As tissue attempts to bridge the fracture gap, it cannot form if the strain at that site causes those tissue elements to rupture. The size of the fracture gap can be increased, either during the reduction, or by bone resorption induced by large local tissue strains. This spreads the fracture movements over a larger area and volume of tissue and therefore reduces those strains experienced by the tissue elements. For bone resorption to result in decreased callus strains, however, the fracture fixation method would have to produce similar fracture movements in the presence of a larger fracture gap. In order to promote callus formation, a certain amount of strain is required, however, the strains must also be kept below certain limits depending on the material in the fracture gap. Perren et al. [105] suggested that "Strain values up to 2% are tolerated by lamellar bone tissue, up to 10% are tolerated by the three-dimensional configuration of woven bone and between 10% and 30% induction of resorption prevails".

Direct healing results from stable fixation and compression of the fracture fragments and is characterised by a lack of callus formation. Instead the process of internal haversian remodelling is able to continue across the fracture site without the osteones being affected by the gap [105]. In internal haversian remodelling specialist cells called osteoclasts tunnel through dead or damaged bone and osteoblasts then follow along these channels filling them with new, healthy bone [106]. Direct healing is not however necessarily any faster than indirect healing and can be substantially slower to complete [5, 104].

2.2.6 Discussion

The human anatomy is a complex, interrelated system that can be extremely difficult to investigate or model. Wide person-to-person and case-to-case variability makes it extremely difficult to use statistical analyses of in vivo outcomes to evaluate treatments or fixations. This is particularly true for long-term scenarios such as PFF treatments where implants are expected to remain in patients for many years. Evaluating the biomechanical

causes for fixation failure due to the cyclic loading that occurs after years of use can be almost impossible when the loading those implants have been subjected to, either during daily activities or at the point of failure, is unknown. Attempting to evaluate treatments based on the success or failure of specific clinical cases is therefore generally impractical. The relevance of long-term clinical follow up studies can also sometimes be limited due to the progression of surgical techniques and technologies. For example Springer et al. [48] evaluated their clinical results from the use of long stem revision treatments. During the course of the time period covered by the analysis, however, they had moved from predominantly using cemented stems to proximally-coated uncemented stems to extensively coated uncemented stems.

The relative benchmarking of constructs or treatment options against each other, under simulated loading conditions, is therefore a common approach for pre-clinical testing. Matching the in vivo scenario, in order to produce relevant comparisons, is difficult however. Regarding PFF treatments the material properties of bone, both cancellous and cortical, are extremely complex, displaying viscoelastoplastic properties and anisotropy as well as regional variations. Additionally the loading scenario under which these fracture fixation devices must operate is extremely complex. Hip contact forces were reported, during day to day activities, in the region of 2.5x body weight [64]. Hip contact forces during stumbling have been reported to be as high as 8.7x body weight [107]. In addition to this there is the effect of muscle forces on the length of the femur and the constraining effect of the acetabular cup and knee.

The in vivo scenario that must be replicated in order to evaluate periprosthetic femoral fracture treatment options in extremely complex. As such great care should be taken when designing testing regimes to match this in vivo scenario as closely as possible and to represent the wide range of characteristics displayed by the patient population.

2.3 Experimental Biomechanical Testing

2.3.1 Introduction

The focus of this section will be on evaluating potential methods for performing experimental testing of the biomechanics surrounding periprosthetic femoral fractures. The areas that will be considered are:

- Possible choices for experimental specimens that can be used to represent the femur.
- Possible methods for simulating the loading and constraints that the femur will experience in vivo, as well as any additional loading scenarios that may be of use biomechanically.
- Possible measurement methods for acquiring data that can compare different treatments.

Based on the information documented in the literature an experimental methodology for the purposes of this study will then proposed.

2.3.2 Specimen Selection and Preparation

The use of synthetic femur surrogates simplifies the complex anisotropic cortical bone to a transversely orthotropic polymer with similar bulk properties [108]. Micromechanical properties such as fracture toughness and propagation and fatigue failure may not be as well represented however [109], particularly in scenarios where natural bone would have the opportunity to heal [110, 111]. Synthetic femurs lack the variable nature of bone which changes its shape and properties over time in response to, among other factors, the loading that the bone is subjected to [111]. The cancellous bone is represented using a foam surrogate. This surrogate does not show the organised inhomogeneous nature of cancellous bone [94], which develops an optimised sub-structure in response to the loading it is subjected to, nor does it match the porosity of cancellous bone [112] with will affect the penetration of, and interdigitation with, cement [113, 114]. Synthetic femurs typically represent a single geometry that does not account for the wide range of femur shapes seen

across the human population. They also typically represent a relatively healthy, young patient [109] rather than an elderly patient, potentially with poor bone stock, as is usually seen in PFF cases [12]. The advantages and disadvantages of synthetic bone are therefore linked in many ways. The advantage of good repeatability of results and uniform geometry and material properties between specimens makes discovering statistically significant differences more likely, however it also limits the applicability of these synthetic femurs by only representing a very small subset of the human population, and possibly an even smaller subset of the patient population. Additionally, the fact that the material properties of the cancellous and cortical bone surrogates are effectively constant across the entire specimen, rather than varying by region as seen in vivo [92, 94], means that they will differ even from a patient with a similar femoral geometry.

The use of animal specimens can provide more realistic bone properties [115-117]. There are still noticeable differences between animal and human bone that make comparisons difficult, however [118]. The geometric differences are more significant, limiting the usefulness of animal studies to investigations requiring biological surroundings and the possibility for healing to occur [119, 120]. Even then differences between animal and human models must be kept in mind when analysing the results [118].

Cadaveric human specimens can provide realistic bone properties and the variability of geometry and properties seen across the human population [109, 121-125]. They are, however, difficult to obtain in large numbers, limiting the effectiveness of statistical comparisons, and preparation of the specimens for experimental testing will still induce differences to real life. The specimens are typically cleaned to remove soft tissue and tested in a dry atmosphere under similar loading conditions to synthetic femurs. As such the bone may behave differently under loading when outside of its natural biological surroundings. In particular, the effects of soft tissue and muscle forces have been lost and the effects of the natural hip bone and lower limb have been removed. Bilateral testing of paired left and right femurs, using one sample for testing and one as an intact control, can be used in order to account for inter-specimen variations [126, 127]. In addition, with both human and animal specimens, there are ethical considerations which must be taken into account regarding whether any additional value that can be gained by selecting to use animal or human specimens is sufficient to justify their use.

Synthetic specimens, human cadaveric specimens and animal specimens all have advantages and disadvantages regarding their use for biomechanical testing. Therefore the selection of specimen type should be made due to the specific aims of the study. Given the relatively low cost and lack of ethical concerns synthetic specimens may be useful in nearly all cases, however, as part of the development and optimisation of testing regimes prior to their application.

2.3.3 Constraints and Loading

In previously reported experimental testing a wide range of loading methodologies have been described. Tests can use either static loading cases [4, 10, 14, 56, 122, 125, 127-140] or cyclic loading [14, 109, 124, 131, 141-146]. They can either constrain the femoral head and knee, preventing relative displacements in the transverse plane [10, 122, 124, 128, 129, 132-135, 137, 138, 141], or leave them unconstrained in the transverse plane [14, 56, 109, 127, 130, 134, 136, 140, 142-144]. They can consider only the load applied to the femoral head [4, 10, 14, 56, 122, 124, 128-138, 142-145] or they can also consider the effect of muscle forces [109, 127-129, 139-141, 146]. They can consider pure bending, compression and torsion, generally described in the literature as isometric loading [4, 10, 14, 56, 125, 130-135] or they can consider loading orientations aimed to represent an approximately physiological femur orientation [4, 10, 14, 56, 109, 122, 124, 127-146]. Finally, they can consider loading within the elastic region of the specimens, typically so that a range of testing scenarios could be investigated [4, 10, 14, 56, 109, 125, 127-146], or they can load the specimens to failure, evaluating both the mode of failure and energy required to cause failure [10, 122, 124, 131, 143].

A single static loading case can be used to investigate how a treatment construct responds to a very specific scenario. Different treatments can be compared against each other in terms of factors such as the overall stiffness of the construct, specific measurements of stress and strain or deformations. Time-dependent effects such as fatigue failure and creep cannot be usefully evaluated however. Several failure modes for periprosthetic femoral fracture treatments, such as stem loosening for long revision stem fixation [53] and fatigue failure of plates due to non-union [141], might not be properly investigated. Time-dependent material properties, and fatigue failure properties are

generally more difficult to match that simple linear elastic properties, however [143]. As such, developing an experimental methodology to accurately investigate failure due to cyclic loading may be more difficult and subject to error. The biological nature of fracture fixation also makes achieving meaningful long-term testing results difficult. Ideally, testing regimes representing a long time period would have to represent fracture healing as well as bone remodelling and osteolysis [147]. As with static loading, however, treatments under cyclic loading can still be compared relative to each other, rather than specific metrics for clinical success or failure. Fewer studies, out of those evaluated during this literature review, considered cyclic loading compared to static loading. Few studies considered loading the specimens to failure either. This suggests that the majority of experimental testing studies are completed with test specimens still undamaged. It is possible some of these authors conducted additional testing and presented these results in future work. In cases where there was no follow up work conducted on the same specimens, however, it would appear that additional testing could have been planned, conducted and presented. Both load-to-failure comparisons and cyclic loading comparisons are relevant to the survival and suitability of implants. Therefore additional, destructive testing would have likely been of value, particularly when using cadaveric specimens where, for ethical reasons, the maximum research value from each specimen should be obtained.

When remaining within the elastic behaviour limit of the specimens they can be repeatedly tested under different scenarios which can be useful given the wide range of activities performed in vivo [64]. Evaluating the elastic behaviour of a treatment can consider how effectively the fracture has been stabilised. It can also show how well the treatment is likely to restore function during normal day-to-day activities. Testing specimens to failure, however, can show how resistance different treatments are to single, high magnitude, loads such as occur during a stumble or fall [107].

Isometric loading, where the load and specimen are orientated such that only a single loading mode is investigated, can divide the response of the construct into its individual components. Understanding how different treatments respond to, for example pure lateral bending, pure axial compression or pure torsion can identify the relative strengths and weaknesses of treatments that achieve fixation in different ways. Long stem revision treatments can struggle to achieve sufficient support against torsion [9], therefore evaluating a range of stem designs under pure torsion could be used to rank designs based

on this important factor. Focussing on the stability of the treatment in these individual directions also allows for easier, more detailed interpretation of the results, with fewer confounding factors to consider. Physiological loading, which attempts to orient the femur and load in such a way as to represent semi-realistic human activity can provide more realistic loading scenarios however. It is unlikely that a treatment would experience pure lateral bending, for example, particularly that caused by three- or four-point bending [130] whereas the forces incurred during walking, stair climbs and other such activities would occur often [148]. Common physiological loading scenarios include heel strike [128, 129, 141] (the point of maximum load during walking) and the anatomical single-legged stance [10, 14, 130-133]. Many studies tested specimens at semi-physiological orientations, or at isometric and semi-physiological orientations but only one experimental study found in this review considered isometric loading alone [125]. Isometric loading has limited applicability to the in vivo scenario and all of the different loading modes that a specimen can experience (lateral bending, medial bending, anterior bending, posterior bending, axial compression and torsion) can be induced through a range of physiologically relevant adduction/abduction, flexion/extension and internal/external rotation angles. Given that isometric loading orientations do no generally seem to be sufficient alone it may be more valuable to, instead, consider a wider range of physiologically relevant loading angles instead.

The constraining effect of the in vivo hip and knee is difficult to determine. Most activities performed on a daily basis involve dynamic movements of much, if not all, of the body. As such interpreting the reaction forces applied to the femur from the hip and knee joints requires the consideration of all of these contributing forces. Although bulk estimations for the relative contributions of the hip and knee can be made from free body diagrams [66, 70, 71] and the analysis of gait data [64- 66] the small scale response of complicated biological tissues, such as cartilage, have not been fully characterised. The deformations that occur in these tissues, at the hip and knee, will depend on the action of the femur. As such, when testing femoral specimens the hip and knee constraints should be dependent on the behaviour of the specimen itself. A review of the literature provides no current methodology for representing the structural properties of the hip and knee joint tissues, and the movements of the remainder of the human body, in an accurate way. Instead, experimental studies typically utilise one of two methodologies, either fully

constraining the relative transverse motion of the hip and knee or leaving this transverse motion completely unconstrained. In reality it is likely that the in vivo scenario, depending on the particular activity being replicated, resides somewhere between these two extremes. Comprehensive testing regimes should therefore perhaps consider and report both cases.

The relative contributions of the various muscles and ligaments to the forces acting around the femur during daily activities are also still undetermined. This may be why only eight studies, out of the twenty-eight reviewed in this section considered their effect. Many methods have been proposed and investigated for recording [149, 150] or calculating [151-154] the muscle forces. It is difficult to validate these values when used experimentally, however, due to the large number of unknown factors involved in the biomechanical system and limited in vivo data. Additionally, experimentally simulating muscle forces can be difficult and is typically done using cables or straps attached via pulleys to hanging weights or additional loading fixtures [128, 129]. Accounting for the full range of muscle forces would therefore require an extensive network of cables and attachments. The most common muscle force simulated experimentally appears to be an abductor force to the greater trochanter and this therefore may be the most relevant force to consider.

2.3.4 Measurements

Across the current literature many different measurement methods have been used to evaluate the biomechanics of long bones, implanted bones and fractured and treated bones. Typical measures that are recorded are the construct stiffness, which is generally defined as the force per unit displacement at the point of load application in the direction of the load [4, 12, 13, 130, 132]. Stiffness is often used to compare the response of different cases to specific, static, loading cases which may either be physiological or isometric. The stiffness is usually calculated as the gradient of the linear portion of recorded force versus displacement data. Failure is often also estimated from this data by referring either to a maximum displacement value, a sharp increase in displacement or the first large drop in force [9, 10]. Lever et al. [4] did however recommend that stiffness should not be used alone to estimate clinical success or failure. Given that stiffness relates to the displacement of a single point it is possible that it would fail to represent the response of the whole structure with sufficient detail to be biomechanically useful.

The relative movement at the fracture site has been shown to be an important factor in fracture healing [155]. Several studies have therefore attempted to measure this movement and use it to evaluate the likelihood of fracture union [4, 9, 13].

The static load to failure has been used to compare the survivability of different constructs and identify the different modes by which they are likely to fail [4, 13].

Strains have been used frequently as an attempt to investigate the likelihood of strain-shielding induced bone resorption, the potential for bone fracture, or refracture, due to high stresses and the localised bending, compressive or tensile, of the bone [13, 14, 129, 133-136, 156, 157]. Similar methods have also been applied to measure the strains in implants and fixation constructs [13, 128]. These can be used to estimate the failure mode of these devices and/or the fatigue cycles-to-failure. Strain gauges are a common method for measuring cortical or implant strains. They are cheap, relatively easy to set up and reliable. Strain gauges are, however susceptible to thermal drift which must be accounted for using reference gauges and the quality of the results depends on how well bonded the gauge is to the specimen [158]. Additionally, attempting to measure strain across several locations and in several directions becomes increasingly complex, requiring many gauges and an increasingly complicated signal processing system. Other methods for measuring strain use high resolution digital imaging during testing. Though there are several methodologies for achieving this the ones most commonly seen in PFF testing are digital image correlation (DIC) and image marker tracking [157, 158]. Image marker tracking uses a system of pre-prepared markers, attached to the specimens, and cameras to track the movement of these specific markers during loading. From this the relative motions between these pre-selected points can be calculated. DIC instead relies on the automatic tracking of an entire region by applying a speckled pattern to that region and tracking all definable points on that surface.

The deformation of the implant, particularly a stem, can be measured during and after loading to estimate the stability of the implant under load and the effect of cyclic loading and fatigue damage on stability and subsidence [4]. A similar comparison can be performed by measuring the relative micro motions between interfaces, for example the stem-bone interface in a press-fit stem, which again provides information on how much the implant displaces under load and how much of that displacement is permanent [48]. Linear variable differential transformers (LVDTs) can also be used to measure displacements of

the specimens when loaded [12]. They can be applied externally to record overall displacements as another way of measuring stiffness, they can be used in combination to measure bending patterns and they have been used in the past, by creating small holes into the interior areas of the specimens, to provide information on the relative motion of components inside the femur [48].

Finally, pressure sensitive films can be used to investigate contact pressures between surfaces, such as at the femoral head to estimate loading magnitude and distribution and between fracture fragments to identify areas of load transfer [159].

2.3.5 Discussion

Fully replicating the in vivo scenario is difficult and, in general, previous experimental testing regimes have therefore simplified the system. The most common simplifications involve removing the effect of muscle forces, arbitrarily constraining the transverse relative motion of the hip and knee and considering only static, elastic loading cases. Although several studies did consider one or more of these factors, for example Talbot et al. [131] tested specimens under cyclic loading and to failure however they did not include muscle forces in their model. No experimental testing regime found during the course of this literature review considered all of these factors in combination however. The focus of the experimental testing proposed in this study is for the validation of finite element models. The complexity of the experimental methodology is therefore linked to the validity of the computational models. Initial experimental testing that considers a relatively simple, linear elastic loading case with no muscle forces is therefore proposed. If computational models can be developed to accurately represent this case additional factors, such as the effects of muscle forces, fatigue, creep and failure can be incrementally investigated and introduced.

2.4 Computational Biomechanical Testing

2.4.1 Introduction

This section focuses on evaluating the possible techniques for using computational modelling to investigate the biomechanics surrounding a periprosthetic femoral fracture. It will include discussions on different constraints and loading scenarios that can be represented and the various outputs that can be selected. Based on the information documented in the literature a computational testing methodology for the purposes of this study is then proposed.

2.4.2 Constraints and Loading

Computational modelling can generally be more flexible regarding the options for loading and constraints as compared to experimental testing. Loads and constraints can be applied directly to any section of the model, without requiring a suitable loading fixture, and their magnitudes and directions can be explicitly controlled without experimental error or variability. As such, computational models, once developed, have the potential to quickly and cheaply consider a wide range of scenarios. The application of cyclic loading, however, can lead to significant increases in computational analysis time and as such few studies have considered cyclic loading with finite element models [160-162]. Muscle forces can be applied relatively easily and many studies have considered them within their computational testing [53, 59, 128, 139, 163-168, 160, 161]. The boundary conditions applied to computational models are often similar to those used experimentally [16, 19, 20, 21, 53, 132, 133, 137, 163, 164,167-169], in that the base of the specimen is fixed. As with the experimental testing the constraint at the head could range from completely fixed, allowing no transverse head movement [16, 19, 20, 132, 137], to completely unconstrained, allowing free bending of the specimen [21, 133, 139, 163, 164, 167, 168]. Alternatively, physiological boundary conditions can be estimated to replicate the effects of the hip, knee and lower leg [160, 161, 165, 166], although given the lack of detailed in vivo measurements validating these models can be difficult. Finally, with computational models

the properties of any interfaces must be defined. In experimental specimens the properties of these interfaces can be complex [170- 172]. Computationally however, in order to achieve reasonable model analysis times or in the absence of accurate interface property data, interfaces can often be simplified. A typical assumption is to assume that surfaces are perfectly bonded and that no relative motion can occur between them [16, 19- 21, 132, 133, 137, 139, 165, 166]. Several studies have investigated the frictional interfaces between some components, however [16, 19, 20, 53, 128, 161, 163-165, 168, 169].

The large number of studies that have included muscle forces shows that it is a feasible and well-tested method of applying physiological loading to a femur model. If the structural response of a computational model can be validated against experimental testing, which would benefit from a less complicated loading scheme, then the addition of muscle forces can be easily justified.

Unlike experimental testing, which is limited by practical concerns such as space and loading assembly complexity, physiological loading and constraints can be simulated computationally without significantly increasing the modelling complexity [160, 161, 165, 166]. As such, if a computational model can be developed and validated against an experimental loading it could therefore be more valuable to then move to a physiological loading scenario that incorporates measurements from in vivo testing.

There are many areas of complexity that can be added to a computational model that will result in an increase in model analysis time. As such the complexity of the model must be balanced against the available computing resources and project time. Combining several factors such as fatigue properties, creep properties, interface properties and dynamic loading may therefore not be feasible. Sensitivity testing can be used to investigate the effects of these factors individually, however, and should be used to interpret how the simplification and assumptions made in the final computational model may affect the results.

2.4.3 Discussion

Finite element modelling has the capacity to consider a wider range of cases, and provide more detailed results, compared to experimental testing. These results are only relevant if the model is validated against experimental results, however. One key area

where computational models appear to have more flexibility that experimental testing is in replicating physiological loading scenarios and constraints. Once a model is well validated it may therefore be recommended to focus the investigations on a range of physiological activities rather than mimicking semi-physiological experimental testing or isometric loading.

2.5 Discussion

Analysing the Vancouver classification [41], and the current range of recommended treatments for Vancouver type B periprosthetic femoral fractures, shows that an improved treatment algorithm is required. Long revision stems have been identified as a potential treatment for type B1 fractures where it is uncertain whether plated fixation can provide adequate support. The suitability of long stem revision treatment for a range of potentially unstable fracture configurations will therefore be evaluated during this study to investigate if it could be a more appropriate treatment.

When considering the in vivo scenario that PFF treatments will be subjected to the muscle forces and constraining effect of the hip and knee appear key. Simulating the in vivo scenario will also require a method of representing realistic bone material properties as these will also influence the survivability of a treatment. In vivo instrumented stem data by Bergmann et al. [64], and a simple free body diagram, suggested that balancing on one leg may minimise the transverse component of the hip contact force. This could therefore be expected to minimise the transverse movement of the femoral head, relative to the knee. As such this may be a suitable test case when data for the in vivo constraining effect of the head and knee is unknown.

Experimentally matching the wide range of bone material properties and geometries would require a prohibitively large number of experimental specimens. Experimentally matching physiological loading scenarios would require an extensive loading assembly. This study will use a combination of experimental and computational testing focussed on capitalising on the advantages of each. Experimental testing will use synthetic femurs to decrease inter-specimen variability, making the results more suitable for model validation.

Specimens will be loading at a range of adduction angles, including one approximating single-leg stance, to investigate the effect of head constraints.

FE testing will account for some of the simplifications of using synthetic femurs by investigating alternate femoral geometries and material properties. Loosening has been identified in the literature as a common cause for failure of cemented long revision stem PFF treatments [48, 53, 54]. The principle stresses in the cement mantle will therefore be used as one way to evaluate the suitability of long stem treatments. Non-union has been described as another reason for failure of long stem revision PFF treatments [44, 56, 57]. Fracture movements will therefore also be evaluated in the FE models in an attempt to identify potential issues that might impair healing.

3. Experimental Investigation into Long Stem Fixation

In this chapter an experimental methodology for testing the mechanical response of the femur to prosthetic femoral fracture and subsequent long stem revision treatment is described. This methodology covers the specimen preparation, the loading regime and application methods and the measurement and data analysis methods. Following this the results for the mechanical behaviour of these experimental specimens is presented for a range of loading angles.

The aim of the work in this chapter is to provide biomechanical data from experimental long stem fracture fixation specimens suitable for the validation of comparable computational models. Specifically, multiple significantly different cases were required against which the FE biomechanical response could be compared.

3.1 Experimental Methods

3.1.1 Specimen Preparation

Six 4th generation large synthetic femurs (large, left, Model #3406, Sawbones, Pacific Research Laboratories Inc., Sweden), designated S10-S15, were used to investigate the experimental response of the femur under load after long stem revision surgery. The femoral condyles of all specimens were removed with a cut, perpendicular to the long axis of the femur, 340mm below the lesser trochanter (Figure 3.1). The specimens were orientated vertically in a steel loading pot, using a potting jig to ensure consistent positioning (Figure 3.2, Left), and the distal 80mm was potted in PMMA cement of 50mm diameter (Figure 3.2, Right). This procedure was developed and described by Mak [16] for the attachment of femoral specimens into a purpose built loading rig (Figure 3.3 -3.4).

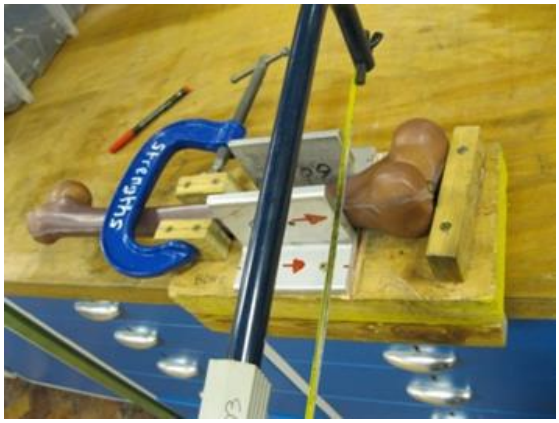

Figure 3.1 Removing the distal condyles using a custom built cutting, taken from [16].

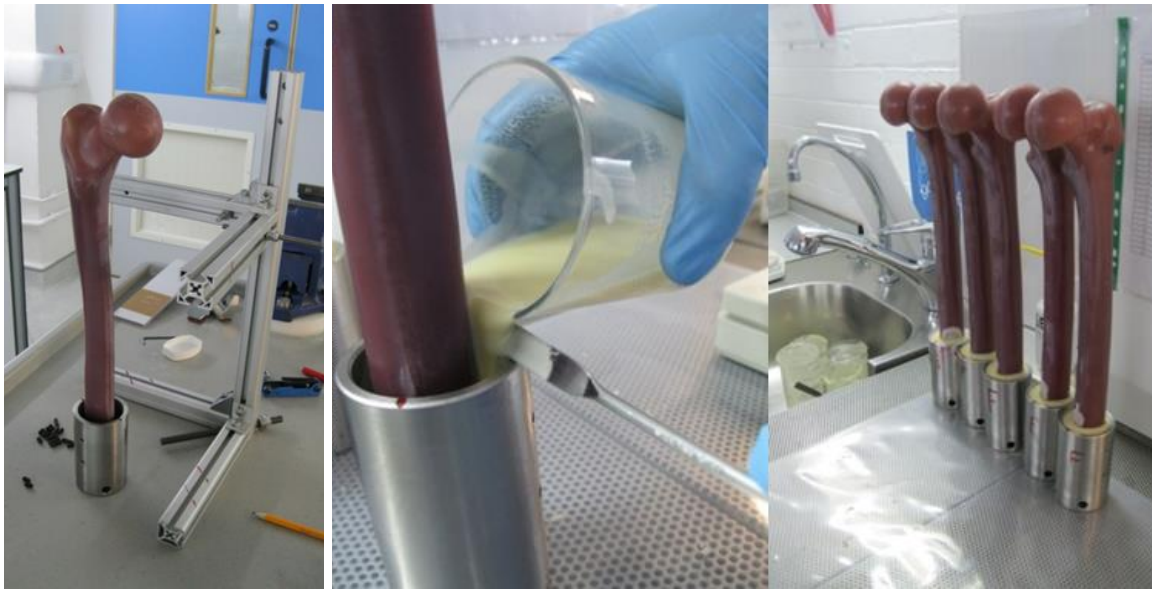

Figure 3.2 Left: The potting jig used to orient the specimens in the loading pots. Right: Distally potting the specimens in PMMA cement, taken from [16].

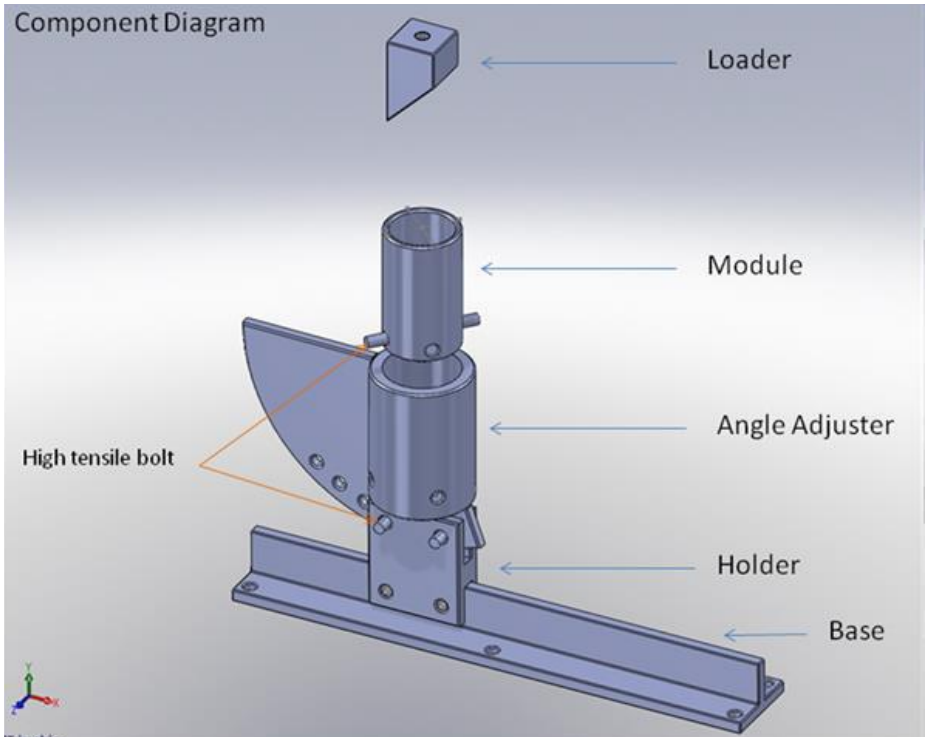

Figure 3.3 A component diagram of the different parts of the loading rig, taken from [16].

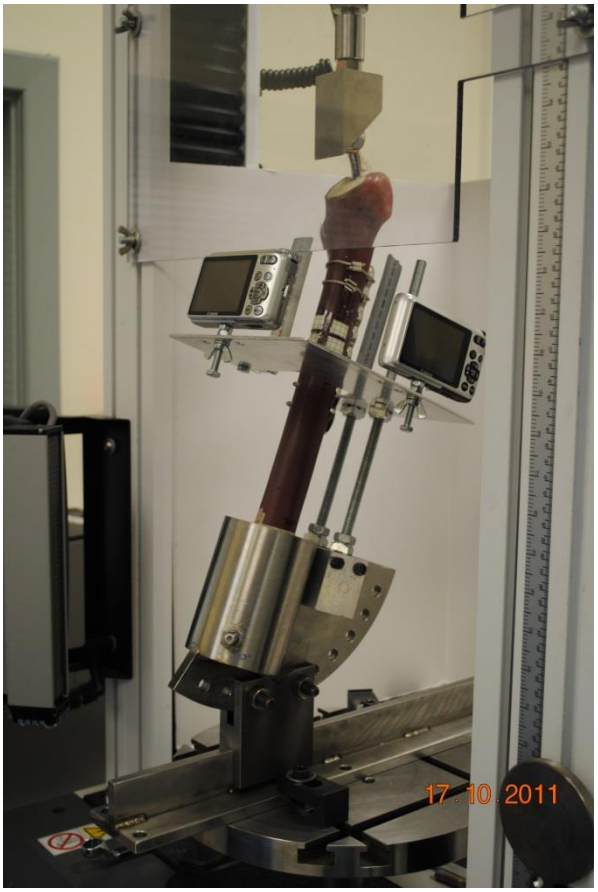

Figure 3.4 Experimental loading rig showing the loading fixture, ability to position the specimen at an angle of adduction and digital cameras recording movement at the fracture site.

For comparison against the long stem revision case and to validate initial FE models the specimens were initially tested with the original femoral head still in place. Loading was applied through direct contact with a flat, steel loading plate instead of the acetabular component shaped loading fixture (Figure 3.5).

Figure 3.5 Intact femur specimen and loading rig fixed into the mechanical testing machine with the load at the femoral head applied via a flat steel plate.

Once testing of the intact specimens had been completed the synthetic femurs were prepared to represent a long stem revision case by two orthopaedic surgeons, Eleftherios Tsiridis (University of Thessaloniki, Greece) and Simon Graham (Royal Liverpool and Broadgreen University Hospital, UK), following surgical procedure as closely as possible. A surgical reciprocating saw was used to remove the femoral head via a cut through the femoral neck (Figure 3.6, Left) and a channel was formed through the proximal cortex and cancellous bone with a drill (Figure 3.6, Right).

Figure 3.6 Left: Removal of the femoral head of a Sawbone femur. Right: Drilling the Sawbone femur.

This channel was extended with a rasp and a chisel (Figure 3.7, Left and Middle) and then reamed to oversize the stem using reamers 37.5 number 1, 44 number 0 and then 44 number 1 (Stryker SA, Switzerland) (Figure 3.7, Right).

Figure 3.7 Left: Opening the drill hole into the synthetic femur with a rasp. Middle: Using a chisel to remove some of the proximal cancellous of the synthetic femur. Right: Creating space for the femoral hip prosthesis with specially designed rasps.

A transverse osteotomy, relative to the long axis of the shaft of the femur, was created 68mm distal to the lesser trochanter using a band saw (blade thickness = 0.6mm) and the two femoral components were aligned together in a vice ready for cementing and stem insertion (Figure 3.8, Left).

Figure 3.8 Left: Clamping the fractured fragments of the synthetic femur ready for cement insertion. Middle: Mixing the surgical cement using the provided kits (Stryker UK Limited, Berkshire). Right: Filling the medullary canal of the synthetic femur with surgical cement from the pressurised cement gun.

Cement restrictors were placed distal to the intended location of the revision stem tip and Simplex surgical cement (Stryker SA, Switzerland) was prepared according to the instructions provided (Figure 3.8, Middle). A pressurised cement gun was used to fill the medullary canals of the specimens with surgical cement (Figure 3.8, Right) and the cement was compressed manually until it reached a sufficiently doughy texture (Figure 3.10, Left). A 205mm long stainless steel Exeter V40 Cemented Hip Long Tapered Stem (Figure 3.9) with 28mm femoral head (Stryker SA, Switzerland) was inserted into the medullary canal, bridging the fracture site, and held in place until the cement set (Figure 3.10, Middle). During this time excess cement at the fracture site and femoral neck cut was removed.

Figure 3.9 The 205mm long Exeter V40 Cemented Hip Long Tapered Stem (Styker SA, Switzerland) used in experimental specimens.

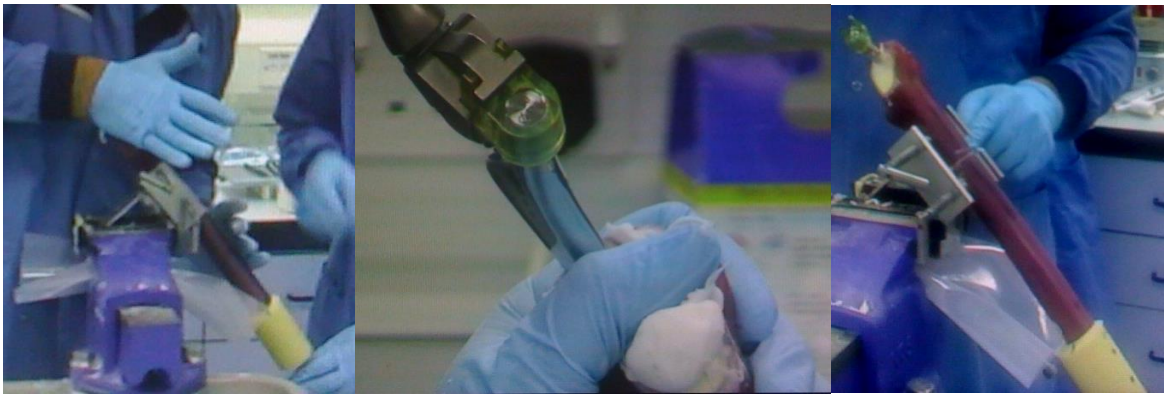

Figure 3.10 Left: Compressing the surgical cement in the medullary canal of the synthetic femur prior to stem insertion. Middle: Inserting the long femoral hip prosthesis into the synthetic femur. Right: The cemented long stem fixation of a transverse fracture in a Sawbone synthetic femur.

The specimens were left for 12 hours before loading to allow the cement to fully set and cool (Figure 3.10, Right).

After loading of all treated long stem specimens had been completed the specimen with the stiffness value closest to the average of the group (S15) was selected and five strain gauges were bonded to the surface at preselected locations (Figure 3.11).

Figure 3.11 Experimental specimen, after implantation of the long revision stem, with the locations of the five strain gauges (marked 1-5). Gauges were located on the medial (1-4) and lateral (5) sides of the specimen at positions 0 (1), 40 (2), 80 (3) and 200mm (4-5) distal to the lesser trochanter.

3.1.2 Loading Regime

The cemented distal 80mm of the specimens was surrounded in the loading rig by a stainless steel pot. Four screws attached the cement to the pot, distally fixing the femurs in place during loading (Figure 3.3). The loading rig was setup in a mechanical testing machine (3365, Instron, MA, USA). A loading cup shaped to conform to the femoral head of the specimens was attached to the load plate of the mechanical testing machine. The femoral head was free to rotate within the cup but prevented from moving in the anatomical transverse plane. The loading rig, developed by Mak [16], allowed for adjustments to the adduction angle (Figure 3.12) and rotation around the axis of the femur (Figure 3.13). Adjustments to the adduction angle were made by adjusting the angle holder component

before attaching to the holder component (Figure 3.3). Adjustments to the angle of internal rotation were made by altering the location of the high tensile bolt that held the module component into the angle adjuster.

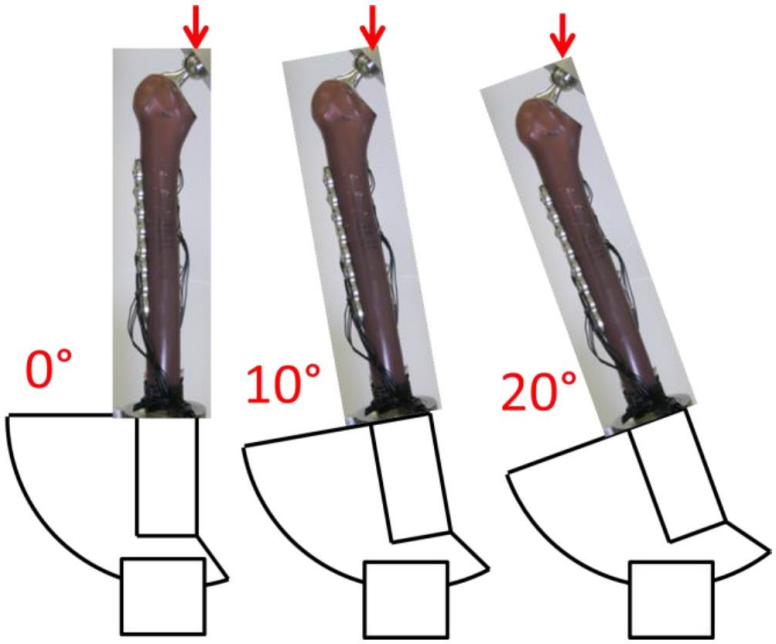

Figure 3.12 The three angles of adduction that the specimens could be placed in using the experimental loading rig, taken from [16].

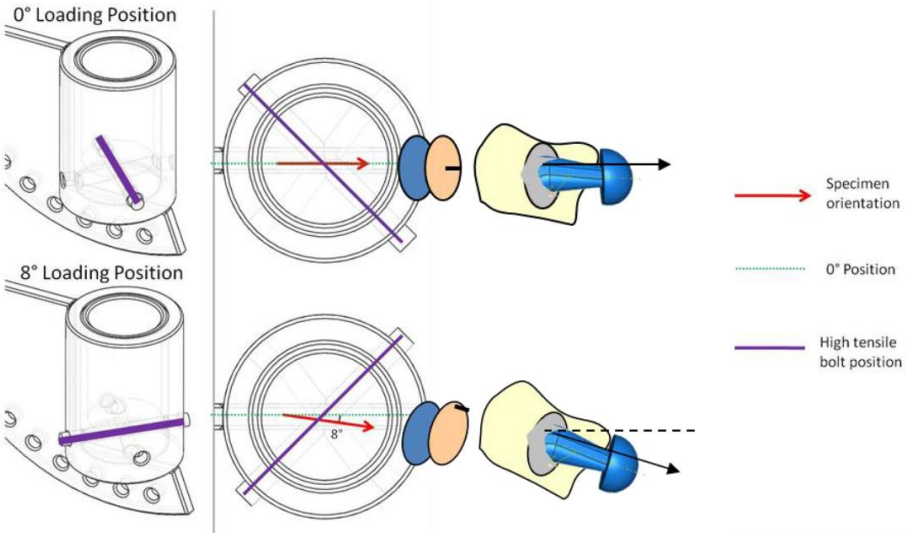

Figure 3.13 The two angles of internal rotation that the specimens could be placed in using the experimental loading rig, taken from [16].

The intact femurs were loaded at 0, 10 and 20 degrees of adduction in the mediolateral plane while vertical in the anteroposterior plane. An element of torsion and posterior bending was also incorporated into the 10 and 20 degree tests by rotating the specimens by 8 degrees around their longitudinal axis (Figure 3.14). When the femur, at an angle of adduction, is rotated about its long axis the point on the femoral head at which the load is applied moves anteriorly. This femoral head load however continues to act through the centre of the femoral head. The femoral head load therefore has a component of force acting in the anteroposterior direction. This component of force in the anteroposterior direction will result in bending in the posterior direction. Due to the offset between the femoral head, where the load is applied, and the long axis of the femur it will also induce torsion around the shaft of the stem.

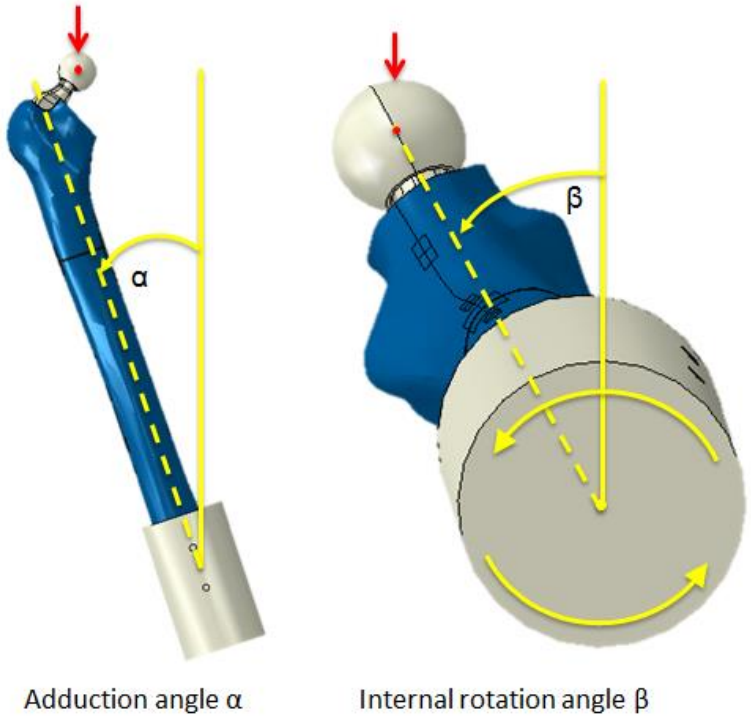

Figure 3.14 Definition of the adduction angle and internal rotation angle, and diagram showing how the combination of adduction and internal rotation results in an element of torsion and posterior bending.

Ten degrees of adduction is comparable to previous studies and represents an approximately physiological stance [142]. The remaining cases allowed a wider range of motions and bending to be considered, therefore providing more information for use in

validating the FE models. Testing the six experimental specimens across five different loading angles resulted in a total of 30 test cases.

The femurs were loaded using displacement control, at a rate of 2mm/minute, to a maximum of 500N to remain in the elastic deformation region of the specimens [10, 14] and avoid damage during testing that would affect repeatability. 500N approximately relates to 25% body weight or 'toe-touch' loading which is the recommended weight-bearing for a patient post-surgery [173, 31]. A 10kN load cell was used with a rated accuracy of ±0.5% down to $1/100^{th}$ of the load cell capacity. This corresponds to an accuracy of ±0.5N at a load of 100N. The mechanical testing machine used for this testing (3365, Instron, MA, USA) was rated to a maximum load of 5kN. Before each testing regime the load cell was calibrated to a reading of 0N with the loading fixture attached but no contact between the loading fixture and specimen.

For each test the specimens were placed into the mechanical testing machine and the load fixture was lowered until a reaction force was measured by the load cell, indicating contact between the fixture and specimen. 20 preconditioning load cycles were used to allow the specimen and loading rig to settle and the results to stabilise and then six cycles were performed across which results were recorded. Between each load cycle the loading fixture returned to its initial starting location. As such the fixture and specimen were still in contact and a small compressive load, typically between 0 and 10N, remained.

3.1.3 Measurement Methods

The load and corresponding vertical displacement of the femoral head were recorded by the Instron mechanical testing machine used for this study. The load-displacement data recorded from the testing typically consisted of two regions, an initial toe-region where the increasing displacement resulted in a negligible increase in load and a linear portion once the recorded exceeded approximately 10N (Figure 3.15).

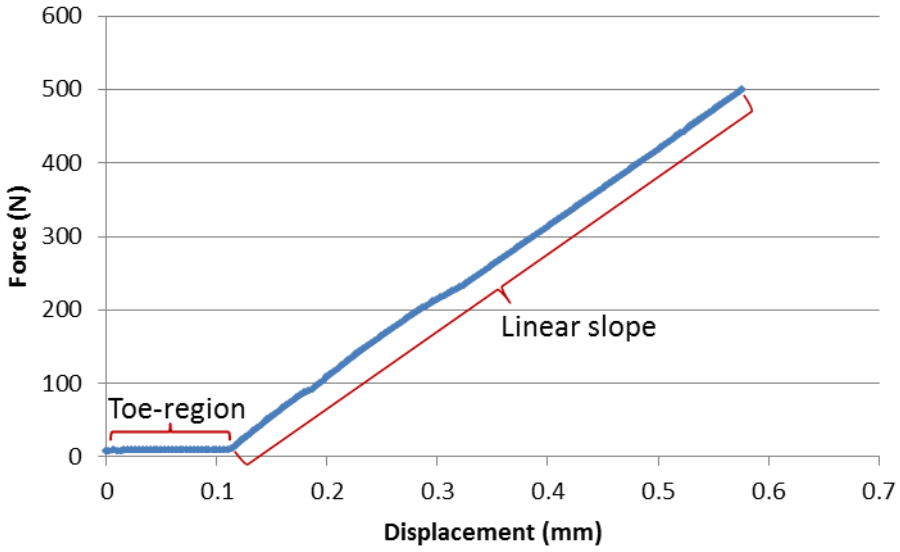

Figure 3.15 Example load-displacement data showing the initial toe-region and then the linear slope used for calculating axial stiffness.

The slope of the linear portion of the load versus displacement curve gave the construct stiffness value. In order to reliably avoid this toe-region the gradient of the load-displacement results (the axial stiffness) was calculated for the results between 50 and 500N. Axial stiffness results were then averaged across 6 load cycles.

After insertion of the cemented revision stem into the specimens, clinical x-ray images (Multix Fusion, Siemens, Erlangen, Germany) were taken through the mediolateral and anteroposterior planes to provide information on the locations of the stem and cement within the femur.

Strain gauges were placed on the medial side of the femur at 0, 40, 80 and 200mm below the lesser trochanter and on the lateral side at 200mm below the lesser trochanter as described by Mak [16] (Figure 3.11). The strain gauges were oriented in line with the long axis of the femur in order to record the long axis compression and tension resulting from mediolateral bending. The data acquisition method for recording the strain made use of a Wheatstone bridge configuration with remote sensing and a dummy gauge [174]. Null offset calibration and shunt calibration was also performed and the strain gauges used in this study (GFLA-3-50, Tokyo Sokki Kenkyujo, Tokyo, Japan) were specifically designed for use with low elastic modulus materials such as the Sawbone cortical surrogate. The strain gauges were connected to a Compact DAQ chassis (9174, National Instruments, USA)

through a Data Acquisition module in a half bridge configuration. The strain data for each gauge was recorded using the Labview Signal Express (SignalExpress Full, National Instruments, USA) software. Strain was measured once the load had reached 500N, and the displacement had therefore stopped increasing, and for each load cycle the average strain across 40 data points was calculated to account for the effect of signal noise. The average strain was then calculated across 6 load cycles.

In addition to recording the stiffness and strain of the test specimens, the relative displacement across the fracture fragments was considered important. Information on the movement in this area could then be used to evaluate the ability of the computational models to represent fracture movement, which is an important factor in fracture healing. Twelve marker points were added to the medial and anterior sides of the femurs, three 5mm above the fracture, three 10mm above the fracture, three 5mm below the fracture and three 10mm below the fracture. Two 10MP digital cameras (A3000 IS, Canon, Tokyo, Japan) were attached to the loading rig to monitor the medial and anterior sides of the fracture and images were taken before and during each of the final six load cycles. A rule was aligned beside the specimens for each camera as a reference. This resulted in two images, one before load and one at 500N, per load cycle. Measuring the relative distances between these marker points and comparing how they changed under load would then describe the movement across the fracture site. The marker points were labelled ‘a’ to ‘l’ representing their location on the specimens as shown in Figure 3.16.

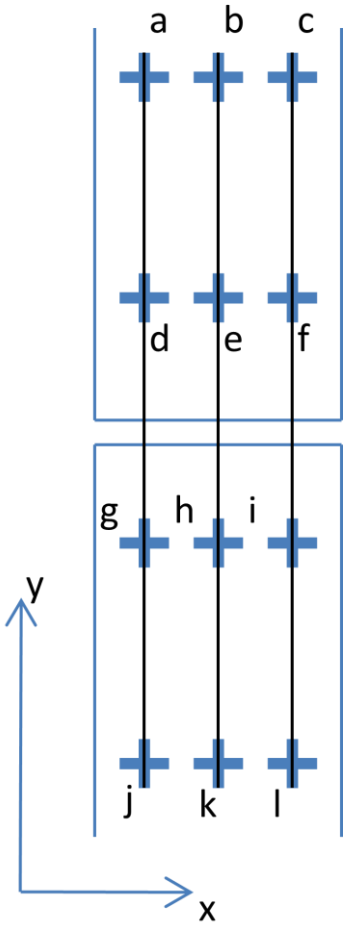

Figure 3.16 Arrangement of the fracture movement marker points on each side on the specimens.

A Matlab program was developed, as a part of this project, which opened the image file and pre-placed four lines per marker point in the appropriate areas (Figure 3.17). This Matlab script is included in the appendices (Section 9.1).

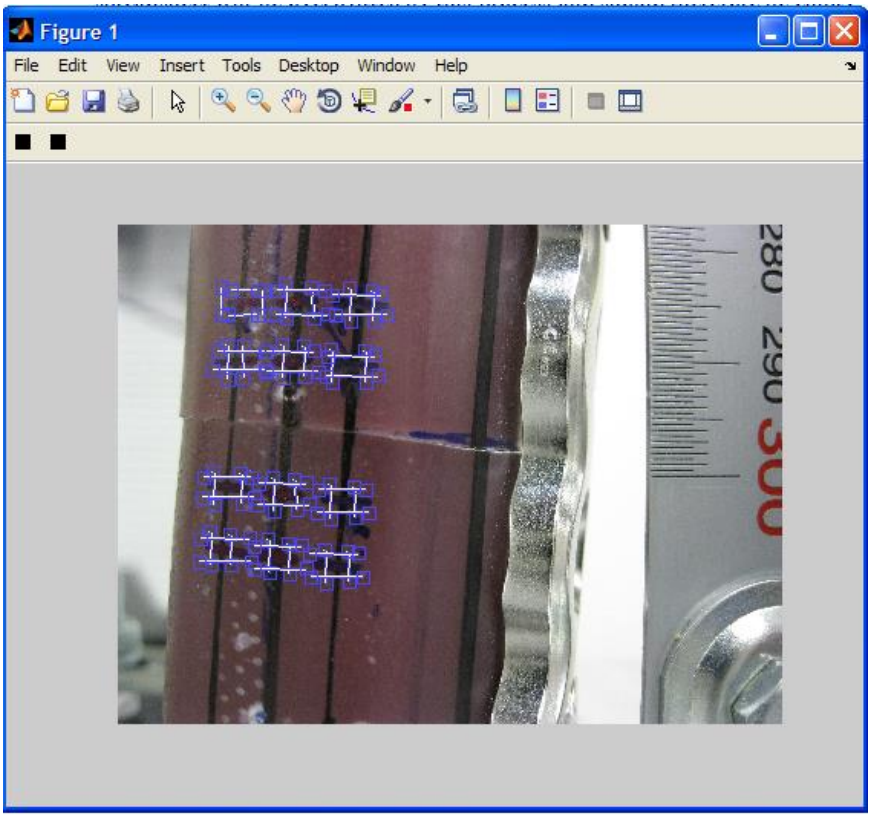

Figure 3.17 Sample fracture movement image after it has been opened by the analysis script. Lines have been pre-placed in the approximate areas of the marker points ready to be arranged by the user.

The user could then align those lines to both edges of both marker lines forming the marker point (Figure 3.18) and then click a command button. The mid-point of each marker was then calculated automatically from the four corners where the lines met. This point was shown on the image so that the user could confirm the results. The values were then exported into a results spreadsheet that was set up to calculate the final fracture movement values from this data.

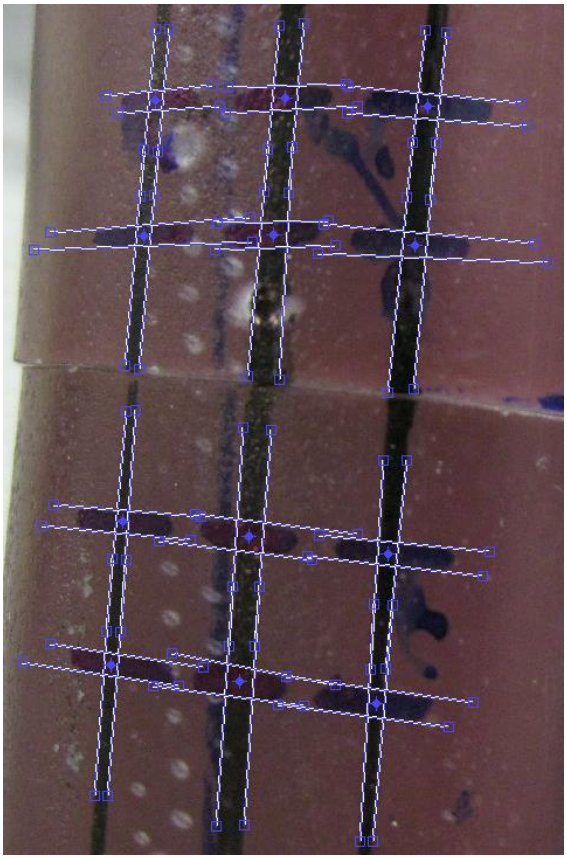

Figure 3.18 Sample image after the user has placed reference lines around each marker point and selected the command button to calculate centre points.

From testing this script, it was found that it took approximately 10 minutes to acquire all points from one image. It had been found from evaluating the script that six repeats were necessary in order to achieve a suitable level of accuracy and given the number of different cases and specimens to consider, the total time required to analyse all cases would be approximately 570 hours. In order to reduce this to a more reasonable timeframe, the analysis process and prioritisation of cases was considered. By performing the analysis on all six load cycles and averaging the results, both human error (by repeating the analysis process six times) and experimental error (by considering the different load cycles) could be accounted for. It was therefore decided that additionally repeating each image analysis six times would not be performed. A test case gave the average standard deviation in results across six repeats to be 0.0156mm (0.97 pixels) which compares favourably to the results of the original manual analysis (1.2 pixels). The standard deviation when averaging across six load cycles was found to be 0.0227mm or 1.42 pixels. Calculating and accounting for the rotation of the distal fracture fragment during loading

dramatically increased the analysis time. A test case was performed and the average change in angle of the distal fracture surface, across six load cycles and six repeats of each load cycle, was found to be 0.01° with a standard deviation of 0.06°. Due to the small angle changes experienced during loading and the negligible effect this had on the final fracture movement results, the image rotation was not considered in the analysis procedure. In addition, because the angle of each fracture fragment was no longer required, only three marker points above and below the fracture site needed to be identified and calculated (a, b, c, j, k and l). To focus the cases on those of greatest relevance, only images from the strain-gauged specimen were analysed. Although this would not allow for interspecimen differences to be compared, the strain-gauged specimen was selected due to having the stiffness value closest to the group average. The fracture movement results could then also be considered together with the strain data. These changes meant that the analyses would require approximately 120 hours which was more reasonable given the timeframe of the overall project.

The fracture movement analysis methodology and script developed here was applied in concurrent studies by Moazen et al. [20] and Mak [16].

3.2 Experimental Results

When reviewing the load-displacement data for the experimental specimens it was found that five out of the six intact specimens experienced ‘jumps’ in the load-displacement data (Figure 3.19). These jumps corresponded to points in the loading where the increasing axial displacement of the femoral head resulted in a momentary reduction in the force experienced by the load cell. These jumps were not experienced by any of the long stem revision specimens. Repeated loading cycles, such as those used to pre-condition the specimens, caused the load at which these jumps occurred to increase until the jumps no longer occurred within the 0-500N region considered in this study.

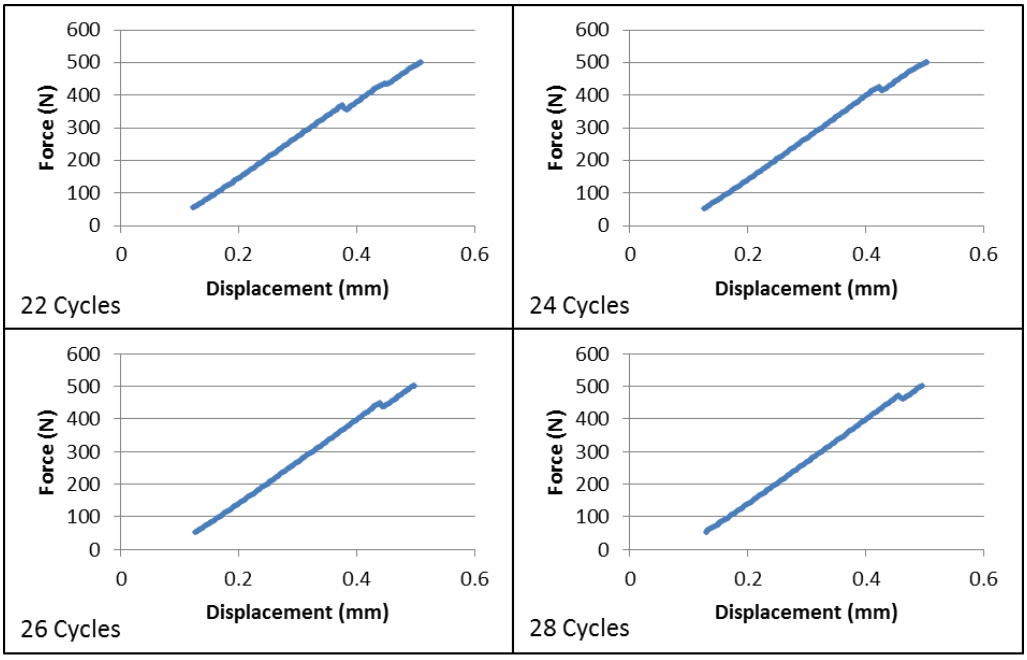

Figure 3.19 Load-displacement data for intact femur specimen S15 after 22, 24, 26 and 28 load cycles showing the momentary jumps in displacement and how they occur at a higher load after repeated load cycles.

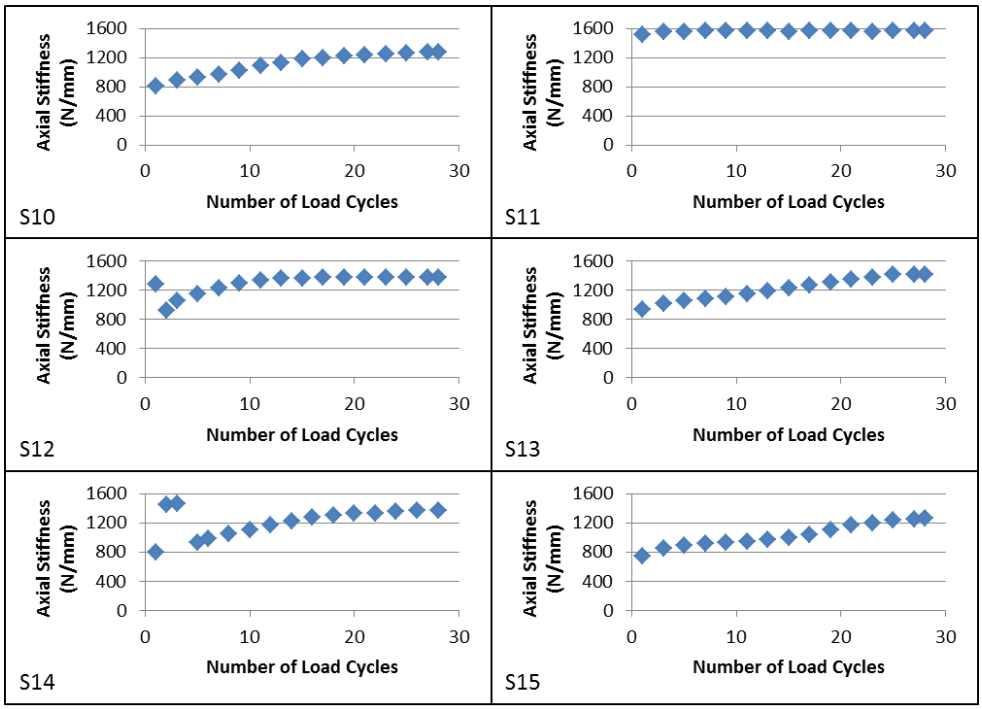

Figure 3.20 Axial stiffness results for all six intact femur specimens across all preconditioning and results gathering load cycles.

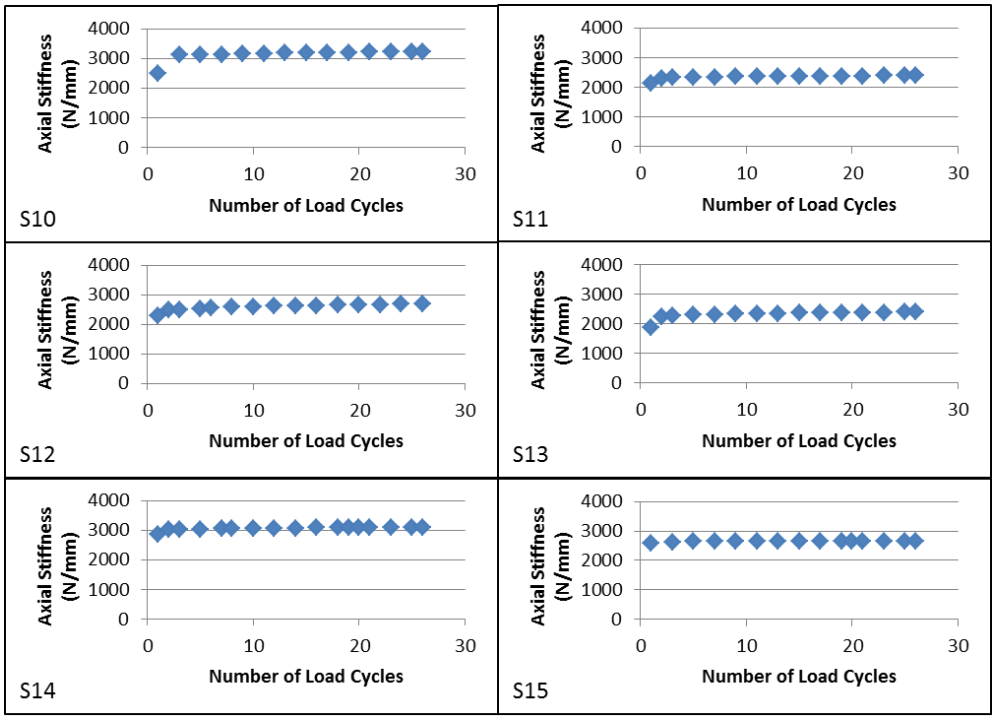

Figure 3.21 Axial stiffness for all six long stem revision PFF specimens across all preconditioning and results gathering load cycles.

For both the intact (Figure 3.20) and the long stem revision (Figure 3.21) specimens the calculated axial stiffness generally increased due to preconditioning load cycles. The axial stiffness of the specimens was found to converge after approximately 20 load cycles. The average increase in axial stiffness was 375 ± 247 N/mm (45%) for the intact femur specimens. The average increase in axial stiffness was 372 ± 244 N/mm (16%) for the long stem revision specimens. The average axial stiffness for the intact femurs at a 0° loading angle was 1363 ± 109 N/mm.

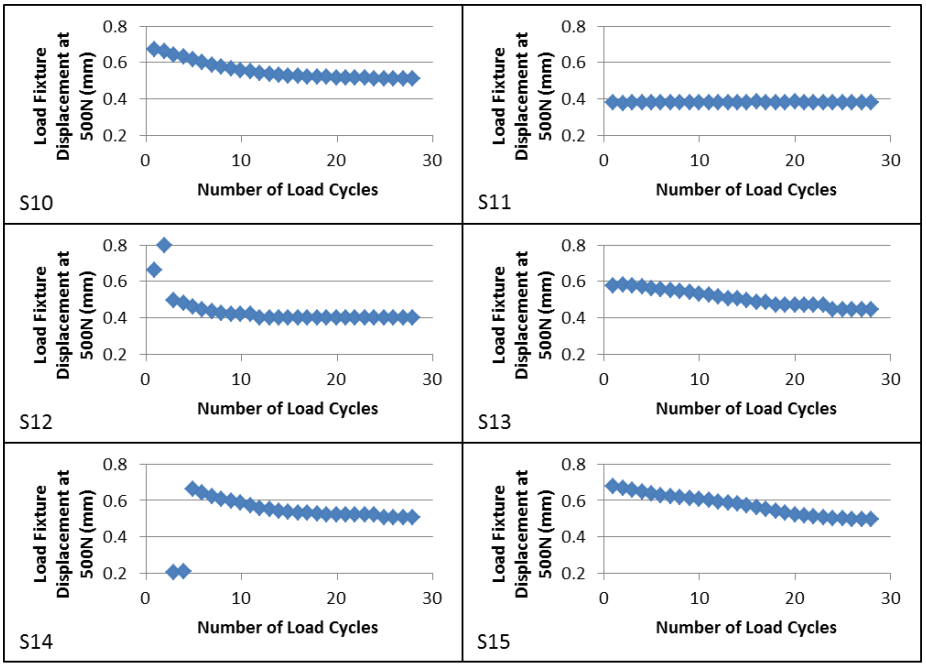

Figure 3.22 Axial displacement of the load fixture when the load reached 500N for all load cycles and all intact femur specimens.

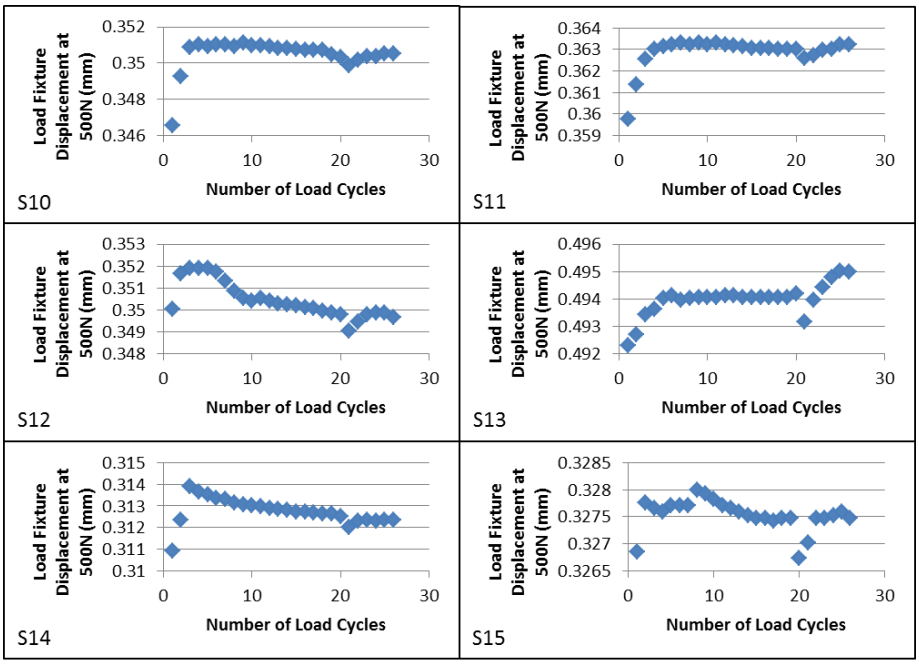

Figure 3.23 Axial displacement of the load fixture when the load reached 500N for all load cycles and all long stem revision specimens.

For the intact specimens the displacement of the femoral head when the load of 500N was reached generally reduced over the preconditioning cycles (Figure 3.22). The

intact femurs therefore had a higher axial stiffness and a lower axial displacement of the femoral head after preconditioning, as would be expected. The average decrease in the maximum displacement of the head, as recorded by the mechanical testing machine, was 0.067mm. For the long stem specimens (Figure 3.23) the change to the displacement of the femoral head at the 500N loading, across all of the preconditioning and results gathering load cycles, generally followed the trend of a relatively sharp increase in maximum displacement followed by a more gentle convergence to a final value. The average change to the maximum displacement of the head, over all preconditioning and results cycles, was however only 0.002mm. The long stem specimens therefore experienced an increasing axial stiffness as they were repeatedly loaded but without the corresponding decrease in the axial displacement of the head.

In between conducting the preconditioning load cycles and results gathering load cycles there was a short pause to change between the two regimes. This pause was estimated to be in the region of ~1 minute. The axial stiffness results for the intact (Figure 3.20) and long stem specimens (Figure 3.21) do not show any noticeable change in the behaviour of the specimens due to this pause (occurring after the 20^{th} load cycle). The axial displacement of the loading fixture at 500N for the intact femur specimens (Figure 3.22) also shows no effect of this pause between loading regimes. The axial displacement of the loading fixture at 500N for the long stem specimens (Figure 3.23) does however show that this short pause affected the results. The short pause caused a reduction in the displacement of the loading fixture when it reached 500N however this effect was counteracted by the six loading cycles used for gathering the experimental results. This reduction in maximum displacement of the loading fixture was also relatively small compared to the total displacements being measured (0.0005mm or 0.1% of the measured maximum displacements) suggesting that its effect on the results would be minimal.

During the experimental testing several specimens were tested multiple times at the same loading angle. In particular specimen S15, which had been chosen to be strain gauged, was retested to record the cortical strains. Strain was not recorded for the same specimen at the same loading angle across multiple test runs however the axial stiffness of the specimens was recorded for all tests (Figure 3.24).

Specimen	Loading Angle	Test Number	Stiffness (N/mm)	Change (N/mm)	Change/Test (N/mm/Test)
S10	0	1	3471		
	0	2	3370	-102	-102
	0	4	3226	-144	-72
S11	0	1	2795		
	0	3	2382	-412.4	-206
S12	0	1	2598		
	0	2	2647	48.9	49
	0	4	2679	32.3	16
S13	0	1	2678		
	0	3	2371	-307.2	-154
S14	0	1	3385		
	0	3	3074	-310.9	-155
S15	0	1	3096		
	0	3	2656	-440	-220
	0	5	2202	-453.8	-227
	10	2	3801		
	10	4	3175	-626	-313
	10+8	6	2615		
	10+8	9	1800	-814.1	-271
	20	7	1228		
	20	11	1029	-198.6	-50
	20+8	8	1451		
	20+8	10	867	-583.7	-292
Average					-154

Figure 3.24 Effect of repeated test runs on the recorded axial stiffness of the long stem specimens. Only repeated tests that occurred on the same specimen at the same loading angle are included. Test number indicates how many times that specimen had been tested, at any loading angle, since it was fractured and implanted.

Repeated testing of the long stem specimens appears to have resulted in a reduction in specimen axial stiffness. Only one specimen experienced an increase in axial stiffness due to repeated loading (specimen S12) and this increase was relatively small (16 to 49 N/mm/Test) compared to the reductions in axial stiffness experienced by all other specimens (-50 to -313 N/mm/Test). The average effect of one full load test on one of the long stem specimens, at any angle, was therefore a permanent axial stiffness reduction of 154 N/mm. The specimen that was most affected by this reduction in stiffness was

specimen S15 due to the repeated testing to gather strain data. Figure 3.25 compares the axial stiffness results for each loading angle, as measured from the 4th to the 8th tests performed on S15 with two different estimations. The first comparison investigates the effect of compensating for the 154 N/mm/Test reduction in axial stiffness by estimating the stiffness at each loading angle at the 4th test on specimen S15. As such the stiffness values are:

$$Axial\ Stiffness = Tested\ Axial\ Stiffness + (154 * (Test\ Number - 4))$$

The second comparison investigates the effect of compensating for this 154N/mm/Test reduction in axial stiffness by estimating the stiffness at each loading angle as if it was the 1st test on specimen S15. This comparison has the advantage of using the experimental data from the first test at each loading angle where the least damage would have been done, rather than selecting the set of loading angle tests that were most closely grouped in the testing order but the estimated stiffness reduction per tests is therefore more heavily used.

$$Axial\ Stiffness = Tested\ Axial\ Stiffness + (154 * (Test\ Number - 1))$$

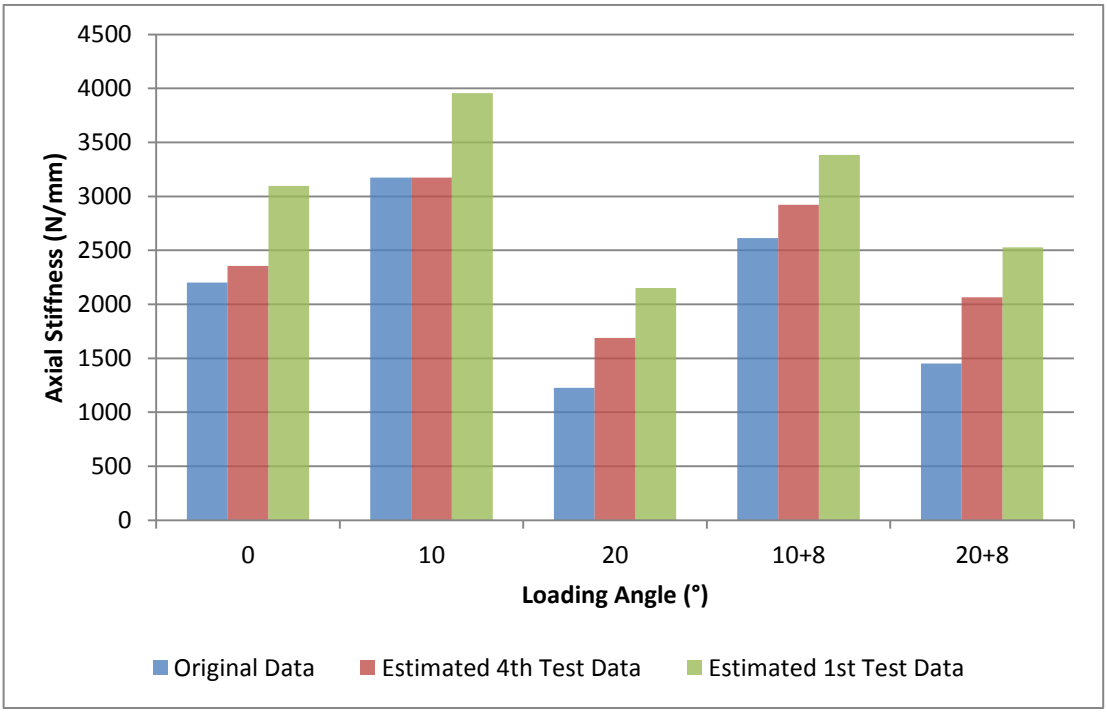

Figure 3.25 Comparison of the original axial stiffness data, across all loading angles, for long stem specimen S15 with 1) the estimated axial stiffness values for the 4th test on S15 and 2) the estimated axial stiffness values for the 1st test on S15.

The results from Figure 3.25 suggest that the overall axial stiffness of specimen S15 would have been higher had no repeated testing of specimens been performed. The relationships between the different loading angles remained consistent however. The 10° case always had the highest stiffness. The 0° case always had a higher stiffness than the 20° case. The 10+8° case was always between the 0° case and the 10° case and the 20+8° case was always between the 20° case and the 0° case.

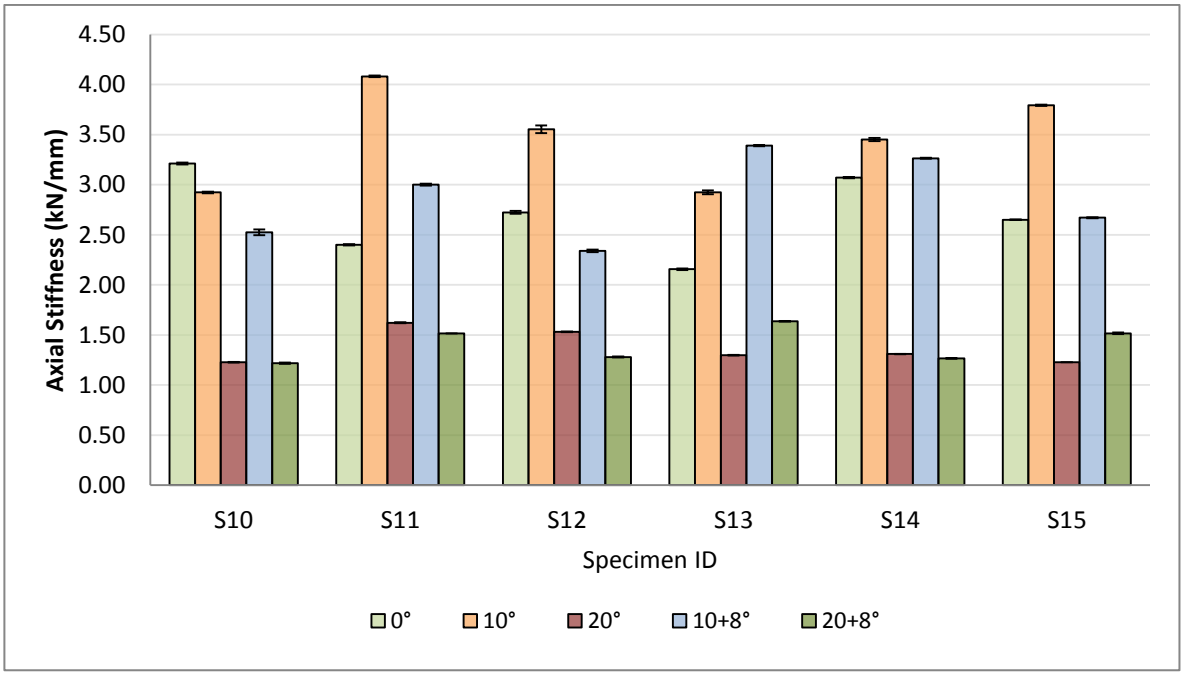

Figure 3.26 Axial stiffness results for each individual specimen at all loading angles. Error bars show ± 1standard deviation (SD) from averaging across 6 load cycles. Specimen S15 was chosen to be strain gauged.

The axial stiffness results of each individual specimen at all loading angles are given in Figure 3.26. The results for specimens S10 and S12 were taken during test numbers 3 to 7. The results for specimens S11, S13 and S14 were taken during test numbers 2 to 6. The results for specimen S15 were taken during test numbers 2, 3, 6, 7 and 8. The standard deviation, which represents the stiffness variations from the final six loading cycles averaged to give each value, is shown to be small suggesting that once suitably preconditioned the specimens were behaving elastically and reliably under testing without noticeable damage occurring between individual cycles.

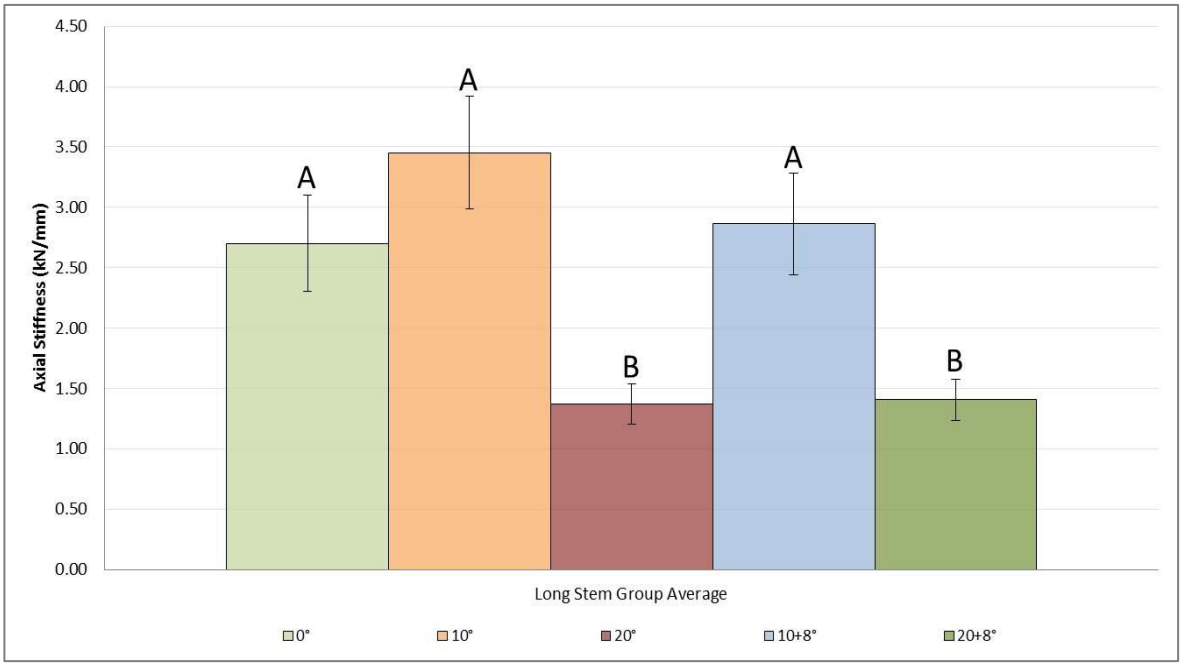

Figure 3.27 Axial stiffness results for the averaged long stem group at all loading angles. Error bars show ± 1 standard deviation (SD) from averaging across all experimental specimens (n=6). Different letters indicate statistically significant differences (ANOVA $p<0.05$, Bonferroni post hoc).

The axial stiffness values for each loading angle as an average of all the experimental specimens are given in Figure 3.27. A much larger standard deviation can be seen, representing the inter-specimen variations. No statistically significant difference (ANOVA $p < 0.05$, Bonferroni post hoc) between the 0°, 10° and 10+8° cases or the 20 and 20+8° cases was found. Significant differences were found however between the 0°, 10° and 10+8° cases compared to the 20° and 20+8° cases (ANOVA $p < 0.05$, Bonferroni post hoc).

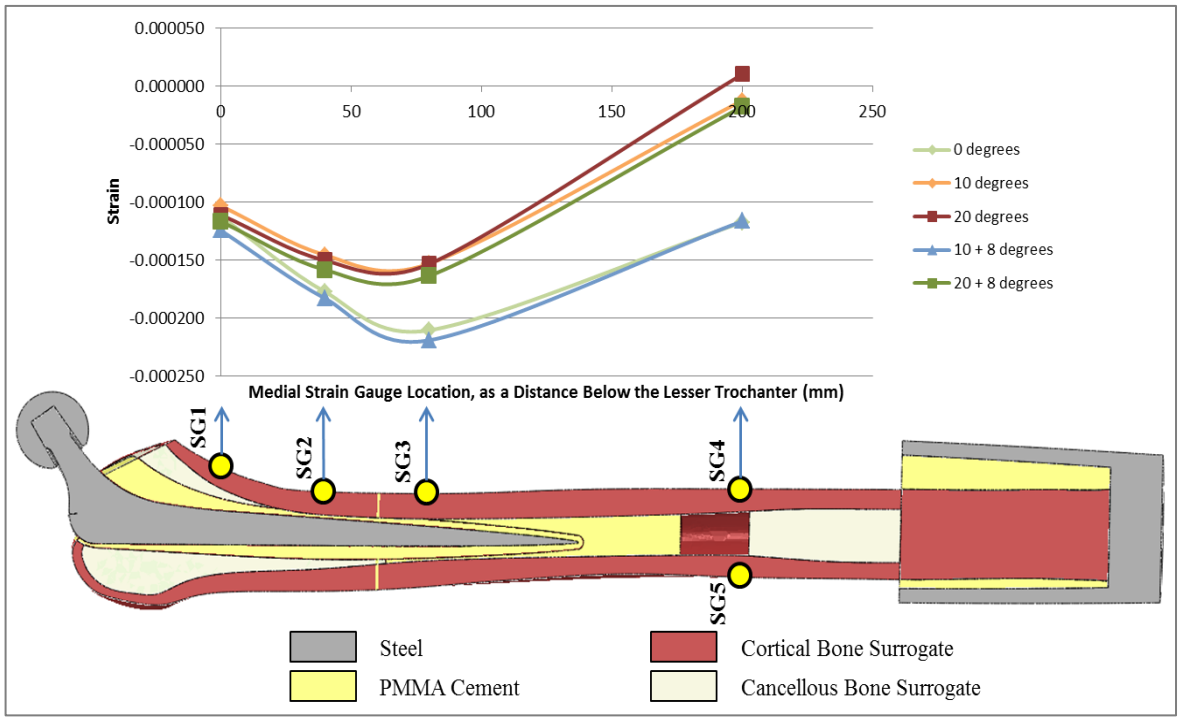

Figure 3.28 Strain results at 4 points along the medial cortex, relating to strain gauges 1-4, of specimen S15. Cross-section of femur showing gauge location, fracture location (60mm below lesser trochanter) and internal configuration.

The strain results for the medial cortex of specimen S15 at all loading angles are given in Figure 3.28. Once again the results can be divided into two distinct groups however these groups do not line up with those from the stiffness changes. The 10°, 20° and 20+8° cases experienced a similar strain distribution, with the highest strains proximally, peaking around the fracture site, and a reduction to almost zero strain at gauge 4. When loaded at 0° and 10+8° the specimens experienced a similar but more extreme pattern, the compressive strains around the fracture site were approximately 27% higher and at gauge 4 the strain was approximately 110μstrain higher and compressive.

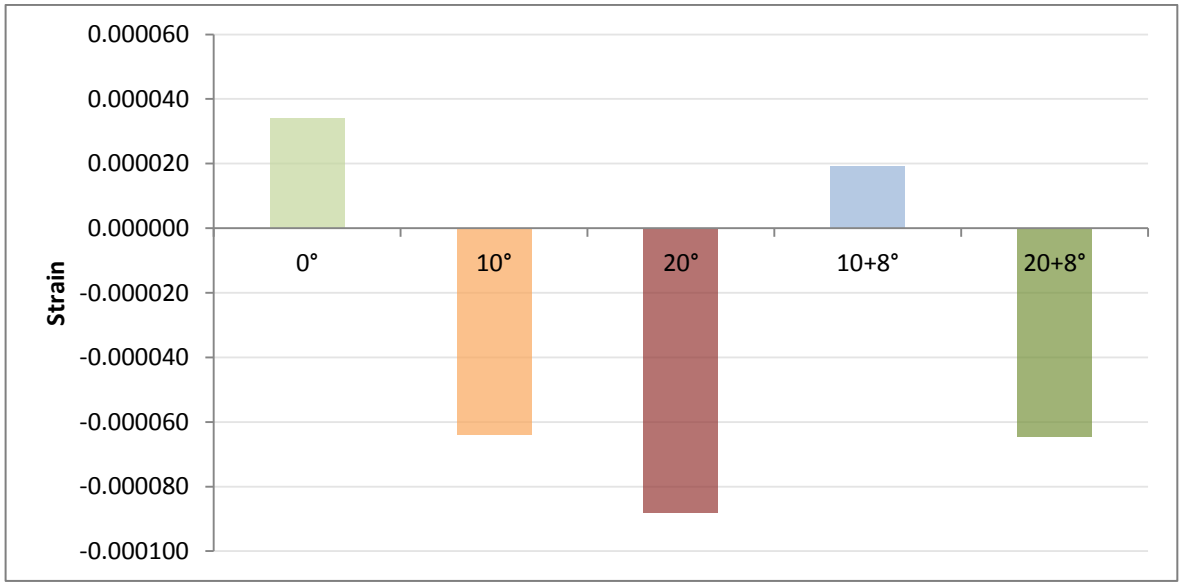

Figure 3.29 Distal lateral strain, 200mm below the lesser trochanter, measured at gauge 5 for all loading angles on specimen S15.

The strain at the distal lateral side of specimen S15 is given in Figure 3.29. The strain at this location displayed the same trends as the corresponding medial strain (gauge 4) but in the opposite direction. The 0° and 10+8° loading angles caused tension on the lateral side. The 20° and 20+8° loading angles, where the medial strain approached 0 at this location, induced noticeable compression laterally.

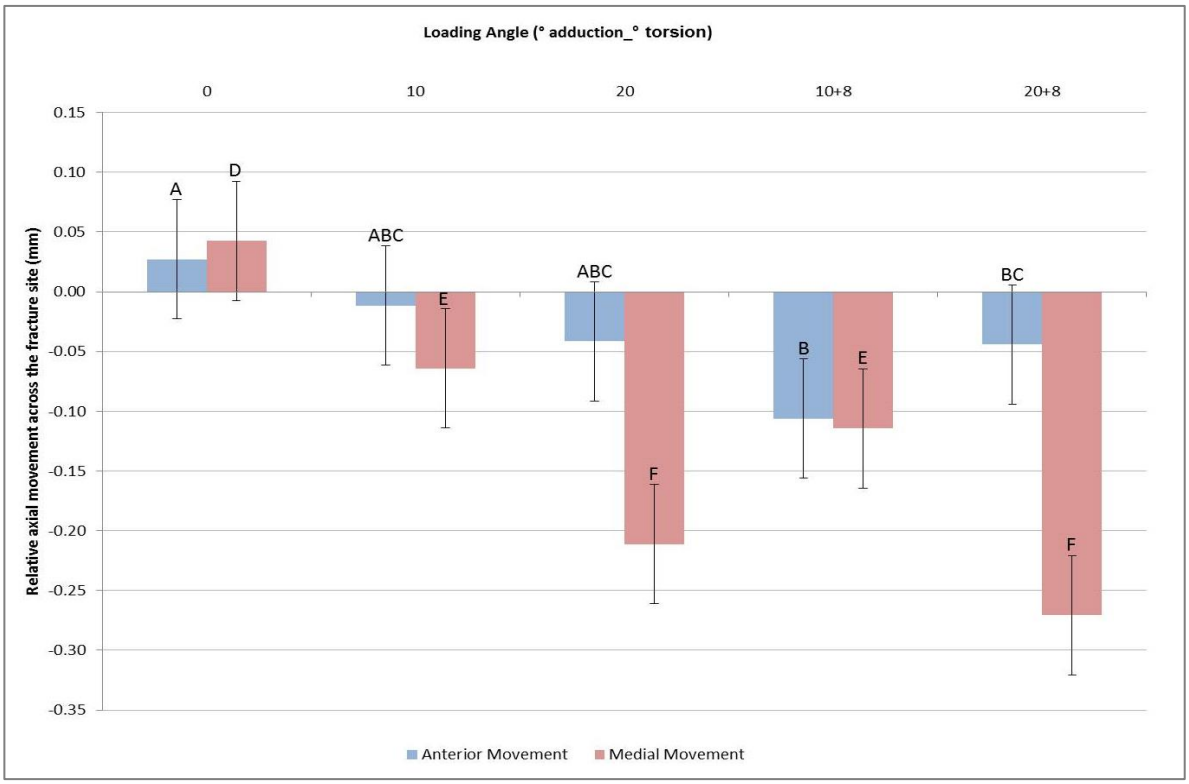

Figure 3.30 Relative axial movement between the proximal and distal fracture fragments across the fracture site from the anterior and medial sides of specimen S15. Error bars represent ±1 standard deviation from the mean after averaging the results of the fracture movement analysis. Statistically significant differences are shown by different letters (ANOVA $p<0.05$, Bonferroni post hoc).

The relative axial fracture movement on the medial and anterior sides of specimen S15 under all loading orientations is given in Figure 3.30. Negative values indicate that the medial or anterior side of the fracture site is in compression while positive values indicate that the medial of anterior side of the fracture site is in tension. The results were averaged across six load cycles, the values for each one calculated using the fracture movement analysis method described in section 2.1.3. The error bars therefore represent the variation due to human error in processing the fracture movement images and the experimental variation between load cycles. The magnitude of these standard deviations compared to the small micromovements being measured makes identifying significant differences between loading angles difficult, particularly on the anterior side where the recorded movements are smaller. Adduction angle did however have a statistically significant effect on the fracture movement. Medial fracture movement can be shown to sit in the approximate range of 0.05mm – 0.30mm.

3.3 Discussion

The results of the intact femur test are compared against other, similar, results from the literature in Table 3.1.

Table 3.1 Summary of published axial stiffness results for intact synthetic femur specimens.

Author/Ref.	Specimen Generation	Adduction Angle (°)	Axial Stiffness (kN/mm)
Mak [16]	4th	0	1.49
This study	4th	0	1.36
Mak [16]	4th	10	1.98
Heiner [135]	4th	11	1.86
Cristofolini et al [14]	2nd	11	1.36
Heiner [135]	3rd	11	1.47
Zdero et al [138]	4th	15	1.74
Mak [16]	4th	20	0.87

The intact femur axial stiffness recorded in this study agrees well with that published by Mak [16] at the same angle of adduction, with only a 0.13 kN/mm difference between the two studies. Heiner [135] performed a comparison of the axial stiffness, at the same loading angle, of the 3rd and 4th generation Sawbone femurs. The axial stiffness of the 4th generation femurs was reported as being 27% higher than that of the earlier generation and this lines up with the relatively low axial stiffness reported by Cristofolini et al [14] using the 2nd generation specimens. It would therefore be expected that the specimens from

this study, if they had been tested at an adduction angle of 10-11°, would have behaved more like the specimens of Mak [16] and the 4th generation specimens of Heiner [135]. Based on the study by Zdero et al [138] the axial stiffness of the specimens at an adduction angle of 15° would be expected to be similar to that of 10-11°. One noteworthy difference between the studies however was that the study by Zdero et al [138] used a steel loading cup to proximally constrain the movement of the femoral head in the transverse plane. Mak [16] loaded the intact specimens using a flat steel plate, against which the femoral head could slide. Heiner [135] used a ball joint and x-y table which would have provided less resistance to transverse movement than a steel conforming cup. Reducing the ability of the femoral head to displace under load may have resulted in a higher recorded stiffness which makes it difficult to compare these studies. Considering the results from these different studies the experimental methodology presented here seems to provide a similar approximation for the behaviour of an intact femur specimen under loading. A review of the literature could find no currently available studies that recorded the axial stiffness of a synthetic femur implanted with a cemented long revision stem, with or without a periprosthetic femoral fracture.

Small jumps were recorded in the load-displacement data for the intact femur specimens but not for the long stem specimens. Typically this behaviour would be expected due to the bedding in of interference fits between components, permanent damage to, or failure of, the specimens or slipping at interfaces. There was no evidence to suggest that sufficient damage was occurring to cause such as effect and this would not explain the jumps occurring at higher loads after reloading. The only area where bedding in would be likely was the base of the specimens where they were fitted into the loading pots and if this was the source of the displacements it would be expected to occur in the long stem specimens as well. The only interface in the intact specimens at which slipping would have been likely was the contact between the flat steel load plate and the femoral head. These jumps may therefore have been the result of friction between these two components which reduced as they continued to move against each other.

The axial stiffness at the 0° loading angle was approximately 75% of the axial stiffness at the 10° loading angle. The axial stiffness at 20° was approximately 50% of the axial stiffness at 10°. There was therefore a significant enough difference between the adduction load angles for them to be used to validate matching FE models. There was no

significant difference in the stiffness results due to the addition of torsion and as such these results would not be as useful for validating FE models. A larger angle of internal rotation may have yielded larger differences but would have also necessitated additional measurements in the anteroposterior plane due to increased bending.

The 0° case caused the largest compressive medial strains, particularly towards the base of the femur, which indicates C-bend style deformation in the medial direction. The 10° case caused the medial strain to approach zero towards the base of the femur, suggesting an S-bend style deformation in the mediolateral plane. The 20° case caused the medial strain to enter tension towards the base of the femur, suggesting movement towards a C-bend in the lateral direction. These different bending modes are illustrated in Figure 3.31. In addition the lack of recorded strain-shielding on the medial side of the specimens immediately proximal and distal to the fracture site suggests that there was compressive load transfer through the medial side of the fracture.

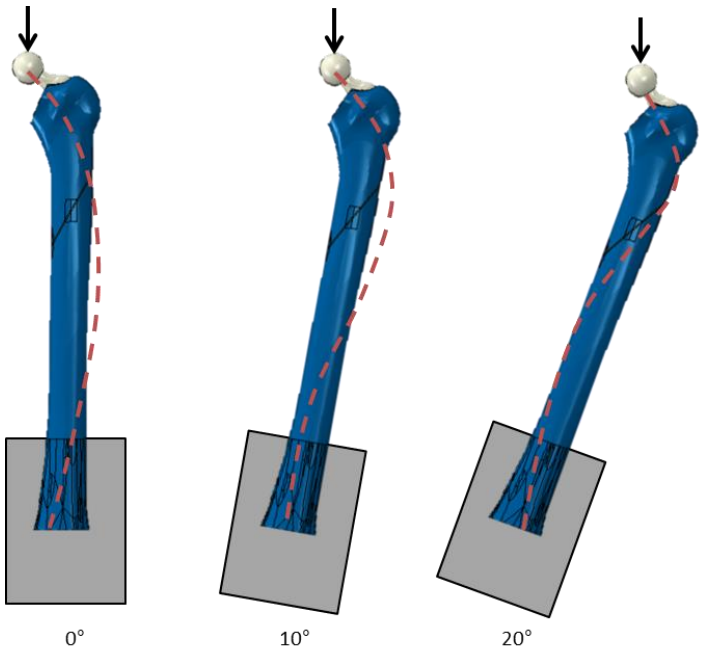

Figure 3.31 Illustration describing how the different loading angles may have affected the bending mode of the specimens. Red dashed lines show simplified estimates of the bending deformations.

The axial fracture movements on the anterior side of the fracture were smaller than those on the medial side of the fracture. This suggests that the majority of the bending was occurring in the mediolateral plane where we had focused the majority of our

measurements. The fracture movement on the medial side was sensitive to the adduction angle of the femur, suggesting that it may be a suitable measure against which to compare FE models. The usefulness of the fracture movement data was limited by the large standard deviations resulting from processing of the digital images. Fracture movement measurement techniques for cemented long stem revision specimens should be selected to be accurate for measurements in the region of 0.02mm and data processing techniques should be reliably and robustly automated to reduce the effects of human error.

There were relatively small intra-specimen stiffness variations, suggesting that the experimental set up was reliable and repeatable. The inter-specimen variation between the intact femur specimens was larger but still relatively small (0.12 kN/mm) suggesting that the synthetic femurs and the process for aligning and potting them in PMMA cement was also relatively similar and repeatable between specimens. The inter-specimen variation between the long stem specimens was larger (0.4 kN/mm). This suggests that the majority of the inter-specimen variation that led to differences in axial stiffness resulted from the process of implanting a femoral stem and/or treating the fracture. This also suggests that it would be unreasonable to compare different cases using a single implanted and/or fractured specimen. Averaging results across multiple specimens is therefore required unless there is evidence to suggest that the single specimen would be representative of a larger group.

The material properties of the synthetic femurs appeared to be slightly time dependent, requiring pre-conditioning cycles before each loading test. This time dependent effect resulted in an increase in specimen axial stiffness for the intact femurs but no notable plastic deformation. The implanted femurs displayed a different pattern, whereby the stiffness increased over initial pre-conditioning in a similar way but a measureable increase in axial deformation occurred as well. This implies that between load cycles the specimens were not returning to their original unloaded position which might be due to semi-permanent displacements such as the closing of gaps between components or the inclusion of a material with a slower load recovery time. The specimens appeared to recover, to a small degree, between the preconditioning loading regime and the results gathering regime. This may support the suggestion that the increased axial deformation was due to a material with time-dependent properties where it did not have time to properly unload between load cycles but could do so between loading regimes. The specific material properties (viscoelastic, viscoplastic, hysteresis, etc.) that caused this effect could not however be

determined from the data available. Zdero et al [138] investigated the effect of different loading rates on 4th generation synthetic femurs and found that although there was a correlation between loading rate and axial stiffness the effect was not sufficient enough to affect the results of a biomechanical study such as this one.

A small reduction in axial stiffness may have occurred due to each loading test. This small reduction (154 N/mm/Test) suggests that the axial stiffness reported from repeated testing may underestimate the actual first test values. This reduction did not appear to alter the trends regarding the effect of loading angle that were shown in the stiffness results and as such these results are still suitable for FE comparisons. The actual mechanism that led to this reduction could not be identified from the axial stiffness data alone however and therefore the effect this might have had on the strain results cannot be determined. This stiffness reduction was not reported by Mak [16] during three repeated testing sessions using the same intact femur specimen and an identical testing methodology which may suggest that it is related to a change made to the specimens when simulating and treating a fracture. This decreasing axial stiffness could be the result of damage to the distal cement at the base of the femur, particularly where it is held into the loading pot by screws, as this might be a focus point for high cement stresses. It could be related to damage to the cement interspersed into the fracture site during stem fixation as again this cement may be subjected to relatively high strains. It could be due to damage occurring between interfaces in the specimens, for example between the stem and cement, the cement and cortical surrogate or the cement and cancellous surrogate. Finally it could be due to biomechanical changes that led to different, possibly larger, localised stresses in the synthetic femur materials that weakened the specimens but were not present in the intact models. It is possible that the stiffness reduction was related to the time-dependent response of the long stem specimens to cyclic loading however further investigation would be required to demonstrate this. Chong et al. [175] evaluated the fracture toughness and fatigue crack propagation rate performance of the materials for 4th generation synthetic femurs against those used in the 3rd generation femurs. They found that the performance of the 4th generation surrogate materials was improved compared to the 3rd generation materials, with a 48% increase in fracture toughness and a 31% reduction in fatigue crack propagation rate. In another study Chong et al [143] evaluated the overall fatigue resistance of the 4th generation synthetic femurs by comparing the cycles to failure and changes to actuator

deflection over repeated high activity loading. The specimens they used were implanted with an Exeter polished, tapered cemented total hip arthroplasty stem, similar but shorter to the ones used in this study. Small changes to the actuator deflection during loading were recorded in the region of ±10-15% of the original values. The authors suggested that changes to the actuator deflection during repeated loading could be indicators of crack formation or implant subsidence. None of the 4th generation specimens they tested failed within 10 million cycles, implying that crack formation was an unlikely cause for the changes in actuator deflection, particularly given the resistance of the 4th generation materials to fracturing. Implant subsidence may therefore have been responsible. A common method for reducing the effect that accumulated damage may have on experimental specimens is to randomise or alter the test order between the specimens [138]. Given the results of this study it would be recommended to apply this practice to studies using synthetic specimens as well to mitigate this potential issue.

3.4 Conclusions

Adduction angle had a statistically significant effect on the axial stiffness and fracture movement, suggesting that it will be a suitable measure by which to compare the validity of FE models. The strain results suggest that these differences occurred, at least in part, due to changes in the bending mode of the specimens at the different angles. An internal rotation angle of 8° was not sufficient to cause statistically significant differences between cases. A larger angle of rotation would therefore be recommended for studies aiming to use the results for FE model validation.

Synthetic femur models are generally reported to have consistent, repeatable material properties during testing [135] and to have a linear elastic response to axial loads in the region of 500N [10, 132]. The results of this study suggest that this may not be the case. Intact femur models require preconditioning load cycles before the axial stiffness results converge. Cemented long revision stem specimens with a fracture also require this preconditioning for the same reason. They also however appeared to experience some degree of time-dependant or plastic deformation as a result of repeated load cycles. More extensive displacement measurements, particularly investigating the overall bending of the

specimens, the movement of the fracture site and any relative motion between the stem and femur, would be recommended to identify the causes for this. There also appeared to be a reduction in axial stiffness each time a specimen was tested. Implanted synthetic femur specimens should therefore not be tested across different cases in the same order. Any changes in the response of the specimens due to repeated loading can then be accounted for when averaging the results across all specimens. The relatively large inter-specimen variation in axial stiffness between the long stem specimens suggests that a single synthetic femur specimen is not sufficient for a biomechanical study and that averaging the results across multiple specimens is required.

4. Long Stem Fixation FE Model Development and Validation

This chapter introduces the development and validation of a 3D, computational, finite element model to mimic the experimental specimens developed and tested in Chapter 3. The models are described and results are presented for a baseline model as well as a range of sensitivity tests investigating different model variables. The applicability and limitations of the models are then discussed.

The aim of the work in this chapter was to develop a finite element model of cemented long stem PFF fixation that replicated the biomechanical behaviour of the experimental specimens when loaded. Although close numerical agreement between the experimental and computational results would be ideal the most important factors were therefore:

1. Whether the trends in the deformation behaviour between different cases were replicated.
2. Whether the computational models were sensitive enough to the different cases that changes to the response of the model could be identified, beyond numerical error, and understood on a biomechanical level.

4.1 Motivation

Before computational models can be used to investigate clinically relevant cases the reliability, accuracy and limitations of those computational models must be evaluated [176-178]. Verification of the model involves investigating possible numerical issues whereby the equations that govern the behaviour of the model are not being solved correctly or with sufficient accuracy [176, 179, 180]. When using established commercial finite element packages, which have been extensively tested and evaluated, this typically takes the form of a mesh convergence study [181]. This type of study compares the effect of different element sizes and types on the results to ensure that they are not being adversely affected by insufficient discretisation of the components. It can also be used to optimise the analysis time of the models. Increasing the number of nodes, and therefore degrees of freedom, in a model generally increases the analysis time so to reduce run times the model should be

meshed with the minimum number of nodes that still achieve suitably accurate results. In this study, mesh sensitivity was performed in order to produce the most realistic model possible within the constraints of the available computational resources.

Validation is used to show that the model represents the case that it is attempting to replicate [176, 179, 180]. Many assumptions and simplifications are made when producing an FE model and these will all change how it behaves. A model can be verified, in that the mesh is converged and there are no numerical issues with the results, but the scenario it is correctly analysing may not correspond to the one it is intended to test. Validation is typically performed by comparing the results from the computational model against one or more additional sources of data [176, 178]. These can be comparable experimental data, though the assumptions in both studies then have to be kept in mind and experimental error can make direct comparisons difficult [177], theoretical data from other numerical simulations such as beam bending theory [182], although the applicability of these will depend on the case being considered, or clinical data, although the limited information these typically provide can make linking cases and outcomes difficult [178, 181]. For this study, the FE models were compared to the corresponding experimental data from Chapter 3.

Sensitivity testing is used to identify how sensitive the results of the model are to different variables [176-178]. Variables that have a large effect on the results of the simulation need to be accurately represented in order to produce an accurate model [182, 183]. Variables which have a small effect on the results can perhaps be modelled using more assumptions and simplifications to save time or avoid additional experimental testing [181]. The outcomes of these tests can also be related to clinical practice; understanding what effect a particular variable has on the model, for example bone material properties, can be related to the effect that the same variable may have clinically. The sensitivity of the results to that variable will show how drastic those changes then might be. Finally, the sensitivity results can be related back to experimental testing [177]. Identifying which factors have the greatest effect on the results shows which factors should be matched most closely to the clinical scenario to produce the most representative simulations. Understanding which factors change the results the most can help identify key sources of error between an experimental set up and clinical practice and therefore recommend routes

for improvement. In this study, sensitivity tests were undertaken on the major model variables by comparison against a baseline case.

The development of the long stem fixation finite element model, along with the verification, validation and sensitivity test methods and results are presented in the following chapter.

4.2 FE Methods

4.2.1 Geometry

The finite element analysis (FEA) software Abaqus (Dassault Systèmes, USA) was used to construct and solve all the computational models in this study. The femur geometry was acquired as a three-dimensional computer aided design (CAD) model from Biomed Town (BEL repository) [184] which included both the cortical shell and cancellous surrogate. The CAD model had been developed based on CT scans of a 3rd generation synthetic femur [166]; however the geometry of the synthetic femurs was not altered between the 3rd and 4th generation models. The long stem and femoral head geometry was provided by CAD file from Stryker (Stryker SA, Switzerland). The femur model was cut and virtually potted in cement to match the experimental set up. A steel pot and screws were created in Abaqus to represent the loading rig used in the experiments.

The locations for the femoral neck cut, fracture and revision stem were identified from the experimental specimens. This was done using measurements from the specimens themselves (Figure 4.1) and from x-ray images (Multix Fusion, Siemens, Erlangen, Germany) taken in the anteroposterior and medioloateral planes. These x-ray images showed the internal location of the stem and cement mantle (Figure 4.2).

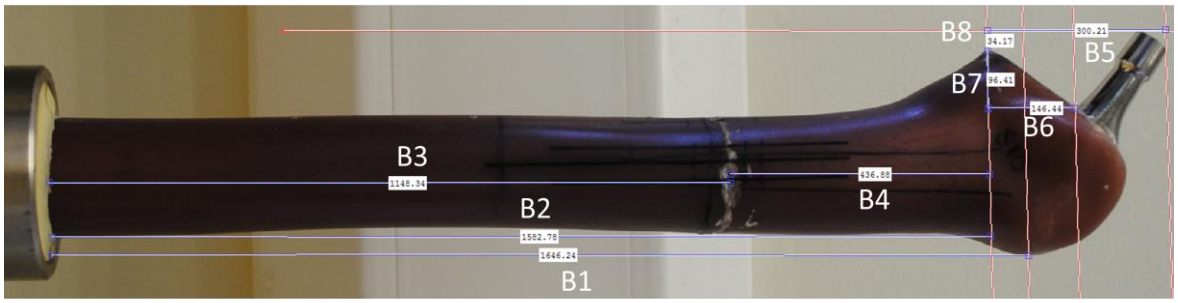

Figure 4.1 Example of measurements taken from the experimental specimens to locate the neck cut, fracture and stem.

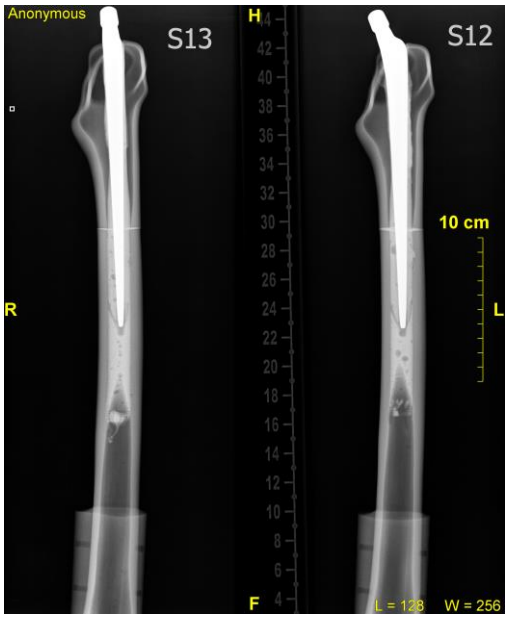

Figure 4.2 X-ray image of the experimental specimens from which the internal location of the stem and cement was identified.

A 3-dimensional geometry for the cement mantle was created using information from the x-ray images of the experimental specimens in a similar manner to that described by Stolk et al. [139]. The distribution of the cement around the stem was measured in both the anteroposterior and mediolateral planes. This information was used to produce two cross-sectional profiles for the cement mantle, one for each plane (Figure 4.3, Left, Middle). These two profiles were then combined to produce one 3D geometry and the edges were smoothed based on the geometry of the stem-shaped surgical reamers (Figure 4.3, Right). This methodology resulted in a geometry that was based on information in only two planes, which therefore would not capture the full variation in cement mantle geometry around the stem. The profile of the stem itself was relatively constant in the anteroposterior direction,

with flat sides on the anterior and posterior faces of the stem, and could therefore, apart from the rounding of edges, be described using only information in these two planes. The space into which the stem was inserted, and into which the cement was shaped, was created using reamers that were an oversized version of this stem. As such the geometry of the cement is likely to be related to the geometry of the stem and could be predominantly described by information in the anteroposterior and mediolateral planes. An alternate method of developing a cement mantle geometry was investigated in a related study [19]. In that study the cement mantle around a normal length femoral stem was measured by performing a CT scan of a reamed experimental specimen. The CT scan data was segmented and a 3D geometry for a cement mantle was developed from the resulting cavity that was created during the reaming process. Although this process potentially produced a more realistic mantle it proved to be a highly time-intensive task. The results also still required manual modifications to deal with segmentation errors and simplifications before they could be implanted into the femur finite element model. As such a simplified approach was selected for this study.

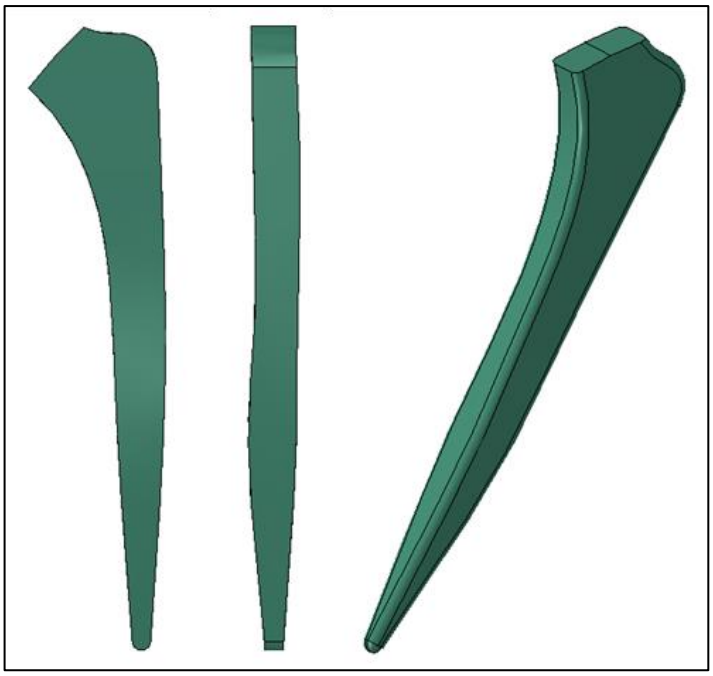

Figure 4.3 Left: Cement mantle profile in the mediolateral plane. Middle: Profile in the anteroposterior plane. Right: Final 3D cement mantle geometry with edges rounded.

The final 3D model geometry is shown in Figure 4.4.

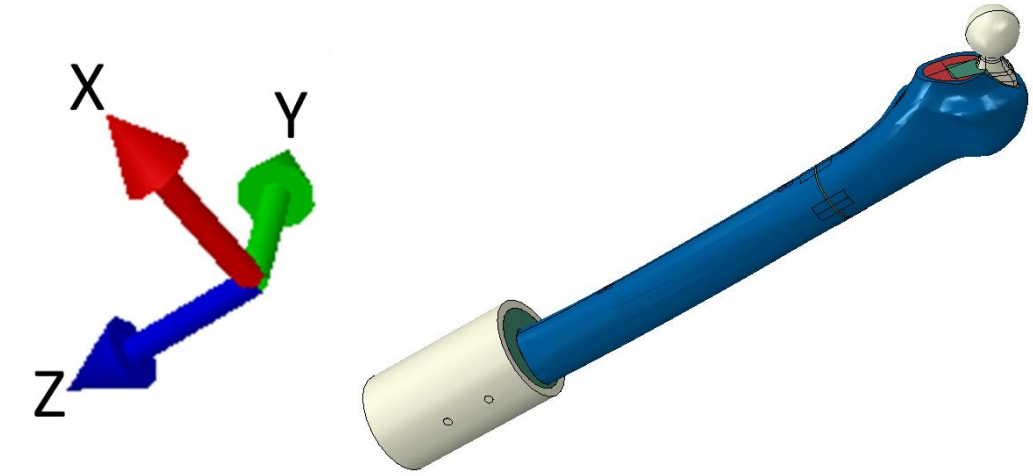

Figure 4.4 The 3D geometry of the finite element model, with global coordinate system specified. The x-axis is positive in the medial direction, the y-axis is positive in the posterior direction and the z-axis is positive in the inferior direction.

4.2.2 Material Properties

The baseline material properties representing stainless steel that were applied to the long revision stem and femoral head were E=200GPa and ν=0.3 [185]. For PMMA cement E=2.45GPa and ν=0.3 were used [186-189]. For the cortical bone surrogate values of E=16.7GPa and ν=0.3 were used [108, 175]. Properties used for the cancellous bone surrogate foam were E=0.155GPa and ν=0.3 [108].

Table 4.1 List of material property sensitivity cases.

Case	Description
0	Baseline model. Cement E = 2.45GPa. Cortex E = 16.7GPa. Cancellous E = 0.155GPa.
1	Baseline with cement E = 1.225GPa.
2	Baseline with cortex E = 10GPa.
3	Baseline with cortical E = transverse orthotropic (compressive E = 16.7GPa, transverse E = 10GPa).
4	Baseline with cancellous bone E = 2.45GPa.

The baseline settings and material property sensitivity cases are described in Table 4.1. The effect of halving the Young's modulus of the cement investigated in Case 1. This was due to the fact that the properties of cement can vary due to the mixing technique and porosity [190-192]. The manufacturer specified material properties for the cortical surrogate [108] described a notable difference between the Young's Modulus in the transverse and longitudinal directions ($E_{transverse}$=10GPa, $E_{longitudinal}$=16.7GPa). An investigation was therefore performed to test the effect of lowered (Case 2) and transverse orthotropic (Case 3) material properties. Case 2 considered an isotropic cortex with E=10GPa, representing a 'worst case scenario' model, and Case 3 considered a model with different elastic modulus values applied in the longitudinal and transverse directions (16.7 and 10GPa, respectively). Mechanical testing of the cortical surrogate used in 4th generation synthetic femurs has suggested that the longitudinal Young's modulus of the material may be closer to the reported transverse Young's modulus [193]. Case 2 therefore also considers the effect that this may have had on the response of the overall structure. During the stem implantation the clinicians performing the procedure commented that the cancellous surrogate required more effort to drill, chisel and ream through than they would typically expect in surgery. Consequently Case 4 was developed where the Young's modulus was increased to 2450MPa which matches that used for the cement. This considered a scenario where the cancellous surrogate had a far greater mechanical stiffness than normal cancellous bone. It also considered a scenario where the cancellous bone had been entirely replaced with surgical cement, either due to excessive reaming by the surgeon or because of extreme cancellous bone loss in the patient.

4.2.3 Interactions

The different interfaces and interactions from the computational model are listed in Table 4.2. These interfaces are also shown visually in Figures 4.5-4.7.

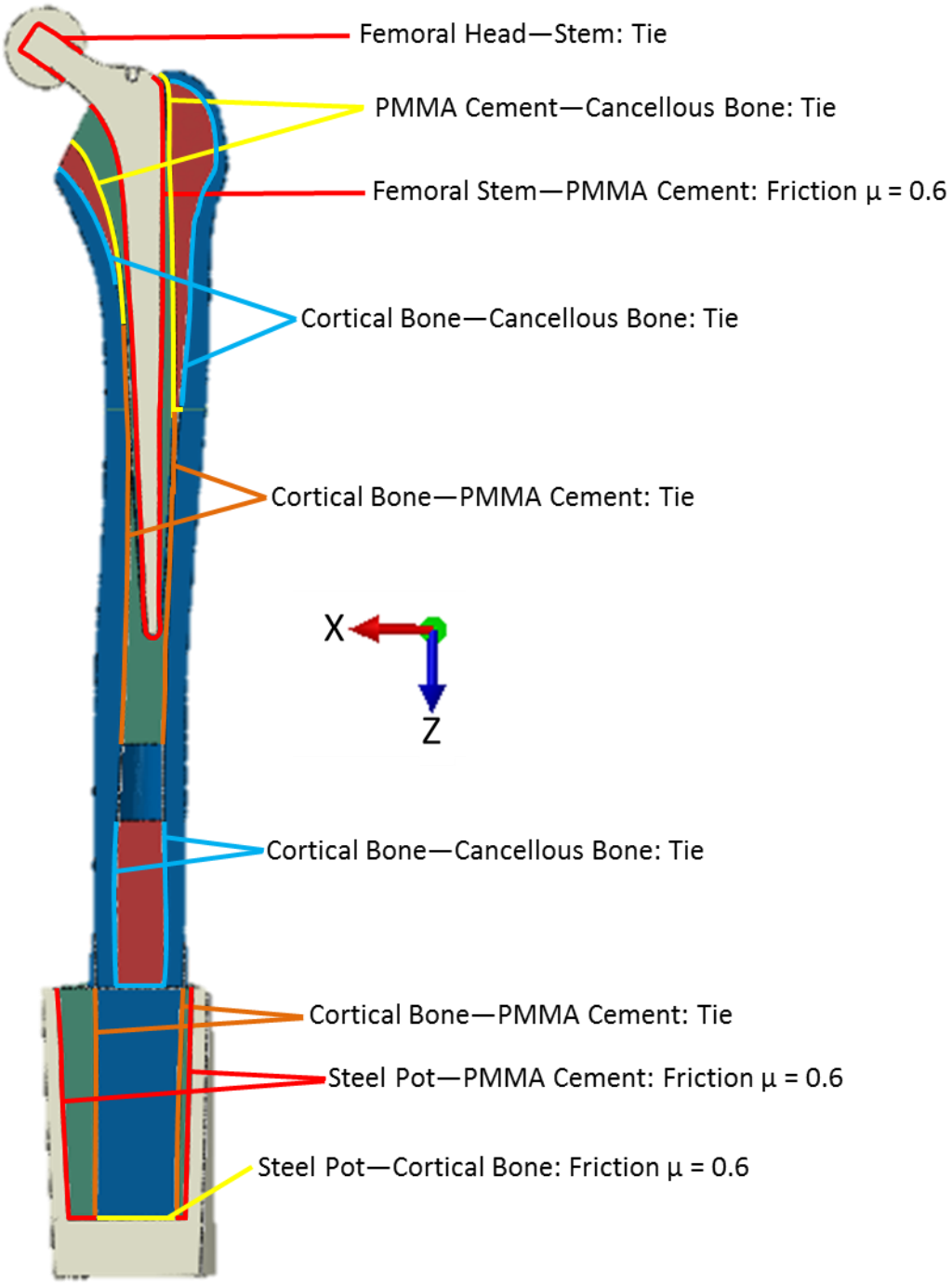

Figure 4.5 Cut-through image of the whole 3D computational model detailing the interfaces between different components.

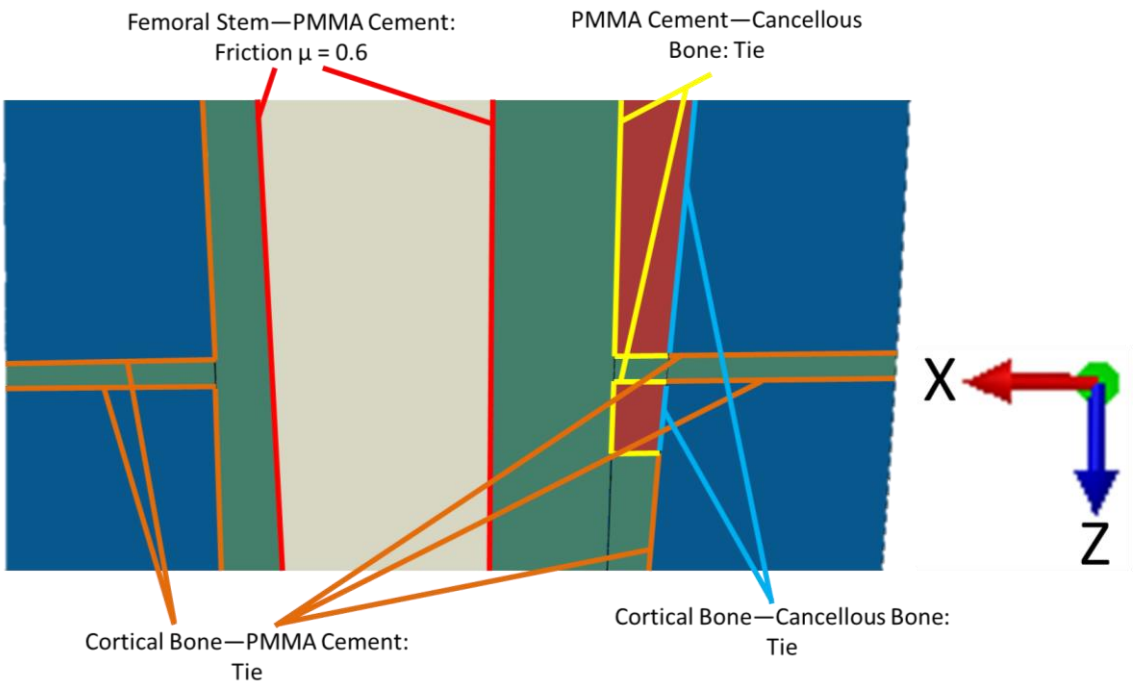

Figure 4.6 Close-up image of a cut-through view of the fracture site, showing the interfaces between different components. View orientation is the same as in Figure 4.5.

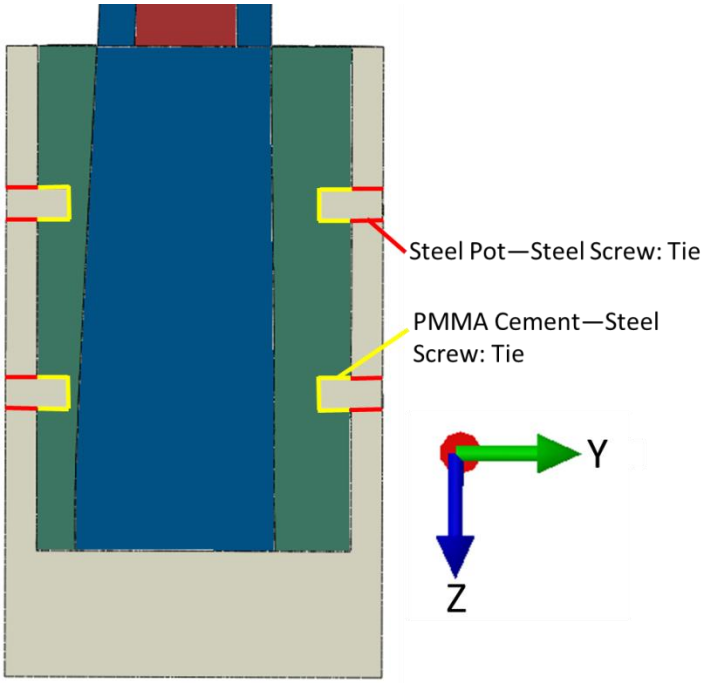

Figure 4.7 Close-up of a cut-through view of the loading pot, showing the interfaces between the screws, loading pot and PMMA cement. Screws were located on the anterior and posterior sides of the specimens; hence the view has been rotated around the z-axis by 90° compared to Figures 4.5 and 4.6.

Table 4.2 List of interactions in the computational model.

Master Surface	Slave Surface	Interaction Type
Femoral Head	Femoral Stem	Tie
PMMA Cement	Cancellous Bone	Tie
Femoral Stem	PMMA Cement	Friction (μ = 0.6)
Cortical Bone	Cancellous Bone	Tie
Cortical Bone	PMMA Cement	Tie
Steel Pot	PMMA Cement	Friction (μ = 0.6)
Steel Pot	Cortical Bone	Friction (μ = 0.6)
Steel Screw	Steel Pot	Tie
Steel Screw	PMMA Cement (Pot)	Tie

The stem-to-cement mantle interface, pot-to-cement interface and pot-to-cortex interfaces were created as a frictional interface (μ=0.6). The value of 0.6 was selected based on available literature [164, 170] and represented the fact that in the experimental setup, due to the comparatively low loading of 500N and limited number of load cycles, the cement to polished interface would still be relatively undamaged. These areas were considered the most important for the application of contact due to the fact that the smooth surfaces of the pot and stem would prevent interdigitation. Experimental testing of polished double-tapered stems by Sangiorgio et al. [146] showed that, regardless of the initial level of attachment of the cement to the stem, relative motion occurred at the stem-to-cement interface after the first few cycles of dynamic loading. The contact parameters selected in Abaqus for these interfaces were:

- Surface to surface discretization (as it, in general, provides more accurate stress and pressure results than node-to-surface discretisation [194]).
- Finite sliding (as it is a more realistic, though potentially less reliable, model than small sliding [194]).
- Path contact tracking (as it is more accurate than state based tracking, which can miss contact due to large incremental motion [194]).
- Penalty-based friction formulation.
- ‘Hard’ normal contact using the classical Lagrange multiplier method of constraint enforcement.

- Strain free adjustment of nodes on the slave surface was used to remove overclosure errors due to the discretisation of curved surfaces.

All other contact was defined as a tie as the cancellous surrogate of the experimental specimens was bonded with cyanoacrylate adhesive and the rough surfaces of the bone would provide better attachment to the cement. The screw-to-pot interface and screw-to-cement interface was also tied. As with the frictional interfaces a surface to surface discretization method was used for the tie constraints. Where possible, strain free adjustments of the slave surface to remove overclosure were used. In several cases however these adjustments led to elements with unsuitable geometries. This prevented slave surface adjustment on the cortical bone-to-PMMA cement, PMMA cement-to-proximal cancellous and cortical bone-to-proximal cancellous interfaces.

In the case of the screw fixation this is a simplification of the true effects of threaded contact. More accurate modelling would however require significant additional time and computational resources [167, 195, 196], providing detail to a small section of the model of limited relevance to the results being drawn. It is expected that the usage of tie constraints would create an overly rigid structure not capturing the small amounts of relative motion between components that would be seen experimentally. As this motion cannot be characterised accurately within the bounds of the current study it cannot however be accounted for in terms of contact conditions within the model. An overestimation of stiffness and underestimation of fracture movement would therefore be expected, predominantly due to unrepresented movements in the loading rig and at the stem-to-cement and cement-to-cortex interfaces. As well as considering time and computational constraints additional contact surfaces reduced the robustness of the model itself and increase the likelihood of convergence failures. This was particularly relevant when having layered contact surfaces such as a combination of contact at both the stem-to-cement and cement-to-bone interfaces and this was another limiting factor.

Table 4.3 List of interaction sensitivity cases.

Case	Description
0	Baseline model. Cement-Steel μ = 0.6. Cement-cortex interface = Tie.
5	Baseline with cement-steel μ = 0.3.
6	Baseline with cement-cortex interface = contact, μ = 0.6.

The baseline settings and interaction sensitivity cases are described in Table 4.3. The effect of altering the cement-to-steel interface's tangential friction to μ=0.3 was considered in Case 5. The baseline value of 0.6 was relatively high compared to the range of values estimated experimentally [164, 170]. Therefore this comparison was performed to provide a measure of how sensitive the FE results were to the cement-to-steel friction coefficient. Additionally Case 5 could be considered as estimating the effects of debonding of the cement-to-stem interface due to either longer periods of cyclic loading or higher static loading. As the cement-to-cortical bone interface would achieve less interdigitation than the cement-cancellous bone interface the effect of altering this tie constraint to a contact with μ=0.6 was considered in Case 6.

4.2.4 Boundary Conditions

The rotational centre of the femoral head was constrained to only allow movement in the direction of the applied load, matching the intended effect of the loading cup on the head. The outside of the distal loading pot was then constrained in all degrees of freedom.

Table 4.4 List of boundary conditions sensitivity cases.

Case	Description
0	Baseline model. Constrained pot at the distal base. Transverse head movement fully constrained.
7	Baseline with transverse head movement unconstrained.
8	Baseline with no distal pot and rotation of femoral base unconstrained.
9	Baseline with 18% of the unconstrained transverse head movement applied as displacement control and 18% of the unconstrained base rotation applied as rotation control.
10	Baseline with no distal pot and distal femur fully constrained.

The baseline settings and boundary condition sensitivity cases are described in Table 4.4. As the loading fixture will allow small deformations the effect of transverse head movement, normal to the load direction, was investigated. The first step was to estimate the direction of the reaction force applied to the loading fixture from the femur. A model was solved for all loading angles with an unconstrained head (Case 7). This model was considered a ‘worst case scenario’. The final position of the centre of the femoral head for these unconstrained head models is shown in Figure 4.8.

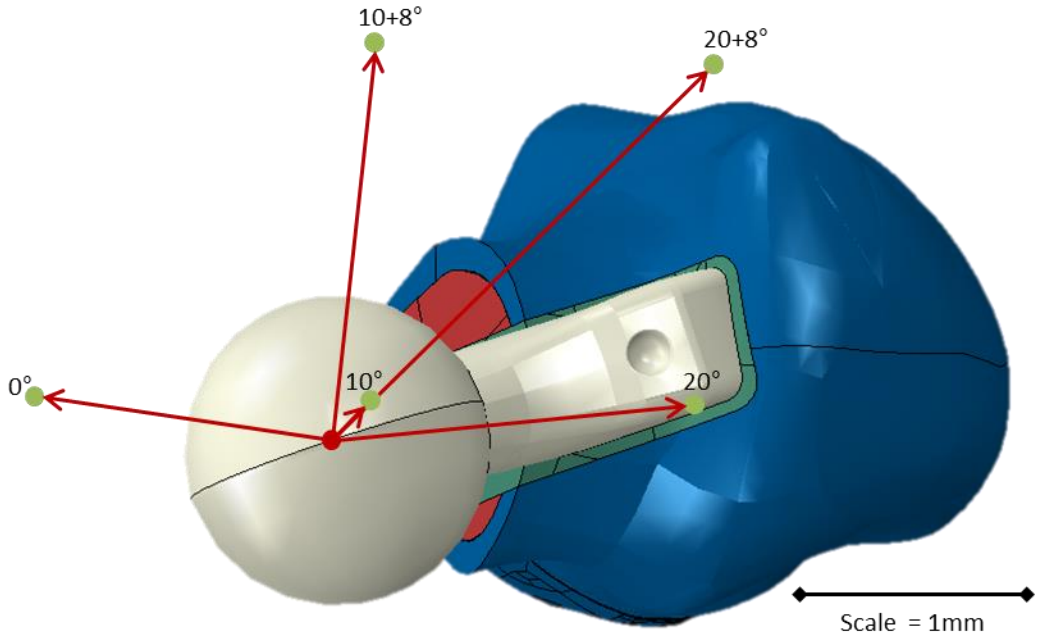

Figure 4.8 Transverse head movements caused by each loading angle when the femoral head was left unconstrained. Movements are scaled to the 1mm scale given but are not scaled to the image of the computational model.

The effect of the loading cup and distal loading rig was then simplified to a linear and constant resisting force to this transverse head movement. This meant that they could be accounted for by scaling down the magnitude of transverse head movement for each loading angle by a fixed proportion, while maintaining the direction of the movement. The actual loading rig and cup will not have an equal stiffness in all directions and to all loads. This was simply a sensitivity study to gauge the effect and importance of head movement by calibrating the model to experimental results however.

From the experimental specimens it could be seen that the most severe changes in strain results with respect to loading angle occurred in the distal portion of the femur, at gauges 4 and 5. The suggested change in bending behaviour, from medial compression and lateral tension at 0° to medial tension and lateral compression at 20°, was the key mechanical aspect affected by head movement. A calibration process was performed whereby a proportion of the unconstrained transverse head movement for each loading angle was applied to the femoral head as a forced displacement. The resulting computational strain at gauge 4 was then compared to the experimental strain at this location.

Several different proportions of the unconstrained head movement were tested until the computational gauge 4 strain approximated the experimental gauge 4 strain. The calibration of the strains at SG4 led to 24% of the unconstrained head movement being applied by displacement control back to the head. This is shown in Figure 4.9.

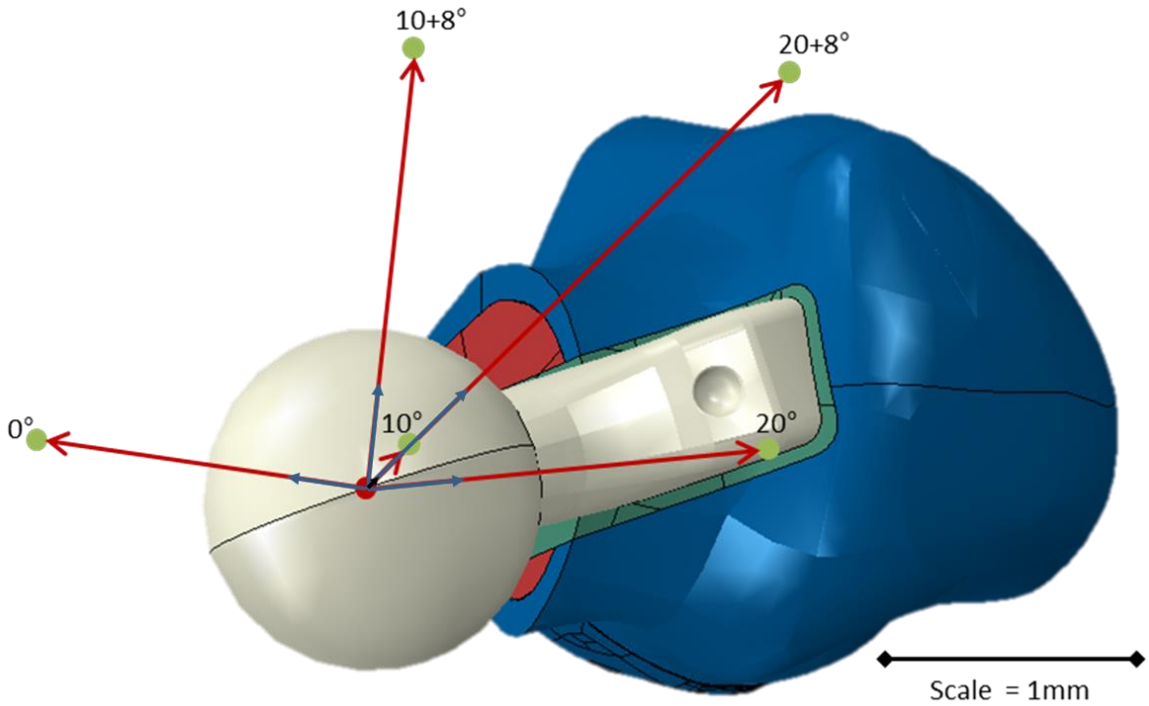

Figure 4.9 The original unconstrained head movements taken from the unconstrained head model and the 24% head movement displacements that were forced onto the boundary condition sensitivity models using displacement control. Movements are to the scale given, not to scale with the image of the computational model.

When comparing against the experimental stiffness and strain results head movement alone significantly improved the sensitivity of the models to loading angle, however the strain pattern could not be matched. In addition to relative transverse micromovement between the head and base there would also be a small amount of rotation of the base within the distal pot. This would be greater than the FE pot components would simulate due to issues such as imperfections and manufacturing tolerances.

The distal pot, screws and cement were removed. The femoral head was constrained against transverse head movement and the centre of the distal base of the femur was constrained against any displacement. Rotation of the base, however, was left

unconstrained. In a similar way as with the head displacements the resulting rotations were considered a ‘worst case scenario’ from which to estimate the direction of the experimental micromovement (Case 8). The unconstrained base rotations for all loading angles are shown in Figure 4.10.

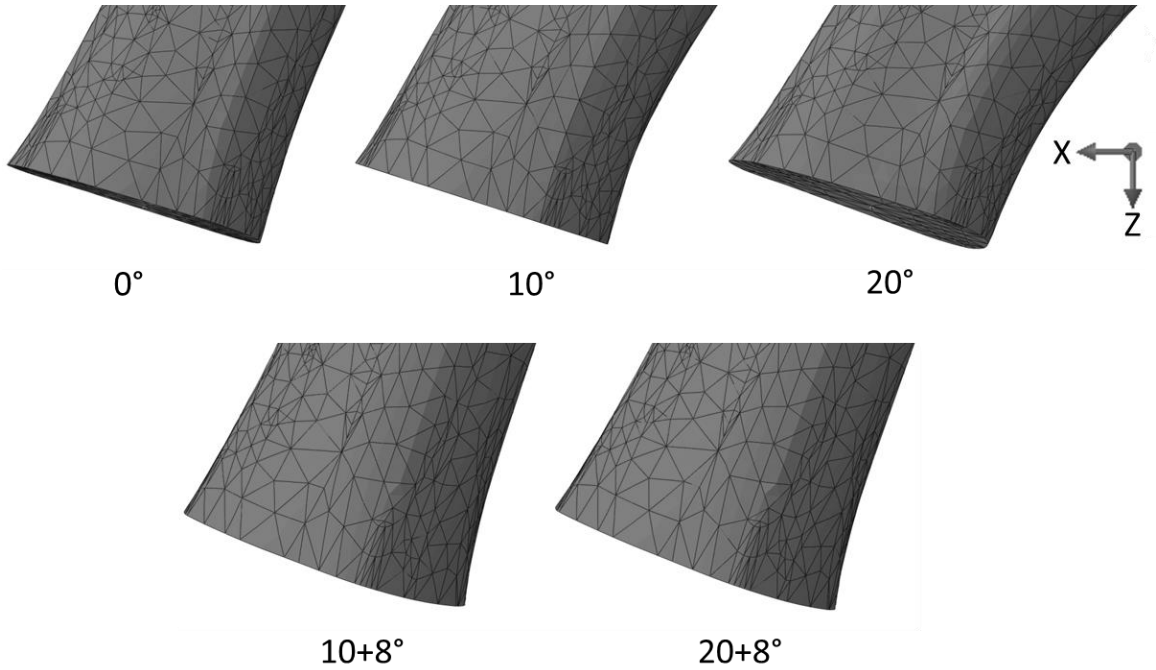

Figure 4.10 Effect of unconstrained base rotations on the displacements of the base of the femur. Displacements for the 0, 10 and 20° cases are increased by a scale factor of 1000x. Displacements for the 10+8 and 20+8° cases are, due to much large displacements, increased by a scale factor of 200x. All cases are shown from the anterior side.

Calibration of the results against SG4 was repeated and this time both transverse movement of the head and distal rotation of the base were considered. When forced onto the model using displacement/rotation control 18% of the unconstrained displacement and rotation was found to provide good agreement with the experimental gauge 4 strains (Case 9).

A final comparison model was created (Case 10) which investigated the effect of removing the distal pot and cement and fully constraining the base of the femur directly. This case tested the effect of simplifying the distal boundary conditions. It also considered the fact that although experimentally there had been a steel loading pot and cement this would not be the case for a clinical patient. As such a case where these components were

not included might be more clinically relevant. Due to the fact that they were investigating the sensitivity of the model to changes in loading angle Cases 0, 7, 8 and 9 were investigated at all loading angles (0, 10, 20, 10+8 and 20+8°).

4.2.5 Loads

The force of 500N was applied as a single point load on the top surface of the femoral head. As the load is rotated for the 10 and 20° of adduction cases, the proximal-most point of the femoral head changes and the load is applied to different points. A modelling investigation was performed in a concurrent study on plate fixation of periprosthetic femoral fractures [16]. This study identified that although modelling the load cup fixture itself and the contact between the two components may be a more accurate way of applying the load it came with a new set of difficulties. Discretisation of the curved surfaces of the femoral head and loading cup resulted in numerical inaccuracies in the stress distribution. Contact between the head and cup was complex and time-consuming to model.

From initial results the models were found to be more representative for the 10° case; as such this was typically used for sensitivity studies. The baseline load settings are summarised in Table 4.5.

Table 4.5. Baseline case settings for load application and direction.

Case	Description
0	Baseline model. 500N point load applied to the proximal-most point of the femoral head. Femur at 10° of adduction.

4.2.6 Fracture Modelling Technique

Identifying the biomechanical situation at the fracture site from the experimental specimens was particularly difficult. From visual inspection and the x-ray images it could be seen that cement had entered the fracture site to an approximate thickness of 1mm. Whether this cement was sufficiently intact to provide structural load bearing or whether it was sufficiently attached to the fracture site surfaces to provide any tangential or tensile support could not easily be determined however. Three different fracture site configurations

were tested to discern the one that most closely replicated the experimental situation. In the original baseline case a 1mm thick transverse slice of the cortex was modified to have the material properties of cement. This represented a situation where the cement provided full support in both compression and tension and was perfectly bonded to both sides of the fracture site. This could be considered a 'best case scenario' in terms of structural support.

Table 4.6 List of fracture modelling sensitivity cases.

Case	Description
0	Baseline model. Fracture site = 1mm thick slice of cement bonded to cortices.
11	Baseline with 1mm thick gap at the fracture site.
12	Baseline with a perfectly reduced fracture and fracture surfaces contact, μ = 0.6.

For the second scenario (Case 11) a 1mm thick transverse slice of the cortex was removed. This represented a situation where the cement provided no structural support at all in any direction. It can therefore be considered a 'worst case scenario' in terms of structural support [52]. The actual experimental situation can be assumed to lie somewhere between the baseline model and this scenario.

For the final scenario (Case 12) the fracture site was perfectly reduced and contact surfaces were defined between the faces of the fracture site (μ = 0.6) (Table 4.6). The normal and tangential contact conditions used for this interface were the same as for the stem-to-cement interface described in Section 4.2.3. In reality the contact conditions between the fracture surfaces would differ from those between polished steel and PMMA cement. This sensitivity study, however, was more focused on the effect of changing to a frictional contact condition rather than the specific properties of that contact. Using contact conditions that had already been successfully applied therefore reduced model development time and improved robustness.

This case represented the surgical ideal where the fracture had been completely reduced and no cement had been allowed to enter the fracture site. This does not match the

evidence from the x-rays of the specimens but may have clinical relevance [60] in terms of how it affects the load response and strain patterns in the model.

4.2.7 Measurement Outputs and Methods

The results taken from the FE models and the methods used to do so are described in this section.

The axial stiffness was defined, as with the experiments, as the force required to cause a 1mm vertical displacement of the femoral head. For each case, the vertical displacement of the point on the femoral head at which the load was applied was recorded and the stiffness was the applied load divided by this value. The points on the femoral used to calculate the axial stiffness for the five different loading cases are shown in Figure 4.11.

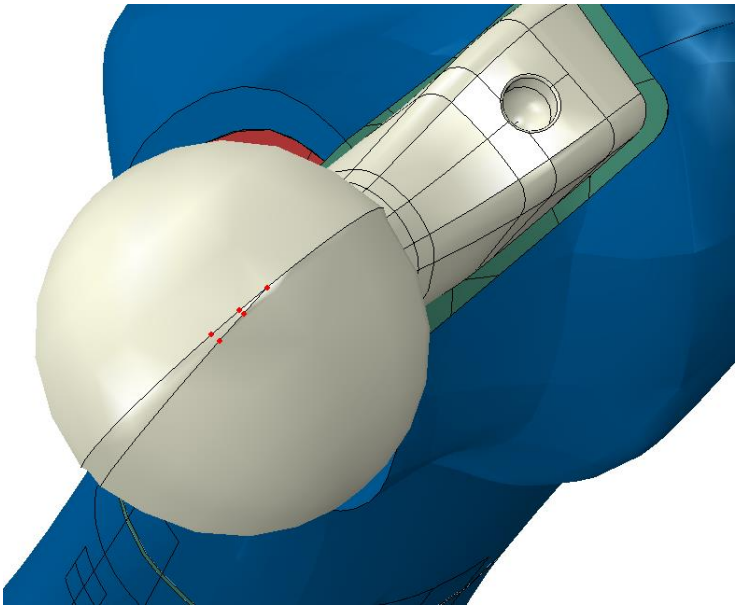

Figure 4.11 The five different points, highlighted red, on the femoral head that were used to calculate the axial stiffness of the models at the five different loading angles.

Elastic strain values were recorded in the axial direction along the medial and lateral sides of the femur for all nodes between 60-220mm below the lesser trochanter (Figure 4.12). At the same points on the medial side the components of the horizontal movement of the femur were also recorded. For strain values at a corresponding location to strain gauge 1, on the lesser trochanter, the surface of the femur was not aligned vertically to the global

axis system and an additional coordinate system was created to record the axial elastic strain at this point. Faces matching the dimensions of the experimental strain gauges were defined on the surface of the cortical bone at locations corresponding to the experimental gauges. These were used to control the mesh quality in these regions and to check for significant strain variations that would have occurred under the experimental gauges (Figure 4.13). The stress and strain results were inspected for unrealistic extreme stress concentrations and where necessary readings from these areas were avoided.

Figure 4.12 Top: Medial regions for which axial cortical strains, and displacements perpendicular to the axis of the shaft, were recorded (highlighted red). Bottom: Lateral regions for which axial cortical strains were recorded (highlighted red).

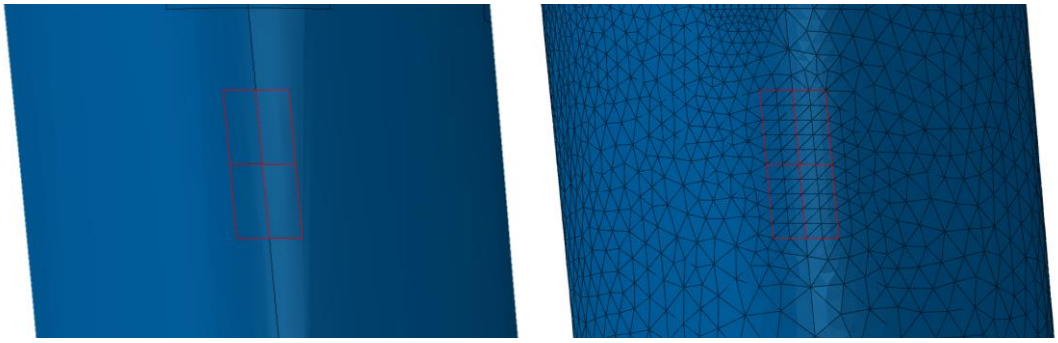

Figure 4.13 Faces created to computationally represent the experimental strain gauges and control the mesh quality in this area (highlighted red).

Points were created on the surface of the cortices 10mm above and below the fracture to match the locations of those used to calculate the experimental fracture movement (Figure 4.14).

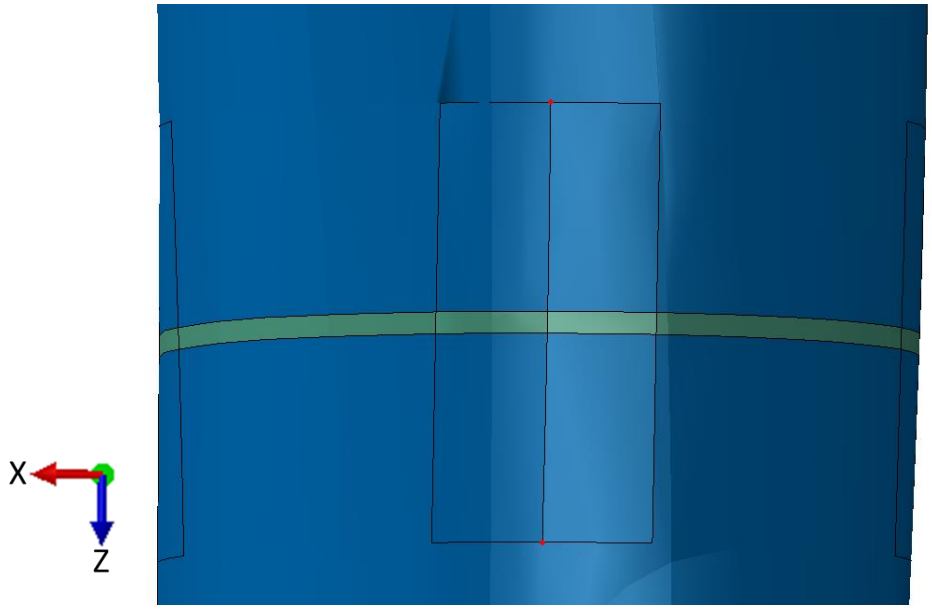

Figure 4.14 The two points (highlighted red), on the anterior side of the model, that were used to calculate the relative axial movement across the fracture site.

Relative vertical motion between these points was then recorded from the FE models on the medial, anterior and lateral sides of the femur. The axial fracture movement was then recorded for all cases at all of these locations.

The vertical movement of the distal most point at the tip of the femoral stem, used as a measure of the axial stability of the stem, was also recorded from the FE models.

4.3 Verification of the Long Stem Fixation Model

Mesh sensitivity testing was performed at several stages during model development to ensure that an appropriate mesh density was being used. Information from the initial development of the FE model was used to select the element type used (C3D10M). Tetrahedral elements were used due to their ability to approximate complex geometries and a quadratic shape function was chosen for improved reliability of results, particularly in the bending of thin walls. The 'modified formulation' option was selected as it is recommended for problems involving contact surfaces [194]. Spiers et al. selected the same element type when creating a THA FE model in order to "accurately calculate the contact stresses at the element corner nodes in the contact interaction" [165]. These models also provided a starting point from which to investigate the effect of element size. An initial mesh was constructed which is described below in Table 4.7.

Table 4.7 Element sizes used for the initial stages of the mesh sensitivity testing.

Model Component	Approximate Element Size
Cortical Surrogate	4mm overall with 1-2mm towards the fracture site and 0.5mm at the fracture site.
Femoral Head	4mm.
Long Revision Femoral Stem	2mm.
Cement Mantle	3mm overall with 0.5mm for the contact surface with the femoral stem.
Proximal Cancellous Surrogate	3mm overall with 0.7mm for some extremely thin areas.
Distal Cement	4mm overall with 1mm for the contact surface with the cement mantle.
Distal Cancellous Surrogate	5mm.
Distal Loading Pot	5mm.
Screws Holding Specimen Into Loading Pot	5mm.
Cortical Surrogate Inside Loading Pot	5mm.
Cement Inside Loading Pot	5mm.

This mesh had in part been selected because it resulted in a model with ~560,000 elements and therefore ~1,300,000 nodes. This made use of the advanced computing facilities available but left sufficient headroom that complexity could be added and testing performed without inducing failures. The models were solved using the Arc1 HPC cluster at the University of Leeds, operating on 6 AMD 8384 (2.7Ghz) processor cores and 48GB of RAM. From this initial mesh the element sizes were modified by ±10% and ±20% of the initial values in order to check for convergence and this was compared across the 0, 10 and 20° loading angles.

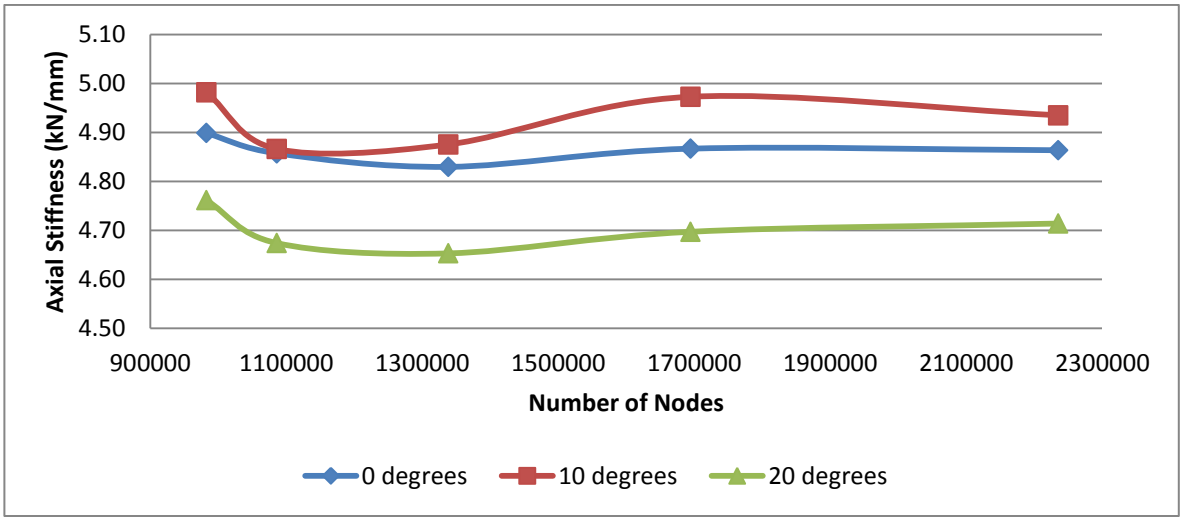

Figure 4.15 Effect of mesh size, and therefore the total number of nodes, on the axial stiffness at 0, 10 and 20° of loading.

Figure 4.15 gives the results of the mesh sensitivity testing on stiffness. 3D solid elements were used; therefore each node had three degrees of freedom (translations in the x-, y- and z-axes). The largest variation was 2.3% of the average and this occurred at the 20° loading angle. A general trend can be seen across the three loading angles where the stiffness initially reduces and then recovers and stabilises. Due to the small changes no obvious issues with the element sizes selected could be discerned. A similarly small effect was seen in strain and fracture movement. The maximum change in element size was ±20% however which would not typically cause any major changes in how geometries were being represented or how contact was being calculated. The whole model could not be refined further without inducing solution failures. In order to optimise the quality of the results without increasing the computational cost, each component of the model was then investigated individually. Considering each component individually allowed for the element sizes to be altered by at least ±50% without causing the solution process to fail.

The proximal cancellous surrogate, distal cement, distal cancellous surrogate and cortical surrogate inside the loading pot were all relatively insensitive to the mesh size. As such a comparison was performed where a 50% coarser mesh was used on all of these components at the same time to check the combined effect of reducing the element sizes. Reducing the number of elements used to represent these components resulted in less than a 1.5% change in all outputs except for strain gauge 4, which changed from 13 μstrain to 8 μstrain (a 36% reduction due to the relatively low starting value). This gave a 5.6%

reduction in the number of nodes in the model which could then be assigned to more influential areas.

The screws that held the specimen into the loading pot and the cement inside the loading pot had an adverse effect on the results when meshed more coarsely, however this aspect was not greatly improved by a finer mesh. As such, the mesh resolution on these components was kept the same.

The cortical bone surrogate, femoral head, long revision stem, cement mantle and distal loading pot all caused a noticeable change in the results when the mesh was refined.

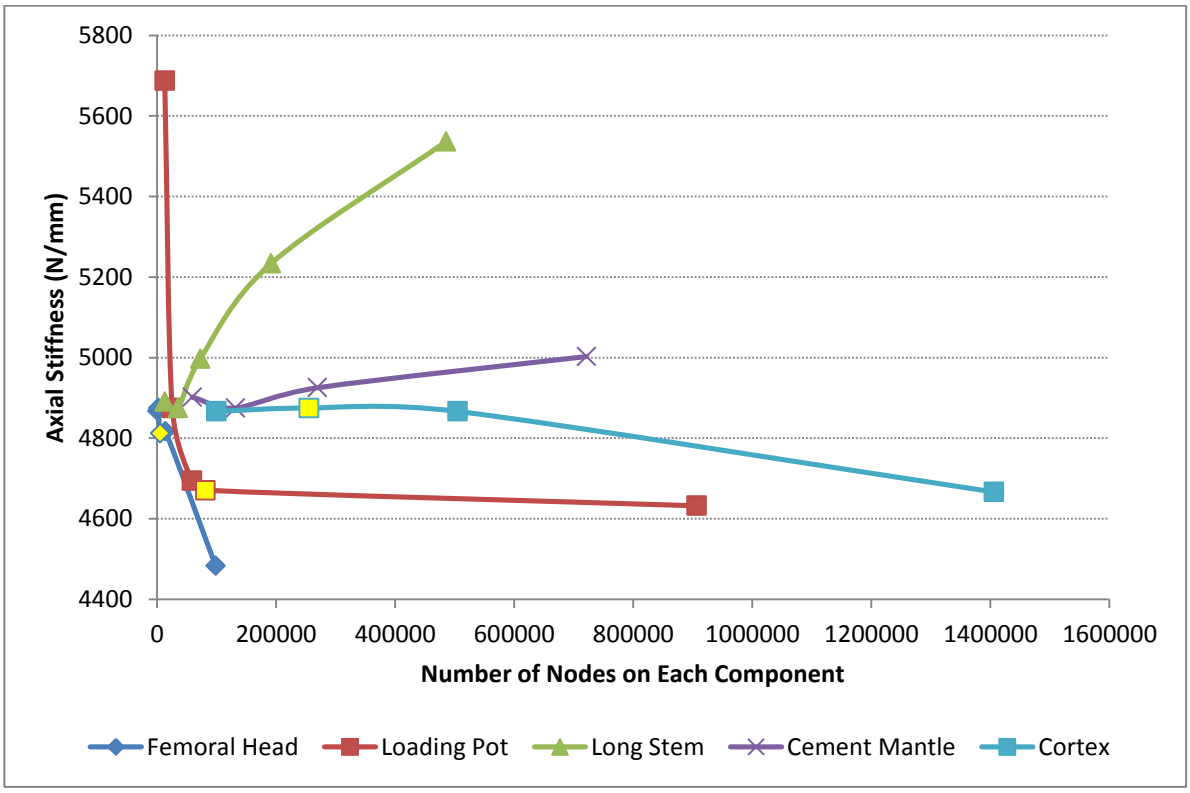

Figure 4.16 Stiffness results for a mesh sensitivity study into the five components most influenced by element size. Yellow markers for the femoral head, loading pot and cortex results indicate the final, selected, mesh size.

Figure 4.16 shows the stiffness results for these five components. Refining the femoral head resulted in a relatively large decrease in stiffness per additional node added and this occurred in two steps. Reducing the element size by 25 or 50% caused a drop in stiffness of around 1.25% with very little difference between the two mesh sizes. Refining further and reducing the element size by 75% caused another drop in stiffness of an

additional 6.75%. Analysing the models more closely showed that this second drop in stiffness was the result of local deformation at the point on the femoral head where the load was being applied. As a concentrated force to one node was being used refining the mesh at the load point resulted in the load effectively being applied to a smaller area. This increase in pressure caused the surface of the femoral head to deform and decreased the recorded stiffness. As this was an unrealistic numerical effect the mesh on the femoral head was refined to the earlier point where it appeared to have converged (-25% element size, marked on Figure 4.16 in yellow).

The distal loading pot and cortical shell displayed more traditional convergence patterns. In terms of the loading pot the stiffness dropped sharply from the coarsest mesh and then settled at approximately 4650 N/mm. An element size 50% smaller than the baseline was selected (marked on Figure 4.16 in yellow) as an appropriate compromise between accuracy and computational cost.

The cortical shell appeared reasonably stable between 100,000 and 500,000 nodes however considering a 50% reduced element size showed that the model was not yet converged. Due to the size of the cortex however decreasing the element size resulted in a significant increase in node count. The baseline element size was kept as the necessary level of refinement to achieve a noticeable difference to the results led to an unreasonable increase in computational time and model failures. In the future, however, this may be the first area that additional computational resources should be assigned to.

Generally mesh refinement leads to a less stiff construct as more degrees of freedom are added [176, 197]. In the case of the cement mantle and the long stem however selecting a smaller element size resulted in a stiffer construct. In both cases the results failed to converge before the number of nodes in the model resulted in failures and given that these components had a much smaller volume than others, such as the cortex, and shared a contact condition at the stem-cement interface further investigation was performed. When investigating the models it was seen that a coarse mesh on the femoral stem resulted in twice the maximum contact pressure between the distal stem tip and cement and higher contact pressures along the shaft of the femur as well. The distal movement of the stem in the coarsely meshed model was 3.4 times higher than in the finely meshed model. This suggested that the coarser mesh was not sufficiently replicating the smooth rounded tip of the femoral stem and was leading to localised points of high and low stress and greater

penetration of the stem into the cement (Figure 4.17). Figure 4.17 shows the view from above the model with all components removed except for the inner surface of the cement mantle, where it is contact with the femoral stem. It therefore looks down into the cavity left by removing the stem from view.

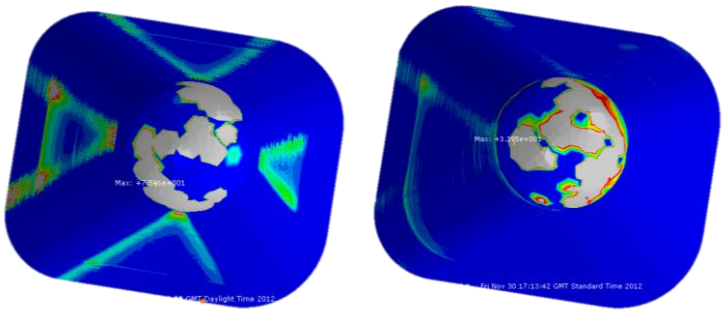

Figure 4.17 Contact pressures in the cement under the tip of the femoral stem. Left: Model with a femoral stem element size 50% larger than the baseline. Right: Model with a femoral stem element size 65% smaller than the baseline. Maximum coarse contact pressure = 76N/mm^2, maximum fine contact pressure = 34N/mm^2. Contact pressure contours shown between 0 and 5N/mm^2 (larger pressures shown grey).

To test this, an analysis was performed where 2mm elements were used for the long stem, except for the distal tip which was meshed with 0.7mm elements. As models had already been created where the entire femoral stem had been meshed with 2mm or 0.7mm elements a comparison could then be made as to whether refining the tip of the stem alone would have the same effect as refining the entire stem. There were negligible differences between the 2-0.7mm mesh case and the 0.7mm case and as such mesh refinement was reanalysed considering only the tip of the femoral stem. Mesh convergence was found to also depend on the element size used for the cement surface in contact with the tip of the stem. The results were found to converge when locally refining the mesh at the tip for the cement and femoral stem to 0.4mm. It was also found that with the cement refined in this location the remaining cement that was in contact with the stem could be meshed with 1mm elements instead of 0.5mm elements, reducing the number of nodes in the model without adversely affecting the results.

Table 4.8 Table of element sizes selected after completion of the mesh sensitivity testing.

Model Component	Final Element Size
Cortical Surrogate	4mm overall with 1-2mm towards the fracture site and 0.5mm at the fracture site.
Femoral Head	3mm.
Long Revision Femoral Stem	2mm overall with 0.4mm at the distal tip.
Cement Mantle	3mm overall with 1mm for the contact surface with the femoral stem and 0.4mm where it meets the distal stem tip.
Proximal Cancellous Surrogate	3.75mm overall with 1mm at the fracture site and 0.7mm for some extremely thin areas.
Distal Cement	6mm overall with 1.5mm for the contact surface with the cement mantle.
Distal Cancellous Surrogate	7.5mm.
Distal Loading Pot	2.5mm.
Screws Holding Specimen Into Loading Pot	5mm.
Cortical Surrogate Inside Loading Pot	7.5mm.
Cement Inside Loading Pot	3mm overall with 1.5mm on the outer surface in contact with the loading pot.

The final element sizes are listed in Table 4.8 and this resulted in a model with 667,015 elements and 1,603,938 nodes. Based on the available computing resources available, this led to an average analysis run time of approximately 19 hours. This final finite element mesh is shown in Figure 4.18.

Figure 4.18 The meshed finite element model used in this study.

4.4 Validation Results

The axial stiffness results for the experimental specimens, the baseline FE models (Case 0) and the FE models with altered boundary conditions (ABC – Case 9) for all loading angles are given in Figure 4.19. The axial strain results for the medial side of the experimental specimens, baseline FE models (Case 0) and ABC FE models (Case 9) for all loading angles are given in Figure 4.20. The distal, lateral strain results for the experimental specimens, baseline FE models (Case 0) and ABC FE models (Case 9) for all loading angles are given in Figure 4.21.

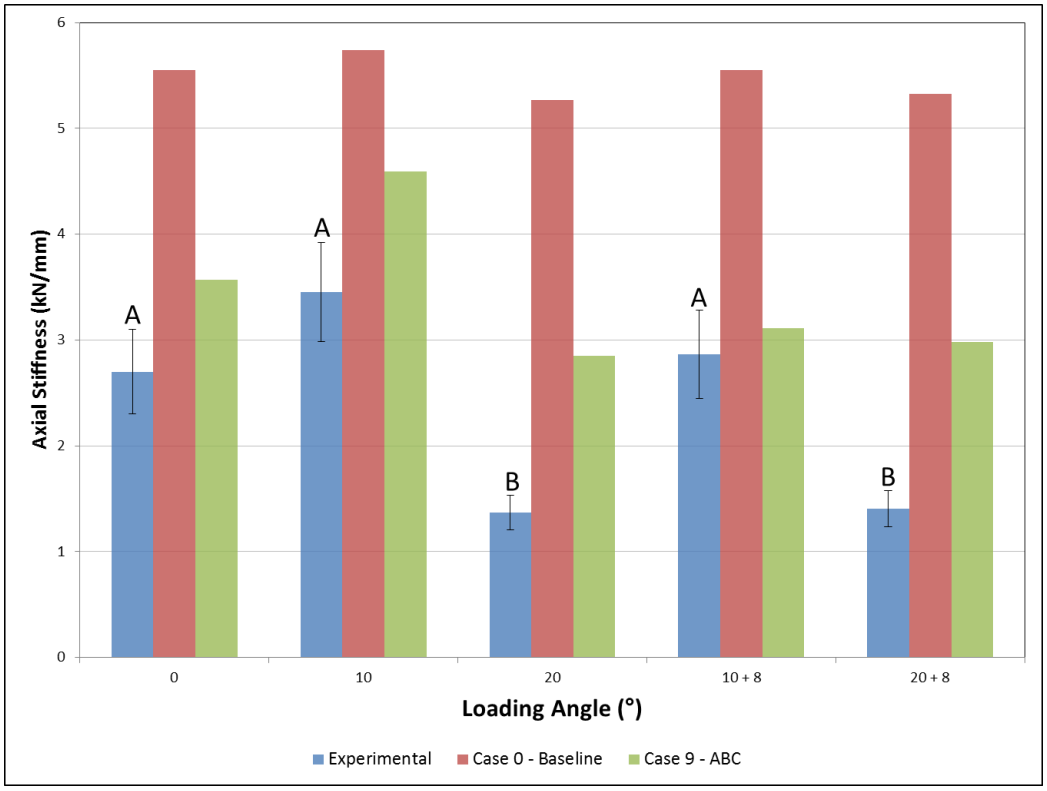

Figure 4.19 Axial stiffness comparison between the experimental specimens, the FE models with a fully constrained femoral head (Case 0) and the FE models with the adjusted boundary conditions (ABC) (Case 9) for all loading angles. Experimental results are averaged across six specimens, error bars indicate ±1SD and different letters indicate statistically significant differences (ANOVA $p<0.05$, Bonferroni post hoc).

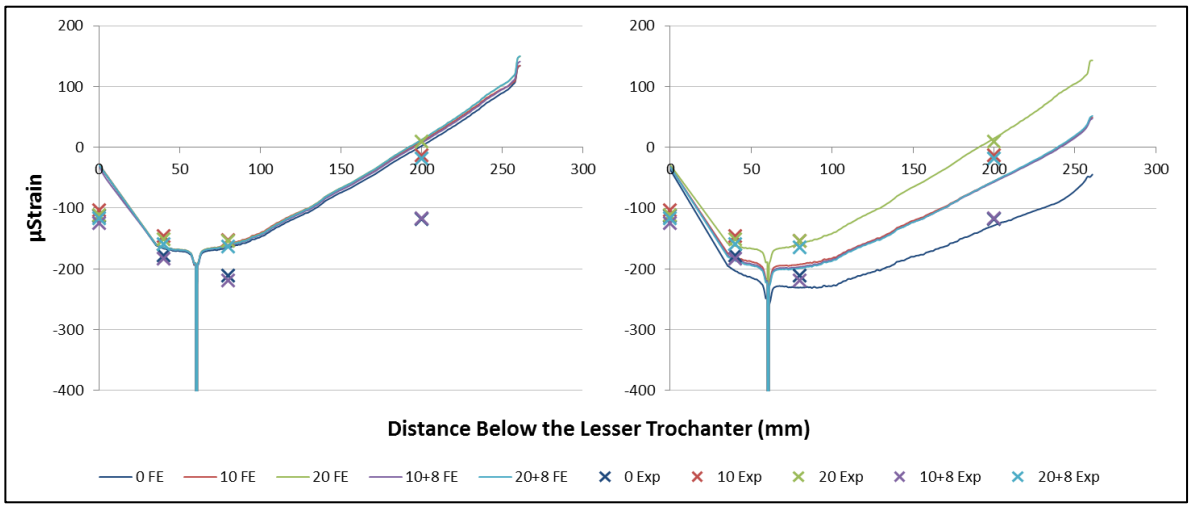

Figure 4.20 Axial strain results from the experimental specimens (both), baseline FE models (Case 0 - left) and ABC FE models (Case 9 - right) at all loading angles. Strains are given for the medial side of the femur between the lesser trochanter and either 200mm below the lesser trochanter, for the experimental specimens, or 260mm below the lesser trochanter, for the FE results.

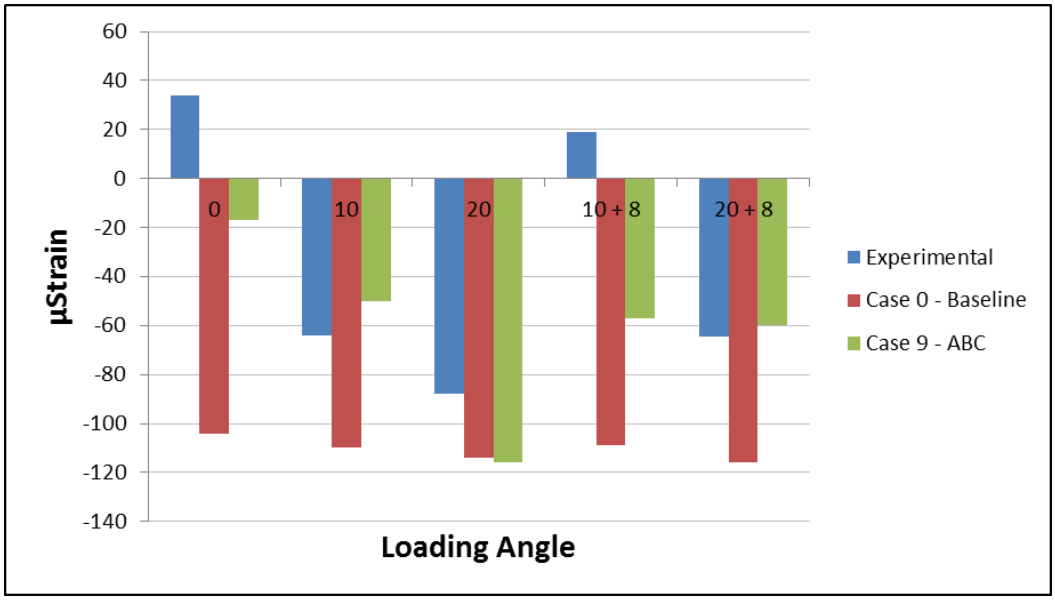

Figure 4.21 Distal lateral strain, 200mm below the lesser trochanter, for the experimental, baseline FE (Case 0) and ABC FE (Case 9) models at all loading angles.

The average stiffness for the experimental specimens was 2.36 kN/mm and the range across all loading angles was 2.08 kN/mm. The average stiffness for the computational specimens with the baseline constraints was 5.49 kN/mm (a 133% overestimate) and the range across all the loading angles was 0.47 kN/mm (a 77% underestimate). The average difference between the experimental and computational strain was 52 ± 44 µstrain. The standard deviation across all the experimental strain readings was 35 µstrain. The standard deviation across all the FE strain readings was 3 µstrain. At the 10° loading angle the computational models overestimated stiffness by 66% and the average difference between the experimental and computational strain was 34 ± 28 µstrain.

The average computational stiffness for Case 9, with the adjusted boundary conditions, was 3.42 kN/mm (a 45% overestimate compared to the experimental average). The computational range was 1.74 kN/mm (a 16% underestimate compared to the experimental range). The average difference between the experimental and adjusted boundary conditions FE strain across all loading angles was 38 ± 29 µstrain. The standard deviation of the strain at each gauge, across all loading angles, is shown in Figure 4.22 for the experimental, baseline FE (Case 0) and ABC FE (Case 9) models. This represents a measure of the sensitivity of each strain gauge to loading angle.

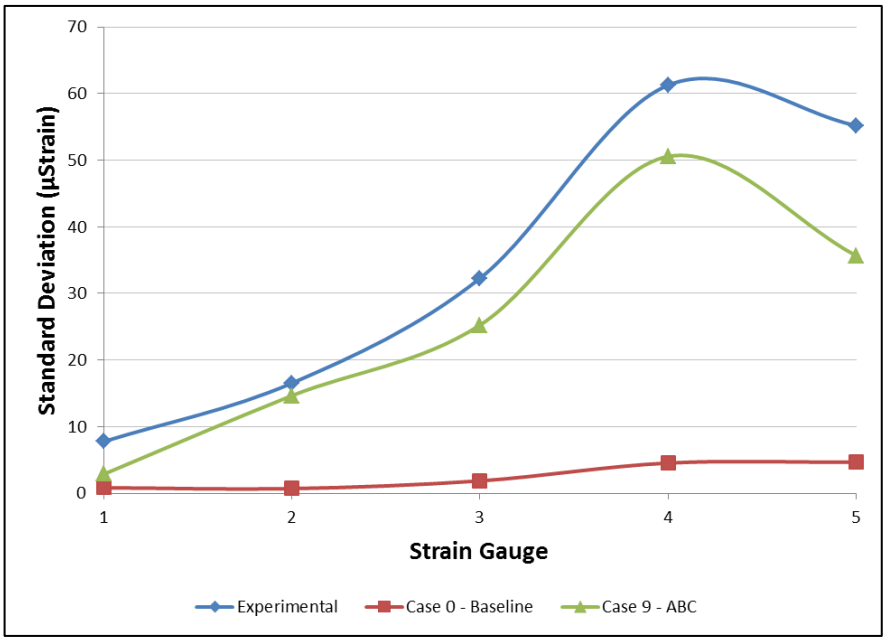

Figure 4.22 Standard deviation of the strain at each strain gauge across all loading angles for the experimental specimens, baseline FE (Case 0) and ABC FE (Case 9).

Table 4.9 Summary of the axial stiffness, medial, anterior and lateral axial fracture movements and distal displacement of the stem tip for the baseline FE model and all sensitivity studies at the 10° loading angle. Positive or negative changes, compared to the baseline model, greater than 20% have been shaded red.

Case	Comparison	Axial Stiffness (kN/mm)	Medial Fracture Gap Change (µm)	Anterior Fracture Gap Change (µm)	Lateral Fracture Gap Change (µm)	Distal Stem Displacement (µm)
0	Baseline	5.7	-4.4	-1.8	2.7	21
1	Cement E=1.225GPa	4.9	-5.2	-2.0	3.3	25
2	Cortex E = 10GPa	4.6	-6.2	-2.4	4.3	25
3	Cortex E = Anisotropic	5.6	-4.4	-1.8	2.7	30
4	Cancellous E = 2.45GPa	6.1	-4.4	-1.8	2.8	22
5	Cement-Steel µ = 0.3	5.4	-4.2	-1.6	2.8	31
6	Cement-Cortex µ = 0.6	4.2	-4.4	-1.8	2.2	29
7	Free Head	5.3	-5.1	-2.6	0.6	22
8	Free Base Rotation	3.4	-6.3	-1.2	7.4	20
9	Adjusted BCs	4.6	-5.1	-1.7	3.3	27
10	No Distal Pot	5.1	-4.7	-1.6	3.3	40
11	1mm Fracture Gap	3.7	-51.2	-16.3	47.4	25
12	Reduced Fracture	5.2	-6.3	1.3	21.1	22

The axial stiffness results are shown in Table 4.9. The average effect of Cases 1-12 on the axial stiffness, compared to the baseline model, was a reduction of 16%. Out of the 12 sensitivity cases presented only one resulted in an increase in model stiffness (Case 4, an

increased Young's Modulus for the cancellous bone surrogate) and the remaining 11 cases resulted in a decrease in model stiffness. The sensitivities which had the greatest effect on the axial stiffness at 10° were: allowing unconstrained rotation of the base of the femur (-41%, Case 8), creating a 1mm gap at the facture site (-36%, Case 11), creating an interface between the cortical bone and cement with a coefficient of friction $\mu = 0.6$ (-27%, Case 6), allowing 18% of the unconstrained head movement and base rotation (-20%, Case 9) and reducing the Young's modulus of the cortical bone by 40% to 10GPa (-20%, Case 2).

The axial relative movement of the fracture surfaces for the medial, anterior and lateral sides of the femur are also given in Table 4.9. When comparing the medial and lateral sides of the femur the baseline case (Case 0) caused the proximal and distal surfaces of the fracture to move together in the axial direction under loading. This was due to greater compressive motion of the medial side than tensile motion on the lateral side. When considering the relative difference between the medial and lateral fracture movements the greatest increases in fracture compression were caused by an unconstrained femoral head (Case 7, 175% increase), a 1mm fracture gap (Case 11, 130% increase) and, to a lesser extent, the inclusion of a frictional interaction between the cortical surrogate and PMM cement (Case 6, 32% increase). Two cases caused the axial fracture movement to change from fracture compression to fracture opening, these were the perfectly reduced fracture (Case 12) and the unconstrained base rotation (Case 8). The relative fracture movements on the medial, anterior and lateral sides of the femur are plotted for some of the more sensitive cases in Figure 4.23.

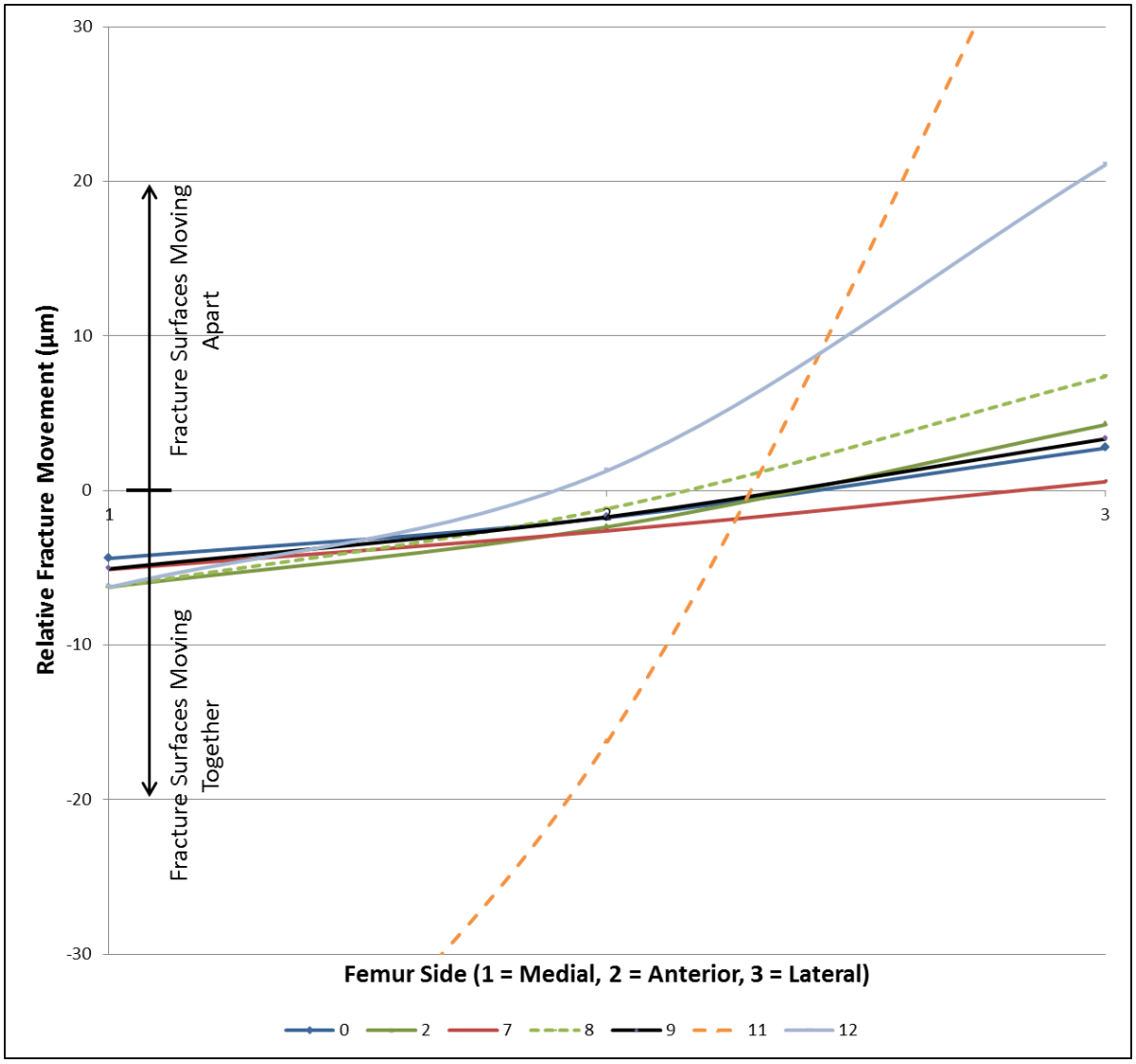

Figure 4.23 The relative fracture movements, on the medial, anterior and lateral sides of the femur, for the sensitivity cases that differed most from the baseline case.

Compared to the baseline case (Case 0), reducing the Young's modulus of the cortical bone (Case 2) caused slightly larger medial compressive and lateral tensile fracture movements. This resulted in a slight increase in bending at the fracture site. Case 7 (an unconstrained femoral head) led to an increase in medial compression and a large decrease in lateral tension. This resulted in a decrease in bending at the fracture site. Case 8 (unconstrained base rotation) caused a relatively large increase in medial compression and a larger increase in lateral tension. This resulted in increased bending at the fracture site. Case 9 (adjusted boundary conditions) caused a very slight increase in both medial compression and lateral bending which resulted in a slight increase in bending at the

fracture site. Case 11 (gap fracture) resulted in a very large increase in both medial compression and lateral tension which resulted in a significant increase in bending at the fracture site. Case 12 (reduced fracture) caused a slight decrease in medial compression but a large increase in lateral tension. This resulted in increased bending at the fracture site. Case 12 also displayed a relatively non-linear trend between the medial, anterior and lateral sides of the fracture which suggests that there was an increase in anteroposterior bending as well. The maximum principle strains in the fracture site cement for Cases 0, 2, 7, 8 and 9 are given in Figure 4.24. The contact pressures acting on the distal fracture surface of Case 12 are given in Figure 4.25.

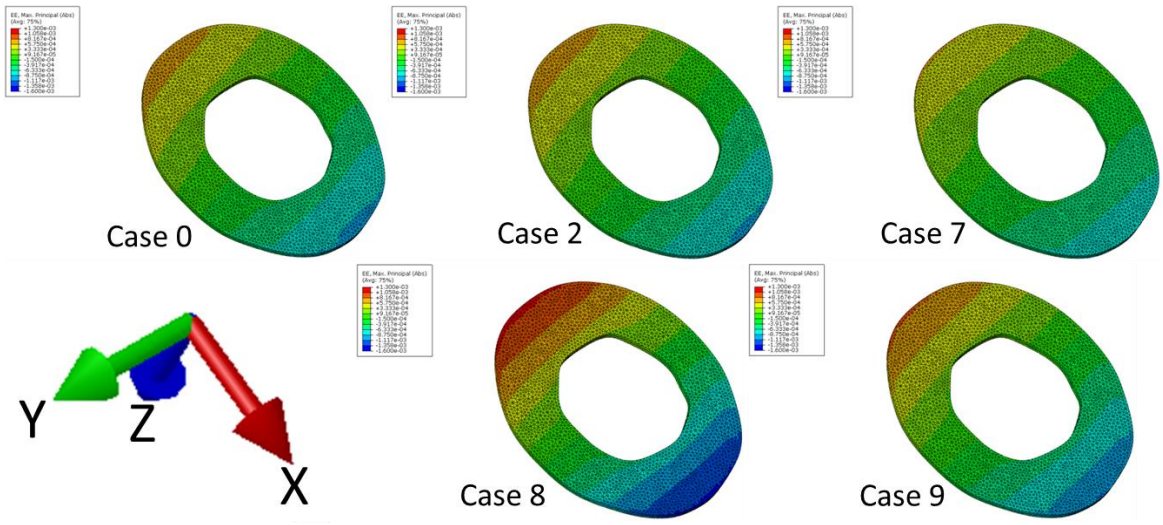

Figure 4.24 Maximum principle strains in the cement at the fracture site for cases 0, 2, 7, 8 and 9. Maximum principle strains are visualised between $1.3e^{-3}$ (red) and $-1.6e^{-3}$ (blue). In the axis system shown the x-axis is positive in the medial direction, the y-axis is positive in the posterior direction and the z-axis is positive in the distal axial direction.

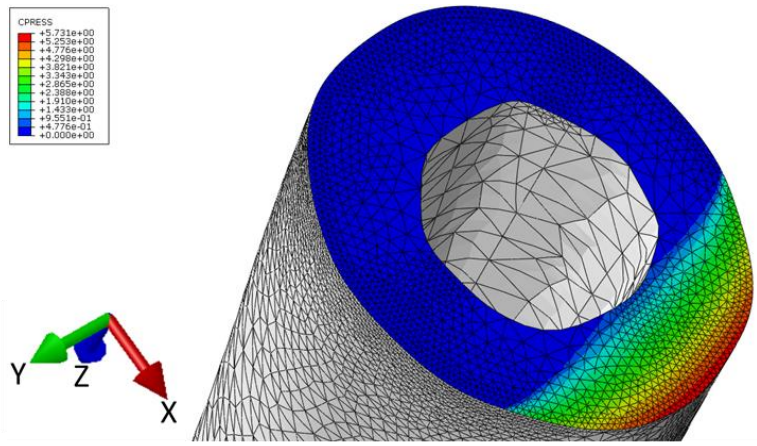

Figure 4.25 Contact pressures on the distal surface of the fracture for Case 12. Grey indicates no value. Blue represents a contact pressure of 0MPa and red represents a contact pressure of 5.73MPa.

The range of sensitivity cases considered caused the maximum tensile strains in the fracture cement to vary between $7.6e^{-4}$ and $1.3e^{-3}$. The maximum compressive strains varied between $8.9e^{-4}$ and $1.6e^{-3}$. The corresponded to maximum compressive cement stresses of 4.7MPa, maximum tensile cement stresses of 3.6MPa and maximum shear cement stresses of 0.46MPa.

The axial displacement of the distal tip of the femoral stem is also given in Table 4.9. Only increasing the Young's Modulus of the cancellous bone (Case 4) resulted in a decrease in distal displacement of the stem tip. The cases with caused a large increase in distal displacement were a frictional interface between the cement and cortical bone (Case 6, 86% increase), decreasing the Young's Modulus of the cement (Case 1, 46% increase), unconstrained base rotation (Case 8, 39% increase), decreasing the Young's Modulus of the cortical bone (Case 2, 36% increase) and reducing the coefficient of friction between the stem and cement (Case 5, 24% increase).

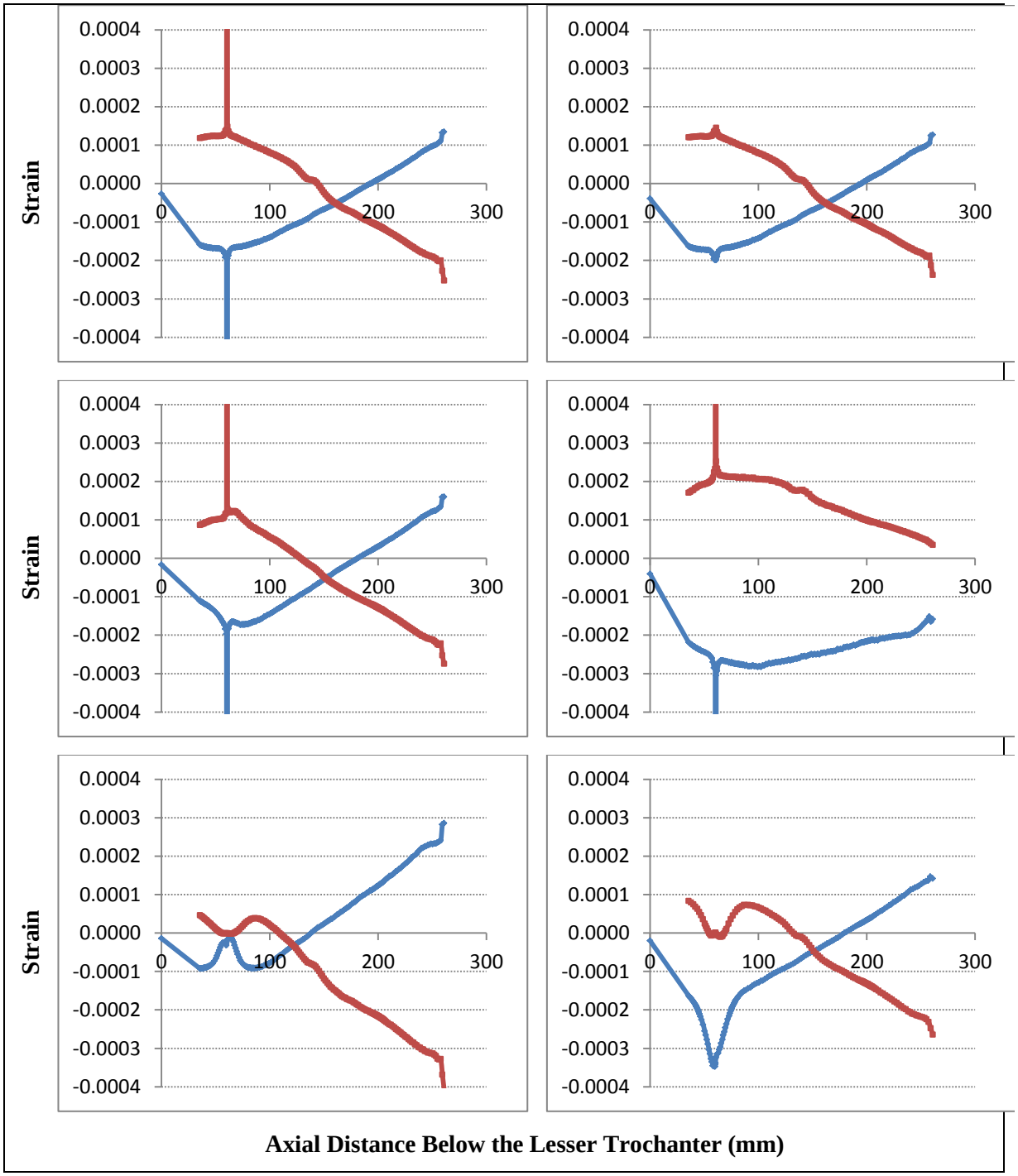

Figure 4.26 Principle axial strain, on the medial (blue) and lateral (red) sides, at the 10° loading angle. Top Left: Baseline FE (Case 0). Top Right: Increased cancellous Young's Modulus (Case 4). Middle Left: Frictional interface between cement and cortex (Case 6). Middle Right: Unconstrained base rotation (Case 8). Bottom Left: 1mm fracture gap (Case 11). Bottom Right: Perfectly reduced fracture (Case 12).

The axial strain along the medial and lateral sides of the femur was recorded for the baseline model and all sensitivity cases. The results for the baseline model (Case 0) and

Cases 4, 6, 8, 11 and 12 (increased cancellous Young's Modulus, inclusion of a frictional interface between the cement and cortical bone, unconstrained rotation of the base of the femur, a 1mm gap at the fracture site and a perfectly reduced fracture, respectively) are shown in Figure 4.26. These cases were specifically chosen because they led to a noticeable change to the strain pattern in the femur. The strain results for these sensitivity cases are compared against the baseline model (Case 0) below.

Case 4 (increased cancellous bone Young's Modulus) showed a very similar pattern of strain compared to the baseline model except for at the fracture site. The increase in stiffness of the cancellous bone reduced the strain concentration in the cement at the fracture site by 77%.

Case 6 (inclusion of a frictional interface between the cortex and cement) caused a reduction in proximal strain (-13%) and increase in distal strain (19%). It also caused a small peak in strain just distal to the fracture site on both the medial and lateral sides of the femur.

Case 8 (unconstrained base rotation) caused increased proximal strain (54%) and significantly decreased distal strain (-292% medially, -128% laterally). Fracture site strains were increased by 62%. It also removed the S-bend pattern of strain with the medial and lateral sides switching between tension and compression. Case 8 caused the medial side to remain solely in compression and the lateral side solely in tension.

Case 11 (1mm fracture gap) altered the overall strain pattern, with no strain peaks for the fracture, a large decrease in proximal strain (-88%) and large increases in distal strain on both the medial (144%) and lateral (65%) sides. Without contact at the fracture site the fracture strains were effectively zero, though fracture movement at the fracture site had increased.

Case 12 (perfectly reduced fracture) also altered the strain pattern. Contact at the medial side of the fracture meant that the strain pattern was more like that of the baseline case. The lack of contact or tensile load transfer on the lateral side however resulted in a lateral strain pattern more like the fracture gap in Case 11. Case 12 caused increased medial strain both proximally (79%) and distally (31%), increased strain distally on the lateral side (14%) and reduced strain proximally on the lateral side (-100%). There was no contact or tensile load transfer at the lateral side of the fracture making the strain effectively zero and on the medial side the compressive strain was reduced by 61% compared to the baseline.

Across all sensitivity studies the most sensitive measure was the medial distal strain, which had a standard deviation of 110% of the average value. Following this the most affected strain locations were the proximal lateral strain (51%), distal lateral strain (48%), medial fracture site strain (45%), lateral fracture site strain (42%) and then the proximal medial strain (36%).

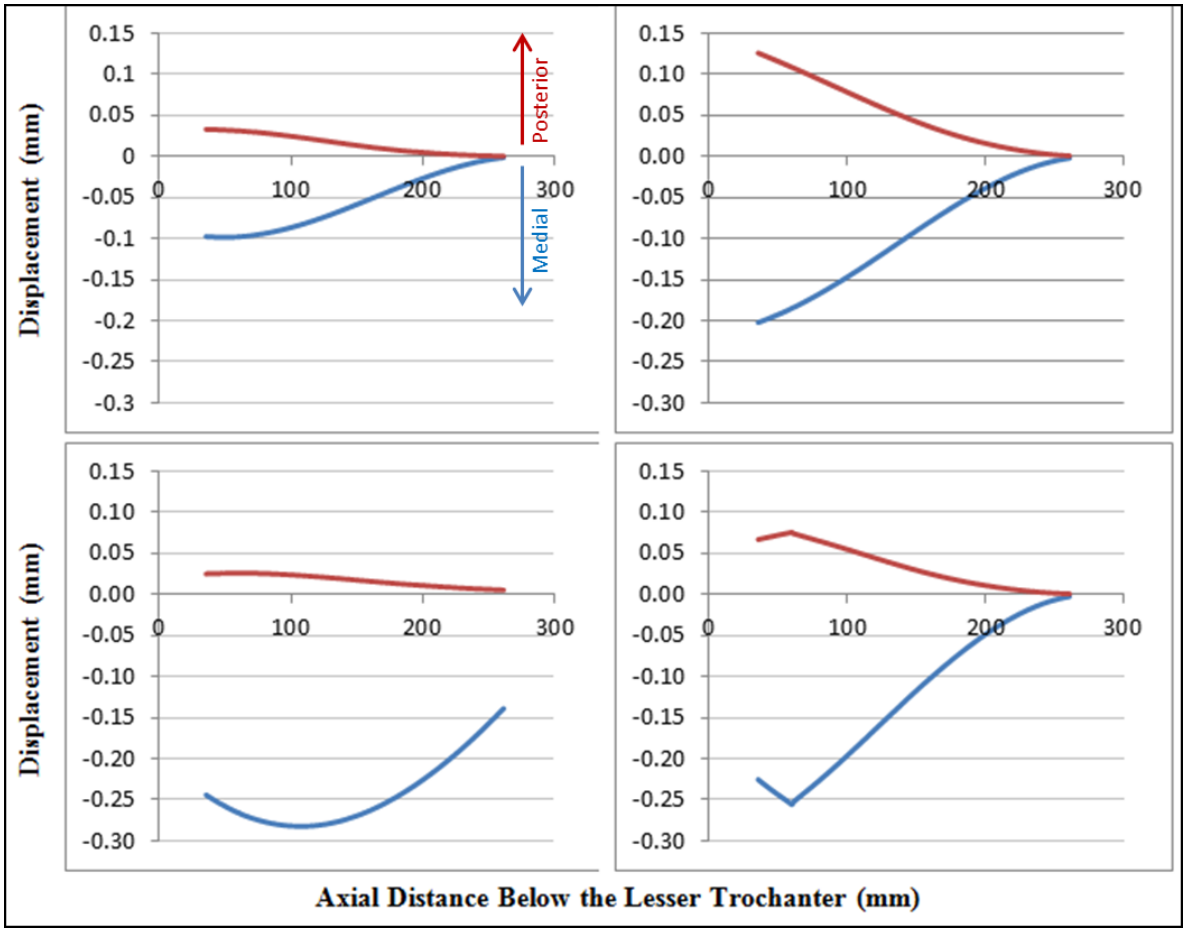

Figure 4.27 Displacements of the femur, along the length of the medial side, in the mediolateral direction (blue) and anteroposterior direction (red). Mediolateral movements are positive in the medial direction and anteroposterior movements are positive in the posterior direction. Top Left: Baseline FE model (Case 0). Top Right: Unconstrained femoral head (Case 7). Bottom Left: Unconstrained base rotation (Case 8). Bottom Right: 1mm fracture gap (Case 11).

The transverse movements of the medial side of the femur, along its axial length, in the mediolateral and anteroposterior directions for the baseline model and all sensitivity cases were recorded at the 10° loading angle. Three sensitivity studies, Cases 7 (unconstrained femoral head), 8 (unconstrained base rotation) and 11 (1mm fracture gap),

resulted in markedly different patterns of bending deformation compared to the baseline model (Case 0). These four cases are presented in Figure 4.27 and the differences between them and the baseline model (Case 0) are described below:

Case 7 (unconstrained femoral head) caused the transverse movement to continue to increase towards the proximal region, rather than changing direction and reducing towards the head as in the baseline case. It resulted in a 106% increase in lateral bending and a 282% increase in posterior bending.

Case 8 (unconstrained base rotation) caused a large lateral movement at the base of 0.14mm and a more distinct C-bend curvature in the mediolateral plane. It resulted in a 188% increase in lateral bending and a 21% reduction in posterior bending.

Case 11 (1mm fracture gap) caused the majority of the bending in the femur to be focused at the fracture site, with a sharp change in direction there and reduced bending in the shaft. It caused a 161% increase in lateral bending and a 127% increase in posterior bending.

On average, across all the sensitivity studies, the lateral bending was 56% higher than the baseline value and the posterior bending was 41% higher than the baseline value.

4.5 Discussion

In this chapter, a finite element model of a long stem PPF treatment was developed to represent the experimental model presented in Chapter 3. The baseline finite element model was successfully solved using a high performance computing facility. A series of cases were then analysed to evaluate the sensitivity to mesh density and input parameters and comparisons were made with the experimental results presented previously. The outcomes and significance of these verification, validation and sensitivity tests are discussed in more detail below.

4.5.1 Verification

In terms of verification, modifying the mesh across the whole model at once did not prove to be a good measure for whether mesh convergence had been reached. This was due

to the fact that significant changes to the element size, such as would alter the way different geometries were being represented, could not be achieved before the solution step began to fail. A component-by-component mesh refinement analysis was therefore required to adequately optimise the mesh distribution. Although a reasonable level of convergence was achieved using the resources available to this study, there were still areas of the model that could have been improved. Based on the convergence patterns displayed by the various mesh sensitivity tests an approximate estimation could be made that results of the model are within 15% of the true, fully converged values. This was estimated as a 10% numerical error based on the mesh refinement of the cortices and a 5% numerical error from the remaining components. Optimisation of a finite element mesh for studies of this type is therefore still an important step in order to improve the quality of the results obtained.

4.5.2 Validation and sensitivity to boundary conditions

In terms of validation, the computational models considerably overestimated the axial stiffness at all loading angles, when compared to the experimental data. In addition, the stiffness predicted by the computational models was much less sensitive to the loading angle than the experimental data. Similarly when the axial strain was compared at the locations of the experimental gauges, the computational models underestimated the strains at all loading angles and also underestimated the sensitivity of the strain to the loading angle. Although the changes were smaller, the computational models did, however, display the same trends as the experimental data regarding the effects of different loading angles.

The reasons for the discrepancies between the experiment and FE models were explored through the sensitivity test cases. The majority of these cases were selected to test assumptions and simplifications made during the modelling process that would potentially make the model more realistic. It is therefore possible that some of the axial stiffness overestimate seen in the computational models was caused by these known issues. The factors considered in the sensitivity testing in this chapter, but not accounted for in the baseline model, that are probably most likely to be contributing to this stiffness overestimate are: 1) Relative motion at the PMMA cement-to-cortical bone interface, 2) Small amounts of micromotion in the experimental loading assembly and 3) A less idealised fracture configuration. On average the various tested sensitivity cases resulted in a stiffness reduction of 16%. In a similar way all bar one of the sensitivity cases resulted in

an increase in the distal displacement of the stem tip. As such, it can be suggested that as well as overestimating the axial stiffness the baseline computational model might be underestimating the distal movement of the stem tip into the femur.

When estimating the direction of experimental micromotions using models with unconstrained boundary conditions, and estimating the magnitude of these experimental micromotions by calibrating against the distal, medial strain the stiffness overestimate, strain underestimate and sensitivity underestimates were reduced. With adjusted boundary conditions the 10+8° case had a reduced axial stiffness compared to the 10° case. Experimentally torsion had little effect on the axial stiffness or strain results. It is possible however that this difference is due to issues with the way this sensitivity case caused bending in the anteroposterior plane which, without comparable strain data, could not be calibrated or validated against experimental strain data.

With the movement of the femoral head and knee constrained, the strain patterns along the medial and lateral side of the femur show that the axial strain changes between compressive and tensile along the length of the femur. This is indicative of an S-shaped bending profile. Allowing free rotation of the base of the femur, which represents the in vivo knee joint, resulted in the formation of a pure C-bend however (Section 3.3, Figure 3.31). In this case, the lateral side of the femur remained in tension all along its length and the medial side of the femur remained in compression. These two bending profiles result in very different strain patterns and it is generally unclear which methodology best represents the in vivo case. It is clear, however, that the behaviour of a femur model is highly sensitive to the choice of boundary conditions at the head and knee and that, experimentally or computationally, the decision of how to constrain a model should be made carefully.

Given that the models appear to be sensitive to small micromotions at the femoral head and base, and that experimental data on the magnitude or direction of these micromotions was not available, a loading angle of 10° will be used for future computational comparisons. This is because the 10° case most closely represented pure compression and therefore produced the least transverse head movement, making the assumption of no transverse head movement most valid.

4.5.3 Sensitivity to material properties

The addition of transverse orthotropic material properties to the cortical surrogate had a negligible effect on the results of the analyses but increased model development time and model analysis time. As such it is likely not necessary or recommended to model this degree of anisotropy for computational comparisons. It may be more important however if the difference between material properties in different directions is more severe, such as might be the case in osteoporotic patients.

The reduction of the cortical bone Young's modulus resulted in a decreased stiffness and increased bending and cortical strain as would be expected from the application of simple beam bending theory. No significant changes in the trends or response of the model were noted however. This suggests that with the geometry of a healthy femur and reasonable treatment options the effect of reduced cortical Young's modulus, in order to represent osteoporotic bone, would not need to be investigated. More realistic cases that account for cortical thinning and realistic osteoporotic material properties (including reduced failure resistance) would likely be required to provide clinically relevant results.

4.5.4 Limitations of axial stiffness measurements

The results for the axial stiffness across the range of sensitivity studies show that differences in axial stiffness can be driven by several different biomechanical mechanisms. A reduction in axial stiffness can be due to increased closing of the fracture site, increased bending of the specimen, increased compression of the specimen or increased relative movement of the stem into the femur. Referring to the axial stiffness as a single value with which different cases can be compared therefore fails to identify these individual causes and their relative contribution, which is important information when attempting to evaluate the efficacy of different treatment options. This may be of particular importance when considering changing loading orientations, which potentially generate different deformation responses, or treatments that provide stability in a fundamentally different way, such as plated fixation against long stem fixation. Load vs. displacement data may be more usefully applied in load to failure testing where the aim is to evaluate the overall survivability of a construct, rather than more subtle differences.

4.5.5 Benefits of FE approach

The various sensitivity studies performed showed that the finite element model was sensitive to changes in fracture configuration, material properties, proximal cement geometry, interface properties and boundary conditions. Moreover, the changes that were caused by these different cases could be identified using the measurements taken from the FE models, namely axial stiffness, principle axial strain, fracture movement, transverse displacement of the femoral shaft and distal movement of the stem tip. Compared to the measurements taken from the experimental specimens, the computational model provided a far more comprehensive description of the response of the specimen to loading. In particular, the ability to gather stress and strain data at almost any location has the potential to thoroughly investigate strain-shielding and the risk of refracture. The ability to fully characterise the deformation of the structure allows for different bending modes to be identified. The ability to accurately determine the movement of the fracture site can be used to compare how well different cases can stabilise and restore function to the fractured bone and the ability to easily analyse the stresses and displacements in areas within the specimen provides information that would be very difficult to obtain experimentally. With all of these results however, the limitations and assumptions of the simulation discussed above must be kept in mind.

4.6 FE Model Case List

Table 4.10 FE sensitivity testing case list.

Case	Description
0	Baseline model. Pot at the distal base. Cement E = 2.45GPa. Cortex E = 16.7GPa. Cancellous E = 155MPa. Cement-Steel μ = 0.6. Cement-cortex interface = Tie. Transverse head movement fully constrained. Fracture site = 1mm thick slice of cement.
1	Baseline with cement E = 1.225GPa.
2	Baseline with cortex E = 10GPa.
3	Baseline with cortical E = anisotropic (compressive E = 16.7GPa, transverse E = 10GPa).
4	Baseline with cancellous bone E = 2.45GPa.
5	Baseline with cement-steel μ = 0.3.
6	Baseline with cement-cortex interface = contact, μ = 0.6.
7	Baseline with transverse head movement unconstrained.
8	Baseline with no distal pot and rotation of femoral base unconstrained.
9	Baseline with 18% of the unconstrained transverse head movement applied as displacement control and 18% of the unconstrained base rotation applied as rotation control.
10	Baseline with no distal pot.
11	Baseline with 1mm thick gap at the fracture site.
12	Baseline with a perfectly reduced fracture and fracture surfaces contact, μ = 0.6.

4.7 Conclusions

A finite element model of a long stem PPF treatment was successfully developed and solved. The verification demonstrated that an adequate level of numerical accuracy had been achieved by refining the mesh on each individual component.

The idealisation of material properties, geometry and interface conditions when producing a finite element model resulted in a simulation that was more resistant to

deformation than reality. The trends displayed by the experimental specimens regarding the effects of loading angle were successfully replicated however. It would therefore be recommended to consider, where possible, less ideal scenarios in order to highlight potential issues and avoid overestimating the suitability of treatment options. Considering the anisotropy of bone however may only have a significant effect on the results in cases where there is a large difference between the material properties in different directions, for example in osteoporotic patients.

The results of the finite element model were extremely sensitive to the boundary conditions used and models with fixed boundary conditions were relatively insensitive to the effect of loading angle, when compared to the experimental results. It is therefore possible that the results of the experimental testing were affected by the choice, and compliance, of loading assembly. Given this the selection of boundary constraints, for both computational and experimental studies of this nature, should be made carefully. During experimental testing measurements of any micromotion in the loading assembly may assist with interpreting the results and/or validating computational models. Performing mechanical testing using a bi-axial loading cell that can give force and displacement data in the transverse plane may be one way to achieve this. When attempting to match experimental data using a computational simulation the effect of any assumptions made at the boundaries of the model should be minimised. In the case of this study this involved focussing comparisons to the 10° case, where the femoral head constraints had the minimum effect on the results.

The results of this study suggest that, when performing a biomechanical analysis of a complex system such as an implanted femur, comparing cases using the overall stiffness values is not sufficient. Depending on the cases being considered, specimens can respond in many different ways and these responses cannot generally be identified without additional information. Therefore in the subsequent studies presented in this thesis, additional measurements such as strain and fracture movement will also be presented.

5. Evaluating the Effect of Cement Thickness and Fracture Configuration

Given that the finite element models had been evaluated and validated against comparative experimental testing, and that the applicability and limitations of the models were understood, the next stage was to investigate a wider range of clinical scenarios. Utilising the same femoral geometry and modelling techniques as reported in Chapter 4, scenarios were considered where the cement mantle distribution differed from the experimental cases and where the fracture height or angle was varied. Performing these comparisons experimentally would have been time consuming, costly and, in some cases, technically very difficult. Given the inter-specimen variability present even when using synthetic femurs, this approach still may not have shown statistically significant differences between cases. Computationally however many cases could be considered relatively quickly. With the comprehensive results provided by finite element analysis, the biomechanical differences between cases could then be analysed in great detail. The overall purpose of these tests was to investigate the suitability of long stem fixation for different fracture heights and angles, the optimum stem length for these fracture cases and the necessary cement mantle distribution for proximal stem fixation.

5.1 Cement Thickness

5.1.1 Motivation

The default cement mantle was developed from x-ray images of the experimental specimens. The thickness of cement surrounding the stem varied across its surface. Clinically, surgeons attempt to produce a cement mantle that is at least 1mm thick surrounding the femoral stem. The experimental specimens however showed that the distribution of cement was not uniform and below the lesser trochanter the cement thickness varied between approximately 1mm and 4mm. The thickness and distribution of the cement mantle is likely to vary between clinical cases and may depend on factors such as surgical technique and bone quality. However it is also something that a surgeon can

control, to some degree, clinically. As such, if the stability and survivability of the implants are sensitive to the cement distribution, then this is an area of clinical practice that could potentially be optimised. The aims of this study were therefore:

- To evaluate whether the experimental cement mantle seen in these x-rays was sufficient to provide proximal stem stability.
- To evaluate the effect that a decreased or increased volume cement mantle might have on the fracture fixation.
- To evaluate the difference between a cement mantle that varies in thickness around the stem and ones that do not.

This information could then be used to identify key areas where cement mantle support is required and also to investigate the level of realism required when representing a cement mantle computationally.

5.1.2 Methods

Two uniform cement mantles were developed, one of 1mm thickness and one of 4mm thickness, by increasing the size of the femoral stem CAD file in all directions by 1 and 4mm respectively. These thickness values were selected due to the fact that they represented the minimum and maximum values from the experimental x-rays. The sensitivity studies presented in Chapter 4 showed that the FE models best matched the experimental data at a 10° angle of adduction loading case. As such all of the models were tested at this orientation.

The effect of cement mantle geometry was compared for both the baseline fracture and fracture gap configurations. In the baseline fracture model, the fracture was bonded together with 1mm of PMMA cement (Case 0 from Chapter 4). The fracture gap model included a gap between the fractured cortical surfaces of 1mm (Case 11 from Chapter 4). The two cases provided both ‘ideal’ and ‘worst-case’ fracture stability scenarios. The three different cement distributions are shown, in the fracture gap configuration, in Figure 5.1. The cement volumes for the experimentally derived, 1mm thick and 4mm thick cement distributions were 38, 24 and 42 cm^3 respectively. These values could be used to gauge

how the models might compare to cement usage in practice. The depth of cement into the femoral canal and cement loss from mixing and insertion would obviously need to be accounted and compensated for however.

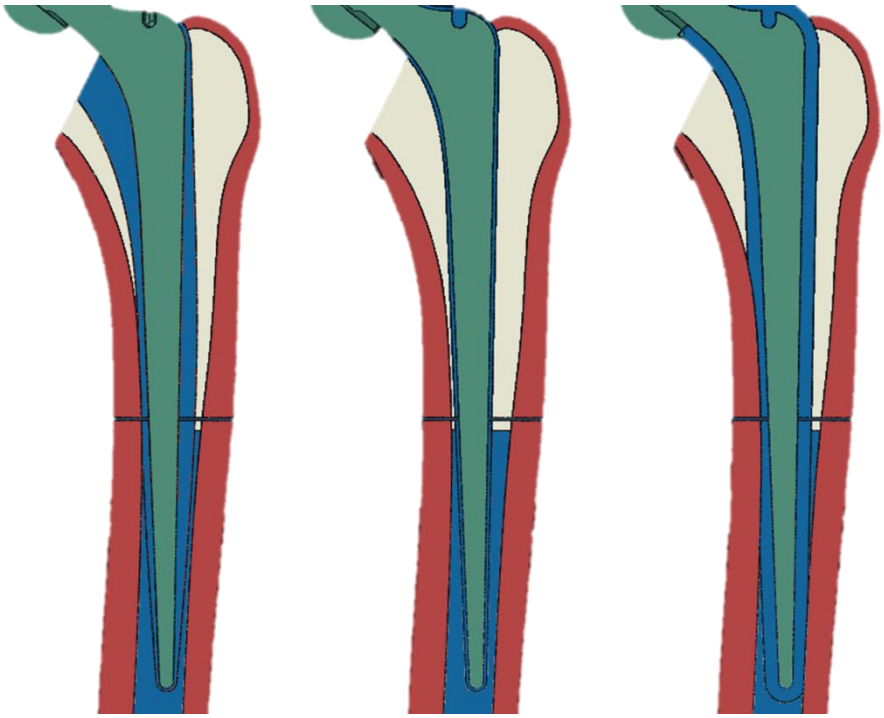

Figure 5.1 Cut-through images, in the mediolateral plane, of the three different cement mantle distributions investigated. Left: The experimentally-derived cement mantle. Middle: The 1mm thick uniform cement mantle. Right: The 4mm thick uniform cement mantle. The cortical bone is coloured red, the cancellous bone is off-white, the PMMA cement is blue and the femoral stem is green.

5.1.3 Results

The axial stiffness results for the experimentally derived, 1mm uniform and 4mm uniform computational cement mantles are shown, for both the standard and gap fracture cases, in Figure 5.2. Only small differences between cement cases can be seen when considering the axial stiffness. For the standard fracture case, the experimental cement mantle resulted in the lowest axial stiffness, with the 1mm uniform and 4mm uniform mantles both slightly increasing the values. The changes were small and did not appear to be due to major differences in the bending or fracture movement however. The stability of the cement bonded fracture sites meant that the fracture movements were also similar

across the cement mantle cases. For the gap fracture cases, the axial stiffness differences between the cases were also small (the range was approximately 10% of the average value) however biomechanical differences could be seen at the less stable fracture sites.

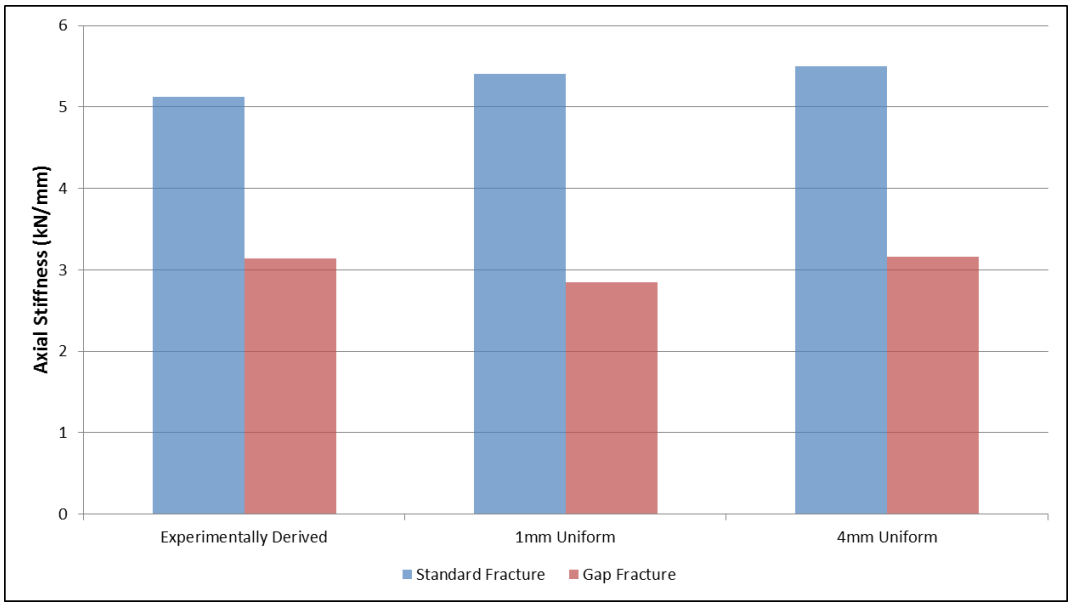

Figure 5.2 Effect of cement mantle geometry on the axial stiffness of the construct for both the standard fracture and gap fracture configurations.

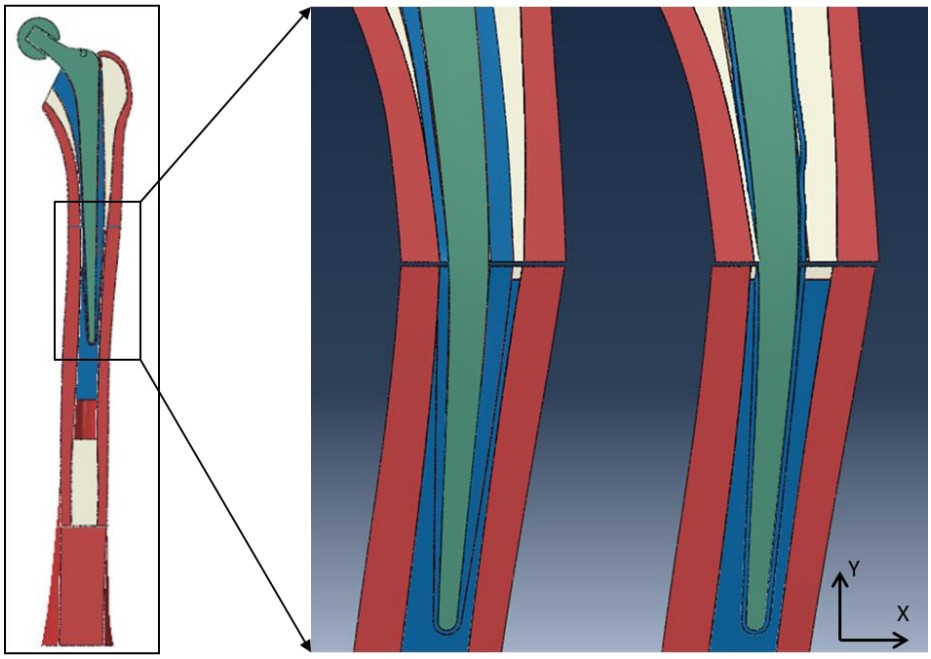

Figure 5.3 Pivoting motion of the stem due to the insufficient support provided by the 1mm thick cement mantle. Left: Cut-through image of the computational model. Middle: Loaded experimentally derived cement distribution model. Right: Loaded 1mm thick uniform cement model. Deformations scaled 50x in the X axis and 1x in the Y axis.

The differences between the fracture site shear movement, in the mediolateral direction, for the experimental and 1mm uniform cement cases are highlighted in Figure 5.3. The results for the overall shear movement for all three cases are provided in Figure 5.4. Differences between cases were only seen clearly in the fracture gap scenario and as such only those results are shown. It can be seen that there was much greater shear in the 1mm cement mantle case than in either the 4mm or experimentally derived cement mantle cases.

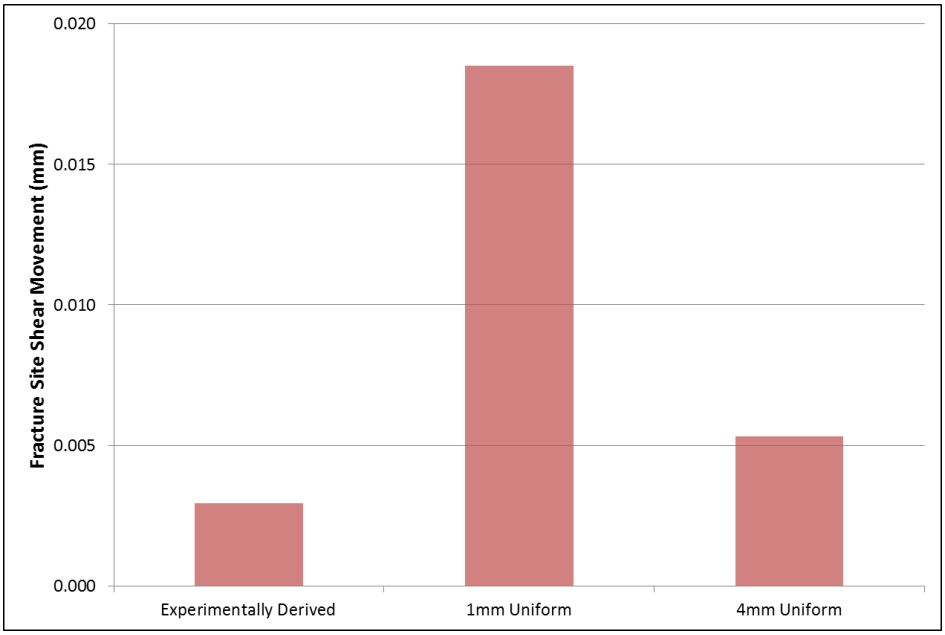

Figure 5.4 Relative shear movement between the proximal and distal fracture surfaces for all three cement distributions with a gap at the fracture site.

The maximum Von Mises stress in the cement surrounding the distal stem tip, for all three mantle geometries, is given in Figure 5.5. The effect of mantle geometry is compared for both the cement-bonded fracture site case and the 1mm fracture gap case. With both fracture configurations the 1mm uniform cement mantle led to significant increases (up to 210%) in cement stresses in this region.

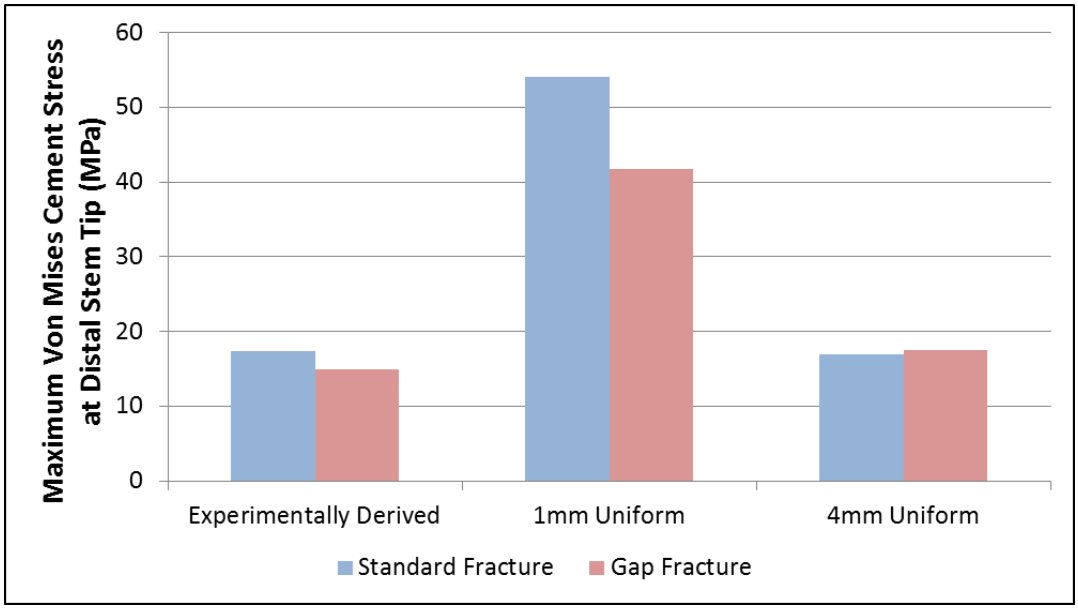

Figure 5.5 Maximum Von Mises cement stress measured in the cement surrounding the distal stem tip for the three mantle geometry cases. Results given for both the cement-filled fracture site case and the 1mm fracture gap case.

The maximum tensile, compressive and shear stresses in the cement mantle are given in Figure 5.6. They are compared against example ultimate tensile, compressive and shear stress properties (UCS, UTS and USS) for PMMA cement [198, 199, 200]. The maximum shear stress at the cement-to-bone interface is also given for all three models and is compared to cement-to-cancellous bone shear yield stress of 6 MPa [172]. Given the reduced interdigitation at the cement-to-cortical bone interface this value is likely to underestimate likelihood of failure of the cement-to-cortical bone interface.

The maximum tensile stresses measured from the experimentally derived and 4mm uniform cement mantles were significantly less (63 - 68%) than the UTS of PMMA cement. The maximum tensile cement stress in the 1mm uniform cement mantle was larger than the UTS of PMMA cement however, suggesting that failure would be expected. A similar pattern was seen with the maximum compressive cement stresses. Both the experimentally derived and 4mm uniform cement mantles did not cause maximum compressive stresses larger than the UCS of PMMA cement. The 4mm uniform cement mantle did lead to an increase in maximum compressive stress when compared to the experimentally derived case, however. The 1mm uniform cement mantle resulted in maximum compressive cement

stresses greater than the UCS of PMMA cement, again suggesting that cement damage would be expected.

None of the maximum shear stresses recorded in the models exceeded the USS of PMMA cement, however the maximum shear stress recorded in the 1mm uniform case was 98% of the USS value and the maximum shear stress in the 4mm case was 72% of the USS value. Considering the shear stresses at the interface between the PMMA cement and cortical bone, only the 4mm uniform cement mantle resulted in no areas where the shear stress exceeded the yield stress. Even this 4mm uniform cement mantle case, which included the greatest surface area between cement and cortical bone over which the shear load could be distributed, experienced 85% of the interface shear yield stress.

The maximum compressive, tensile and shear stresses in the cement near to the tip of the femoral stem are shown in Figure 5.7. None of the recorded stress values exceeded the corresponding yield values for PMMA cement. Both the experimentally derived and 4mm uniform cement mantles resulted in relatively low maximum shear stresses around the distal stem tip. The 1mm uniform cement mantle resulted in the highest maximum stresses in all directions for both the entire cement mantle, the cement near the distal stem tip, and the cement-to-bone interface. The maximum shear stress near the distal stem tip for the 1mm uniform cement mantle case was more than double the maximum shear stresses for the two other mantle geometries.

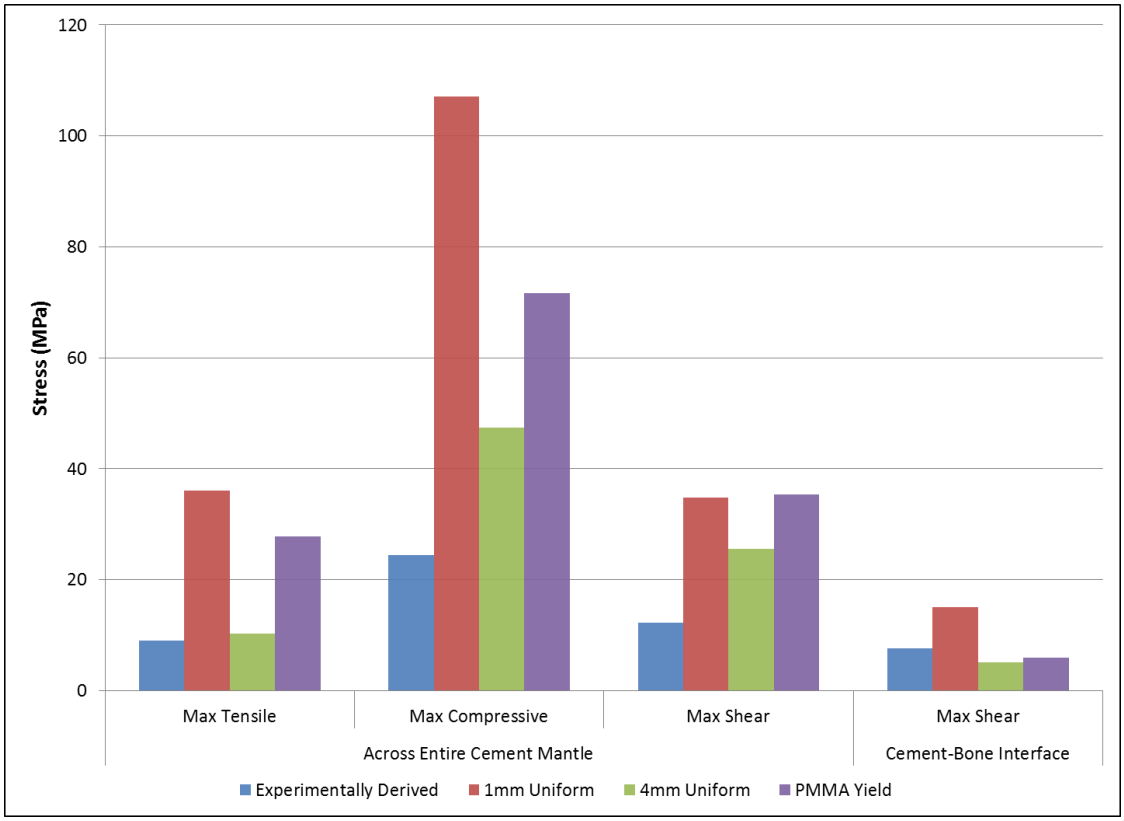

Figure 5.6 Maximum tensile, compressive and shear stresses measured in the cement mantle of the three cement mantle geometry computational models, at 10° of adduction with a fracture gap, compared against the UTS, UCS and USS properties of PMMA cement. The maximum shear stress between the cement and bone is also presented.

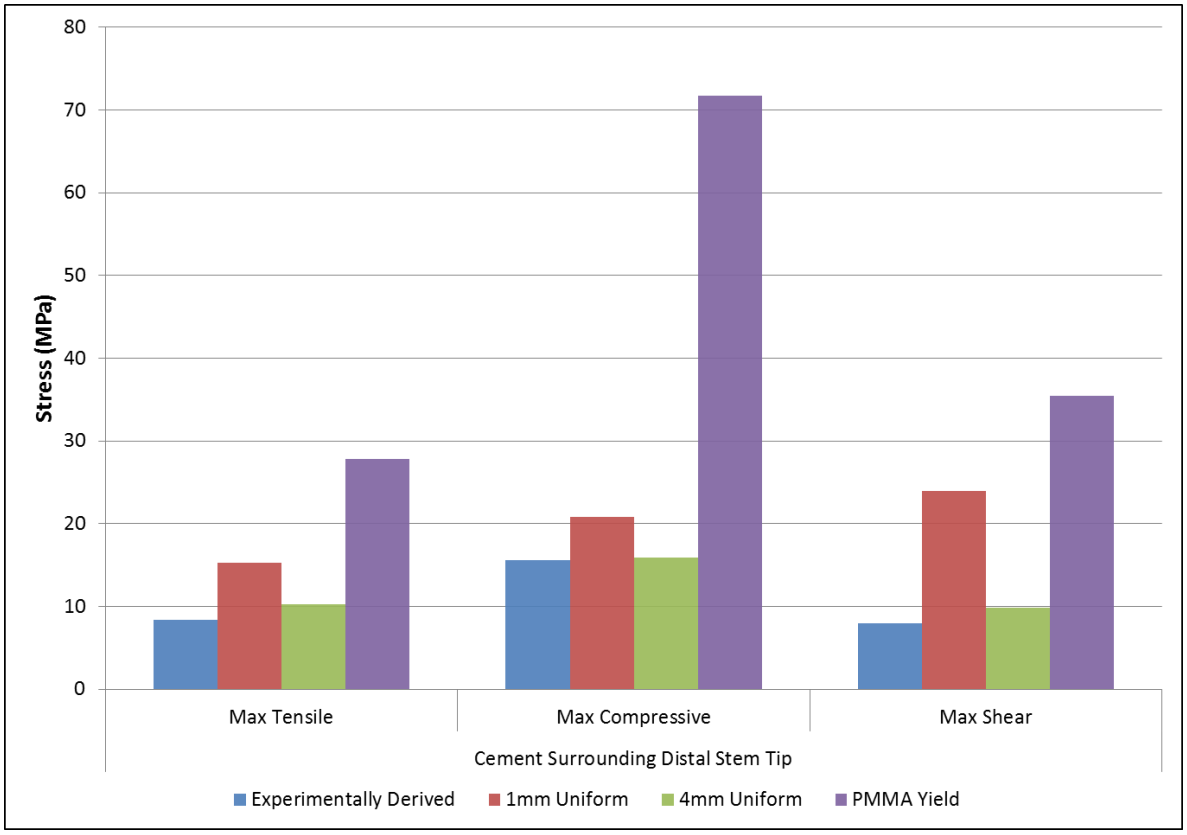

Figure 5.7 Maximum tensile, compressive and shear stress measured in the cement in the region of the distal tip of the femoral stem for the three cement distribution models. Models load at 10° of adduction with a 1mm fracture gap. UTS, UCS and USS for PMMA cement provided for comparison.

The von Mises stress distributions for cut-through views of the FE models, sectioned through the stem in the mediolateral plane, are given in Figure 5.8. As well as leading to an increase in the maximum cement stress, the 1mm uniform cement model also caused the location of this maximum stress to change. In the experimentally derived and 4mm uniform cement mantle cases, the maximum Von Mises stresses in the cement around the stem tip were located beneath the tip of the stem. For the 1mm uniform cement mantle case, the maximum cement stress had moved to the lateral side of the stem tip.

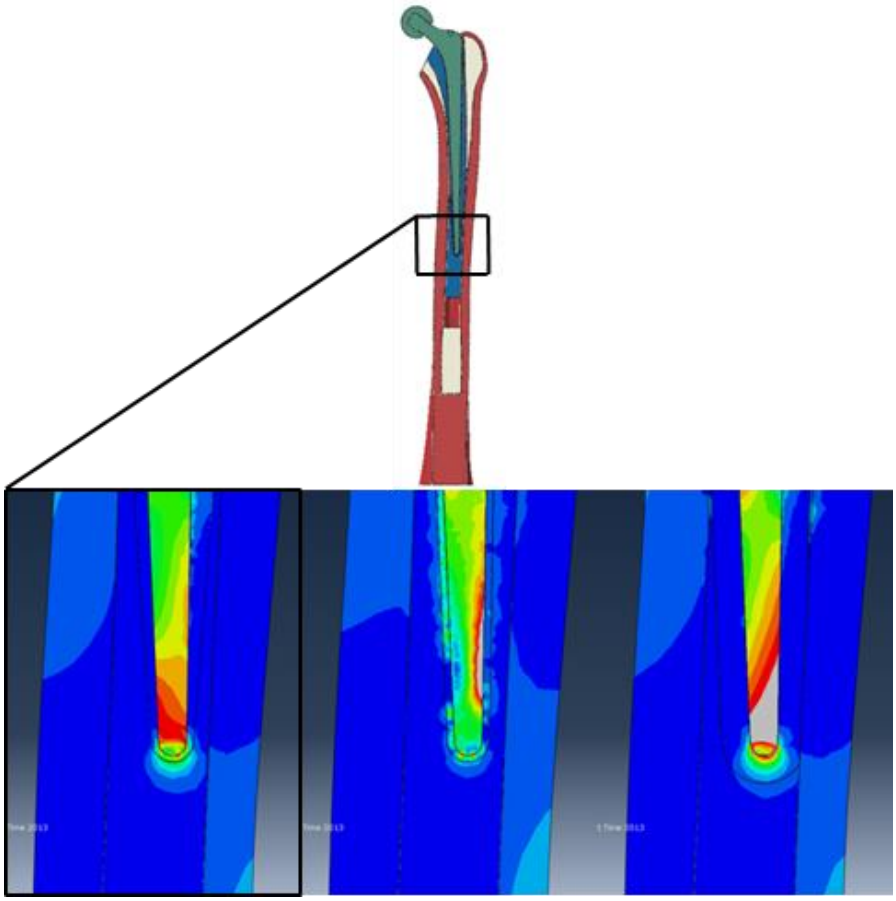

Figure 5.8 Von Mises stress in the cortex, cement and stem for the three cement distribution cases. Stresses shown between 0MPa (Blue) and 10MPa (Red), larger stresses are shown as grey. Left: Experimentally derived cement distribution. Middle: 1mm uniform cement. Right: 4mm uniform cement.

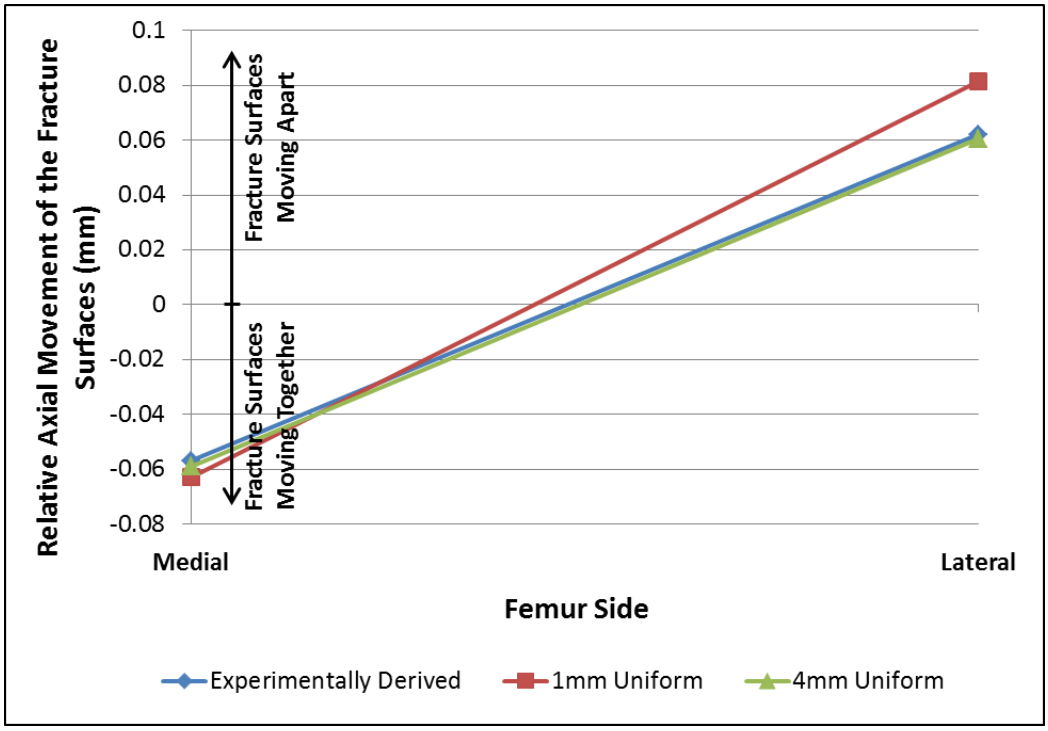

Figure 5.9 Relative axial movement of the medial and lateral sides of the fracture for all three cement distributions with a fracture gap.

The results for the relative axial movements of the medial and lateral sides of the fracture are given in Figure 5.9. The fracture movements on the medial side of the fracture were relatively similar for all cases. The fracture movements from the experimentally derived and 4mm uniform cement mantles were also relatively similar on the lateral side of the fracture. The 1mm uniform cement mantle resulted in the fracture surfaces moving further apart, by approximately 30%, on the lateral side of the fracture.

5.1.4 Discussion

The results for the models representing the experimentally derived cement mantle and the 4mm uniform cement mantle were relatively similar at the loading angle used in this study. There were differences in the fracture site shear movement and the cement stress distribution between cases, however the general trends and overall biomechanical response agreed well. This suggests that increasing the amount of cement providing proximal fixation had a limited mechanical effect on the treatment. The experimentally derived cement mantle geometry therefore appeared to provide sufficient support to the stem to be

suitable for further investigation. The good agreement between the results of the 4mm uniform cement mantle and the experimentally derived cement mantle also suggests that if the geometry for a realistic mantle is not available, for example during FE studies without comparable experimental specimens, a more simplified geometry can be used. This technique of representing the cement mantle with a uniform thickness was used previously by Mann et al. [164] with a 3mm thick uniform cement mantle to investigate methods for computationally representing the stem-to-cement interface. The differences between the 1mm cement mantle and the other two cases, however, does show that if a uniform cement mantle is to be used it must be sufficiently thick to provide adequate stem fixation.

The different cement mantle cases were evaluated with both a perfectly bonded, cement-filled fracture site and with a 1mm fracture gap. The sensitivity of the models to the cement mantle thickness and distribution was small when the cement-filled fracture configuration was used. With a fracture gap however notable biomechanical differences occurred between the cases. It therefore appears more useful to represent a ‘worst case scenario’ fracture configuration when evaluating the performance of the different cement mantle geometries rather than the most stable ‘best case scenario’.

An increased cement thickness under the medial side of the neck of the stem was seen in the experimentally derived cement mantle that was not present in the 4mm uniform cement mantle. This additional cement did not seem to provide a marked increase in stem fixation as the results from the experimentally derived and 4mm uniform cement mantles were relatively similar. The fact that the thicker cement under the neck of the stem did not seem to have a substantial effect on stem fixation may suggest that more cancellous bone could be retained clinically in the proximal region without adversely affecting stem survival. This additional cement may however provide improved support against stem subsidence over repeated loading so further investigation using a model that simulates cyclic loading, material failure and interface debonding would be required.

The axial stiffness of the different cases was not a useful indicator for differences between the cases. It was relatively insensitive to the cement mantle distribution, with the value changing by less than 10% of the average, despite the relatively large differences in fracture movement and cement stresses.

The use of a 1mm thick uniform cement mantle, with a gap fracture, resulted in a large increase in fracture site shear movement in the mediolateral direction. Specifically,

the proximal section of the femur moved laterally relative to the distal section. This appeared to be due to the fact that there was cancellous bone remaining on the medial side of the stem at the level of, and proximal to, the fracture site. This cancellous bone, due to its low Young's modulus, had the ability to compress and allow the medial cortex to move closer to the femoral stem.

The use of a 1mm thick uniform cement mantle, compared to the experimentally derived or 4mm uniform cement mantles, resulted in increased cement stresses at the tip of the femoral stem. These increased cement stresses occurred on the lateral side of the stem tip, unlike in the other two cases where the maximum cement stresses occurred under the tip of the stem. If large cement stresses under the tip of the stem lead to cement failure then the stem will subside distally. With a tapered stem this distal subsidence will result in increased support from the cement mantle above the stem tip and reduce the risk of continued damage (Figure 5.10). If cement failure occurs to the sides of the stem tip, however, this would result in an increased ability for the stem to 'toggle' within the femur. This toggling motion would be accentuated by the cyclic loading in alternating directions caused by many daily activities such as walking and would not be resisted due to the tapered stem geometry. It would therefore likely increase the risk of further cement damage and further stem destabilisation until the stem became loose. The increased stresses in the lateral cortex, caused by the stress riser effect of the stem tip, may also be of concern in osteoporotic patients with especially weak bone as they could increase the risk of re-fracture.

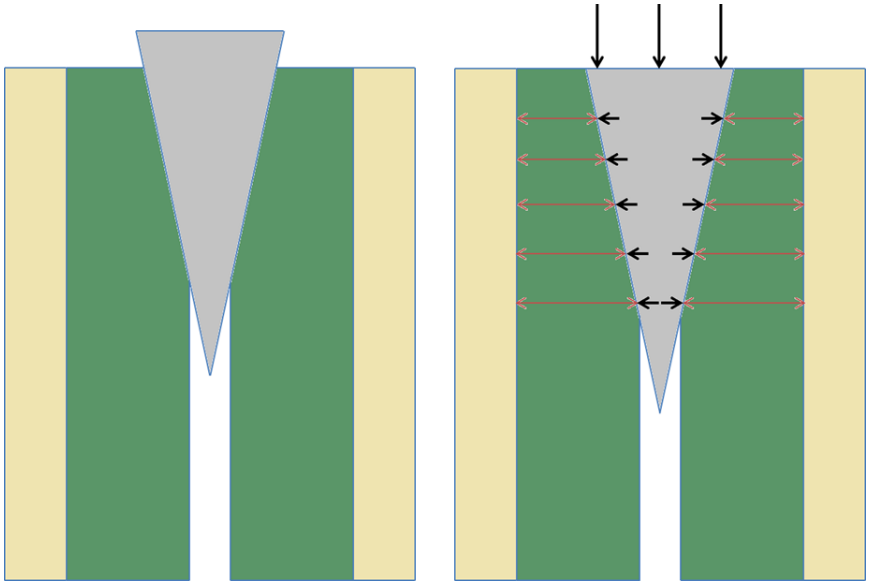

Figure 5.10 Illustration demonstrating how, with a tapered stem, subsidence of the stem into the canal can increase stem stability. Left: The initial unloaded position of the stem (grey) surrounded by cement (green) and the cortices (off-white). Right: The loaded (black) stem subsides, applying a transverse load on the cement which results in transverse compression of the cement (red). The cement therefore applies a transverse reaction force back on the stem, providing additional resistance to further subsidence. Additionally subsidence of the stem into the cement results in an increase in stem-to-cement contact area.

Given the idealised material and interface properties used to create the computational models it is likely that a real-life scenario would provide less resistance to the types of toggling motion that were indicated by the results of the 1mm cement mantle case. Insufficient proximal cement fixation may therefore be a more severe problem in reality than in the computational simulations.

The main concern regarding the 1mm uniform cement mantle was that it allowed this toggling motion to develop, which was signified by increased shear movements at the fracture site and increased stresses in the cement at the lateral side of the stem tip. This toggling motion appeared to develop due to a lack of support on the medial side of the stem at the level of, and proximal to, the fracture site. Simplifying the cement mantle to a uniform thickness, or otherwise altering the cement distribution, may therefore only be suitable if good cement-to-cortical bone fixation is maintained in this area. The loading orientation considered in this study however generated compression on the medial side of the femur, particularly in this region. It is therefore possible that the apparent importance of

the support in this area is only relevant to the loading scenario selected and other areas of cement support could prove to be more important at different loading angles.

High shear stresses were recorded at the interface between the cement and cortical bone for all cases. These stresses were large enough, compared to experimentally derived mechanical properties for PMMA cement [171, 172, 198- 200], to induce failure of the cement and/or cement-to-bone interface. If these values are representative they suggest that in the initial stages of post-surgical rehabilitation, before there has been the opportunity for bony ingrowth, it is possible that these interfaces would experience debonding or failure in some areas. This is made more likely due to the relatively low shear yield properties of the cement-to-bone interface, when compared to their compressive yield properties. The subsidence of the stem and cement into the femoral canal may therefore predominantly be resisted by friction between the cement and bone and the inhomogeneous geometry of the femoral canal. It is difficult to interpret the cement stress values clinically when they could not be validated from the experimental data, however the load case considered in this study included a relatively low magnitude hip contact force. Even if the computational simulations are underestimating the cement stresses, the fact that the in vivo scenario would be expected to induce higher peak loads [201] still means that these values would be concerning. The effect of a reduced thickness cement mantle has also been evaluated previously by Cristofolini et al. and Ramos et al. using experimental techniques [144, 145]. Similar to this study, they found that a thin cement mantle resulted in increased cement damage and increased stem subsidence, which supports the conclusions from this study and the applicability of the computational model.

5.2 Fracture Height

5.2.1 Motivation

When applying a long revision stem to treat a PFF, it is generally recommended that the tip of the stem bypass the fracture by approximately two femoral diameters (FD) [2, 17, 44, 136, 202]. Previous studies [53] have shown an increase in distal cement stresses corresponding to shorter bridging distances between the fracture site and stem tip. The

fracture height in the experimental specimens resulted in an 80mm fracture bridging distance (FBD) between the fracture and the distal stem tip, compared to a 34mm femoral diameter. Previous work has already investigated the optimal bridging distance and this has been supported by clinical outcomes. As insufficient bridging distances were unstable enough to lead to clinical failures an investigation into the effect of bridging distance on the current FE models was an effective way to test their sensitivity to a structurally relevant variable. The results from treatments which would typically result in clinical success could be compared against the results of treatments that would typically fail in practice. Key failure mechanisms could then be identified and appropriate output measures selected for quantifying success and failure. Additionally, the increased level of detail of these models compared to others previously tested [53] may mean that the mechanisms at work, and reasons for this optimal bridging distance, can be better identified and quantified.

5.2.2 Methods

The original fracture case resulted in a fracture bridging distance (FBD) of 80mm. There were two main options for investigating the effect of fracture bridging distance. Either the fracture height could be varied, such that the fracture moved closer to, or further away from, the stem tip or the fracture could be kept constant and the length of the stem could be altered. Neither technique can independently investigate the effect of fracture bridging distance. Moving the fracture site to a different location will alter the biomechanics of the femur and the bending moments around the fracture site, as well altering the geometry of the fracture site. Increasing the stem length will require additional cement in the medullary canal to compensate, will increase the overall stiffness of the construct and will move the tip of the femoral stem closer to the distal boundary conditions.

Part of the purpose of this study was to evaluate the performance of the computational models to a relatively well understood variable. Moving the fracture site required no new modelling techniques or significant changes to the computational model. Modifying the stem length, however, would have required altering both the stem geometry and cement distribution, moving the model further away from the validation case.

Computationally the fracture was therefore moved to four other locations in order to compare the effect of a reduced or increased FBD on the biomechanics of the fixation

construct. In total five fracture cases were created to produce 100, 80, 60, 40 and 20mm FDB, as shown in Figure 5.11. These FBDs were selected so that, although the biomechanics of the different cases may be affected by the changing location of the fracture site, the drastic differences in the amount of distal stem fixation should be the dominating factor. The models were loaded, as before, at 10° of adduction as recommended by the results of the model validation. As with the cement mantle case, it was seen in initial testing that the standard, bonded fracture provided such stability to the construct that differences between the models were extremely small. As such, the fracture gap configuration was used for these models in order to test the effect of FBD in a less idealised scenario. This gap fracture could be considered, for the simple transverse fracture being modelled, as a worst case scenario. Experimentally or clinically, as the stability of the fracture site increases, the changes described here would be likely to reduce in severity.

To compare with the five fracture cases, an additional model with a cemented long stem but no fracture was also created and tested. The Von Mises stresses were recorded along the medial and lateral sides of the stem. Average stress values for different heights along the length of the stem were then estimated by averaging between the medial and lateral sides of the stem. This provided a measure for how the stress in the stem varied along its length, irrespective of a fracture. The variation in stem stress at different locations was then compared against the changing bending moments around different points along the length of the femur. Given that stress is equal to the force per unit area, and that the variation of the cross-sectional area of the stem along its length was known, the force causing bending of the stem was also estimated. This was done by multiplying the calculated average stress values by the cross-sectional area of the stem at the corresponding point along its length. The difference between this estimated force and the bending moments at different points along the length of the femur were then also compared.

Cases with a reduced FBD were used to evaluate the usefulness of different outputs from the model for estimating failure. Outputs that were not sensitive to a drastically reduced FBD were unlikely to be good indicators for potential failure of the construct. Conversely outputs that clearly identified failure mechanisms in the 20-40mm FBD cases may also be useful indicators of the likelihood of failure in other, less well understood, comparisons.

Previous studies that have attempted to recommend an optimal fracture bridging distance when using a long revision stem have generally focussed on a few specific output measures. Mann et al. [53] investigated the relative motion between the cement and bone and the stresses in the cement. Panjabi et al. [136] recorded the lateral strain and used this to evaluate the effect of stem length. It is possible however that different output measures will result in different recommendations for the optimal fracture bridging distance, and that the best recommendation would come from considering the entire response of the model. Each output measure was used, as best as possible, to recommend an optimal FBD. The differences between these recommendations were compared to investigate whether the output measures used by a study will impact its conclusions in terms of the optimal FBD. To do this, linear or 2nd order polynomial lines of best fit, selected depending on the distribution of the data, were used to interpolate between data points. The outputs that were investigated, and the method used to suggest an optimal FBD, are listed in Table 5.1.

Table 5.1 The outputs investigated from the fracture height FE cases and the methods used to recommend, from these outputs, an optimal fracture bridging distance.

Output Metric	Method of Selecting an 'Optimal' FBD
Axial Stiffness	Maximise.
Stem Stress in Unfractured Case	Maximum FBD that would place the fracture around a minimally stressed region of the stem.
Fracture Movement (Axial and Shear)	Minimise.
Distal Stem Tip Movement	Minimise.
Maximum Von Mises Cement Stress (at Tip of Stem)	Minimise.
Maximum Compressive Cement Stress	Minimise.
Maximum Tensile Cement Stress	Minimise.
Maximum Shear Cement Stress	Minimise.
Maximum Cement-to-Bone Shear Stress	Minimise.

For some of the outputs listed in Table 5.1 the method of recommending an optimal FBD would not be suitable for any sort of clinical recommendation. For example simply

maximising axial stiffness does not take into account many of the biomechanical requirements for stable fixation. Minimising fracture movement is also a simplification as some fracture movement is required to induce healing, although the optimal values are not yet known. The aim of this comparison was to evaluate the relative usefulness of the different output measures, and test the sensitivity of recommendations for optimal FBD to the output measures investigated. As such these ‘best possible estimates’ were used despite having limited clinical applicability as this could be considered a limitation of that particular output.

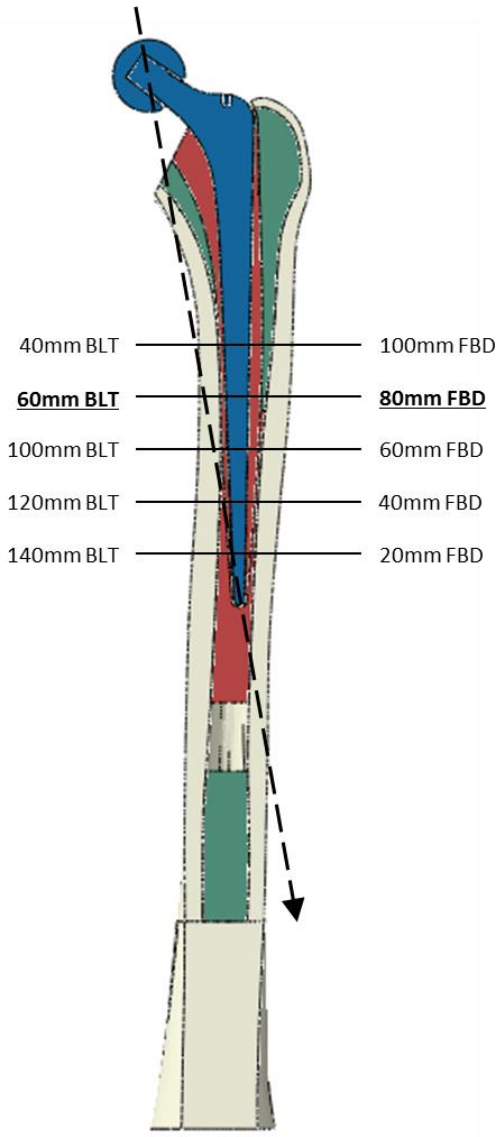

Figure 5.11 Locations of the five different transverse fracture cases. The five fractures are labelled with their distance below the lesser trochanter (BLT) and their distance from the distal stem tip (FBD). The baseline case, which corresponds to the experimental setup, is bold and underlined. The 10° offset load path is shown as a dashed line.

5.2.3 Results

The normalised bending moment distribution along the length of the femur, calculated from the perpendicular distance between the offset load path at 10° of adduction and the centroid of the transverse cross-section of the femoral canal, is given in Figure 5.12. The normalised average Von Mises stem stress along the length of the stem is also given, as well as the estimated force required to cause that stress.

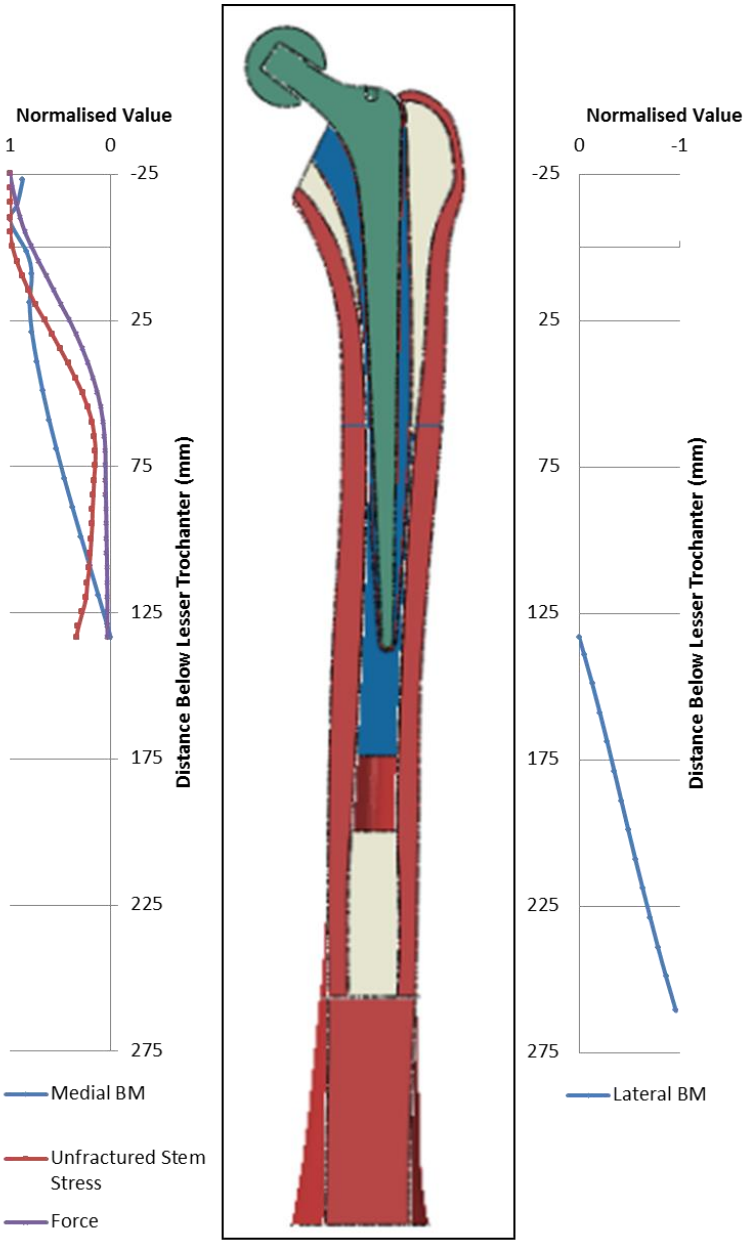

Figure 5.12 Normalised values for the bending moment, average Von Mises stem stress without a PFF and estimated force causing this stem stress along the axial length of the FE model. Bending moments causing medial compression are marked as positive and bending moments causing lateral compression are marked as negative. A to scale image of the computational mode, cut-through in the mediolateral plane to show the stem and cement, is given for reference.

A comparison of the FE axial stiffness values for all five fracture heights is given in Figure 5.13.

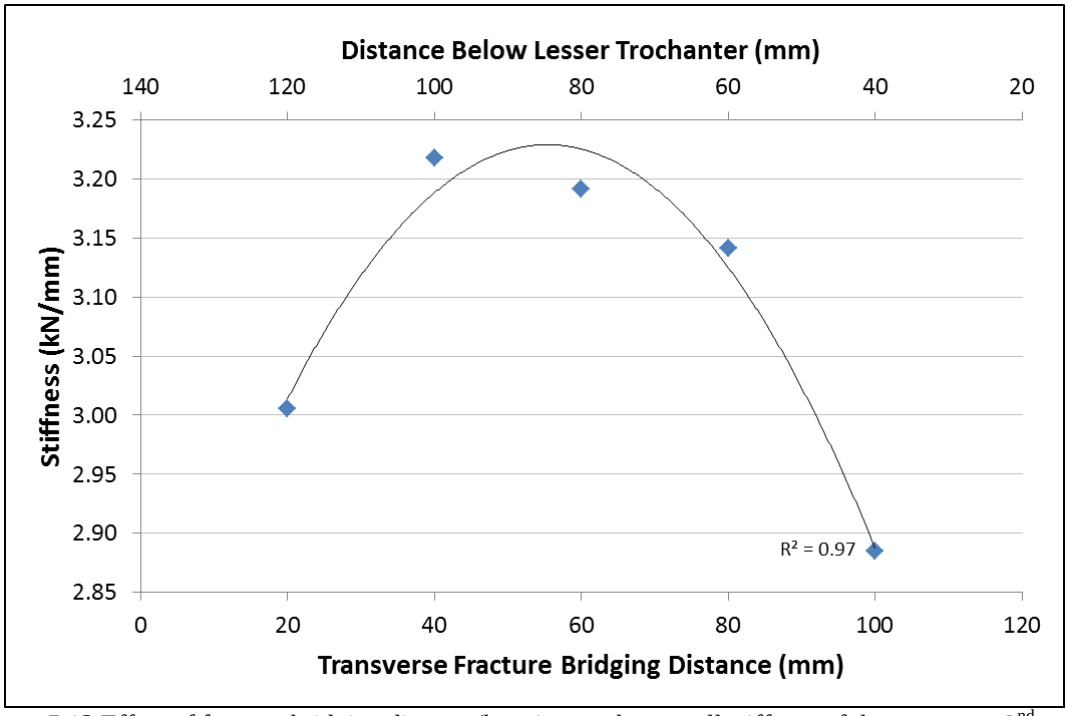

Figure 5.13 Effect of fracture bridging distance/location on the overall stiffness of the construct. 2nd order polynomial line of best fit with R^2 value included.

Axial stiffness and FBD appeared to have a non-linear relationship. Axial stiffness reduced with both a very short (20mm) or very long (100m) FBD. The labelled FBDs of 20, 40 60, 80 and 100mm correspond to fracture locations of approximately 40, 60, 80, 100 and 120mm below the lesser trochanter. The fracture case that resulted in the highest axial stiffness value was the 40mm FBD case while the 100mm FBD case resulted in the lowest axial stiffness.

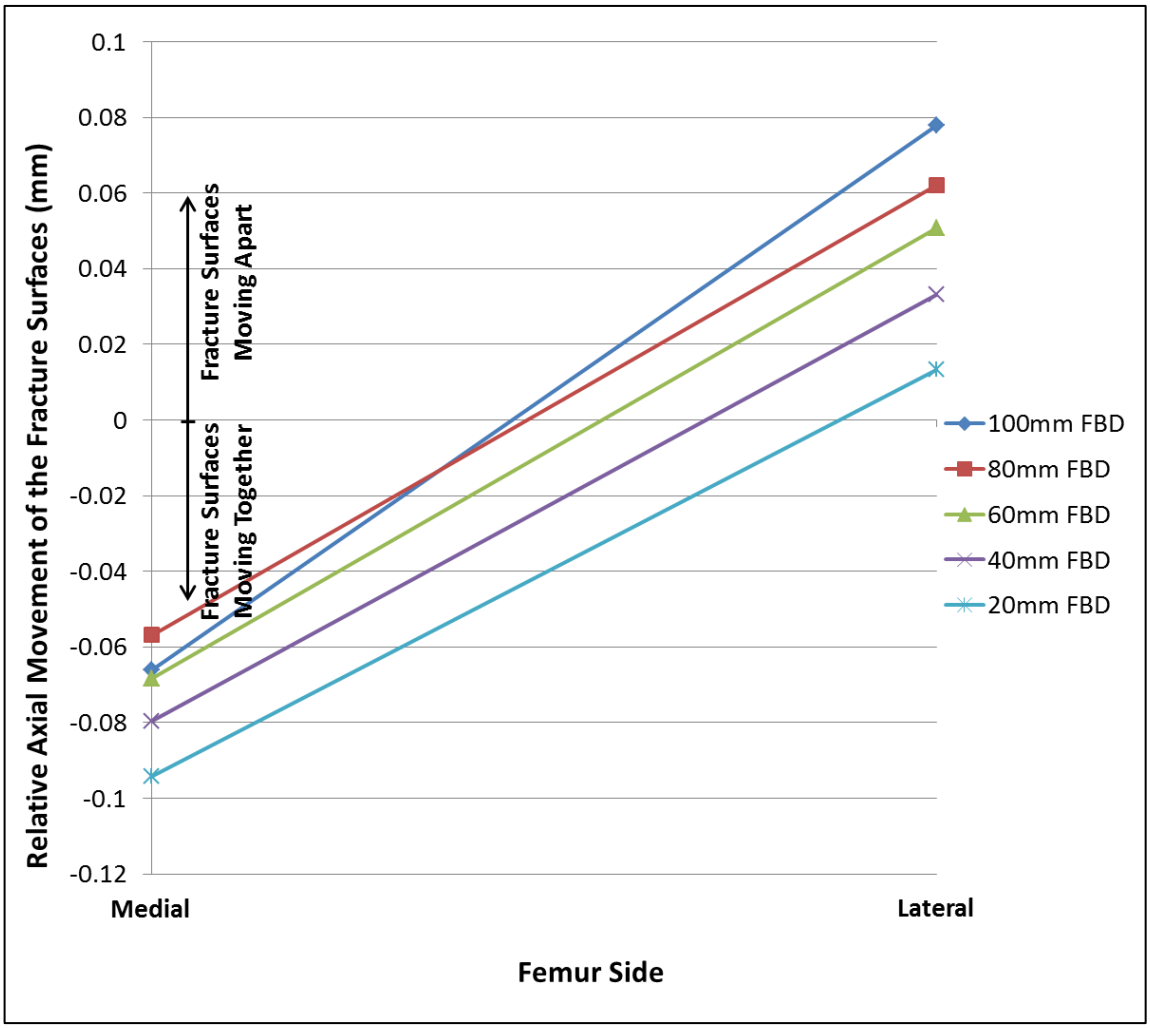

Figure 5.14 Relative axial movement of the medial and lateral sides of the fracture for the five fracture height cases. Positive values indicate that the fracture surfaces are moving apart. Negative values indicate that the fracture surfaces are moving together.

The relative axial movement of the medial and lateral sides of the fracture, for the five cases, is given in Figure 5.14. The 80mm FBD case resulted in relatively similar, but opposite, medial and lateral movements. Reducing the FBD did not have a notable effect on the relative angle of the fracture surfaces, in that the magnitude axial movement difference between the medial and lateral sides of the fracture was relatively constant. Reducing the FBD did, however, result in increasing compression on the medial side and reducing fracture opening on the lateral side. This indicates that the proximal fracture surface was, in total, moving closer to the distal fracture surface. Increasing the FBD to 100mm resulted in increased compression on the medial side and increased fracture opening on the lateral side. This resulted in the fracture surfaces remaining, on average, a similar distance apart when

compared to the 80mm FBD case. The relative change in angle of the fracture surface was higher for the 100mm FBD than for the 80mm FBD however. This may be related to the increased bending moments acting around the more proximal fracture site. The change in angle of the proximal fracture surface, relative to the distal fracture surface was 19% larger in the 100mm FBD compared to the 80mm FBD. The bending moment around the 100mm FBD fracture site was 20% larger than the bending moment around the 80mm FBD fracture site.

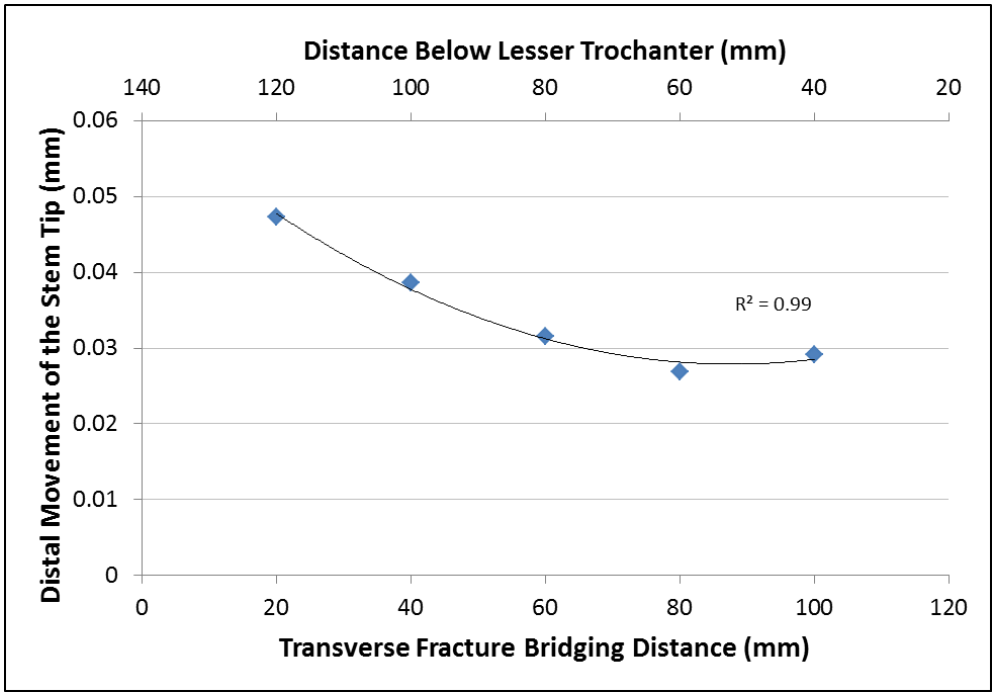

Figure 5.15 Comparison of the axial displacement of the distal tip of the stem against the corresponding fracture bridging distance/location for the five fracture height cases. 2nd order polynomial best fit line and R^2 value included.

The results for the distal movement of the stem tip are given for all five cases in Figure 5.15.The results showed a good agreement with a 2nd order polynomial line of best fit (R^2 = 0.99). This suggests that, at least in the computational models, the effect of the FBD on the distal movement of the stem tip could be reliably estimated and controlled. The lowest amount of distal stem tip movement occurred at a FBD of 80mm.

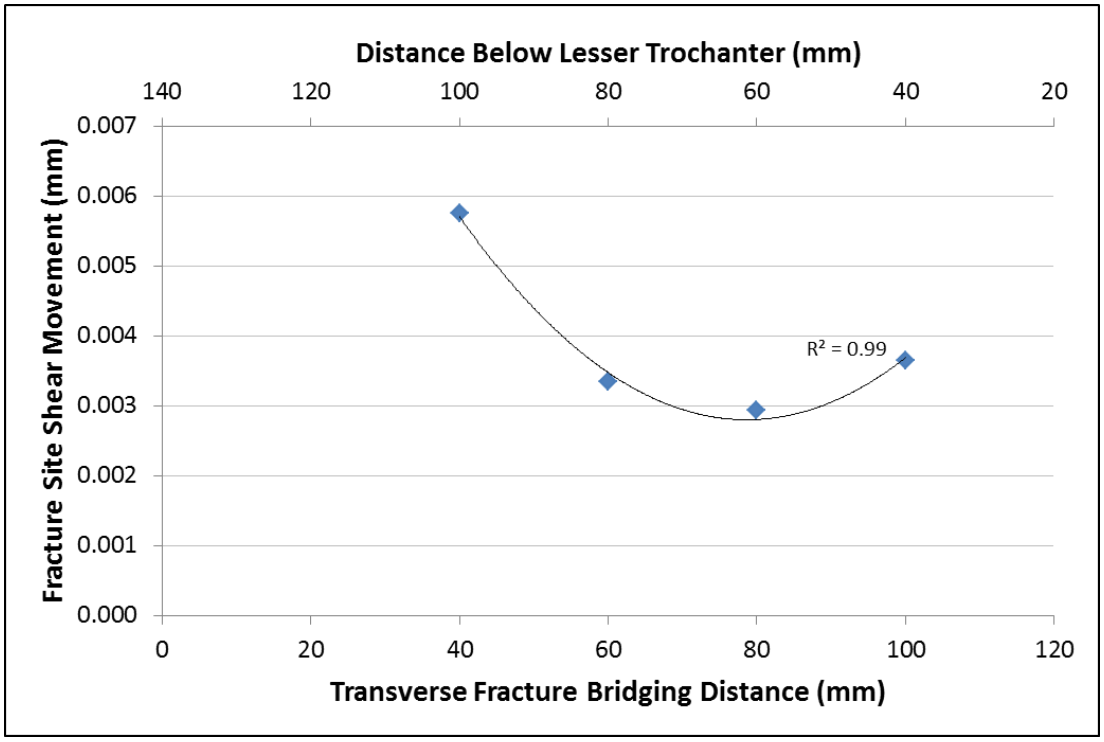

Figure 5.16 The relative transverse shear motion between the proximal and distal surfaces of the fracture for four of the fracture height cases, specifically the cases with FBDs of 40, 60, 80 and 100mm. 2nd order polynomial line of best fit with R^2 value included. Shear movement for the 20mm FBD case was 0.087mm.

The results for the fracture site shear movement for only four of the FBD cases, without the shortest bridging distance case, are given in Figure 5.16. The 20mm FBD case caused shear movement to increase by nearly 15x compared to the highest value for the other cases. Given that the 20mm case was not a clinically relevant one, as no PFF would be treated in this fashion, the results were plotted without it. Such a large value dominated the placement of a 2nd order polynomial line of best fit so leaving that data point out meant that the trends from the more relevant cases to be identified and focussed on. The shear movement was minimised by the case with a FBD of approximately 80mm.

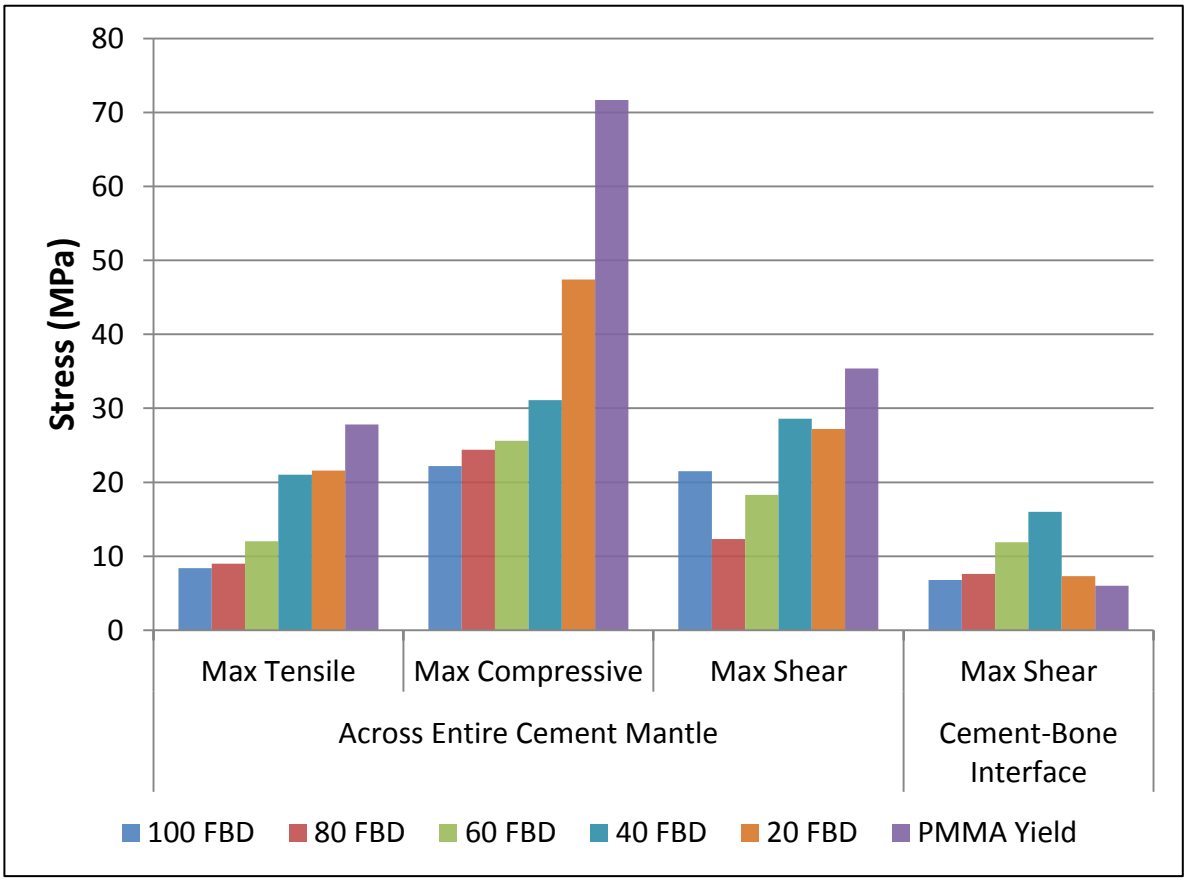

Figure 5.17 Maximum tensile, compressive and shear stresses in the PMMA cement for the five fracture height cases. 2nd order polynomial line of best fit with R^2 value included.

The maximum cement stress at the tip of the stem is given in Figure 5.17. The maximum tensile and maximum compressive cement stresses show a relatively clear trend of a decreasing FBD resulting in increasing maximum stresses. The maximum shear stresses in the cement mantle appeared to follow a non-linear relationship. The minimal shear stresses occurred with the 80mm FBD and both an increased or decreased FBD caused the shear stresses to increase. The maximum shear stresses recorded at the cement-to-bone interface were all larger than the yield shear stress for the cement-to-bone interface. Failure at this interface would therefore be expected. Again the effect of FBD on the stresses appeared to be non-linear. The maximum interface shear stresses occurred at the 40mm FBD case and either a reducing or increasing FBD then caused the maximum interface shear stress to reduce.

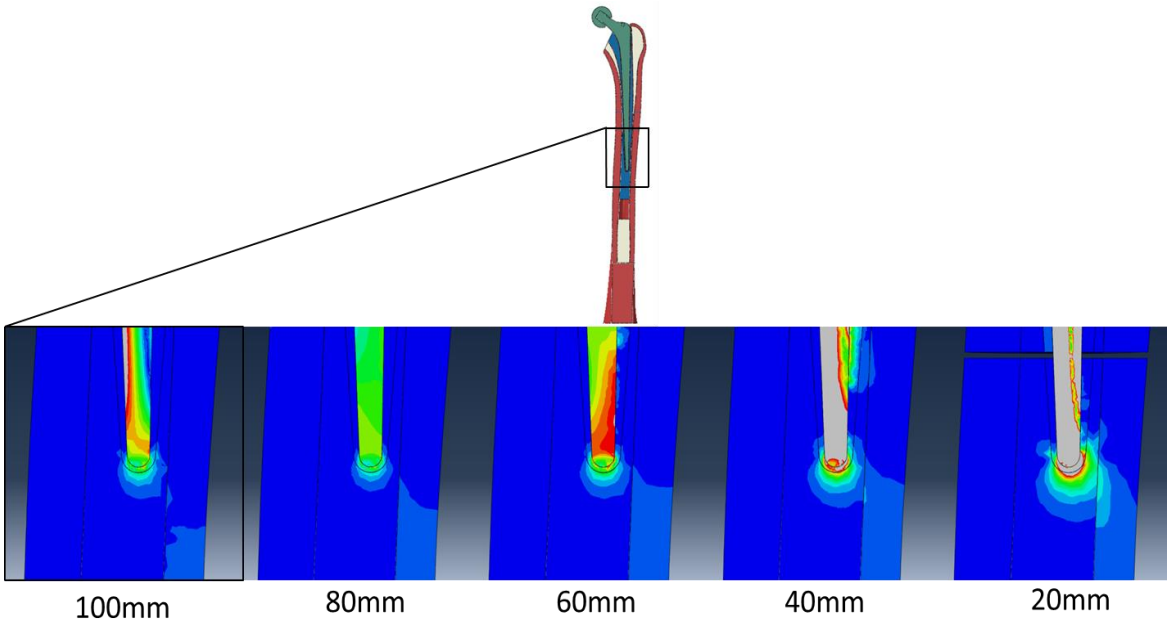

Figure 5.18 Von Mises stress maps for the stem tip and surrounding cement for all five fracture height cases. From left to right: 100, 80, 60, 40 and 20mm FBD. Stress contours displayed between 0 (blue) and 15 (red) MPa, stresses larger than this are shown grey. For each model the left side of the image is the medial side and the right side of the image is the lateral side.

The stress maps of the stem tips and surrounding cement are shown in Figure 5.18. These images show the stresses in a mediolateral slice through the tip if the stem in the stem, cement and cortical bone.

5.2.4 Discussion

The optimal bridging distances recommended by each model output, and the sensitivity of that output to FBD, are summarised in Table 5.2.

Table 5.2 Summary table of the recommended fracture bridging distances from each output measure and the sensitivity to FBD of each output measure. Sensitivity was calculated as the range across the five fracture height cases as a percentage of the average value.

Output Metric	Recommended FBD (mm)	Recommended FBD (FD)	Sensitivity of Output (Range as a % of the Average)
Axial Stiffness	56	1.6	11
Stem Stress in Unfractured Case	85	2.5	180
Axial Fracture Movement	80	2.4	365
Shear Fracture Movement	80	2.4	420
Distal Stem Tip Movement	88	2.6	57
Maximum Von Mises Cement Stress (at Tip of Stem)	80	2.4	103
Maximum Compressive Cement Stress	100	2.9	84
Maximum Tensile Cement Stress	100	2.9	92
Maximum Shear Cement Stress	80	2.4	76
Maximum Cement-to-Bone Shear Stress	100	2.9	93

Comparing the different output measures that were investigated the recommended optimal fracture bridging distance was seen to vary between 1.6 and 2.9 femoral diameters. The optimal fracture bridging distance recommended by a biomechanical study will therefore depend on the specific output that is being investigated. The actual optimal bridging distance will depend on a combination of factors, however, and studies should take care to consider as many relevant factors as possible.

All measures apart from the axial stiffness showed large differences (with a range of greater than 50% of the average value) when moving from a treatment that would be expected to heal (100-80mm FBD) to a treatment method that would be expected to fail

(20-40mm FBD). As such, the FE models developed here appear to be sufficiently sensitive to FBD that clinically relevant conclusions can be made.

The changes caused by an insufficient bridging distance were very sensitive to the fracture configuration. A very stable fracture site was only slightly affected by a shortened bridging distance, while a very unstable fracture site required the bridging distance to be carefully controlled.

Reducing the FBD resulted in exponentially increasing shear movements at the fracture site. The difference between the 40mm and 20mm FBD cases resulted in a 15x increase in fracture site shear movement. Shear movements have been shown to adversely affect fracture healing so this may have an impact on the likelihood of delayed-, mal- or non-union in clinical practice.

There was a linear relationship between the fracture bridging distance and the relative height of the fracture. There was also a linear relationship between the fracture bridging distance and the amount of stem-to-cement contact area (range 251-2176 mm^2), or cement-to-bone contact area that remained beneath the fracture site. As such all of the results presented above that showed a good agreement with FBD showed the same trends and good agreement when compared against either the fracture height or the distal surface area. This means that although the results for several outputs may compare well to FBD the cause for these changes may actually be due to either the location of the fracture or the amount of contact area supporting the stem and cement mantle.

Decreasing the FBD resulted in increasing distal stem stresses, increasing maximum cement stresses near the tip of the stem, a movement of the maximum cement stresses from underneath the stem tip to the lateral side of the stem tip and increased stresses in the lateral cortex at the height of the stem tip. All of these changes signify an increased likelihood of stem fixation failure due to a toggling motion and cement failure at the lateral side of the stem tip. In the 20mm FBD case the significantly increased cortical stresses also suggest an increased risk of re-fracture. This suggests that an important factor when selecting stem length is achieving sufficient support to prevent this toggling motion. The increased fracture site shear movements recorded in the 20 and 40mm FBD cases may also be another useful indicator of this toggling motion however.

The interface shear stresses between the PMMA cement and bone reached a maximum at the 40mm FBD. The 20mm FBD case experienced reduced interface shear

stresses despite providing less supporting contact beneath the fracture site. The 20mm FBD case caused the cement stresses around the stem tip to move from beneath the stem tip to the lateral side of the stem tip. It also resulted in a significant increase in fracture site shear movement. It is therefore possible that this decrease in interface shear for the 20mm FBD case is due to the reduced FBD causing the loading to act more in the transverse plane than in the axial direction. This increased toggling motion therefore induced higher compressive cement stresses at the stem tip towards the cortex and reduced shear stresses.

In a case with a cemented long stem and no PFF, the stresses in the stem varied along its length. If the stresses at different points along the femur vary then fractures at different locations will behave in different ways even when treated with the same bridging distance. The bending moments that would act around a fracture site also varied along the length of the femur. These two factors however did not appear to correlate particularly well with each other. This suggests that the changing stresses along the length of the stem, without a PFF, are affected by other variations such as the non-uniform geometry of the femur, cement and stem. There also appears to be a stress riser effect in the stem towards the distal tip, this may be related to the high stresses in the surrounding cement and could possibly be reduced by modifying the stem design.

The current recommendation of a two femoral diameter bridging distance seems reasonable based on the results of this study. This is further supported by the fact that the clinical recommendation of a two FD bridging distance comes not only from other biomechanical studies [2, 17, 53, 136] but also from analysing previous clinical outcomes [57].The optimal fracture bridging distance should ideally be evaluated for a range of fracture heights and a range of different stem designs however if the aim is to select the optimal treatment.

Although using a minimum suitable fracture bridging distance may be a clinically useful rule of thumb, a more accurate required stem length could be ascertained by suggesting two case specific parameters, based on actual biomechanical mechanisms. A maximum allowable force that can be required at the tip of the stem to counteract the toggling of the stem around the fracture site and a minimum amount of contact area in the distal portion of the femur, between the cortex and cement and between the cement and stem, to resist subsidence. The maximum force required to counteract toggling around the fracture site will be dependent on the bending moments acting around the fracture site and

will therefore vary with fracture height. It will also relate to the magnitude of the hip contact force and may therefore depend on the weight of the patient and their activity level. The stem-to-cement and cement-to-bone contact areas required to prevent subsidence would depend on the stem dimensions, the inner diameter of the femoral canal and, again, the weight and activity level of the patient.

5.3 Fracture Angle

5.3.1 Motivation

Based on the Vancouver classification system and treatment algorithm, fracture height is considered when selecting an appropriate PFF treatment method, however the type of fracture is not. Given that different fracture angles and types will likely create very different biomechanical situations, it is possible that they may respond differently to treatment. The sensitivity studies in Chapter 4 showed that the models were sensitive to the way in which the fracture site was represented and Section 5.2 showed that the results were also sensitive to the height of the fracture. The hypothesis of this study was that the results of the FE models would also be sensitive to the angle of the fracture, that this may also be biomechanically important and that it may affect the optimal treatment for each patient. A range of fracture angle cases were therefore created and tested using the computational models. Given that with the 10° of adduction loading angle, the majority of the bending acts in the mediolateral plane, these fractures were created at different orientations in this plane where the greatest differences would be expected.

5.3.2 Methods

From the baseline 0° transverse fracture orientation, fractures were created at ± 45° and ±60°. An additional fracture orientation of 70° was also generated. Due to interference with the proximal neck area however, this could only be created for the case with the fracture highest on the lateral side and lowest in the medial side. Fractures that were highest on the medial side and lowest on the lateral side are referred to as ML and negative.

Fractures highest on the lateral side and lowest on the medial side are referred to as LM and positive. The six fracture angle cases investigated are shown in Figure 5.19. As with the fracture height study in Section 5.2, the models were analysed with a 1mm gap at the fracture site to consider a structural worst case scenario and the models were loaded at an adduction angle of 10°.

The sensitivity of different model outputs to the angle of the fracture was evaluated in order to identify whether the angle of the fracture had an effect on the results. The sensitivity of the model to fracture angle was compared to the sensitivity of the model to the fracture height to identify whether the effect of fracture angle was biomechanically important. Potential indicators for failure that had been highlighted by the results of Section 5.2 (namely toggling of the stem and high cement stresses) were used to attempt to identify possible failure cases and failure mechanisms relating to the angled fracture cases described in this section.

Current clinical practice is to account for an angled fracture by applying the two femoral diameter bridging distance rule to the distal-most point of the fracture. Effectively the angle of the fracture is accounted for by considering the minimum fracture bridging distance (MFBD). A treatment rule of thumb, such as the recommendation for a two FD bridging distance, works by relating something that can be measured to the output(s) that need to be controlled. It does this by using an approximation. The current method for dealing with angle cases is to assume that their behaviour can be approximated based on the height of the distal-most point of the fracture. If the angle of the fracture has little to no effect on the biomechanics, then a range of different fracture angle cases will all behave in a similar manner when treated with the same MFBD. If the angle of the fracture has a significant effect on the biomechanics, however, these different fracture angle cases would behave differently despite being treated with the same MFBD. Therefore the sensitivity of the results to the angle of the fracture will change how reliably the effects of an angled fracture can be approximated using the MFBD.

If it is possible to reliably estimate the likelihood of failure based solely of the height of the distal-most point of the fracture, irrespective of angle, the resulting treatment recommendation will be suitable for most cases. If it is not possible to reliably estimate the likelihood of failure based on the height of the distal most point of the fracture, then the treatment selected using that approximation will be unsuitable for many cases. The ability

to approximate different outputs using 1) the minimum fracture bridging distance (equivalent to the distal height of the fracture), 2) the fracture bridging distance on one specific side of the femur, 3) the fracture angle and 4) the fracture angle and direction was compared using the R^2 values of either a linear or 2^{nd} order polynomial line of best fit. The aim of this comparison was to suggest a good metric that reliably represented the effects of changing fracture angles upon which a surgical rule of thumb could be based.

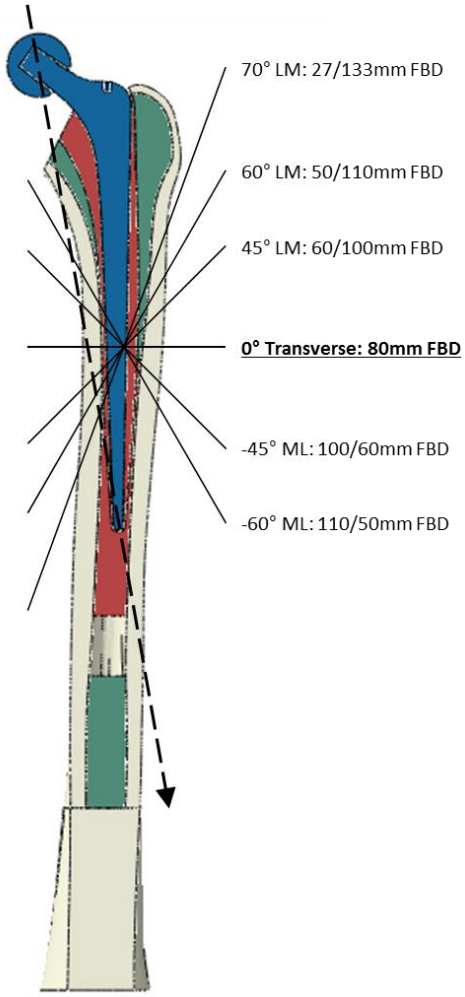

Figure 5.19 Locations of the six fracture angle cases investigated with the fracture angle and direction labelled. The baseline case is labelled bold and underlines and the 10° offset load path is shown as a dashed line. As well as the fracture angle the fracture bridging distances on the medial and lateral sides of the model are given.

5.3.3 Results

The axial stiffness results for the six fracture angle cases, compared against both MFBD and fracture angle with direction, are given in Figure 5.20. The results suggested a non-linear relationship between stiffness and fracture angle, with the construct stiffest with an approximately transverse fracture. As fracture angle increased, in either direction, the construct stiffness decreased. The maximum decrease in stiffness, caused by the 70 LM fracture, was only 8% compared to the transverse fracture however. The linear relationship between axial stiffness and MFBD suggests that a reducing MFBD results in a decreased axial stiffness.

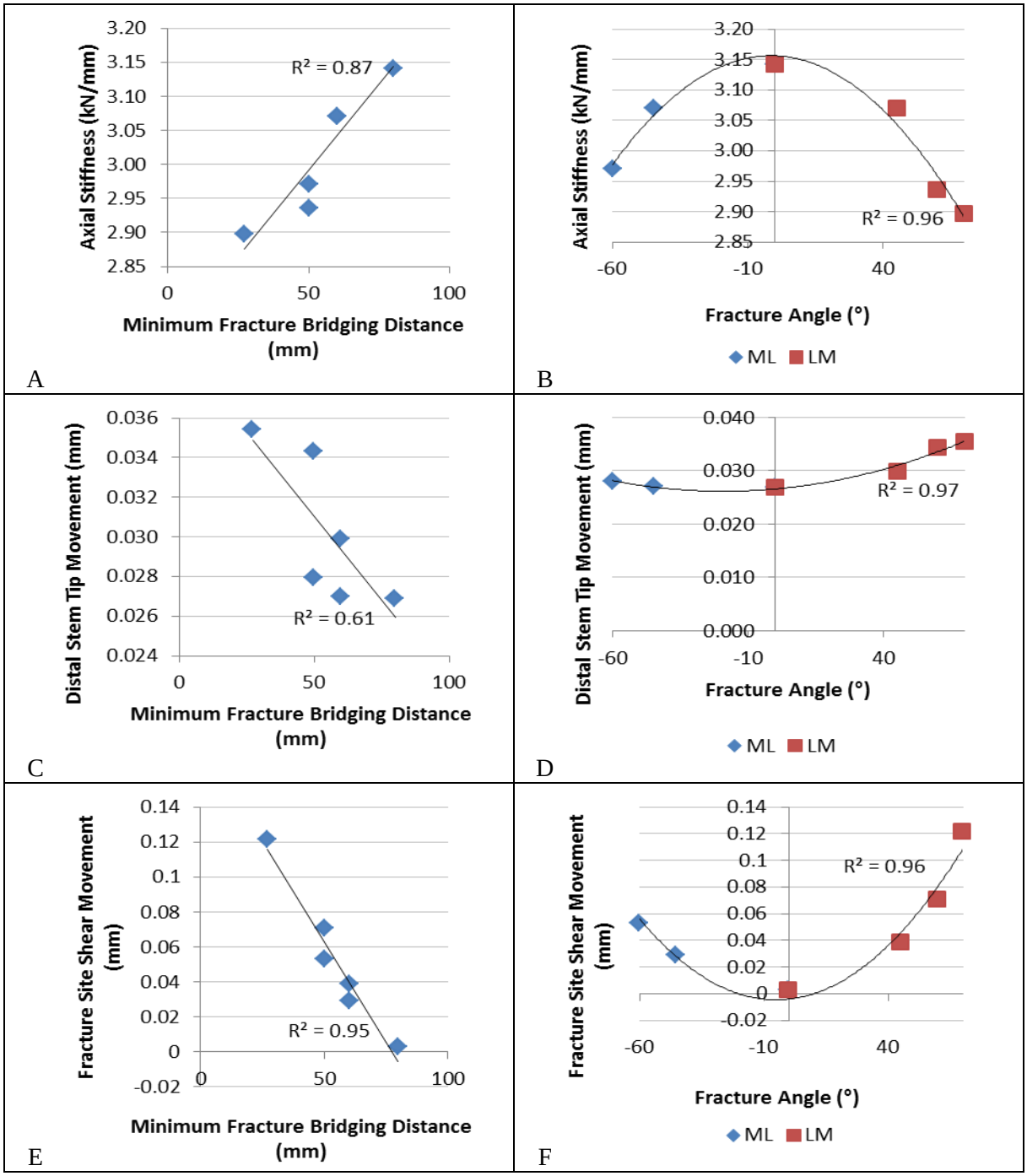

Figure 5.20 A+B: Axial stiffness of the six fracture angle cases compared against the MFBD and the fracture angle (with direction). C+D: Distal stem tip movement compared against MFBD and the fracture angle (with direction). E+F: Fracture site shear movement against MFBD and the fracture angle (with direction). A, C and E include linear lines of best fit with R^2 values. B, D and F include 2nd order polynomial lines of best fit with R^2 values.

The distal stem tip movement results are also given in Figure 5.20. The minimum amount of distal stem tip movement occurred at the transverse fracture case. Fractures in

the LM direction had a greater effect on the results than similarly angled fractures in the ML direction. The linear relationship between distal stem tip movement and MFBD suggests that a reducing MFBD caused increased distal stem tip movement.

The fracture site shear movement results are also given in Figure 5.20. The minimum amount of fracture shear movement occurred, again, at the transverse fracture case. The linear relationship between MFBD and fracture site shear movement suggests that a reducing MFBD results in increased fracture site shear movements.

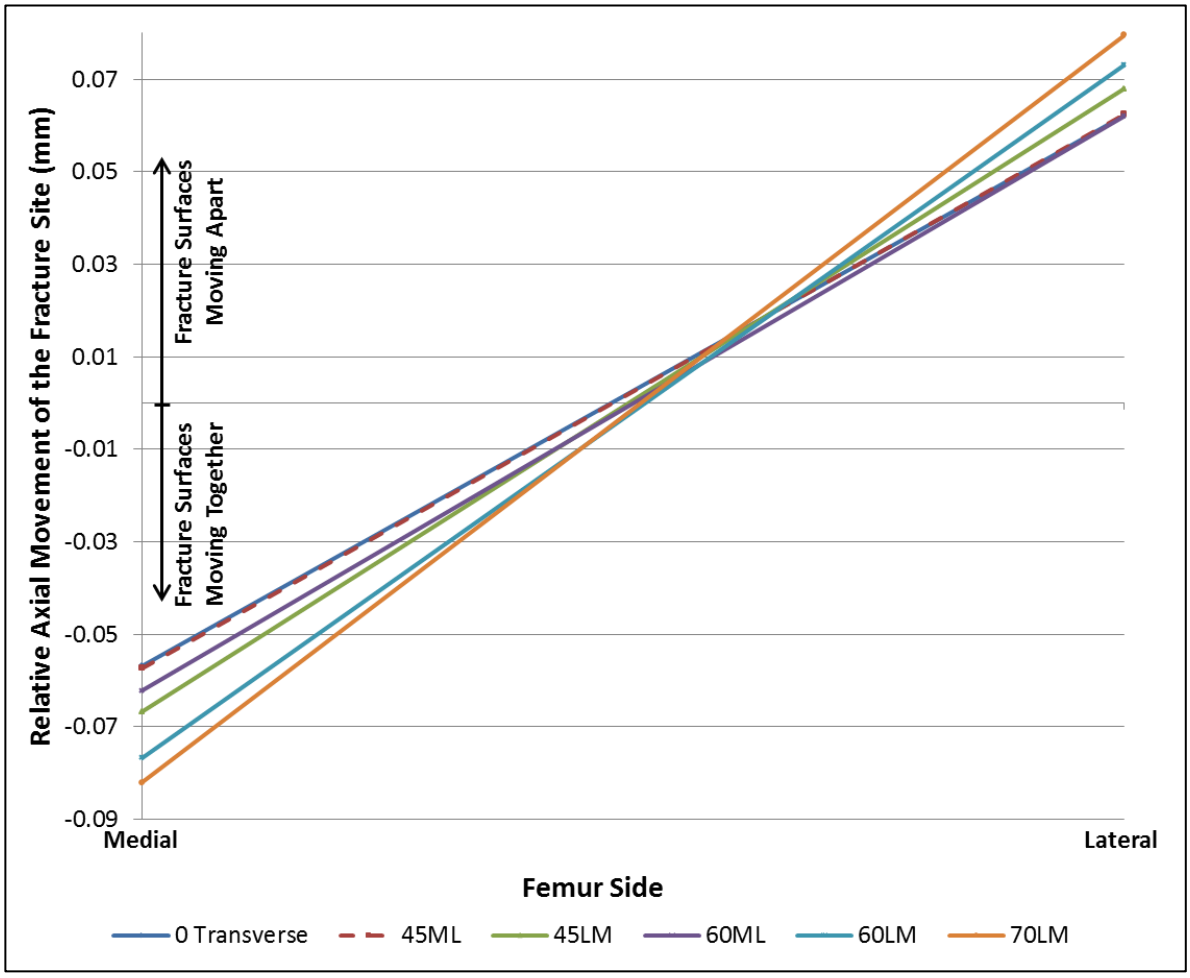

Figure 5.21 Relative axial fracture movements on the medial and lateral sides of the fracture for all angle cases.

The relative axial movement of the medial and lateral side of the fracture for all six fracture angle cases is given in Figure 5.21. The transverse fracture and 45ML fracture axial movements were relatively similar. The 60ML case experienced larger compression

on the medial side but a similar amount of fracture opening on the lateral side. This therefore caused the angle change of the proximal fracture surface, relative to the distal fracture surface, to increase. The LM fractures caused both the medial axial compression to increase and the lateral axial fracture opening to increase. This resulted in the LM fractures causing the relative angle change of the fracture surfaces to increase more than the comparable ML fractures. The average movement between the medial and lateral sides of the fracture remained relatively constant across all cases. This indicates that the proximal fracture surface was not, on average, moving closer to, or further away from, the distal fracture surface.

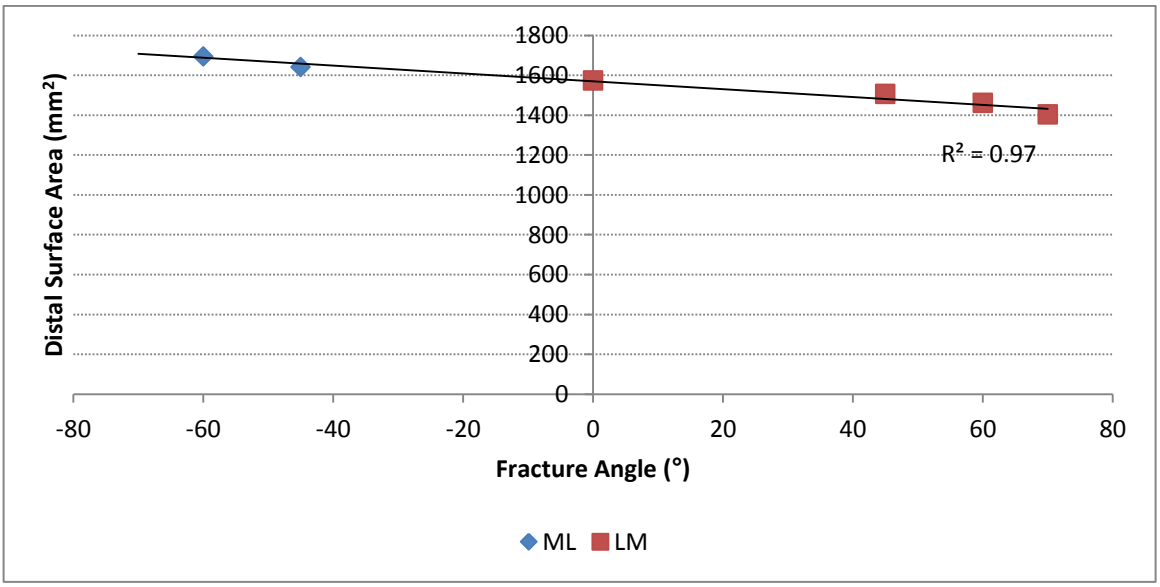

Figure 5.22 Comparison of the surface contact areas between the stem and the cement distal to the fracture for the six fracture angle cases. Linear best fit line and R^2 value included.

The effect of changing the angle of the fracture on the amount of remaining contact between the stem and cement below the fracture is given in Figure 5.22. The variation between cases is small, with the range across all cases 20% of the average value; however a reliable linear relationship exists. Fracture direction does seem to have a noticeable effect on the remaining contact area, with ML angled fractures resulting in an increase in contact and LM fractures resulting in a decrease in contact area. This difference is likely to be due to the inhomogeneous geometry of the femur, cement and stem and would be expected to vary depending on the initial fracture location and clinical case.

None of the outputs investigated, including the distal stem tip movement and maximum cement stresses, experienced a linear trend when compared against fracture angle. This meant that, for example, when comparing the distal stem tip movement against the distal surface area the relationship suggested that either increasing or decreasing the contact area from the transverse case resulted in increasing distal stem tip movement. There were therefore no results that could be linked to the increasing or reducing contact area in a logical way.

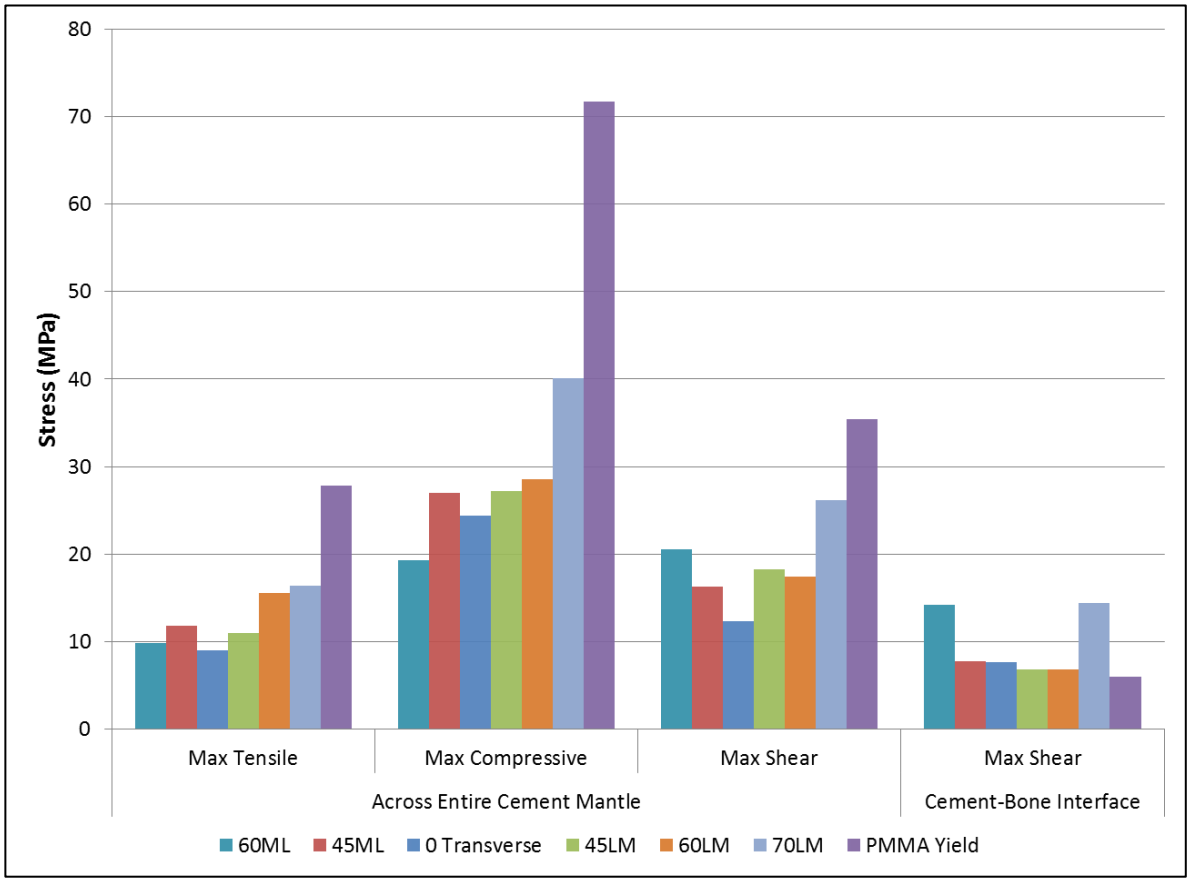

Figure 5.23 Comparison of the maximum tensile, compressive and shear stresses in the cement mantle for the six fracture angle cases. The maximum shear stresses at the cement-to-bone interface are also included.

The effect of the fracture angle on the maximum stresses in the cement is shown in Figure 5.23. In general the ML cases appeared to produce lower maximum tensile and compressive stresses than the LM cases. Increasing LM fracture angle resulted in an increase in both the maximum tensile and maximum compressive cement stresses. The maximum shear stress in the cement appeared to be more sensitive to ML fractures, with

fracture angle cases in either direction resulting in increased maximum shear stresses in the cement mantle. None of the reported cement mantle stresses were larger than the corresponding yield stresses of PMMA cement so failure would not be expected from these results. All of the cases however produced cement-to-bone interface shear stresses that were larger than the yield values for PMMA cement. Some degree of interface failure could therefore be expected for all cases. Regarding the interface shear stresses, the 45 degree fracture angles performed similarly to the transverse fracture case, as did the 60LM case. The 60ML case and 70LM case experienced interface shear stresses approximately twice those of the other cases however which may suggest that larger areas of interface failure would be expected.

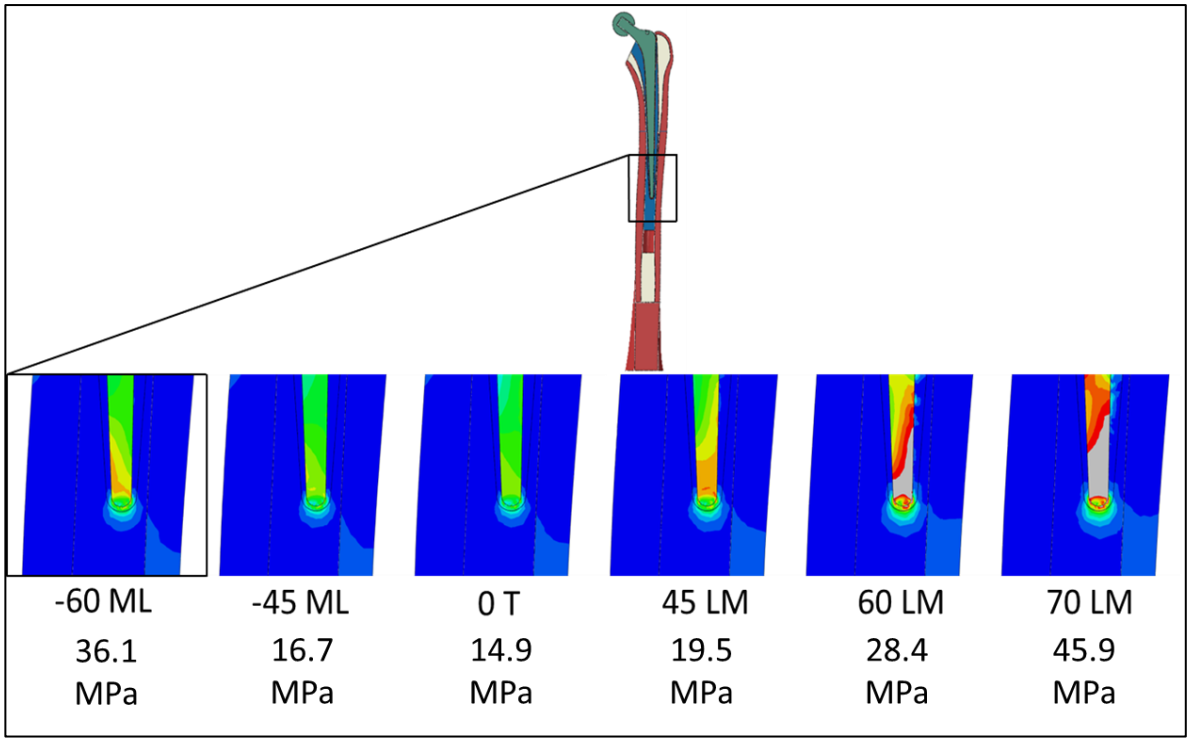

Figure 5.24 Cement and stem Von Mises stress maps, in the mediolateral plane, of the six fracture angle cases. From left to right: -60° ML, -45° ML, 0° Transverse, 45° LM, 60° LM and 70° LM. Stresses shown between 0 MPa (blue) and 15 MPa (red). Stresses above this value are shown grey. For all images the medial side of the femur is to the left and the lateral side is to the right. The maximum Von Mises cement stress for each case is included.

The cement and stem tip stresses are shown as stress maps in Figure 4.28. Starting from the 0° transverse fracture case, which displayed the lowest cement stresses, increasing

fracture angles in the ML direction resulted in increasing stem stresses on the medial side but little noticeable change in the cement or cortical stress distribution. Increasing fracture angles in the LM direction however caused more severe increasing stresses on the lateral side of the stem and increasingly radiating cement stresses. The stress riser effect of the stem tip on the lateral cortex also increased with fracture angle.

5.3.4 Discussion

The sensitivity of each output measure to the fracture height and fracture angle cases is given, in terms of the range of values found, in Table 5.3. In general the computational model was slightly less sensitive to fracture angle than fracture height. Sufficiently large differences occurred across the fracture angle cases however to suggest that the fracture angle may have a noticeable effect on the biomechanics of a potential treatment. Axial stiffness was relatively insensitive to both factors which limited its usefulness as a measure for evaluating the suitability of a treatment.

Table 5.3 Sensitivity of the various FE output measures to the angle of the fracture and the height of the fracture.

Output	Sensitivity of Output to Fracture Height (Range)	Sensitivity of Output to Fracture Angle (Range)
Axial Stiffness	2.9 – 3.2 kN/mm	2.9 – 3.1 kN/mm
Fracture Site Medial Axial Compression	56.9 – 94.1 µm	56.9 – 82.0 µm
Fracture Site Lateral Axial Opening	13.4 – 78.0 µm	62.0 – 79.5 µm
Fracture Site Shear Movement	2.9 – 86.6 µm	2.9 – 121.5 µm
Distal Stem Tip Movement	26.9 – 47.3 µm	26.9 – 35.4 µm
Distal Stem-Cement Surface Area	251 – 2176 mm^2	1403 – 1695 mm^2
Maximum Tensile Cement Stress	8.4 – 21.6 MPa	9.0 – 16.4 MPa
Maximum Compressive Cement Stress	22.2 – 47.4 MPa	19.3 – 40.1 MPa
Maximum Shear Cement Stress	12.3 – 28.6 MPa	12.3 – 26.2 MPa
Maximum Cement-to-Bone Interface Shear Stress	6.8 – 16.0 MPa	6.8 – 14.4 MPa

The variations in the axial movement of the medial side of the fracture site were relatively similar between the height and angle studies. The axial movement of the lateral side of the fracture was far more sensitive in the fracture height study however. This was due to the fact that while the fracture angle cases cause the amount of bending at the fracture site to change, leading to changes in the relative angle between the proximal and distal fracture surfaces, the fracture height cases led to increased movement of the proximal fracture surface towards the distal surface. The large fracture site shear movements experienced by the more extreme fracture height cases were likely indicators for potential fixation failure. The fact that the fracture angle cases led to even greater changes in shear

movement may suggest that appropriate fixation, for example by selecting a sufficiently long stem, is even more important when an angled fracture is present.

The maximum stresses in the cement and cement-to-bone interface were less sensitive to fracture angle than fracture height. The variations were still much larger than the estimated numerical error in the computational models (in the region of <15%) however. Some of the recorded stresses also moved sufficiently close to, or beyond, the failure properties of PMMA cement that the results indicate the potential for cement damage.

Table 5.4 Comparison of the ability of different metrics to approximate the response of the models to different fracture angle cases. Metrics considered are the MFBD, the side specific FBD, the angle of the fracture and the angle of the fracture including direction. The type of relationship between each output and each metric is specified and the level of agreement between the data and this approximation is given. An R^2 value of <0.6 is considered very poor, 0.6-0.7 is poor, 0.7-0.8 is reasonable, 0.8-0.9 is good and 0.9-1 is very good.

Output	MFBD	Side Specific FBD	Frac Angle	Frac Angle + Direction
Axial Stiffness	Linear, Good	Non-Linear, Reasonable	Non-Linear, Good	Non-Linear, Very Good
Max Cement Stress	Linear, Good	Non-Linear, Good	Non-Linear, Very Good	Non-Linear, Good
Fracture Shear Movement	Linear, Very Good	Non-Linear, Very Good	Non-Linear, Very Good	Non-Linear, Very Good
Fracture Compression	Linear, Poor	Non-Linear, Very Poor	Non-Linear, Reasonable	Non-Linear, Good
Fracture Angle Change	Linear, Poor	Non-Linear, Good	Non-Linear, Poor	Non-Linear, Very Good
Distal Tip Movement	Linear, Poor	Non-Linear, Good	Non-Linear, Poor	Non-Linear, Very Good
Max Femur Transverse Displacement	Linear, Reasonable	Non-Linear, Good	Non-Linear, Reasonable	Non-Linear, Very Good

The ability of some different metrics to approximate the way different outputs vary across a range of fracture angle cases are compared in Table 5.4. The metric MFBD effectively represents the concept of selecting a treatment based on the height of the distal-most point of the fracture. The side-specific FBD metric represents selecting a treatment based on the height at which the fracture meets one specific side of the femur. The fracture angle metric represents selecting a treatment based on the angle of the fracture, without

specifying the direction (treating ML and LM fractures as identical) and the fracture angle and direction considers both of these factors.

In terms of the outputs considered, the fracture compression is the average axial movement of the proximal fracture surface towards the distal fracture surface. The fracture angle change is the relative change in angle of the proximal fracture surface compared to the distal fracture surface, representing the amount of bending at the fracture site. Two key outputs that appeared to be good indicators for potential fixation failure, the maximum cement stress and the fracture site shear movement, have been highlighted.

Using the MFBD as a guide for how to treat angled fractured provided a reasonable approximation of how the maximum cement stresses and fracture site shear movements were affected by the different cases. As these are key outputs that can identify potential loss of fixation due to a toggling motion and cement damage near the stem tip this may be why using the MFBD has provided good results clinically. The MFBD provides a poor approximation of other outputs, such as the axial compression and relative angle change of the fracture site. These factors may not be as structurally important in terms of leading to failure but they will still have an effect on the biomechanics. Fracture movements affect fracture healing and as such using an approximation based on the MFBD might not give sufficient control to select a treatment to optimise this.

Using a side specific FBD provided improved agreement with some factors and reduced agreement with others. This may suggest that the changes to some outputs are dominated more by the fracture location on one side of the femur, as opposed to the distal-most point. Due to the fact that the fracture angles in this study led to equal but opposite changes to the FBD on the medial and lateral sides of the femur however it could not be ascertained which side was most important.

Using the fracture angle, without specifying the direction of the fracture, appears to perform similarly to the MFBD. Several outputs are poorly represented and this is predominantly due to the fact that ML and LM fractures behaved differently in several ways. The results were generally more sensitive to fractures angled in the LM direction than fractures angled in the ML direction and, just like when using the MFBD, this information was not captured in an approximation based on angle alone.

When considering both the angle of the fracture and its direction all outputs could be reliably approximated using 2^{nd} order polynomial lines of best fit. This may suggest that

a better treatment recommendation could be made using a rule of thumb that considered both the angle and direction of the fracture than by using either the FBD or fracture angle alone. Identifying the fracture configuration from radiographs, for example differentiating between an oblique or spiral fracture, may be difficult however which would make such a system more difficult to apply.

5.4 Conclusions

Based on the cement mantle geometry study presented in Section 5.1 the experimentally derived cement mantle geometry used in this study appears to provide sufficient stem fixation.

Representing the fracture site as cement-filled and perfectly bonded produced a model that was relatively insensitive to changes in cement mantle geometry. Computationally representing a less ideal case is recommended to produce distinctly different biomechanical responses.

A reduced thickness cement mantle resulted in an increased risk of cement damage, which could lead to stem loosening. It also increases the risk of subsidence of the stem and cement into the femur due to increased shear stresses at the cement-to-bone interface. A lack of cement on the medial side of the stem near to the level of the fracture site appeared to also allow shear movements at the fracture site which could lead to a toggling motion and increase the risk of fixation failure.

The FE models developed here appear to be sufficiently sensitive to FBD that clinically relevant conclusions can be made.

Using a minimum suitable fracture bridging distance may be a clinically useful rule of thumb, and the current two FD FBD recommendation seems reasonable. An important factor when selecting stem length is achieving sufficient support to prevent a mediolateral toggling motion. As opposed to specifying a minimum FBD a more accurate required stem length could possibly be ascertained by suggesting two case specific parameters, based on actual biomechanical mechanisms. A maximum allowable force that can be required at the tip of the stem to counteract the toggling of the stem around the fracture site and a

minimum amount of contact area in the distal portion of the femur, between the cortex and cement and cement and stem, to resist subsidence.

Measuring different output measures will lead to a different recommendation for the optimal fracture bridging distance. Care must therefore be taken to consider a suitably wide range of biomechanical responses that can identify the different ways that a treatment can fail.

The effects of different fracture angles can be approximately dealt with by assuming a generic minimum bridging distance starting from the distal-most point of the fracture. A more accurate approximation could be made by considering the direction, angle and distal-most point of the fracture. In general however the models were less sensitive to fracture angle than they were to fracture height.

The limitation that this study only considered loading at 10° of adduction may not have conclusively investigated the sensitivity of the models to fracture height or fracture angle. Different loading angles lead to different bending moment distributions along the length of the femur. A more comprehensive set of cases and loading orientations would therefore be recommended to investigate how these factors inter-relate.

6. Evaluating Alternative Revision Stem Fixation Techniques and Scenarios

The effects of fracture location, fracture bridging distance and fracture angle were investigated in Chapter 5. It was difficult to develop cases to differentiate the effects of each individual factor, however, without modifying the geometry of the femoral stem. Generating an angled fracture decreased the FBD on one side of the femur and increased it on the other. Generating different angled fractures with the same minimum FBD would have required also changing the fracture location. This would have limited the angled cases that could be created without interfering with the proximal region of the femur. In this chapter, two different stem lengths are considered. This allows the effects of fracture location, fracture bridging distance and fracture angle to be evaluated in a more independent way. For example, by using two different stem lengths a comparison can be made between fractures in two different locations while maintaining the same fracture angle and FBD. An osteoporotic femoral geometry is also presented, incorporating wider, thinner cortices and reduced material properties, to compare how the different treatment methods and fracture configurations respond to a patient with reduced bone quality.

6.1 Motivation

The lowered fracture height models described in Chapter 5 intentionally resulted in an insufficient bridging distance to test the effect this had on the results. In actual fact however this had two effects; the bridging distance was reduced but the fracture was also moved to a different location on the femur. A relatively simple investigation was undertaken to look at the differences in stress at different heights on the stem without a fracture and large variations along its length were found. The bending moments acting around the fracture site also varied along the length of the femur. This was due to the offset loading at the femoral head and 10° of adduction femur orientation. It is therefore likely that some of the differences between the fracture height cases were related to the fracture location rather than the distance between the fracture and stem tip.

The fracture angle models also described in Chapter 5 involved rotating the fracture line from the baseline case. The distal most point of the fracture therefore moved towards the tip of the femoral stem, reducing the fracture bridging distance on one side of the femur while increasing it on the other. Given that the current treatment recommendation is to bridge the fracture by at least two femoral diameters, this meant that the fracture had been insufficiently bridged. Insufficiently bridging similarly angled fractures in different directions was useful to identify any differences between those different directions, particularly in terms of where and how failure might follow. This comparison showed that fracture angle can have an impact on the results from the computational models. It also showed that fractures in different directions can behave differently under loading. In order to better understand and apply the conclusions from these studies, however, information was needed on more clinically relevant cases.

Appropriately treated angled fractures in the ML and LM directions were required to investigate whether a two femoral diameter FBD is suitable for all fracture angle cases. An appropriately treated transverse fracture at a different height was required to investigate whether a two femoral diameter bridging distance is suitable for all fracture locations.

The synthetic femurs, upon which the original experimental work and validated FE models were based, represent, in terms of both geometry and material properties, a relatively young and healthy patient. This was due to the relatively high material properties of the cortical and cancellous bone surrogates and the relatively thick bone stock [109]. Periprosthetic fractures, particularly those that require a revision stem, often occur in patients suffering from some degree of osteoporosis and or bone loss from previous surgeries. Given the lack of available synthetic femurs representing osteoporotic bone, analysing this experimentally would be infeasible. It could be considered computationally with relatively small changes to the FE model however. This would then allow for biomechanical comparisons with much greater clinical relevance. Additionally, little work has been performed in which osteoporotic bone was simulated, particularly in terms of combining the geometric and material property changes that occur, either experimentally or computationally. This may mean that there is room for improvement in the treatment methods used currently.

6.2 Methods

Using the original, healthy femoral geometry a model with a lengthened long stem was produced. The stem was lengthened from 205mm long to 245mm long. Models with 60° ML and 60° LM fracture angles, at the same location as before, and this lengthened 245mm stem were created, in order to show the effects of treating these fractures with an appropriate length stem.

A model with the 245mm stem and the transverse fracture lowered by 60mm was also produced. This tested the effect of an appropriately treated fracture at a more distal position on the femur. Treating the 60° angled fractures with the 245mm lengthened long stem resulted in a MFBD of 90mm (2.6 FD). Treating the 60mm lowered transverse fracture with this stem resulted in a FBD of 60mm (1.7 FD). These FBD do not match exactly to the two FD recommendation, however they were also selected to compare directly to the results from models shown in Chapter 5. The cases are shown in Figure 6.1.

The 245mm long stem was created from the CAD file of the original 205mm stem. An 85mm section of the stem, from 165 to 80mm above the distal stem tip, was removed and the remaining distal 80mm translated distally by 40mm. The two disconnected stem segments were then reconnected with a 125mm long lofted section. Due to the increased length with the same taper this created additional material, particularly in the proximal region, and the stem was trimmed back medially by 2.6mm between 170 and 110mm above the stem tip to prevent a reduction in the cement mantle thickness and impingement on the cortical wall. This process is illustrated in Figure 6.2. The cement in the medullary canal was also extended distally by a further 40mm to compensate for the lengthened stem.

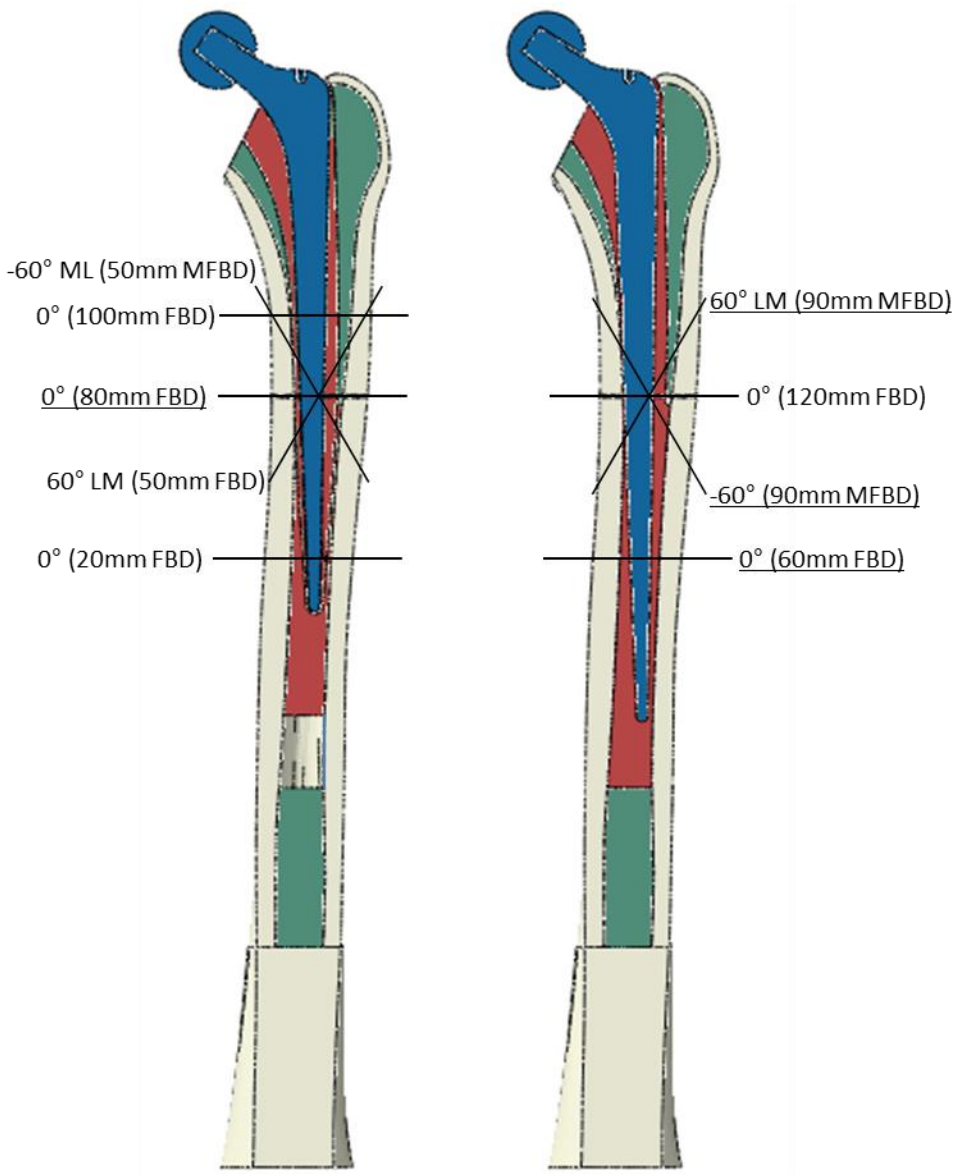

Figure 6.1 The nine fracture cases considered in this section. Fracture angle, direction and (minimum) fracture bridging distance are labelled. Left: Standard 205mm long revision stem. Right: Lengthened 245mm long revision stem. Cases which are being used in this study to represent a typical recommended treatment are underlined.

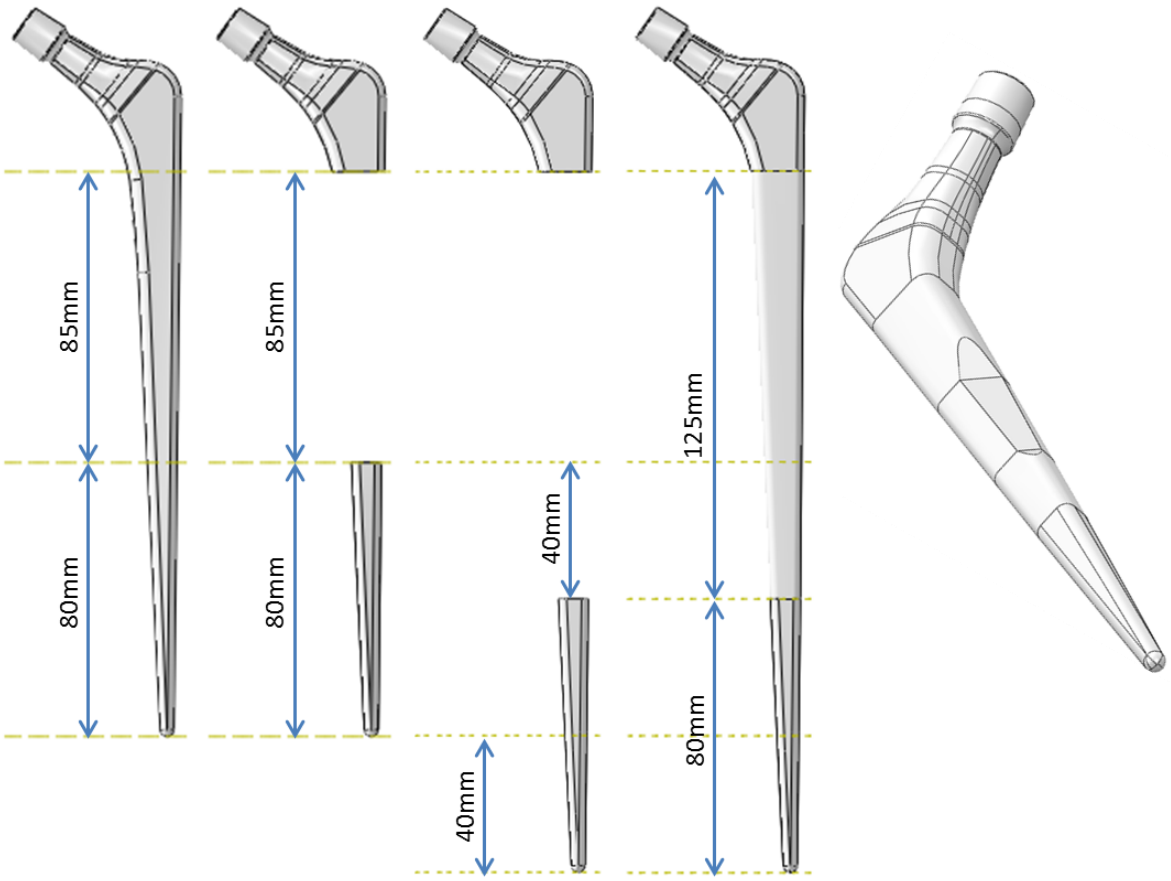

Figure 6.2 Development of the 3D model for the 245mm long revision stem. From left to right: An 85mm section of the stem was removed, the remaining distal portion was translated 40mm distally, the sections were united using a loft operation and finally the medial side was altered to prevent impingement on the cortices.

Several studies have used FE modelling to represent osteoporotic femurs in the past by varying the material properties [12,128]. To create osteoporotic patient models the Young's Modulus values of the cortical and cancellous bone were therefore altered to 12.4GPa and 67MPa respectively. The FE bone material properties used a linear elastic model without incorporating any form of failure criteria. The increased brittleness and reduced fracture resistance of the bone that is typically also associated with osteoporosis was therefore not accounted for [110]. It is unlikely however that under a single static toe-touch loading scenario failure would occur on any but the most unsuitable treatment options.

As well as reducing material properties, osteoporosis also has the effect of altering the femoral geometry. Bone resorption causes the intramedullary canal to widen. In order to compensate the diameter of the femur can increase in an attempt to regain some structural

integrity. A typical measure of the effect of osteoporosis is the cortical thickness ratio (CTR). The cortical thickness ratio is defined as the combined thickness of both cortices divided by the outer cortical diameter. A healthy femur would usually have a CTR of 0.5-0.6 while the CTR of an osteoporotic femur may be around 34% lower [203]. This percentage reduction in CTR has been used in computational and experimental studies [132] to investigate the effect of osteoporosis. As it is a reduction in the ratio of the outer and inner diameters it does not provide information on the relationship between expansion of the outer and inner diameters however. The expansion of the outer cortical diameter is an attempt to counteract the loss of stiffness caused by the cortical thinning. Changes to the inner and outer diameter of the femur were selected that reduced the CTR by approximately 34% but maintained the second moment of area of the cross-section of the femur. To do this, cross-sections of the femur were taken at 10mm intervals along the length of the shaft. In total 32 cross-sections were used to describe the geometry of the femur. Coordinate points defining the outer and inner edge were recorded and the centroid of each cross-section was calculated. The distance of each point from the centroid could then be scaled to create a series of altered cross-sections. The outer diameter of the femur was increased by 6.1% and the inner diameter was increased by 28.2%. Microsoft Excel (Microsoft, USA) was used to calculate the altered coordinate points and SolidWorks (Dassault Systèmes, USA) was used to build, from these points, a new 3D model of the femur. This allowed the testing of the effect of both osteoporotic geometry and material properties on, in effect, the femur from the original healthy case. Additionally, because the second moment of area remained constant the results could be interpreted with the knowledge that differences in the models were due to the shape and material properties alone. Transverse fractures were created at heights 60mm and 90mm below the lesser trochanter. These fractures were treated with both the 205mm long stem and the 245mm long stem. This resulted in in FBDs of 80 and 50mm on the 205mm stem and 120 and 90mm on the 245mm stem. The transverse fracture 60mm below the lesser trochanter was rotated, for both stem lengths, to produce angled 60ML and 60LM fractures. With the 205mm stem these angled fractures had a MFBD of 50mm and with the 245mm stem these angled fractures had a MFBD of 90mm. The eight cases are shown in Figure 6.3.

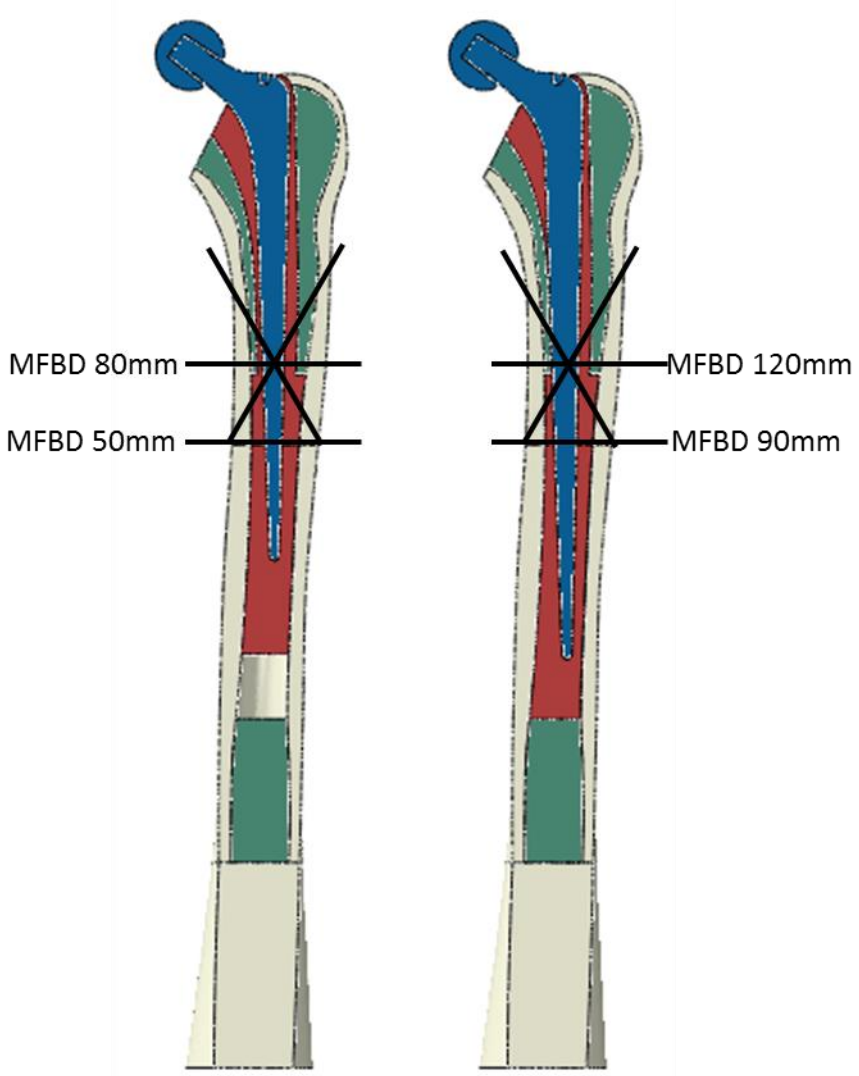

Figure 6.3 The eight fracture cases considered using the osteoporotic femoral geometry. This consisted of two transverse fracture cases and two 60° angled fracture cases for each stem length option.

The results from the models were used to evaluate differences between the cases in a similar way to the work presented in Chapters 4 and 5. Additionally the correlation between different output measures was investigated across the range of cases considered in this chapter. This was done to identify outputs that responded to changes in model configuration in a similar way. A change to the model, for example a reduced stem length, can lead to multiple independent mechanisms that will alter the response of the structure. For the case of a reduced stem length the reduced metalwork might lead to increased bending of the entire structure. The reduced surface area of the stem could also to increased relative motion of the stem into the femur. Different outputs may then be dominated by one

of the mechanisms or the other. Other outputs may be sensitive to both. These two mechanisms do not need to occur together however. For example reducing the Young's modulus of the cortical bone would also result in increased bending of the femur. It might not however result in increased relative motion of the stem into the femur. Outputs that are changing in response to similar mechanisms, irrespective of the cause, would correlate well with each other. Outputs that were changing due to different mechanisms that are behaving in different ways would not necessarily correlate as well. Identifying these mechanisms and understanding which outputs they affect, and how, could be useful in estimating the effect of different treatment options. It could be used to identify better, more focused, ways to measure these mechanisms and it could be used to assist the interpretation of results. This hypothesis is illustrated in Figure 6.4.

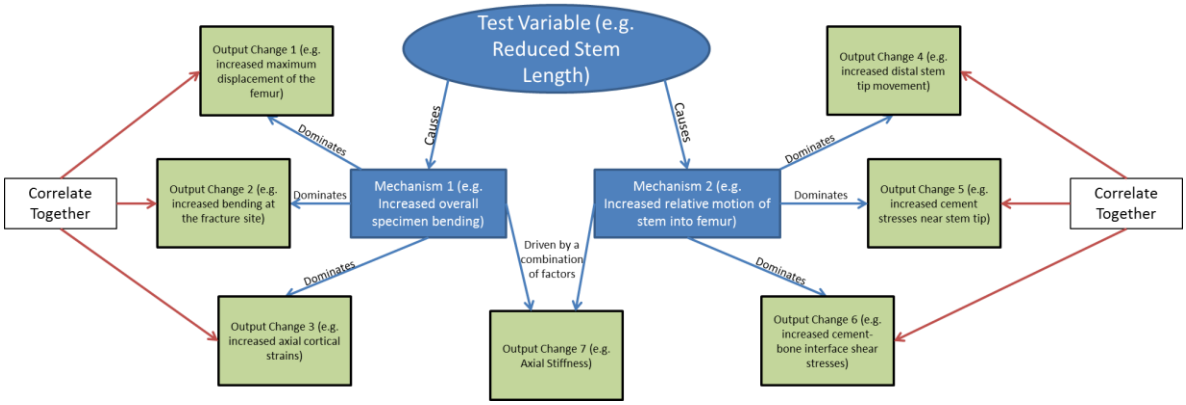

Figure 6.4 Diagram detailing how different mechanisms could dominate the response of certain outputs and how correlations between these outputs could be used to identify them.

6.3 Results

The results for all cases are summarised in Table 6.1.

Femur Type	Stem Length (mm)	Fracture Height Below Lesser Trochanter (mm)	Fracture Angle (°)	MFBD (mm)	Axial Stiffness (kN/mm)	Medial Axial Fracture Movement (µm)	Lateral Axial Fracture Movement (µm)	Distal Stem Tip Movement (µm)	Max Transverse Femur Bending (mm)	Fracture Site Shear Movement (µm)	Distal Surface Area (mm^2)	Max Tensile Cement Stress (Mpa)	Max Compressive Cement Stress (Mpa)	Max Shear Cement Stress (Mpa)	Max Cement-Bone Shear Stress (Mpa)
Healthy	205	40	0	100	2.88	-66	78	29	0.35	4	2176	8	22	22	7
Healthy	205	60	0	80	3.14	-57	62	27	0.34	3	1574	9	24	12	8
Healthy	205	120	0	20	3.01	-94	13	47	0.36	87	251	22	47	27	7
Healthy	205	60	-60° ML	50	2.97	-62	62	28	0.36	53	1695	10	19	21	14
Healthy	205	60	60° LM	50	2.94	-77	73	34	0.41	71	1461	16	29	17	7
Healthy	245	60	0	120	4.05	-37	43	20	0.25	2	2820	15	19	15	4
Healthy	245	120	0	60	4.34	-50	13	28	0.22	5	1048	7	29	18	13
Healthy	245	60	-60° ML	90	3.78	-44	47	21	0.26	33	2978	14	26	25	25
Healthy	245	60	60° LM	90	3.99	-42	50	22	0.27	32	2654	42	53	27	12
Osteoporotic	205	60	0	80	2.54	-86	98	35	0.46	41	1575	9	17	10	6
Osteoporotic	205	90	0	50	2.89	-85	52	41	0.38	6	795	16	22	25	7
Osteoporotic	205	60	-60° ML	50	2.54	-93	84	35	0.46	119	1714	11	16	11	6
Osteoporotic	205	60	60° LM	50	2.59	-90	95	39	0.47	97	1446	14	25	16	7
Osteoporotic	245	60	0	120	3.31	-60	69	26	0.33	31	2820	8	17	13	5
Osteoporotic	245	90	0	90	3.79	-51	35	28	0.27	4	1827	10	20	12	5
Osteoporotic	245	60	-60° ML	90	3.28	-67	62	27	0.33	78	2980	8	15	12	9
Osteoporotic	245	60	60° LM	90	3.41	-56	67	29	0.32	50	2652	10	20	11	6
											PMMA Yield Stress (MPa)	27.8	71.7	35.4	6

Table 6.1 Comparison of results for different height and angle fracture cases between the original and additionally lengthened stem and healthy and osteoporotic femur. Case descriptions highlighted red denote appropriately treated transverse fractures and case descriptions highlighted blue denote appropriately treated angled cases, as recommended clinically.

The relative axial movement of the fracture surfaces for cases investigating the effect of a more distal fracture, treated with a longer stem, are given in Figure 6.5. Cases with a FBD of as close as possible to two femoral diameters were compared on the 205mm and 245mm long revision stems. Appropriately treated fractures at two different fracture heights were therefore compared. Both the original, healthy, femoral geometry and the osteoporotic femoral geometry were used.

Key results for these same cases, selected from Table 6.1, are summarised in Figure 6.6. The maximum tensile, compressive and shear stresses in the cement, and the maximum shear stress at the cement-to-bone interface are compared to the failure properties of PMMA. The maximum reported cement stresses were all less than 50% if the corresponding PMMA yield stress. The maximum reported shear stress at the cement-to-bone interface was either similar to, or larger than, the yield stress, implying that failure would be expected. In nearly all cases the more distal fracture resulted in larger maximum stresses. The less distal fracture resulted in a lower maximum tensile stress in the healthy bone and a lower maximum interface shear stress in the osteoporotic bone, however. The maximum compressive and shear cement stresses, and maximum interface shear stress, were larger in the healthy bone than in the osteoporotic bone.

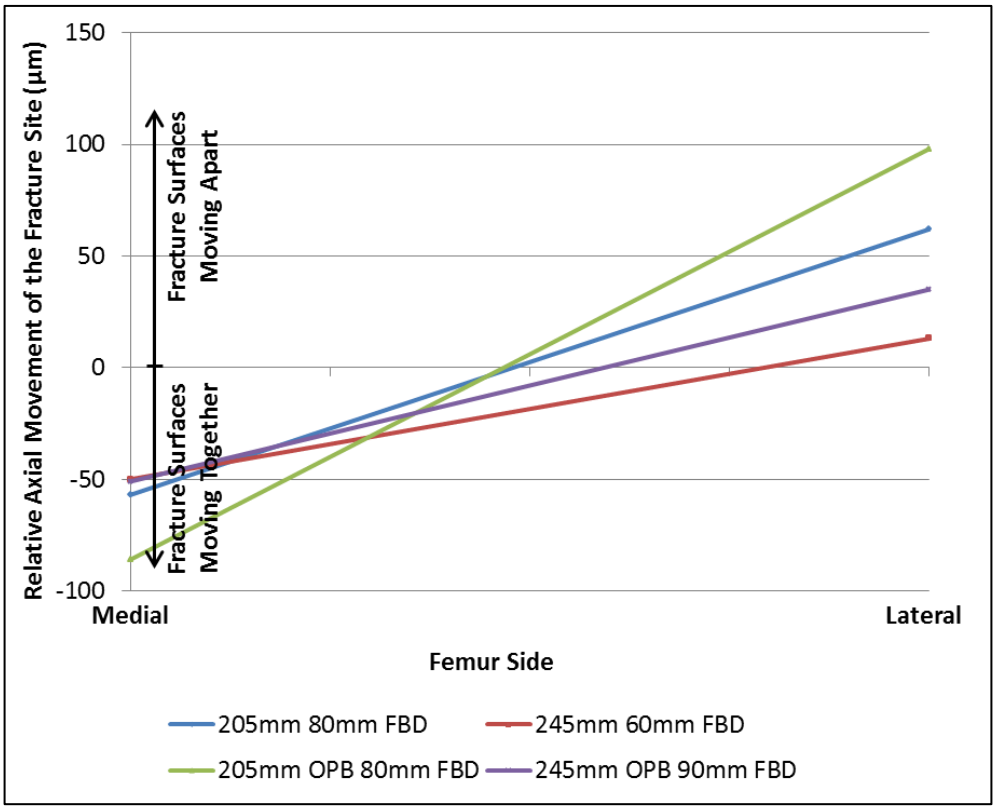

Figure 6.5 Effect of a more distal fracture, treated with a longer stem, on the relative axial fracture movements on the medial and lateral sides of the fracture. Compared for both the healthy and osteoporotic cases. Cases are described in terms of the stem length, bone quality and FBD.

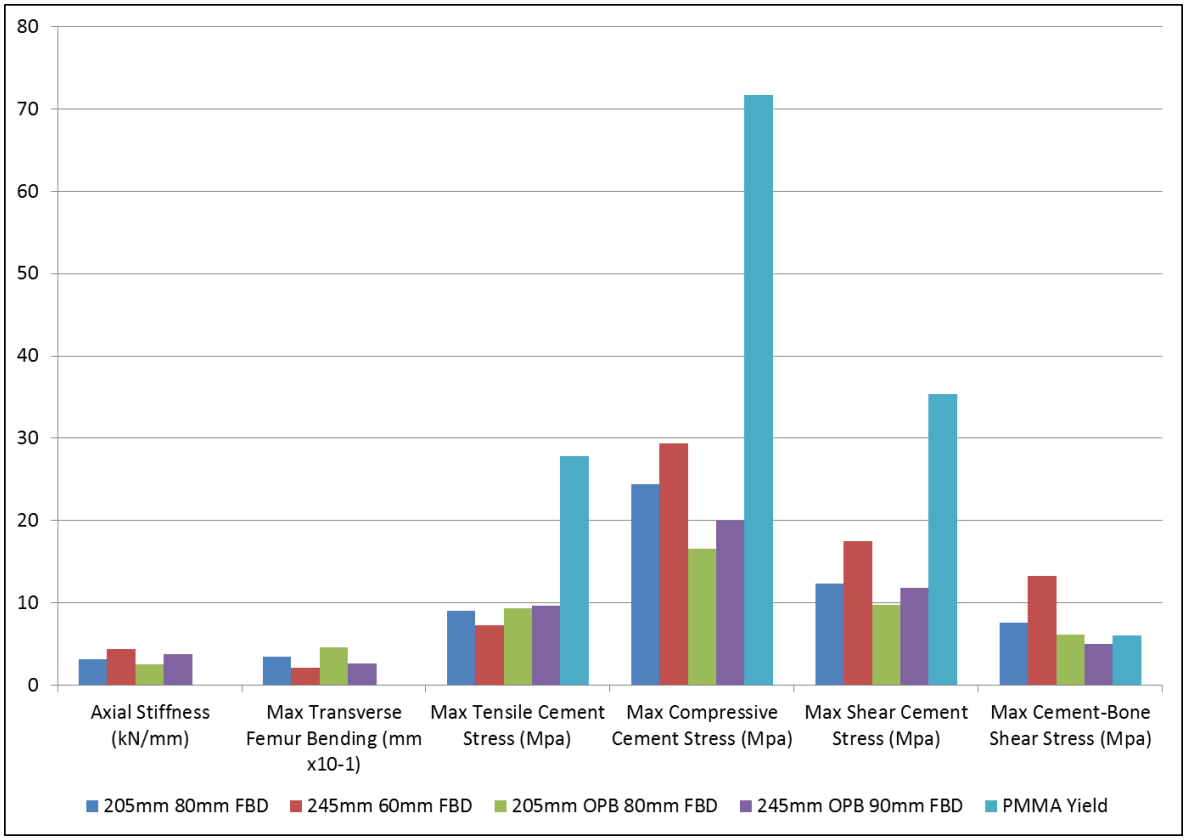

Figure 6.6 Effect of a more distal fracture, treated with a longer stem. Compared for both the healthy and osteoporotic cases. Results given for axial stiffness, maximum displacement of the medial side of the femur in the transverse plane, maximum cement stresses and maximum cement-to-bone interface shear stress. Cases are described in terms of the stem length, bone quality and FBD.

The relative axial movement of the fracture surfaces for cases investigating the effect of using a longer than two femoral diameter FBD are given in Figure 6.7. Cases with a FBD of as close as possible to two FD were compared to cases with a longer than two FD FBD on the 205mm and 245mm long revision stems. Both the original, healthy, femoral geometry and the osteoporotic femoral geometry were used.

Key results for these same cases, selected from Table 6.1, are summarised in Figure 6.8.

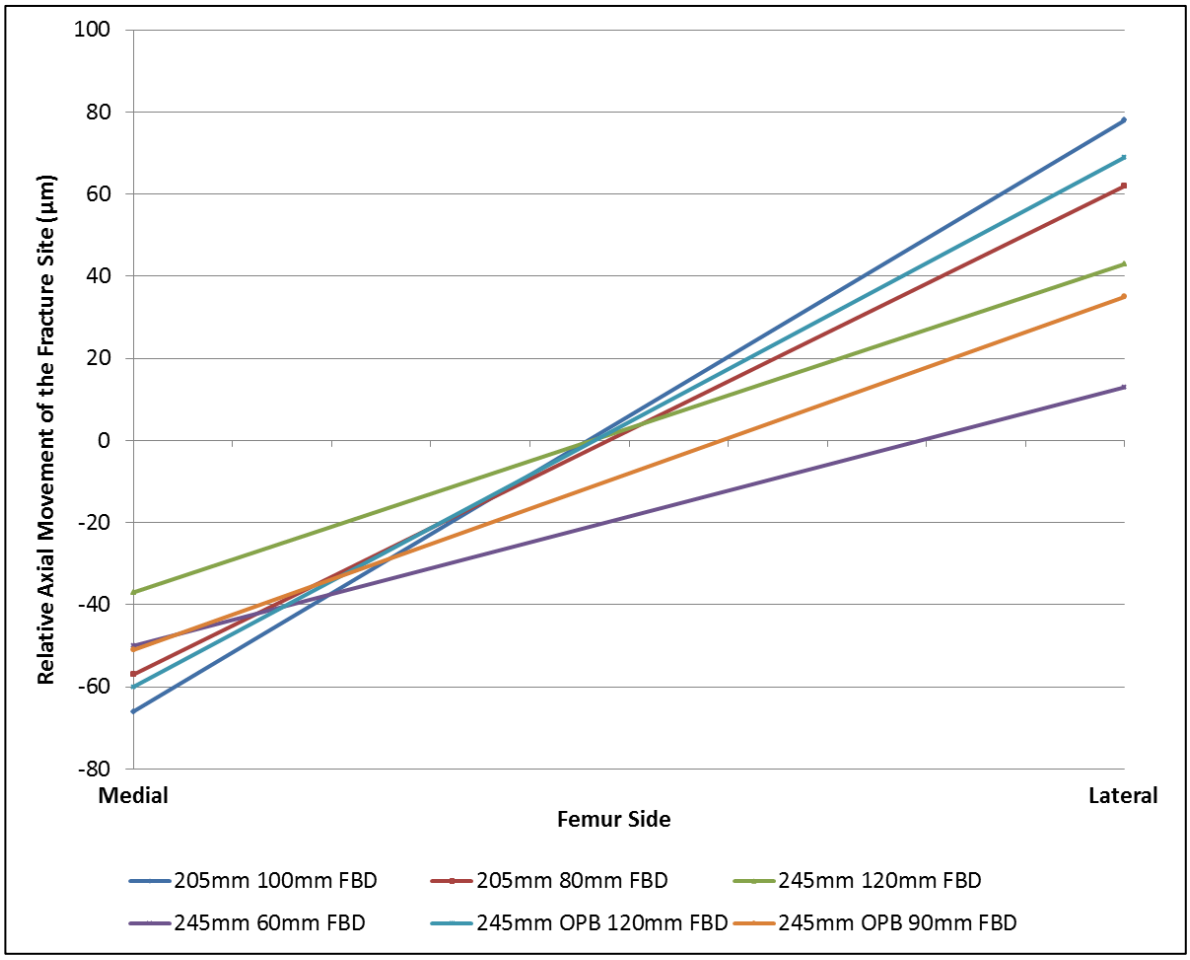

Figure 6.7 Effect of a longer FBD on the relative axial fracture movements on the medial and lateral sides of the fracture. Compared for both the healthy and osteoporotic cases. Cases are described in terms of the stem length, bone quality and FBD.

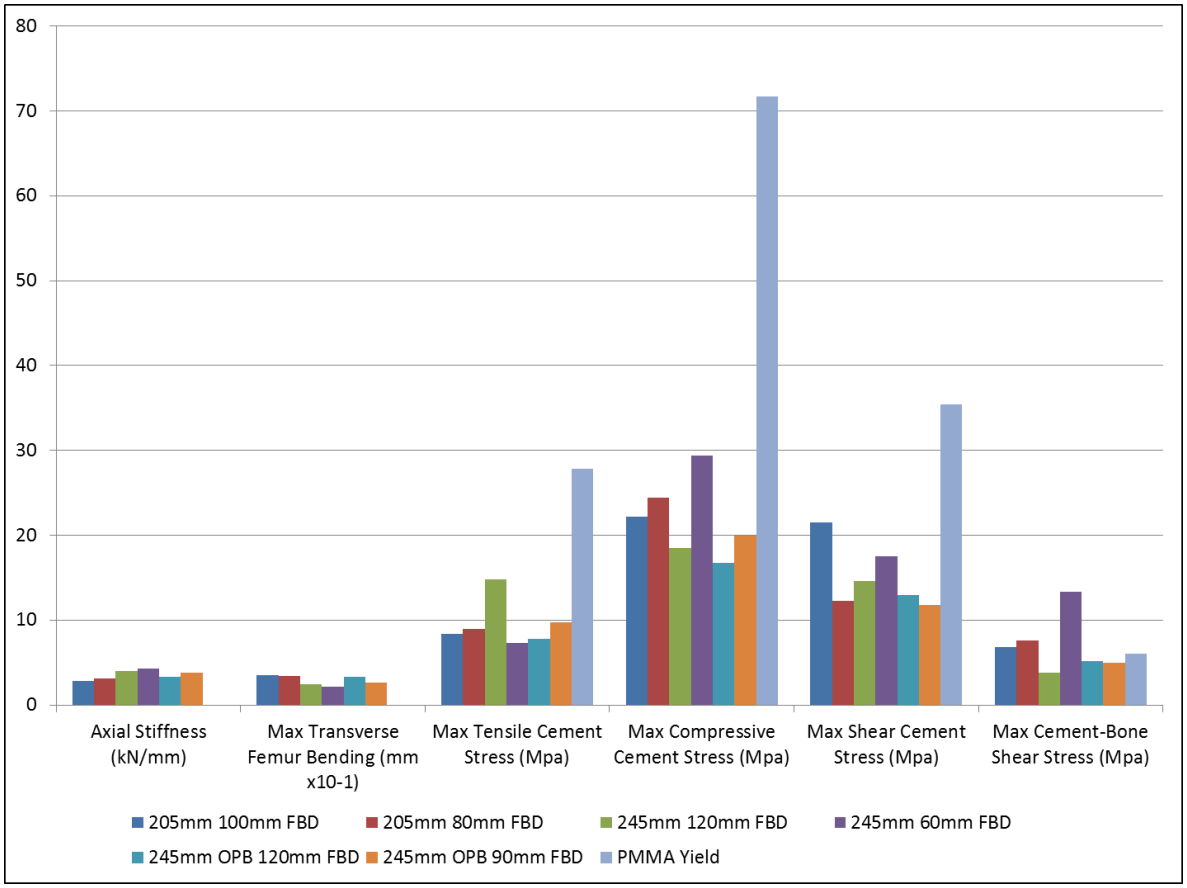

Figure 6.8 Effect of a longer FBD. Compared for both the healthy and osteoporotic cases. Results given for axial stiffness, maximum displacement of the medial side of the femur in the transverse plane, maximum cement stresses and maximum cement-to-bone interface shear stress. Cases are described in terms of the stem length, bone quality and FBD.

The relative axial movement of the fracture surfaces for cases investigating the effect of insufficiently bridged angled fractures are given in Figure 6.9. Transverse fracture cases with a FBD of as close as possible to two FD were compared to angled cases, centred at the same height, that resulted in a reduced MFBD. 60ML and 60LM fracture angle cases were used. Only cases with the 205mm stem were compared. Both the original, healthy, femoral geometry and the osteoporotic femoral geometry were used.

Key results for these same cases, selected from Table 6.1, are summarised in Figure 6.10.

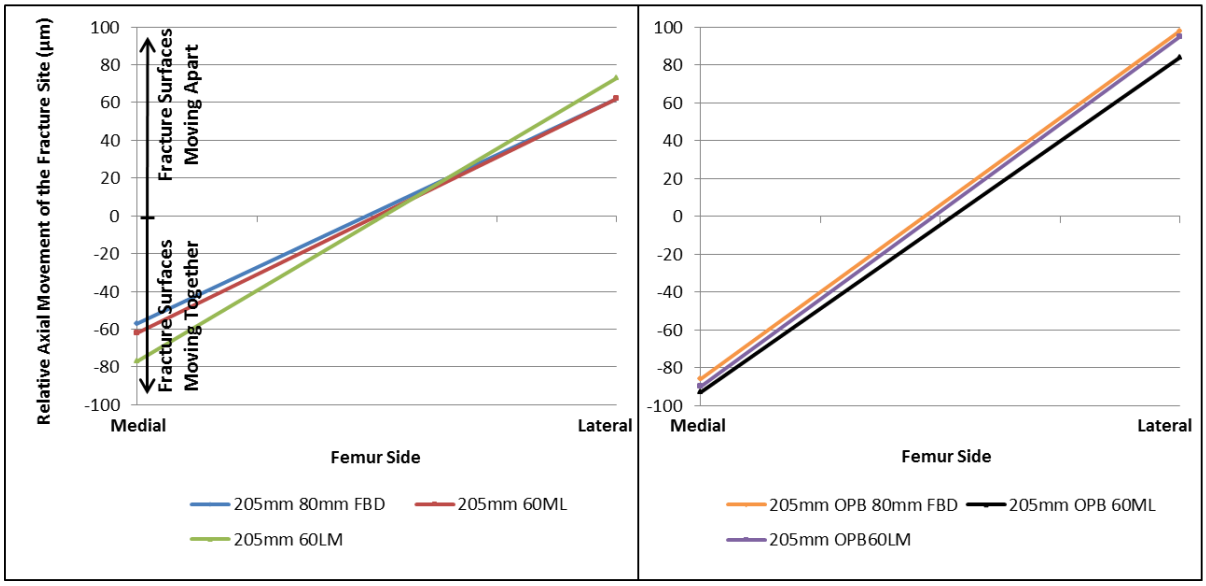

Figure 6.9 Effect of insufficiently bridged angled fractures on the relative axial fracture movements on the medial and lateral sides of the fracture. Compared for both the healthy and osteoporotic cases. Cases are described in terms of the stem length, bone quality and either FBD (transverse fractures) or fracture angle and direction.

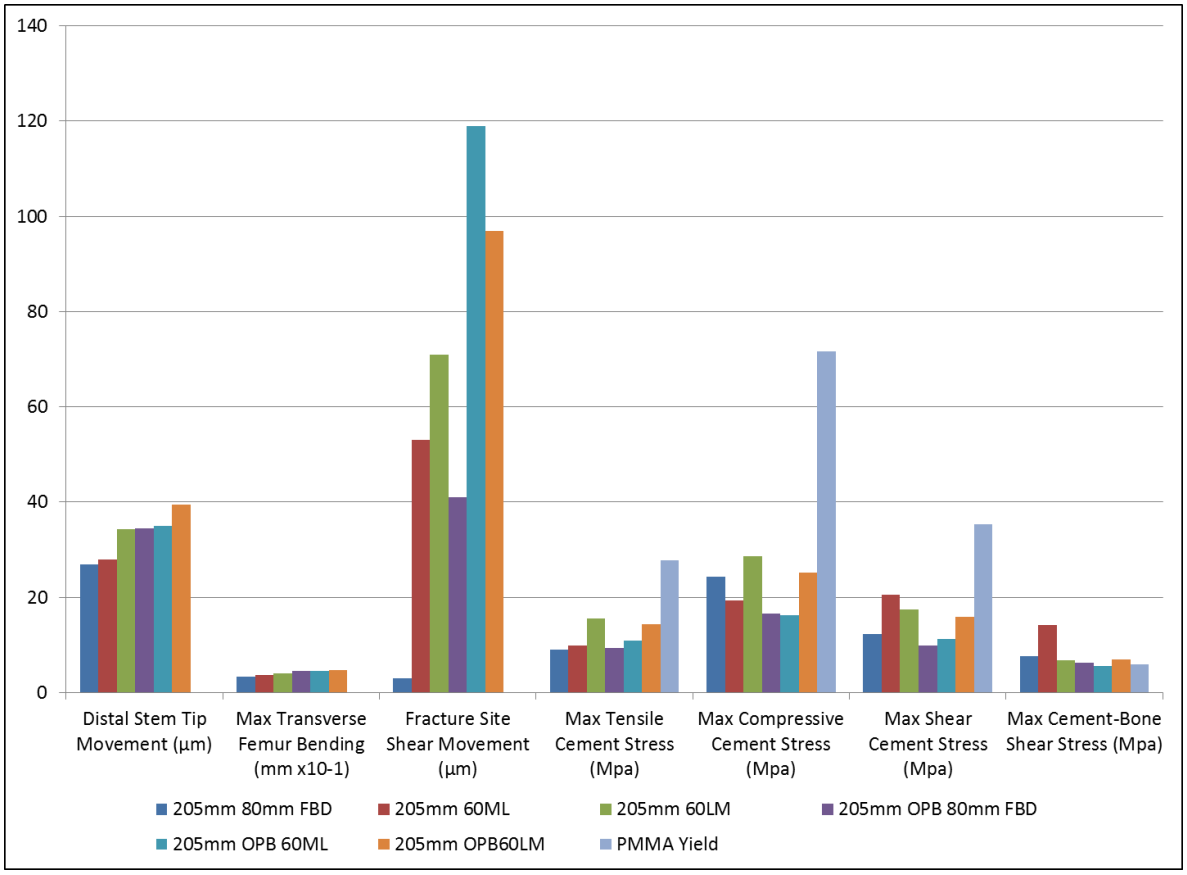

Figure 6.10 Effect of insufficiently bridged angled fractures. Compared for both the healthy and osteoporotic cases. Results given for distal movement of the stem tip, maximum displacement of the medial side of the femur in the transverse plane, maximum cement stresses and maximum cement-to-bone interface shear stress. Cases are described in terms of the stem length, bone quality and either FBD (transverse fractures) or fracture angle and direction.

The relative axial movement of the fracture surfaces for cases investigating the effect of sufficiently bridged angled fractures are given in Figure 6.11. Only cases with the 245mm long stem appropriately treated angled fractures. Given that the transverse fractures created on the 245mm stem models either resulted in a relatively short (60mm) or relatively long (120mm) FBD the angled fractures were compared to both transverse cases. The angled cases resulted in a MFBD of 90mm. As such an ideal transverse fracture comparison case would lie between the 120mm and 60mm FBD cases. 60ML and 60LM angled cases were used for this comparison. Both the original, healthy, femoral geometry and the osteoporotic femoral geometry were used.

Key results for these same cases, selected from Table 6.1, are summarised in Figure 6.12.

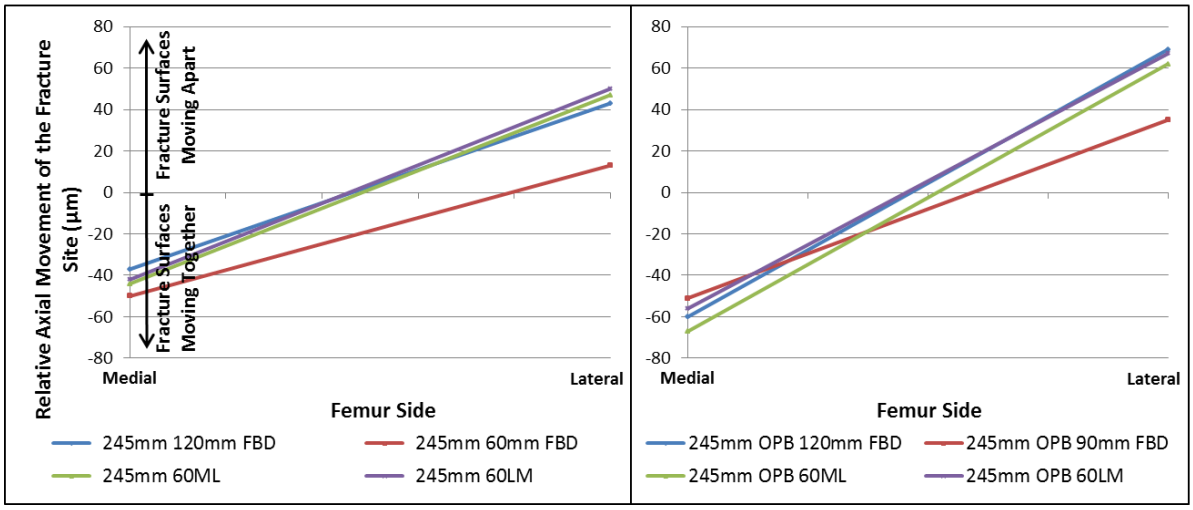

Figure 6.11 Effect of sufficiently bridged angled fractures on the relative axial fracture movements on the medial and lateral sides of the fracture. Compared for both the healthy and osteoporotic cases. Cases are described in terms of the stem length, bone quality and either FBD (transverse fractures) or fracture angle and direction.

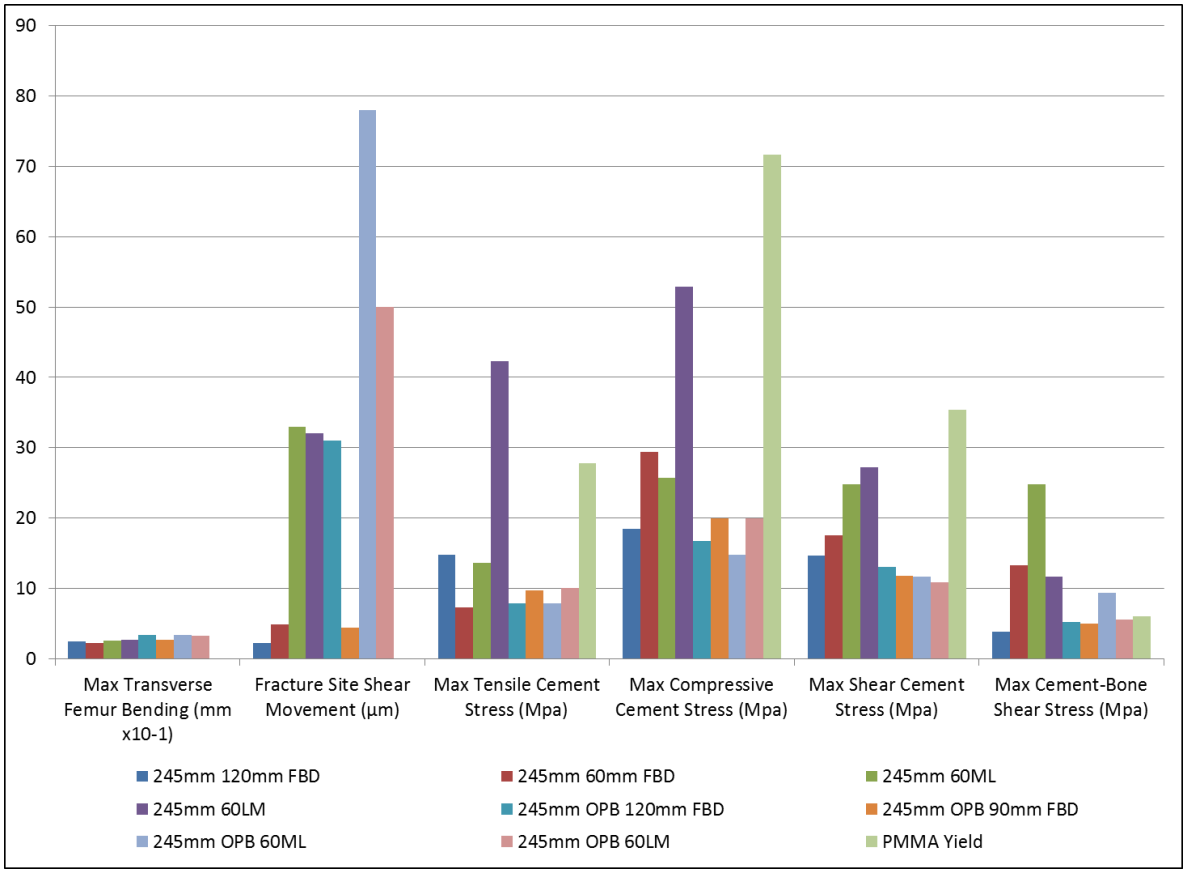

Figure 6.12 Effect of sufficiently bridged angled fractures. Compared for both the healthy and osteoporotic cases. Results given for distal movement of the stem tip, maximum displacement of the medial side of the femur in the transverse plane, maximum cement stresses and maximum cement-to-bone interface shear stress. Cases are described in terms of the stem length, bone quality and either FBD (transverse fractures) or fracture angle and direction.

6.4 Discussion

Treating a more distal fracture with the same FBD requires a longer stem. This therefore increases the amount of metalwork added to the patient and increases the bending stiffness of the overall construct. The increase in measured axial stiffness, decrease in relative angle change between the proximal and distal fracture surfaces and decrease in maximum transverse femur displacement may therefore all be caused by the increased stem length.

The movement of the fracture site distally resulted in a reduction in the bending moments acting around the fracture site. With a reduced bending moment, the forces would act more in compression and less in bending at that point. This may also have contributed

to these changes. This increased compressive loading and decreased bending loading may therefore explain the increased axial movement of the fracture site, increased distal movement of the stem tip, increased maximum cement stresses near to the stem tip and decreased bending at the fracture site.

Some of these effects may be due to the fixed constraints at the femoral head and base however. A treatment with a very well fixed and supported fracture site would bend less at the fracture site than one with a very unstable fracture. If there is less bending at the fracture site and the final location of the head and base are dictated by fixed boundary conditions then then bending in the rest of the structure has to change. Either the bending above and below the fracture site can increase to result in a similar amount of overall deformation or the bending above and below the fracture can remain similar and the overall bending deformation of the structure will reduce. This would not necessarily be the case without these fixed boundary conditions, however. The bending at the fracture site could reduce and the bending in the rest of the structure could stay the same. This is because the femoral head and/or base would have the freedom to displace to compensate. Similarly, increasing the bending stiffness of the areas above or below the fracture site, when using fixed boundary conditions, would mean that less bending would have to take place at the fracture site as well, whether increased fracture site stability had been achieved or not. This concept is illustrated in Figure 6.13.

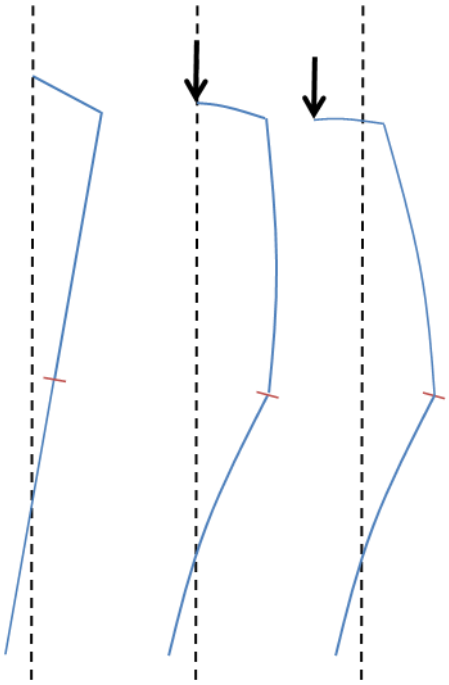

Figure 6.13 Simplified illustration of how the BCs might affect the bending pattern in the model. Left: An unloaded simplified femur. Middle: A loaded femur induces bending at the fracture site (red) and bending in the femur. With fixed BCs this leads to no transverse head movement. Right: If, in a different case, the bending in the femur is the same but the bending at the fracture site is larger this would result in transverse head movement. To meet the requirements of the BCs the bending in the femur or fracture site would have to alter.

An increased FBD with the 205mm stem (by moving the fracture site proximally by 20mm) resulted in little change to the overall axial movement of the proximal fracture surface relative to the distal surface. It did however increase the fracture site compression on the medial side of the fracture and the fracture site opening on the lateral side of the fracture. This meant that the bending at the fracture site had increased and this may have been due to the increased bending moments acting on the raised fracture site (relative change in angle of the fracture surfaces increased by 21%, bending moment around the more proximal fracture increased by 20%). For the 245mm stem, the more proximal fracture also experienced greater bending, with the relative change in angle of the fracture surfaces increasing by 27% for the more proximal fracture. This coincided with a much larger increase in bending moment however (approximately 400%).

The difference between the fracture heights on the 245mm stem was much larger (60mm) than the difference on the 205mm stem (20mm). The 245mm 60mm FBD case

resulted in relatively large amount of overall movement of the proximal fracture surface towards the distal surface (~20μm). Moving from an 80mm FBD to a 60mm FBD in the fracture height study in Section 5.2 resulted in the proximal fracture surface moving approximately 10μm towards the distal surface. Some of this effect is therefore likely to be due to the FBD of below 80mm. The difference appears to be more pronounced with the longer stem and more distal fractures however. In terms of reducing the overall movement of the proximal section of the femur, and the stem, into the distal section of the femur it is possible that more distal fractures could respond better to a greater than two femoral diameter bridging distance.

Angled fractures appeared to result in significantly increased fracture site shear movements when compared to transverse fractures. These increased shear movements occurred even when adequately treated using a FBD of more than two femoral diameters. Fracture site shear movements were identified as an indicator for potential failure. This may therefore support the hypothesis that the angle of the fracture needs to be considered when selecting an appropriate treatment. With transverse fractures a two femoral diameter FBD was shown to drastically reduce fracture site shear movements. If a long FBD cannot produce a similar reduction in angled fractures then another method for controlling this factor may be required.

Angled fractures, even when appropriately treated, appeared to also have a noticeable effect on the stresses on the PMMA cement. A 60ML fracture resulted in large shear stresses at the cement-to-bone interface that would be likely to lead to failure at that interface. A 60LM fracture did not cause a similar increase, compared to the transverse fracture cases. Both the 60ML and 60LM fractures increased the maximum shear stresses in the cement mantle, moving the recorded values to within 30% of the failure stress of PMMA. The 60ML fracture angle gave similar maximum tensile and compressive stresses to the comparably bridged transverse fracture cases. The 60LM fracture case resulted in significantly increased maximum tensile and compressive cement stresses, however. In the case of the maximum tensile stress, the recorded value was larger than the UTS of PMMA by approximately 50%. For the maximum compressive stress the value for the 60LM case was almost double that found from the transverse cases. Fractures angled in the ML direction therefore appeared to result in increased shear stresses in the cement mantle and at the cement-to-bone interface. They might therefore be expected to experience a higher risk

of subsidence into the femur. Conversely LM angled fractures appeared to lead to higher tensile and compressive stresses within the cement mantle. LM angled fractures might therefore be expected to have an increased risk of failure due to cement damage. These increased stresses occurred even with a relatively long MFBD of 90mm.

Longer stem treatments had a higher axial stiffness than shorter stem treatments. They also experienced smaller amounts of distal stem tip movement. Considering the effect of a longer stem in an actual patient stiffening the femur may have an effect on the deformations of the hip, knee, tibia and foot under load as well as the general gait pattern of the patient. This might then affect the effective loading angle of the femur as well as the magnitude and application points of the load. Longer revision stems may therefore have a much more complicated effect on the biomechanics, especially if the effect of muscle forces is also considered.

Widening the inner and outer diameters of the femur results in an increase in fracture site shear movement (Appendix Section 9.2). Thinning the cortical wall increases the shear movement and weakening the material properties of the cortical wall caused a small reduction in shear movement. Widening the diameter of the femur while keeping the cortical wall thickness constant increased the distance between the stem and the cortices. Given that this gap was filled with the relatively weak PMMA cement it is likely that this increase in shear movement came from the increased flexibility of the distal stem fixation within the canal. Thinning the cortices while maintaining the outer femoral diameter also resulted in an increased distance between the stem and cortices, allowing for more relative motion between the stem and cortices. In this case, the movement of both the proximal and distal fracture fragments increased. The relative shear increased because the increase in movement of the proximal side was larger than the increase in movement of the distal side. This suggests however that weakening the cortical walls might reduce the shear movement by making the rigidity, and therefore movement, of the distal portion more similar to that of the proximal portion. The fact that reducing the material properties of the cortical bone caused a slight reduction in shear movement supports this theory. Using osteoporotic cortical material properties also caused a small increase to the transverse movement of the proximal fragment, however it caused a much larger increase to the transverse movement of the distal fragment and this resulted in an overall reduction in shear movement. These results suggest that changes that reduce the fixation of the stem into the distal portion of the

femur lead to increased shear and changes which result in increased flexibility of the distal portion of the femur result in reduced shear. The osteoporotic femur was generated by widening the femoral diameter, reducing the cortical wall thickness and reducing the material properties of the bone. The simple cylinder models showed that the overall effect of these changes would be to increase fracture site shear movement. This is supported by the fact that in all comparisons the OPB models had larger fracture site shear movements that the healthy femur models.

Increasing the stem length counteracted all of the effects of osteoporosis, including leading to a reduction in fracture site shear movement. Shear movement may be a contributing factor to poor clinical outcomes. Recommending a FBD of longer than two femoral diameters for OP patients might therefore provide more suitable treatments. Using a longer bridging length for osteoporotic patients may also improve stem stability and reduce the otherwise increased risk of failure. Care must be taken however as increased stem length resulted in stress shielding in the cortices, which could induce further bone loss. Proximal strain transfer in the FE models was investigated further in Appendix Section 9.3. A longer bridging distance can also lead to an increased stress riser from the tip of the stem. This stress riser, in a well-fixed stem would still probably be less likely to induce failure than the stress riser caused by a loose stem of any length. Therefore the main issue may be selecting a longer than normal stem that does not reduce the cortical strain enough to cause loosening.

The correlation between outputs from the model was compared in an attempt to identify the mechanisms to which each output was most sensitive. Across all cases, there appeared to be a very reliable relationship between axial stiffness, the maximum transverse displacement of the femur and the change in angle of the fracture site (R^2 0.9-0.95 with linear lines of best fit). The most likely mechanism that would dominate the response of these outputs in this way is increasing or decreasing transverse displacement of the femur. As the bending of the femur in the mediolateral plane increases, the vertical height of the femur must reduce, leading to a reduction in axial stiffness. As the bending of the femur increases, the bending at the fracture site is also likely to increase which would lead to a larger change in angle of the fracture.

Another possible relationship was found linking the distal surface area between the stem and cement, the distal movement of the stem tip and the maximum Von Mises cement

stress near to the stem tip (R^2 0.6-0.7 with linear lines of best fit). The distal surface area relates to the amount of stem-to-cement surface area that provides fixation for the stem in the distal femur. Increasing distal surface area linked to a decrease in distal movement of the stem tip and maximum cement stress, likely due to the increased contact area reducing the stem-to-cement contact pressures. This could be investigated further however using FE models with a constant stem length but varying surface contact areas. Differences between cases to the distal movement of the stem tip and/or maximum cement stresses near the stem tip may therefore be related to distal stem support.

Given these two relationships it might be possible to make basic estimates on how different cases will respond based on an understanding of 1) how they will affect the overall bending stiffness of the femur and 2) how they will affect the distal stem support.

The effect of simple structural changes, such as lengthening the stem or changing the material properties of the stem or femur, on the bending stiffness of the construct, could be easily estimated using simple beam bending theory. This would allow an estimation of how the maximum transverse displacement of the femur would change. From the link suggested by this comparison, when concentrating on bending in the mediolateral plane, a 0.1mm increase in the maximum transverse displacement of the femur corresponded to:

- A 0.7 kN/mm decrease in axial stiffness.
- A 0.07° increase in the change in angle of the proximal fracture surface, relative to the distal fracture surface.

The effect of different femoral geometries, fracture configurations and stem geometries/lengths on the contact surface area between the stem-to-cement and cement-to-bone could be estimated from basic geometric measurements. Based on the link found in this comparison a 500mm^2 decrease in distal surface area (stem-to-cement) corresponded to:

- A 0.005mm increase in recoverable (elastic) distal displacement of the stem tip.
- An 8.8MPa increase in the maximum von Mises stress near the distal stem tip.

6.5 Conclusions

From the cases presented in this chapter it appears that the location of the fracture does make a difference to the mechanical behaviour of the structure under the loading case used in this study. It is therefore possible that the optimal FBD will vary along the length of the femur as opposed to being one single value.

Angled fractures also had an effect on the biomechanics. In some ways this was mitigated by applying a two FD MFBD rule. As such, this clinical recommendation appears reasonable. Some effects from angled fractures, including increased fracture site shear movements and maximum cement stresses, were not counteracted through this MFBD recommendation. There may, therefore, be the potential to improve the design or application of long stem revision techniques for angled PFF.

The majority of the effects of osteoporosis could be counteracted by using a longer femoral stem. Osteoporotic patients may therefore benefit from a longer than two FD MFBD. Other issues, such as increased fracture site shear movement, may relate to the increased medullary canal diameter and resulting increase in distance between the stem and cortices. Taking this into account in treatment design and selection might therefore have the potential to lead to improved clinical outcomes.

7. Future Work, Recommendations and Final Summary

Over the course of this project the use of cemented long stem revision was evaluated using both experimental and computational testing. The experimental testing evaluated the biomechanics of a transverse Type B2 periprosthetic femoral fracture treated with a long revision stem. Axial stiffness, medial axial strain, distal lateral axial strain and movement of the fracture site were recorded. Computational models were developed to represent this experimental testing scenario and they were used to investigate how accurately a computational model could the replicate the results from the experimental work.

The limitations of the computational models, and the extent to which they could be used to investigate the treatment of PFF, were evaluated. Sensitivity studies testing a range

of variables in the FE models identified possible causes for some of the differences between the experimental and computational results. These possible causes included factors such as simplification of the boundary conditions and idealisation of the interfaces between sections of the model. Sensitivity testing, combined with the experimental comparisons, identified possible areas for improvement in the experimental testing regime. These improvements consisted of additional measurements that would be needed to properly quantify the response of the specimens and areas where the clinical relevance of the experimental specimens and testing could be improved. Moving forward with the computational modelling the biomechanical effects of the cement mantle thickness, fracture location, fracture angle, fracture bridging distance, femoral stem length and bone quality were investigated.

Many different points were raised by the results of the experimental and computational simulations. The key outputs from this study can be summarised, however, in terms of suggested improvements to pre-clinical testing methods and suggested improvements to the clinical treatment of Type B periprosthetic femoral fractures.

7.1 Pre-Clinical Testing Recommendations

The synthetic femur specimens used in this study required 20 pre-conditioning load cycles to provide repeatable results. Repeated loading tests appeared to have a measurable effect on axial stiffness, even with a loading magnitude of only 500N. Testing regimes using a similar magnitude load have been reported in several studies specifying that it was chosen in order to prevent specimen damage [10, 132].

The axial stiffness variations measured between treated specimens were relatively large compared to the measured values. This inter-specimen variability appeared to be due to surgical variations as opposed to material variations, despite efforts to minimise this during specimen preparation.

Based on the results of this study it would be recommended, when using synthetic femur models, to perform pre-conditioning loading before gathering results. It would also be recommended to randomise or vary the test order between specimens and to use at least

six test specimens for all comparisons. If possible averaging between more than six test specimens should be used as it may better identify trends and statistically significant differences. As the variation between specimens appeared to predominantly occur during the creation and treatment of the fracture these variations may be an important factor to consider. When evaluating or comparing potential treatments the variability between specimens, when using synthetic femurs, may represent the relative in vivo clinical variability associated with that operation. It may therefore be important to compare between the 'worst performing specimens', for example in terms of load-to-failure tests, as well as the group averages to determine which treatments are suitable.

A greater range of outputs from the experimental specimens than the stiffness, strain and fracture movement recorded in this study would have allowed the experimental testing to better support the development of the computational model. Axial stiffness can be useful to compare the overall response of very similar treatments or identify failure through a sudden loss in stiffness. It is less useful for comparing different types of fixation however as optimal stiffness values cannot be recommended. Additionally stiffness alone does not provide sufficient information to understand the cause of differences between results as it is dependent on many factors.

Strain is a biomechanically useful measurement in that the bending of the specimens can be characterised. Testing the experimental specimens at different loading angles showed that the mode of bending altered between cases. Comprehensively measuring the response of the specimen and loading assembly using only strain gauges would require a prohibitively large and costly data acquisition system however. Digital image correlation (DIC) and image marker tracking methods have shown the potential to provide extensive and accurate deformation data for test specimens. They may therefore be a more suitable method for recording the experimental response of simulated PFF treatments.

Accurate displacement data across the whole length of the specimens and loading assembly would have made validation of the corresponding FE models much more effective. Additional factors such as micromotion from the loading assembly and relative motion between components such as the stem and cortices could have also been recorded. The sensitivity testing presented in Chapter 4 showed that the bending behaviour of the models was extremely sensitive to small motions at the head and base of the femur. Therefore recording these displacements would improve both the accuracy of, and the

confidence in, the results from the FE models. From this displacement data the strain could also be estimated and strain gauges would then be a useful comparison to validate these calculated strains.

The use of relatively simple loading regimes for testing PFF treatment options makes interpreting the results easier. It therefore enables the identification of key, fundamental aspects of how the different treatments respond to loading. These relatively simple loading regimes significantly limit the clinical applicability of results from either experimental or computational studies however. The results of the computational models were extremely sensitive to the boundary conditions. To achieve results representing the in vivo scenario in vivo loads and boundary conditions are therefore required. This would suggest that adding physiological loading, including muscle forces and the true constraining effect of the acetabular cup and knee, will be an important step in improving PFF treatment options. The experimental medial fracture movement was shown to be sensitive to the adduction angle of the femur. The natural gait pattern of specific patients may therefore also have an effect on fracture strains and, as a result, fracture healing.

As a general consideration of the current state-of-the-art FE models for PFF treatments an acceptable level of mesh refinement can be achieved using modern high performance computing resources. This resulted in a level of convergence that could be estimated to result in a mesh refinement based numerical error of no more than 15%. With increasing computing power however further mesh refinement to the cortical bone would be recommended as the most effective way to reduce this numerical error. Further detail and complexity is required in the models however in the form of more realistic interface and material failure properties. In particular this should focus on the cement and cement-to-bone interfaces as the results of many of the computational models suggested that failure should have occurred in these regions.

When using computational models to identify an increased likelihood of failure, cases that represented a ‘worst case scenario’ were more useful. The idealisation of material properties, geometry and interface conditions generally result in a structure that is more resistant to deformation and failure than in reality. Worst case scenarios, however, highlighted potential failure modes and made the differences between treatment options more clear. An example of this was the combination of a fracture gap and a thin cement mantle (Section 5.1), allowing a toggling motion of the stem inside the femur that would

likely lead to cement failure and stem loosening. Given the practical difficulties and time constraints of surgical procedures all treatments cannot be expected to match the theoretically optimal scenario [52]. Accounting for these less optimal cases is therefore an important part of providing clinically relevant treatment evaluations.

When attempting to select an 'optimal treatment' analysing different output measures can lead to very different recommendations. Care must therefore be taken to consider the behaviour of the entire construct, using a variety of outputs, before making a treatment recommendation.

7.2 Implant Design and Application Recommendations

The main failure mode for stem fixation, as indicated by the computational models, was a toggling motion of the stem in the femur. This occurred due to either insufficient proximal stem fixation (due to a thin cement mantle) or insufficient distal stem fixation (due to an insufficient fracture bridging distance). It was characterised by increased shear movements at the fracture site and increased cement stresses near the distal stem tip. The increased fracture site shear movements would have the potential to adversely affect fracture healing by callus formation. The increased cement stresses, located on the lateral side of the stem tip, could result in cement failure. Cement failure in this area would then reduce the ability of the cement to resist stem toggling, possibly leading to further cement damage. Karrholm et al. [204] measured migration of the femoral head from 84 cemented hip arthroplasties in 81 patients with an up to 8 year follow-up. They identified a failure pattern that included "medial, distal and posterior migration". Migrations in these directions would be expected based on the toggling motion indicated by the computational models, which may suggest that there is clinical evidence for this failure mode. Another effect of this failure mode was, in extreme cases, an increasing stress riser from the distal stem tip acting on the lateral cortex. Beals et al. [30] performed a review of 93 clinical PFF cases and found that periprosthetic femoral fractures occurring in patients with a loose cemented stem "nearly always fractured at the stem tip". Again, this may suggest that this toggling failure mode is clinically relevant.

All comparisons were relatively sensitive to the stability of the fracture site. A cement-filled, perfectly bonded fracture site generally provided sufficient support to prevent any significant increase in the likelihood of failure. A 1mm fracture gap however required careful treatment selection in order to avoid indicators for potential loss of fixation. Clinical cases where fracture reduction is difficult to achieve may therefore be at a higher risk for failure, particularly if there are other contributing factors.

A wide range of cases, including those modelling typically successful PFF treatments, led to high shear stresses at the cement-to-bone interface. These shear stresses were either larger than, or of a similar magnitude to, the experimentally derived yield shear stress of this interface [172]. It is therefore possible that in vivo cemented stems experience some degree of debonding at this interface during initial loading. The initial post-operative resistance to stem subsidence may therefore come from the geometric inhomogeneity of the femoral canal and cement rather than bonding at the cement-to-bone interface. Gie et al. [26] recorded trabecular remodelling after cemented revision THA which may suggest that remodelling can, given time, provide additional support to an implanted stem. They used a combination of impaction grafting and cement to achieve stem fixation, however, and the morselised bone may have induced this healing response. One of the sensitivity tests performed on the computational model (Chapter 4) investigated changing the tied interface between the cement and bone to a frictional interface. This resulted in a small amount of subsidence of the stem and cement into the femur. Several studies have recorded stem subsidence clinically and found that it commonly occurs in THA and PFF patients. One of the effects of this subsidence in the computational model was increased hoop stresses immediately distal to the fracture site. These increased hoop stresses could lead to fracture propagation from the already damaged fracture site. It may be possible reduce the risk of this, if it is suspected to be a concern clinically, by applying a supporting cable just distal to the fracture.

The current surgical recommendation that a long revision stem should bypass most distal point of the fracture by at least two femoral diameters appears reasonable. Fractures treated with a bridging distance of approximately two femoral diameters appeared to have sufficient distal stem fixation to prevent stem loosening due to cement damage.

It is generally suggested that tapered stems will provide additional support as they subside [26, 168, 205]. This is due to the increased cross-sectional area of the stem

providing increased pressure against the cortical walls. This effect would only occur however in the case of subsidence of the stem into the cement. If the stem and cement subside as one then the increased stem diameter would be counteracted by the correspondingly decreased cement thickness. It is therefore important to investigate whether the subsidence of the stem that is seen clinically is due to movement of the stem or movement of the stem and cement. If the subsidence comes from relative motion at the cement-to-bone interface then resisting this subsidence requires providing more support to the cement, not to the stem.

Gie et al. [26] recorded relative motion of the stem into the cement and of the cement into the femur for 56 revision THA patients with a mean follow-up time of 30 months (range 18-49 months). The most common level of subsidence of the stem into the cement was 1-2mm (22 stems), with 2 stems experiencing more than 10mm of stem into cement subsidence. The most common cement into bone subsidence measured was no subsidence (45 stems) with recorded values ranging from 0-7mm. They suggested that this stem into cement subsidence may have been the result of time-dependent cement material properties such as creep. The results of this project may suggest that cement into bone subsidence is more likely in long revision stem PFF treatments. This could possibly be due to the fact that with any degree of fracture gap the region of the cement-to-bone interface preventing subsidence could be limited to that occurring below the fracture site. This would reduce the effectiveness of the proximal cement-to-cancellous interdigitation to provide support and might lead to increased levels of cement into bone subsidence. If the relationship between stem into cement subsidence and cement into bone subsidence is altered by the existence of a fracture site, this may also affect the ability of a tapered stem geometry to achieve a ‘taper-lock’ [168] mode of support in PFF cases.

The majority of the effects that osteoporosis had on the fracture fixation construct could be counteracted, to some degree, through the use of a longer revision stem. It may therefore be possible to improve the clinical outcomes from PFF treatment in osteoporotic patients by recommending a minimum fracture bridging distance that is greater than two femoral diameters. Other effects from osteoporosis appeared to be due to the increased distance between the stem and cortices. Wider stems might be therefore be advantageous for osteoporotic patients who have experienced a widening of the medullary canal.

In summary potential areas for improvement in both how implants are tested and how they are applied have been suggested. The experimental and computational simulations used in this study complimented each other well, providing more detailed information in combination than could be gathered by focussing on only one form of testing. There are key areas however in the simulation of the in vivo scenario that require further development if the clinical outcomes of PFF treatments are to be improved. Some of these, such as the measurement of experimental micro-motions in the loading assembly, have been recommended as a direct result of this work. Other potential improvements have been recommended as subjects for further study, such as the incorporation of realistic boundary constraints, due to their apparent importance to the simulation results.

8. References

1. National Joint Registry, 2013. Executive summary: public and patient guide to the NJR's 10th annual report 2013. Hemel Hempstead: NJR. Available at www.njrcentre.org.uk [Accessed May 2014].

2. Tsiridis, E., Pavlou, G., Venkatesh, R., Bobak, P., Gie, G., 2009. Periprosthetic femoral fractures around hip arthroplasty: Current concepts in their management. Hip International 19 no. 2, 75-86.

3. Nho, S.J., Kymes, S.M., Callaghan, J.J., Felson, D.T., 2013. The burden of hip osteoarthritis in the United States: Epidemiologic and economic considerations. J. Am. Acad. Orthop. Surg. 21, S1-6.

4. Lever, J.P., Zdero, R., Nousiainen, M.T., Waddell, J.P., Schemitsch, E.H., 2010. The biomechanical analysis of three plating fixation systems for periprosthetic femoral fracture near the tip of a total hip arthroplasty. Journal of Orthopaedic Surgery and Research 5, 45.

5. Chen, G., Schmutz, B., Wullschleger, M., Pearcy, M.J., Schuetz, M.A., 2009. Computational investigations of mechanical failures of internal plate fixation. Proc. IMechE Vol. 224 Part H: J. Engineering in Medicine, 119-126.

6. Lindahl H, Malchau H, Oden A, et al. Risk factors for failure after treatment of a periprosthetic fracture of the femur. J Bone Joint Surg Br 2006;88:26.

7. Buttaro MA, Farfalli G, Paredes Nunez M, et al. Locking compression plate fixation of Vancouver type-B1 periprosthetic femoral fractures. J Bone Joint Surg Am 2007;89:1964.

8. Graham SM, Moazen M, Leonidou A, et al. Locking plate fixation for Vancouver B1 periprosthetic femoral fractures: a critical analysis of 135 cases. J Orthop Sci 18, 426-436.

9. Schmotzer, H., Tchejeyan, G.H., Dall, D.M., 1996. Surgical management of intra-and postoperative fractures of the femur about the tip of the stem in total hip arthroplasty. J. Arthroplasty 11, 709-717.

10. Zdero, R., Walker, R., Waddell, J.P., Schemitsch, E.H., 2008. Biomechanical evaluation of periprosthetic femoral fracture fixation. J. Bone Joint Surg. Am. 90, 1068-1077.

11. Tsiridis, E., Haddad, F.S., Gie, G.A., 2003. Dall-Miles plates for periprosthetic femoral fractures a critical review of 16 cases. Injury, Int. J. Care Injured 34, 107-110.

12. Sommers, M.B., Fitzpatrick, D.C., Madey, S.M., Zanderschulp, C.V., Bottlang, M., 2007. A surrogate long-bone model with osteoporotic material properties for biomechanical testing of fracture implants. J. Biomech. 40, 3297-3304.

13. Moazen, M., Jones, A.C., Jin, Z., Wilcox, R.K., 2011. Periprosthetic fracture fixation of the femur following total hip arthroplasty: A review of biomechanical testing. Clin. Biomech. 26 (1), 13-22.

14. Cristofolini, L., Viceconti, M., Cappello, A., Toni, A., 1996. Mechanical validation of whole bone composite femur models. J. Biomechanics, Vol. 29, No. 4, 525-535.

15. Cristofolini, L., Viceconti, M., 2000. Mechanical validation of whole bone composite tibia models. J. Biomech. 33, 279-288.

16. Mak, J.H., 2013. Optimisation of locking plate fixation methods for periprosthetic fractures. PhD thesis. University of Leeds.

17. Briant-Evans, T.W., Veeramootoo, D., Tsiridis, T., Hubble, M.J., 2009. Cement-in-cement stem revision for Vancouver type B periprosthetic femoral fractures after total hip arthroplasty. Acta Orthopaedica 80 (5), 548-552.

18. Mak, J.H., Moazen, M., Jones, A.C., Jin, Z., Tsiridis, E., Wilcox, R.K., 2012. J. Bone Joint Surg. Br. 94-B (74).

19. Moazen, M., Mak, J.H., Etchels, L.W., Jin, Z., Wilcox, R.K., Jones, A.C., Tsiridis, E., 2014. Periprosthetic femoral fracture - a biomechanical comparison between Vancouver Type B1 and B2 fixation methods. J. Arthroplasty 29, 495-500.

20. Moazen, M., Mak, J.H., Etchels, L.W., Jin, Z., Wilcox, R.K., Jones, A.C., Tsiridis, E., 2013. The effect of fracture stability on the performance of locking plate fixation in periprosthetic femoral fractures. J. Arthroplasty 28, 1589-1595.

21. Moazen, M., Jones, A.C., Leonidou, A., Jin, Z., Wilcox, R.K., Tsiridis, E., 2012. Rigid versus flexible plate fixation for periprosthetic femoral fracture - computer modelling of a clinical case. Med. Eng. Phys. 34, 1041-1048.

22. Moazen, M., Mak, J.H., Jones, A.C., Jin, Z., Wilcox, R.K., Tsiridis, E., 2013. Evaluation of a new approach for modelling the screw-bone interface in a locking plate fixation:a corroboration study. Proc. IMechE Part H: J. Engineering in Medicine 227(7), 746-756.

23. Moazen, M., Mak, J.H., Etchels, L.W., Jones, A.C., Jin, Z., Wilcox, R.K., Tsiridis, E., 2013. Why do periprosthetic femoral fracture fixations fail - a biomechanical investigation. Bone & Joint Journal Orthopaedic Proceedings Supplement 95 (16), 62.

24. Moazen, M., Jones, A.C., Mak, J., Jin, Z., Wilcox, R.K., Tsiridis, E., 2011. The computational evaluation of a locking plate fixation - locking versus far cortical screws. Proceedings of the ASME 2011 Summer Bioengineering Conference.

25. Cox, B.D., 2006.Measurement of bone cement properties using self-sensing techniques. PhD thesis, University of Leeds.

26. Gie, G.A., Linder, L., Ling, R.S.M., Simon, J-P., Slooff, T.J.J.H., Timperley, A.J., 1993. Impacted cancellous allografts and cement for revision total hip arthroplasty. J. Bone Joint Surg. (Br) 75-B, 14-21.

27. Kusakabe, H., Sakamaki, T., Nihei, K., Oyama, Y., Yanagimoto, S., Ichimiya, M., Kimura, J., Toyama, Y., 2004. Osseointegration of a hydroxyapatite-coated multilayered mesh stem. Biomaterials 25, 2957-2969.

28. Lakstein, D., Kopelovitch, W., Barkay, Z., Bahaa, M., Hendel, D., Eliaz, N., 2009. Enhanced osseiointegration of grit-blasted, NaOH-treated and electrochemically hydroxyapatite-coated Ti-6Al-4V implants in rabbits. Acta Biomaterialia 5, 2258-2269.

29. Kelley, S.S., 1994. Periprosthetic femoral fractures. J. Am. Acad. Orthop. Surg. 2, 164-172.

30. Beals, R.K., Tower, S.S., 1996. Periprosthetic fractures of the femur: An analysis of 93 fractures. Clin. Orthop. Relat. Res. 327, 238-246.

31. Corten, K., Vanrykel, F., Bellemans, J., Reynders Frederix, P., Simon, J.-P., Broos, P.L.O., 2009. An algorithm for the surgical treatment of periprosthetic fractures of the femur around a well-fixed femoral component. J. Bone Joint Surg. (Br) 91-B (11), 1424-1430.

32. Masri, B.A, Meek, R.M.D, Duncan, C.P., 2004. Periprosthetic fractures evaluation and treatment. Clin. Orthop 420, 80-95.

33. Adolphson, P., Jonsson, U., Kalen, R., 1987. Fractures of the ipsilateral femur after total hip arthroplasty. Arch. Orthop. Trauma Surg. 106, 353-357.

34. Cooke, P.H., Newman, J.H., 1988. Fractures of the femur in relation to cemented hip prostheses. J. Bone Joint Surg. (Br) 70-B, 386-9.

35. Johansson, J.E., McBroom, R., Barrington, T.W., Hunter, G.A., 1981. Fracture of the ipsilateral femur in patients with total hip replacement. J. Bone Joint Surg. (Am) 63 (9), 1435-1442.

36. Kavanagh, B.F.,1992. Femoral fractures associated with total hip arthroplasty. Orthop. Clin. North Am. 23, 249-257.

37. Mallory, T.H., Kraus, T.J., Vaughn, B.K., 1989. Intraoperative femoral fractures associated with cementless total hip arthroplasty. Orthopedics 12, 231-239.

38. Schwartz, J.T., Mayer, J.G., Engh, C.A., 1989. Femoral fracture during non-cemented total hip arthroplasty. J. Bone Joint Surg. (Am) 71 (8), 1135-1142.

39. Stuchin, S.A., 1990. Femoral shaft fracture in porous and press-fit total hip arthroplasty. Orthop. Rev. 19 (2), 153-9.

40. Roffman, M., Mendes, D.G., 1989. Fracture of the femur after total hip arthroplasty. Orthopedics 12 (8), 1067-1070).

41. Duncan, C.P., Masri, B.A., 1995. Fractures of the femur after hip replacement. Instr. Course Lect. 45, 293-304.

42. Kamineni, S., Vindlacheruvu, R., Ware, H.E., 1999. Peri-prosthetic femoral shaft fractures treated with plate and cable fixation. Injury Int. J. Care Injured 30, 261-268.

43. Grammatopoulos, G., Pandit, H., Kambouroglou, G., Deakin, M., Gundle, R., McLardy-Smith, P., Taylor, A., Murray, D., 2011. A unique peri-prosthetic fracture pattern in well fixed femoral stems with polished, tapered, collarless, design of total hip replacement. Injury Int. J. Care Injured 42 (11), 1271-6.

44. O'Shea, K., Kutty, S., Quinlan, J.F., Brady, O.H., Mulcahy, D., 2005. The use of uncemented extensively porous-coated femoral components in the management of Vancouver B2 and B3 periprosthetic femoral fractures. J. Bone Joint Surg. (Br) 87-B (12), 1617-21.

45. Leonidou, A., Moazen, M., Lepetsos, P., Graham, S.M., Macheras, G.A., Tsiridis, E., 2015. The biomechanical effect of bone quality and fracture topography on locking plate fixation in periprosthetic femoral fractures. Injury Int. J. Care Injured 46, 213-217.

46. Yoshida, Y., Osaka, S., Kojima, T., Taniguchi, M., Osaka, E., Tokuhashi, Y., 2012. Revision of tumor prosthesis of the knee joint. Eur. J. Orthop. Surg. Traumatol. 22, 387-394.

47. Cannon, S.R., 1997. Massive prostheses for malignant bone tumours of the limbs. Eu. Instr. Course Lect. 3.

48. Springer, B.D., Berry, D.J., Lewallen, D.G., 2003. Treatment of periprosthetic femoral fractures following total hip arthroplasty with femoral component revision. J. Bone Joint Surg. Am. 85, 2156-2162.

49. Venu, K.M., Koka, R., Garikipati, R., Shenava, Y., Madhu, T.S., 2001. Dall-Miles cable and plate fixation for the treatment of peri-prosthetic femoral fractures - analysis of results in 13 cases. Injury, Int. J. Care Injured 32, 395-400.

50. Tadross, T.S.F., Nanu, A.M., Buchanan, M.J., Checketts, R.G., 2000. Dall-Miles plating for periprosthetic B1 fractures of the femur. J. Arth. 15 (1), 47-51.

51. Lewallen, D.G., Berry, D.J., 1997. Periprosthetic fracture of the femur after total hip arthroplasty. J. Bone Joint Surg. (Am) 79-A (12), 1881-1890.

52. Oh, J.K., Shau, D., Ahn, Y.H., Lee, S.J., Tsutsumi, S., Hwang, J.H., Jung, D.Y., Perren, S.M., Oh, C.W., 2009. Effect of fracture gap on stability of compression plate fixation: a finite element study. J. Orthop. Res. 28 (4), 462-7.

53. Mann, K.A., Ayers, D.C., Damron, T.A., 1997. Effects of stem length on mechanics of the femoral hip component after cemented revision. J. Orthop. Res. 15, 62-68.

54. Pellicci, P.M., Wilson Jr, P.D., Sledge, C.B., Salvati, E.A., Ranawat, C.S., Poss, R., Callaghan, J.J., 1985. Long-term results of revision total hip replacement. A follow up report. J. Bone Joint Surg. (Am) 67 (4), 513-516.

55. Froberg, L., Troelsen, A., Brix, M., 2012. Periprosthetic Vancouver type B1 and C fractures treated by locking-plate osteosynthesis. Acta Orthopaedica 83 (6), 648-652.

56. Otani, T., Whiteside, L.A., White, S.E., 1993b. Effect of femoral component material properties on cementless fixation in total hip arthroplasty. J. Arthrop. 8, 67-74.

57. Tsiridis, E., Narvani, A.A., Haddad, F.S., Timperley, J.A., Gie, G.A., 2004. Impaction femoral allografting and cemented revision for periprosthetic femoral fractures. J Bone Joint Surg. (Br) 96-B, 1124-32.

58. Moreland, J.R., Bernstein, M.L., 1995. Femoral revision hip arthroplasty with uncemented, porous-coated stems. Clin. Orthop. Relat. Res. 319, 141-150.

59. Huiskes, R., Weinans, H., Rietbergen, B.V., 1992. The relationship between stress shielding and bone resorption around total hip stems and the effects of flexible materials. Clin. Orthop. Relat. Res. 274, 124-134.

60. Marsland, D., Mears, S.C., 2012. A review of periprosthetic femoral fractures associated with total hip arthroplasty. Geriatr. Orthop. Surg. Rehabil. 2012, 3(3), 107-120.

61. Byrne, D.P., Mulhall, K.J., Baker, J.F., 2010. Anatomy & Biomechanics of the hip. The Open Sports Medicine Journal 4, 51-57.

62. Schuenke, M., Schulte, E., Schumacher, U., 2006. THIEME Atlas of Anatomy. In: Ross L, Lamperti E, Eds. General Anatomy of the Musculoskeletal System. Thieme, New York.

63. Marieb, E.N. Human Anatomy and Physiology. 2004.

64. Bergmann, G., Deuretzbacher, G., Heller, M., Graichen, F., Rohlmann, A., Strauss, J., Duda, G.N., 2001. Hip contact forces and gait patterns from routine activities. J. Biomech. 34, 859-871.

65. Rohrle, H., Scholten, R., Sigolotto, C., Sollbach, W., Kellner, H., 1984. Joint forces in the human pelvis-leg skeleton during walking. J. Biomech. 17 (6), 409-424.

66. Thornton-Trump, A.B., Daher, R., 1975. The prediction of reaction forces from gait data. J. Biomech. 8, 173-178.

67. Paul, J.P., 1974. Techniques of gait analysis. Proc. Roy. Soc. Med. 67, 401-404.

68. Brand, R.A., Pedersen, D.R., Davy, D.T., Kotzar, G.M., Heiple, K.G., Goldberg, V.M., 1994. Comparison of hip force calculations and measurements in the same patient. J. Arthrop. 9 (1), 45-51.

69. Aamodt, A., Lund-Larson, J., Eine, J., Anderson, E., Benum, P., Schnell Husby, O., 1997. In vivo measurements show tensile axial strain in the proximal lateral aspect of the human femur. J. Orthop. Res. 15, 927-931.

70. Genda, E., Iwasaki, N., Li, G., MacWilliams, A., Barrance, P.J., Chao, E.Y.S, 2001. Normal hip joint contact pressure distribution in single-leg standing - effect of gender and anatomic parameters. J. Biomech. 34, 895-905.

71. Seireg, A., Arvikar, R.J., 1975. The prediction of muscular load sharing and joint forces in the lower extremities during walking. J. Biomech. 8, 89-102.

72. Paul, J.P., 1967. Forces at the human hip joint. PhD Thesis, University of Glasgow.

73. Crowninshield, R.D., Johnston, R.C., Andrews, J.G., Brand, R.A., 1978. A biomechanical investigation of the human hip. J. Biomech. 11, 75-85.

74. Horak, F.B., Henry, S.M., Shumway-Cook, A., 1997. Postural perturbations: New insights for treatment of balance disorders. Phys. Ther. 77, 517-533.

75. Johnson, F., Leitl, S., Waugh, W., 1980. The distribution of load across the knee, a comparison of static and dynamic measurements. J. Bone Joint Surg (Br) 62-B (3), 346-349.

76. Hagstedt, B., Norman, O., Olsson, T.H., Tjornstrand, B., 1980. Technical accuracy in high tibial osteotomy for gonarthrosis. Acta Orthop. Scand. 51, 963-970.

77. Koshino, T., Tsuchiya, K., 1979. The effect of high tibial osteotomy on osteoarthritis of the knee. Int. Orthop. 3, 37-45.

78. Yang, N.H., Canavan, P.K., Nayeb-Hahemi, H., 2010. The effect of the frontal plane tibiofemoral angle and varus knee moment on the contact stress and strain at the knee cartilage. J. Applied Biomechanics 26, 432-443.

79. Karachalios, T.H., Sarangi, P.P., Newman, J.H., 1994. Severe varus and valgus deformities treated by total knee arthroplasty. J. Bone Joint Surg. (Br) 76-B (6), 938-942.

80. Lotz, J., Gerhart, T.,N., Hayes, W.C., 1991. Mechanical properties of metaphyseal bone in the proximal femur. J. Biomech. 24 (5), 317-329.

81. Carter, D.R., Hayes, W.C., 1976. Fatigue life of compact bone - I Effects of stress, amplitude, temperature and density. J. Biomech. 9, 27-34.

82. Rho, J-Y, Kuhn-Spearing, L., Zioupos, P., 1998. Mechanical properties and the hierarchical structure of bone. Med. Eng. & Phys. 20, 92-102.

83. Shahar, R., Zaslansky, P., Barak, M., Friesem, A.A., Currey, J.D., Weiner, S., 2007. Anisotropic Poisson's ratio and compression modulus of cortical bone determined y speckle interferometry. J. Biomech. 40, 252-264.

84. Reilly, D.T., Burstein, A.H., 1975. The elastic and ultimate properties of compact bone tissue. J. Biomech. 8 (6), 393-396.

85. Morgan, E.F., Bayraktar, H.H., Keaveny, T.M., 2003. Trabecular bone modulus-density relationships depend on anatomic site. J. Biomech. 36, 897-904.

86. Morgan, E.F., Keaveny, T.M., 2001. Dependence of yield strain of human trabecular bone on anatomic site. J. Biomech. 34, 569-577.

87. Bayraktar, H.H., Morgan, E.F., Niebur, G.L., Morris, G.E., Wong, E.K., Keaveny, T.M., 2004. Comparison of the elastic and yield properties of human femoral trabecular and cortical bone tissue. J. Biomech. 37, 27-35.

88. Reilly, D.T., Burstein, A.H., Frankel, V.H., 1974. The elastic modulus for bone. J. Biomech. 7, 271-275.

89. Rho, J-Y., Ashman, R.B., Turner, C.H., 1993. Young's modulus of trabecular and cortical bone material: Ultrasonic and microtensile measurements. J. Biomech. 26 (2), 111-119.

90. Turner, C.H., Rho, J., Takano, Y., Tsui, T.Y., Pharr, G.M., 1999. The elastic properties of trabecular and cortical bone tissues are similar: results from two microscopic measurement techniques. J. Biomech. 32, 437-441.

91. Berteau, J-P., Baron, C., Pithioux, M., Launay, F., Chabrand, P., Lasaygues, P., 2014. In vitro ultrasonic and mechanic characterization of the modulus of elasticity of children cortical bone. Ultrasonics 54, 1270-1276.

92. Abdel-Wahab, A.A., Alam, K., Silberschmidt, V.V., 2011. Analysis of anisotropic viscoelastoplastic properties of cortical bone tissues. J. Mech. Behav. Biomed. Mater. 4, 807-820.

93. Johnson, T.P.M., Socrate, S., Boyce, M.C., 2010. A viscoelastic, viscoplastic model of cortical bone valid at low and high strain rates. Acta Biomaterialia 6, 4073-4080.

94. Brown, S.J., Pollintine, P., Powell, D.E., Davie, M.W.J., Sharp, C.A., 2002. Regional differences in mechanical and material properties of femoral head cancellous bone in health and osteoarthritis. Calcif. Tissue Int. 71, 227-234.

95. Linde, F., Hvid, I., Pongsoipetch, B., 1989. Energy absorptive properties of human trabecular bone specimens during axial compression. J. Orthop. Res. 7, 432-439.

96. Homminga, J., McCreadie, B.R., Ciarelli, T.E., Weinans, H., Goldstein, A., Huiskes, R., 2002. Cancellous bone mechanical properties from normals and patients with hip fractures differ on the structural level, not on the bone hard tissue level. Bone 30 (5), 759-764.

97. Chevalier, Y., Pahr, D., Allmer, H., Charlebois, M., Zysset, P., 2007. Validation of a voxel-based FE method for prediction of the uniaxial apparent modulus of human trabecular bone using macroscopic mechanical tests and nanoindentation. J. Biomech. 40, 3333-3340.

98. Rho, J-Y., Tsui, T.Y., Pharr, G.M., 1997. Elastic properties of human cortical and trabecular lamellar bone measured by nanoindentation. Biomaterials 18, 1325-1330.

99. Ulrich, D., Hildebrand, T., Van Rietbergen, B., Ruegsegger, P., 1997. The quality of trabecular bone evaluated with micro-computed tomography, FEA and mechanical testing. Stud. Health Technol. Inform. 40, 97-112.

100. Zysset, P.K., Guo, X. E., Hoffler, C.E., Moore, K.E., Goldstein, S.A., 1999. Elastic modulus and hardness of cortical and trabecular bone lamellae measured by nanoindentation in the human femur. J. Biomech. 32, 1005-1012.

101. Ninomi, M., 2002. Recent materials for biomedical applications. Metallurgical and Materials Transactions A 33A, 477-486.

102. Hermawan, H., Ramdan, D., Djuansjah, J.R.P., 2011. Metals for Biomedical Applications, Biomedical Engineering - From Theory to Applications, Prof. Reza Fazel (Ed.), ISBN: 978-953-307-637-9, InTech, Available from: http://www.intechopen.com/books/biomedical-engineering-from-theory-toapplications/metals-for-biomedical-applications.

103. Uhthoff, H.K., Poitras, P., Backman, D.S., 2005. Internal plate fixation of fractures: Short history and recent developments. J. Orthop. Sci. 11, 118-126.

104. Claes, L.E., Cunningham, J.L., 2009. Monitoring the mechanical properties of healing bone. Clin. Orthop. Relat. Res. 467, 1964-1971.

105. Perren, S.M., 2002. Evolution of the internal fixation of long bone fractures. J. Bone Joint Surg. [Br] 84-B, 1093-1110.

106. Perren, S.M., Cordey, J., Rahn, B.A., Gautier, E., Schneider, E., 1988. Early temporary porosis of bone induced by internal fixation implants. Clin. Orthop. Relat. Res. 232, 139-51.

107. Berhmann, G., Graichen, F., Rohlmann, A., 1993. Hip joint loading during walking and running, measured in two patients. J. Biomech. 26 (8), 969-990.

108. Sawbones, 2014. Biomechanical Test Materials 2014. Available at www.sawbones.com [Accessed January 2015].

109. Basso, T., Klaksvik, J., Syversen, U., Foss, O.A., 2014. A biomechanical comparison of composite femurs and cadaver femurs used in experiments on operated hip fractures. J. Biomech. 47, 3898-3902.

110. Brock, G.R., Chen, J.T., Ingraffea, A.R., MacLeay, J., Pluhar, G.E., Boskey, A.L., van der Meulen, M.C.H., 2015. The effect of osteoporosis treatments on fatigue properties of cortical bone tissue. Bone Reports 2, 8-13.

111. Birkhold, A.I., Razi, H., Weinkamer, R., Duda, G.N., Checa, S., Willie, B.M., 2015. Monitoring in vivo (re)modeling: A computational approach using 4D microCT data to quantify bone surface movements. Bone 75, 210-221.

112. Lerebours, C., Thomas, C.D.L., Clement, J.G., Buenzli, P.R., Pivonka, P., 2015. The relationship between porosity and specific surface in human cortical bone is subject specific. Bone 72, 109-117.

113. Mann, K.A., Ayers, D.C., Werner, F.W., Nicoletta, R.J., Fortino, M.D., 1997. Tensile strength of the cement-bone interface depends on the amount of bone interdigitated with PMMA cement. J. Biomech. 30 (4), 339-346.

114. Bohner, M., Gasser, B., Baroud, G., Heini, P., 2003. Theoretical and experimental model to describe the injection of a polymethylmethacrylate cement into a porous structure. Biomaterials 24, 2721-2730.

115. Teo, J.C.M., Si-Hoe, K.M., Keh, J.E.L., Teoh, S.H., 2006. Relationship between CT intensity, micro-architecture and mechanical properties of porcine vertebral cancellous bone. Clin. Biomech. 21, 235-244.

116. Walsh, M.P., Wijdicks, C.A., Parker, J.B., Hapa, O., LaPrade, R.F., 2009. A comparison between a retrograde interference screw, suture button, and combined fixation on the tibial side in an all-inside anterior cruciate ligament reconstruction.Am. J. Sports Med. 37 (1), 160-167.

117. Feng, L., Chittenden, M., Schirer, J., Dickinson, M., Jasiuk, I., 2012. Mechanical properties of porcine femoral cortical bone measured by nanoindentation. J. Biomech. 45, 1775-1782.

118. Peric, M., Dumic-Cule, I., Grcevic, D., Matijasic, M., Verbanac, D., Paul, R., Grgurevic, L., Trkulja, V., Bagi, C.M., Vukicevic, S., 2015. The rational use of animal models on the evaluation of novel bone regenerative therapies. Bone 70, 73-86.

119. Proffen, B.L., McElfresh, M., Fleming, B.C., Murray, M.M., 2012. A comparative anatomical study of the human knee and six animal species. The Knee 19, 493-499.

120. Osterhoff, G., Loffler, S., Steinke, H., Feja, C., Josten, C., Hepp, P., 2011. Comparative anatomical measurements of osseous structures in the ovine and human knee. The Knee 18, 98-103.

121. Steinberg, E.L., Blumberg, N., Dekel, S., 2005. The fixion proximal femur nailing system: biomechanical properties of the nail and a cadaveric study. J. Biomech. 38, 63-68.

122. Kukla, C., Gaebler, C., Pichl, R.W., Prokesch, R., Heinze, G., Heinz, T., 2002. Predictive geometric factors in a standardized model of femoral neck fracture. Experimental study of cadaveric human femurs. Injury, Int. J. Care Injured 33, 427-433.

123. Maier, A., Regazzoni, P., 2000. Prevention of malunions in the rotation of complex fractures of the distal femur treated using the Dynamic Condylar Screw (DCS): An anatomical graphic analysis using computed tomography on cadaveric specimens. Injury, Int. J. Care Injured 31, S-B63-S-B69.

124. Kukla, C., Pichl, W., Prokesch, R., Jacyniak, W., Heinze, G., Gatterer, R., Heinz, T., 2001. Femoral neck fracture after removal of the standard gamma interlocking nail: a cadaveric study to determine factors influencing the biomechanical properties of the proximal femur. J. Biomech. 34, 1519-1526.

125. McNamara, B.P., Cristofolini, L., Toni, A., Taylor, D., 1994. Evaluation of experimental and finite element models of synthetic and cadaveric femora for pre-clinical design-analysis. Clin. Mat. 17, 131-140.

126. Pierre, M.A., Zurakowski, D., Nazarian, A., Hauser-Kara, D.A., Snyder, B.D., 2010. Assessment of the bilateral asymmetry of human femurs based on physical, densitometric, and structural rigidity characteristics. J. Biomech. 43, 2228-2236.

127. Sedlacek, R.C., O'Connor, D.O., Lozynsky, A.J., Harris, W.H., 1997. Assessment of the symmetry of bone strains in the proximal femoral medial cortex under load in bilateral pairs of cadaver femurs. J. Arthrop. 12 (6), 689-694.

128. Eberle, S., Gerber, C., von Oldenburg, G., Högel, F., Augat, P., 2010. A biomechanical evaluation of orthopaedic implants for hip fractures by finite element analysis and in-vitro testing. Proc. IMechE Vol. 224 Part H: J. Engineering in Medicine, 1141-1152.

129. Simoes, J.A., Vaz, M.A., Blatcher, S., Taylor, M., 2000. Influence of head constraint and muscle forces on the strain distribution within the intact femur. Med. Eng. Phys. 22, 453-59.

130. Choi, J.K., Gardner, T.R., Yoon, E., Morrison, T.A., Macaulay, W.B., Geller, J.A., 2010. The effect of fixation technique on the stiffness of comminuted Vancouver B1 periprosthetic femur fractures. J. Arth. 25, 124-128.

131. Talbot, M., Zdero, R., Schemitsch, E.H., 2008. Cyclic loading of periprosthetic fracture fixation constructs. J. Trauma 64, 1308-1312.

132. Zdero, R., Bougherara, H., Dubov, A., Shah, S., Zalzal, P., Mahfud, A., Schemitsch, E.H., 2009. The effect of cortex thickness on intact femur biomechanics: a comparison of finite element analysis with synthetic femurs. Proc. IMechE Vol. 224 Part H: J. Engineering in Medicine, 831-40.

133. Shah, S., Kim, S.Y.R., Dubov, A., Schemitsch, E.H., Bougherara, H., Zdero, R., 2011. The biomechanics of plate fixation of periprosthetic femoral fractures neat the tip of a total hip implant: cables, screws, or both? Proc. IMechE Vol 225 Part H: J. Engineering in Medicine, 845-856.

134. Otani, T., Whiteside, L.A., White, S.E., 1993a. Strain distribution in the proximal femur with flexible composite and metallic femoral components under axial and torsional loads. J. Biomed. Mater. Res. 27, 575-585.

135. Heiner, A.D., 2008. Structural properties of fourth-generation composite femurs and tibias. J. Biomech. 41, 3282-84.

136. Panjabi, M.M., Trumble, T., Hult, J.E., Southwick, W.O., 1985. Effect of femoral stem length on stress raisers associated with revision hip arthroplasty. J. Orthop. Res. 3, 447-455.

137. Ebrahimi, H., Rabinovich, M., Vuleta, V., Zalcman, D., Shah, S., Dubov, A., Roy, K., Siddiqui, F.S., Schemitsch, E.H., Bougherara, H., Zdero, R., 2012. Biomechanical properties of an

intact, injured, repaired, and healed femur: An experimental and computational study. Journal of the Mechanical Behavior of Biomedical Materials 16, 121–135.

138. Zdero, R., Shah, S., Mosli, M., Schemitsch, E.H., 2009. The effect of load application rate on the biomechanics of synthetic femurs. Proc. IMechE Vol 224 Part H: J. Engineering in Medicine, 599-605.

139. Stolk, J., Verdonschot, N., Cristofolini, L., Toni, A., Huiskes, R., 2002. Finite element and experimental models of cemented hip joint reconstructions can produce similar bone and cement strains in pre-clinical tests. J. Biomech. 35, 499-510.

140. Cordey, J., Borgeaud, M., Frankle, M., Harder, Y., Martinet, O., 1999. Loading model for the human femur taking the tension band effect of the ilio-tibial tract into account. Injury, Int. J. Care Injured 30, S-A26-S-A30.

141. Barker, R., Takahashi, T., Toms, A., Gregson, P., Kuiper, J.H., 2006. Reconstruction of femoral defects in revision hip surgery: risk of fracture and stem migration after impaction bone grafting. J. Bone Joint Surg. Br. 88, 832-836.

142. Wilson, D., Frei, H., Masri, B.A., Oxland, T.R., Duncan, C.P., 2005. A biomechanical study comparing cortical onlay allograft struts and plates in the treatment of periprosthetic femoral fractures. Clin. Biomech. 20, 70-76.

143. Chong, A.C.M., Friis, E.A., Ballard, G.P., Czuwala, P.J., Cooke, F.W., 2007. Fatigue performance of composite analogue femur constructs under high activity loading. Annals of Biomedical Engineering 35 (7), 1196-1205.

144. Cristofolini, L., Erani, P., Savigni, P., Grupp, T., Thies, O., Viceconti, M., 2007. Increased long-term failure risk associated with excessively thin cement mantle in cemented hip arthroplasty: A comparative in vitro study. Clin. Biomech. 22, 410-421.

145. Ramos, A., Simões, J.A., 2009. The influence of cement mantle thickness and stem geometry on fatigue damage in two different cemented hip femoral prostheses.

146. Sangiorgio, S.N., Longjohn, D.B., Dorr, L.D., Ebramzadeh, E., 2011. The influence of proximal stem geometry and surface finish on the fixation of a double-tapered cemented femoral stem. J. Biomech. 44, 22-27.

147. Ghosh, R., Gupta, S., 2014. Bone remodelling around cementless composite acetabular components: The effects of implant geometry and implant-bone interfacial conditions. J. Mech. Behav. Biomed. Mat. 32, 257-269.

148. Lin, B.A., Thomas, P., Spiezia, F., Loppini, M., Maffulli, N., 2013. Changes in daily physical activity before and after total hip arthroplasty. A pilot study using accelerometry. The Surgeon 11, 87-91.

149. Agnostini, V., Ganio, D., Facchin, K., Cane, L., Carneiro, M., Knaflitz, M., 2014. Gait parameters and muscle activation patterns at 3, 6, and 12 months after total hip arthroplasty. J. Arthrop. 29, 1265-1272.

150. Horstmann, T., Listringhaus, R., Haase, G-B., 2013. Changes in gait patterns and muscle activity following total hip arthroplasty: A six-month follow-up. Clin. Biomech. 28, 762-769.

151. Nishida, I., Maeda, M., Gordon, D., Robertson, E., Shirase, K., 2011. Development of an ergonomic musculoskeletal model to estimate muscle forces during vertical jumping. Procedia Eng. 13, 338-343.

152. Sverdlova, N.S., Witzel, U., 2010. Principles of determination and verification of muscle forces in the human musculoskeletal system: Muscle forces to minimise bending stress. J. Biomech. 43, 387-396.

153. Lloyd, D.G., Besier, T.F., 2003. An EMG-driven musculoskeletal model to estimate muscle forces and knee joint moments in vivo. J. Biomech. 36, 765-776.

154. Gagnon, D., Arjmand, N., Plamondon, A., Shirazi-Adl, A., Lariviere, C., 2011. An improved multi-joint EMG-assisted optimization approach to estimate joint and muscle forces in a musculoskeletal model of the lumbar spine. J. Biomech. 44, 1521-1529.

155. Augat, P., Penzkofer, R., Nolte, A., Maier, M., Panzer, S., Oldenburg, G., Pueschl, K., Simon, U., Buhren, V., 2008. Interfragmentary movement in diaphyseal tibia fractures fixed with locked intramedullary nails. J. Orhtop. Trauma 22, 30-36.

156. Milgrom, C., Finestone, A., Hamel, A., Mandes, V., Burr, D., Sharkey, N., 2003. A comparison of bone strain measurements at anatomically relevant sites using surface gauges versus strain gauged bone staples. J. Biomech. 37, 947-952.

157. Verhulp, E., van Rietbergen, B., Huiskes, R., 2003. A three-dimensional digital image correlation technique for strain measurements in microstructures. J. Biomech. 37, 1313-1320.

158. Yang, P.F., Sanno, M., Bruggemann, G.P., Rittweger, J., 2012. Evaluation of the performance of a motion capture system for small displacement recording and a discussion for its application potential in bone deformation in vivo measurements. Proc. IMechE Vol 226(11) Part H: J. Engineering in Medicine, 838-847.

159. Troy, K.L., Brown, T.D., Conzemius, M.G., 2009. Contact stress distributions on the femoral head of the emu. J. Biomech. 42, 2495–2500.

160. Senalp, A.Z., Kayabasi, O., Kurtaran, H., 2007. Static, dynamic and fatigue behavior of newly designed stem shapes for hip prosthesis using finite element analysis. Mat. Des. 28, 1577-1583.

161. Kayabasi, O., Ekici, B., 2007. The effects of static, dynamic and fatigue behavior on three-dimensional shape optimization of hip prosthesis by finite element method. Mat. Des. 28, 2269-2277.

162. Jeffers, J.R.T., Browne, M., Lennon, A.B., Prendergast, P.J.,

163. Mihalko, W.M., Beaudoin, A.J., Cardea, J.A., Krause, W.R., 1992. Finite-element modelling of femoral shaft fracture fixation techniques post total hip arthroplasty. J. Boimech. 25, 469.

164. Mann, K.A., Bartel, D.L., Wright, T.M., Burstein, A.H., 1995. Coulomb frictional interfaces in modeling cemented total hip replacements: a more realistic model. J. Biomechanics 28, 1067-1078.

165. Spiers, A.D., Heller, M.O., Taylor, W.R., Duda, G.N., Perka, C., 2007. Influence of changes in stem positioning on femoral loading after THR using a short-stemmed hip implant. Clin. Biomech. 22, 431-439.

166. Cheung, G., Zalzal, P., Bhandari, M., Spelt, J.K., Papini, M., 2004. Finite element analysis of a femoral retrograde intramedullary nail subject to gait loading. Medical Engineering & Physics 26, 93-108.

167. Gefen, A., 2002. Computational simulations of stress shielding and bone resorption around existing and computer-designed orthopaedic screws. Med. Biol. Eng. Comput. 40, 311-322.

168. Norman, T.L., Thyagarajan, G., Saligrama, V.C., Gruen, T.A., Blaha, J.D., 2001. Stem surface roughness alters creep induced subsidence and 'taper-lock' in a cemented femoral hip prosthesis. J. Biomech. 34, 1325-1333.

169. Chen, D.W., Lin, C.L, Hu, C.C., Wu, J.W., Lee, M.S., 2012. Finite element analysis of different repair methods of Vancouver B1 periprosthetic fractures after total hip arthroplasty. Injury, 1-5.

170. Nuno, N., Groppetti, R., Senin, N., 2006. Static coefficient of friction between stainless steel and PMMA used in cemented hip and knee implants. Clin. Biomech. 21, 956-962.

171. Köbel, R., Bergmann, G., Boenick, U., 1976. Mechanical engineering of the cement-bone bond. In: Engineering in Medicine 347-357. Springer-Verlag, New York.

172. Bean, D.J., Convery, F.R., Woo, S.L.Y., Lieber, R.L., 1987. Regional variation in shear strength of the bone-polymethylmethacrylate interface. J. Arthrop. 2 (4), 293-298.

173. Ryf CR, Arraf J. Postoperative fracture treatment: general considerations. In: Ruedi TP, Buckley RE, Moran CG, editors. AO principal of fracture management. 2nd ed. Davos: AO Publishing; 2007. p. 447.

174. National Instruments, 2014. Measuring Strain with Strain Gages. Available at www.ni.com/white-paper/3642/en [Accessed March 2015]

175. Chong, A.C.M., Miller, F., Buxton, M., Friis, E.A., 2007. Fracture toughness and fatigue crack propagation rate of short fiber reinforced epoxy composites for analogue cortical bone. Journal of Biomechanical Engineering 129, 487-493.

176. Anderson, A.E., Ellis, B.J., Weiss, J.A., 2007. Verification, validation and sensitivity studies in computational biomechanics. Computer Methods in Biomechanics and Biomedical Engineering 10 (3), 171-184.

177. Oberkampf, W.L., Trucano, T.G., Hirsch, C., 2002. Verification, validation, and predictive capability on computational engineering and physics. Foundations for Verification and Validation in the 21st Century Workshop, Johns Hopkins University, 2002.

178. Viceconti, M., Olsen, S., Burton, K., 2005. Extracting clinically relevant data from finite element simulations. Clinical Biomechanics 20, 451-454.

179. Blottner, F.G., 1990. Accurate Navier-Stokes results for the hypersonic flow over a spherical nosetip. J. Spacecraft 27 (2).

180. Boehm, B.W., 1981. Software engineering economics. Prentice Hall, Englewood Cliffs, New Jersey.

181. Jones, A.C., Wilcox, R.K., 2008. Finite element analysis of the spine: Towards a framework of verification, validation and sensitivity analysis. Medical Engineering and Physics 30, 1287-1304.

182. Sargent, R.G., 2011. Verification and validation of simulation models. Proceeding of the 2011 Winter Simulation Conference, 183-198.

183. Henninger, H.B., Reese, S.P., Anderson, A.E., Weiss, J.A., 2010. Validation of computational models in biomechanics. Proc. Inst. Mech. Eng. H 224 (7), 801-812.

184. Desmarais-Trépanier C. femur_sawbone.zip, From the Biomechanics European Laboratory _BEL_, Finite Element Mesh Repository, http://www.tecno.ior.it/VRLAB. 2009.

185. Benham, P.P., Crawford, R.J., Armstrong, C.G., 1996. Mechanics of Engineering Materials. Prentice Hall, Singapore.

186. Kusy, R.P., 1978. Characterization of self-curing acrylic bone cements. Journal of Biomedical Materials Research 12, 271-305.

187. De Wijn, J.R., Slooff, T.J.J.H., Driessens, F.C.M., 1975. Characterization of bone cements. Acta Orthop. Scand. 46. 38-51.

188. Holm, N.J., 1977. The modulus of elasticity and flexural strength of some acrylic bone cements. Acta Orthop. Scand. 48, 436-442.

189. Davies, J.P., O'Conner, D.O., Greer, J.A., Harris, W.H., 1987. Comparison of the mechanical properties of Simplex P, Zimmer Regular, and LVC bone cements. Journal of Biomedical Materials Research 21, 719-730.

190. Dunne, N.J., Orr, J.F., 2001. Influence of mixing techniques on the physical properties of acrylic bone cement. Biomaterials 22, 1819-1826.

191. Dunne, N.J., Orr, J.F., Mushipe, M.T., Eveleigh, R.J., 2003. The relationship between porosity and fatigue characteristics of bone cements. Biomaterials 24, 239-245.

192. Wilkinson, J.M., Eveleigh, R., Hamer, A.J., Milne, A., Miles, A.W., Stockley, I., 2000. Effect of mixing technique on the properties of acrylic bone-cement. The Journal of Arthroplasty 15 (5), 663-667.

193. Gilroy, D., Younge, A.M., Phillips, A.T.M., Wheel, M., Riches, P.E., 2014. Characterisation and Validation of Sawbones Artificial Composite Femur Material. 7th World Congress of Biomechanics.

194. Abaqus, 2012. ABAQUS 6.12 Documentation. Dassault Systèmes, Providence, RI, USA.

195. Zdero, R., Olsen, M., Bougherara, H., Schemitsch, E.H., 2008. Cancellous bone screw purchase: a comparison of synthetic femurs, human femurs, and finite element analysis. Proc. IMechE Vol. 222 Part H: J. Engineering in Medicine, 1175-1183.

196. Wieding, J., Souffrant, R., Fritsche, A., Mittelmeier, W., Bader, R., 2012. Finite element analysis of osteosynthesis screw fixation in the bone stock: an appropriate method for automatic screw modelling. PLoS ONE 7(3), 1-10.

197. Liu, G.R., Quek, S.S., 2013. The finite element method: a practical course. Elsevier, Oxford.

198. Litchman, H.M., Richman, M.H., Warman, M., Mitchell, J., 1978. Improvement of the mechanical properties of polymethylmethacrylate by graphite fiber reinforcement. Trans. Orthop. Res. Soc., 2, 86.

199. Saha, S., Warman, M.L., 1979. Compressive and shear properties of graphite fiber reinforced bone cement. Orthop. Trans., 3, 169.

200. Saha, S., Warman, M.L., 1979. Improved mechanical properties of graphite fiber reinforced polymethylmethacrylate. Trans. 17th Int. Biomater. Symp. and 5th Ann. Meeting SOC. Biomater., 3, 174.

201. Heller, M.O., Bergmann, G., Deuretzbacher, G., Dürselen, L., Pohl, M., Claes, L., Haas, N.P., Duda, G.N., 2001. Musculo-skeletal loading conditions at the hip during walking and stair climbing. J. Biomech. 34, 883-893.

202. Retpen, J.B., Jensen, J.S., 1993. Risk factors for recurrent aseptic loosening of the femoral component after cemented revision. J. Arthroplasty 8 (5), 471-478.

203. Blain, H., Chavassieux, P., Portero-Muzy, N., Bonnel, F., Canovas, F., Chammas, M., Maury, P., Delmas, P.D., 2008. Cortical and trabecular bone distribution in the femoral neck in osteoporosis and osteoarthritis. Bone 43, 862-868.

204. Karrholm, J., Borssen, B., Lowenhielm, G., Snorrason, F., 1994. Does early micromotion of femoral stem prostheses matter? J. Bone Joint Surg. (Br) 76-B, 912-7.

205. Alfaro-Adrian, J., Gill, H.S., Murray, D.W., 2001. Should total hip arthroplasty femoral components be designed to subside? J. Arthrop. 16 (5), 598-606.

9. Appendix

9.1 Experimental Fracture Movement Matlab Script

```
clear all
% Image processing of fracture movement images

I = imread('C:\Documents and
Settings\men6lwe\Desktop\Testphoto_unloaded.jpg');
imshow(I, 'InitialMagnification','fit');

vert1(1) = imline(gca,[580,351;580,500]);
vert2(1) = imline(gca,[804,361;804,502]);
horiz1(1) = imline(gca,[628,361;770,362]);
horiz2(1) = imline(gca,[608,492;767,496]);

vert1(2) = imline(gca,[922,333;930,519]);
vert2(2) = imline(gca,[1068,347;1077,516]);
horiz1(2) = imline(gca,[876,367;1141,361]);
horiz2(2) = imline(gca,[867,495;1156,490]);

vert1(3) = imline(gca,[1274,349;1282,535]);
vert2(3) = imline(gca,[1402,362;1411,532]);
horiz1(3) = imline(gca,[1185,386;1450,379]);
horiz2(3) = imline(gca,[1198,502;1487,497]);

vert1(4) = imline(gca,[601,662;609,848]);
vert2(4) = imline(gca,[697,667;687,847]);
horiz1(4) = imline(gca,[547,703;812,697]);
horiz2(4) = imline(gca,[526,805;815,801]);

vert1(5) = imline(gca,[901,659;909,845]);
vert2(5) = imline(gca,[1022,667;1031,836]);
horiz1(5) = imline(gca,[816,700;1081,694]);
horiz2(5) = imline(gca,[819,810;1108,806]);

vert1(6) = imline(gca,[1174,686;1182,872]);
vert2(6) = imline(gca,[1358,695;1367,865]);
horiz1(6) = imline(gca,[1154,726;1419,720]);
horiz2(6) = imline(gca,[1146,831;1435,826]);

vert1(7) = imline(gca,[524,1354;532,1541]);
vert2(7) = imline(gca,[677,1364;686,1533]);
horiz1(7) = imline(gca,[472,1393;737,1387]);
horiz2(7) = imline(gca,[467,1502;756,1498]);

vert1(8) = imline(gca,[854,1387;862,1573]);
vert2(8) = imline(gca,[975,1398;984,1568]);
horiz1(8) = imline(gca,[775,1422;1040,1415]);
horiz2(8) = imline(gca,[770,1540;1058,1535]);
```

```
vert1(9) = imline(gca,[1167,1427;1175,1613]);
vert2(9) = imline(gca,[1300,1437;1309,1606]);
horiz1(9) = imline(gca,[1104,1459;1369,1453]);
horiz2(9) = imline(gca,[1098,1584;1386,1579]);

vert1(10) = imline(gca,[512,1684;520,1871]);
vert2(10) = imline(gca,[621,1702;630,1871]);
horiz1(10) = imline(gca,[459,1723;724,1717]);
horiz2(10) = imline(gca,[452,1854;740,1849]);

vert1(11) = imline(gca,[832,1726;840,1912]);
vert2(11) = imline(gca,[939,1749;949,1918]);
horiz1(11) = imline(gca,[752,1767;1017,1761]);
horiz2(11) = imline(gca,[749,1891;1038,1887]);

vert1(12) = imline(gca,[1143,1785;1151,1971]);
vert2(12) = imline(gca,[1264,1793;1274,1962]);
horiz1(12) = imline(gca,[1058,1811;1323,1805]);
horiz2(12) = imline(gca,[1061,1939;1350,1935]);
for i = 1:12;
    spacelist(i,1) = [' '];
end;
fcn = makeConstrainToRectFcn('imline',get(gca,'XLim'),get(gca,'YLim'));

ht = uitoolbar();
A = zeros(10,10,3);

for i = 1:12;
api_vert1(i) = iptgetapi(vert1(i));
api_vert1(i).setPositionConstraintFcn(fcn);
api_vert2(i) = iptgetapi(vert2(i));
api_vert2(i).setPositionConstraintFcn(fcn);
api_horiz1(i) = iptgetapi(horiz1(i));
api_horiz1(i).setPositionConstraintFcn(fcn);
api_horiz2(i) = iptgetapi(horiz2(i));
api_horiz2(i).setPositionConstraintFcn(fcn);
end
pointlist = ['a';'b';'c';'d';'e';'f';'g';'h';'i';'j';'k';'l'];

midcalcbutton = uipushtool('CData',A,'TooltipString','Press to calculate
midpoints','ClickedCallback',sprintf('for i = 1:12; \n temp =
api_vert1(i).getPosition(); \n v1x(i,1) = [temp(1,1)]; \n v1x(i,2) =
[temp(2,1)]; \n v1y(i,1) = [temp(1,2)]; \n v1y(i,2) = [temp(2,2)]; \n
temp = api_vert2(i).getPosition(); \n v2x(i,1) = [temp(1,1)]; \n v2x(i,2)
= [temp(2,1)]; \n v2y(i,1) = [temp(1,2)]; \n v2y(i,2) = [temp(2,2)]; \n
temp = api_horiz1(i).getPosition(); \n h1x(i,1) = [temp(1,1)]; \n h1x(i,2)
= [temp(2,1)]; \n h1y(i,1) = [temp(1,2)]; \n h1y(i,2) = [temp(2,2)]; \n
temp = api_horiz2(i).getPosition(); \n h2x(i,1) = [temp(1,1)]; \n h2x(i,2)
= [temp(2,1)]; \n h2y(i,1) = [temp(1,2)]; \n h2y(i,2) = [temp(2,2)]; \n
end; \n for i = 1:12; \n x1 = [v1x(i,1) h1x(i,1); v1x(i,2) h1x(i,2)]; \n
y1 = [v1y(i,1) h1y(i,1); v1y(i,2) h1y(i,2)]; \n dx1 = diff(x1); \n dy1 =
diff(y1); \n den1 = dx1(1)*dy1(2)-dy1(1)*dx1(2); \n ua1 = (dx1(2)*(y1(1)-
y1(3))-dy1(2)*(x1(1)-x1(3)))/den1; \n ub1 = (dx1(1)*(y1(1)-y1(3))-
dy1(1)*(x1(1)-x1(3)))/den1; \n xi1(i) = x1(1)+ua1*dx1(1); \n yi1(i) =
y1(1)+ua1*dy1(1); \n x2 = [v1x(i,1) h2x(i,1); v1x(i,2) h2x(i,2)]; \n y2 =
[v1y(i,1) h2y(i,1); v1y(i,2) h2y(i,2)]; \n dx2 = diff(x2); \n dy2 =
```

```
diff(y2); \n den2 = dx2(1)*dy2(2)-dy2(1)*dx2(2); \n ua2 = (dx2(2)*(y2(1)-
y2(3))-dy2(2)*(x2(1)-x2(3)))/den2; \n ub2 = (dx2(1)*(y2(1)-y2(3))-
dy2(1)*(x2(1)-x2(3)))/den2; \n xi2(i) = x2(1)+ua2*dx2(1); \n yi2(i) =
y2(1)+ua2*dy2(1); \n x3 = [v2x(i,1) h1x(i,1); v2x(i,2) h1x(i,2)]; \n y3 =
[v2y(i,1) h1y(i,1); v2y(i,2) h1y(i,2)]; \n dx3 = diff(x3); \n dy3 =
diff(y3); \n den3 = dx3(1)*dy3(2)-dy3(1)*dx3(2); \n ua3 = (dx3(2)*(y3(1)-
y3(3))-dy3(2)*(x3(1)-x3(3)))/den3; \n ub3 = (dx3(1)*(y3(1)-y3(3))-
dy3(1)*(x3(1)-x3(3)))/den3; \n xi3(i) = x3(1)+ua3*dx3(1); \n yi3(i) =
y3(1)+ua3*dy3(1); \n x4 = [v2x(i,1) h2x(i,1); v2x(i,2) h2x(i,2)]; \n y4 =
[v2y(i,1) h2y(i,1); v2y(i,2) h2y(i,2)]; \n dx4 = diff(x4); \n dy4 =
diff(y4); \n den4 = dx4(1)*dy4(2)-dy4(1)*dx4(2); \n ua4 = (dx4(2)*(y4(1)-
y4(3))-dy4(2)*(x4(1)-x4(3)))/den4; \n ub4 = (dx4(1)*(y4(1)-y4(3))-
dy4(1)*(x4(1)-x4(3)))/den4; \n xi4(i) = x4(1)+ua4*dx4(1); \n yi4(i) =
y4(1)+ua4*dy4(1); \n midpointx(i) = (xi1(i) + xi2(i) + xi3(i) + xi4(i)) /
4; \n midpointy(i) = (yi1(i) + yi2(i) + yi3(i) + yi4(i)) / 4; \n cpoint(i)
= impoint(gca,midpointx(i),midpointy(i)); \n temp1 =
cpoint(i).getPosition(); \n centrepointx(i,1) = temp1(1); \n
centrepointy(i,1) = temp1(2); \n end; \n ; \n xlist =
num2str(centrepointx); \n ylist = num2str(centrepointy); \n xy =
[pointlist,spacelist,spacelist,xlist,spacelist,spacelist,ylist]'));
resultsfile = 'M:\000_Phd\Results\FractureMovementSpreadsheet.xlsx';
resultsworksheet = 'Exported co-ordinate points';
outputbutton = uipushtool('CData',A,'TooltipString','Press to export to
excel','ClickedCallback','xlswrite(resultsfile,[centrepointx,centrepointy
],resultsworksheet)');
```

9.2 Investigating Shear Movement in Simple Cylinder Models

In order to investigate the effect of cortical diameter, cortical thickness and bone material properties on the amount of shear movement at the fracture a simple cylinder model was created. This model consisted of proximal and distal cylindrical surrogates for the diaphysis of a femur, with a 1mm transverse fracture gap between them. They were stabilised with a steel stem which was held in place with PMMA cement. A transverse point load was applied a point on the proximal-most surface of the proximal fracture fragment. The distal end of the distal fracture fragment was fully constrained (Figure 9.1). A baseline model was created with a cortical diameter of 35mm and a cortical thickness of 5mm. A wide diameter model was created with a 45mm cortical diameter and 5mm cortical thickness. A widened and thinned model was created with a 45mm cortical diameter and a 2.5mm cortical thickness. Finally, with the 45mm cortical diameter and 2.5mm cortical thickness, the material properties were reduced from healthy cortical bone (E = 16.7GPa) to osteoporotic bone (12.4GPa).

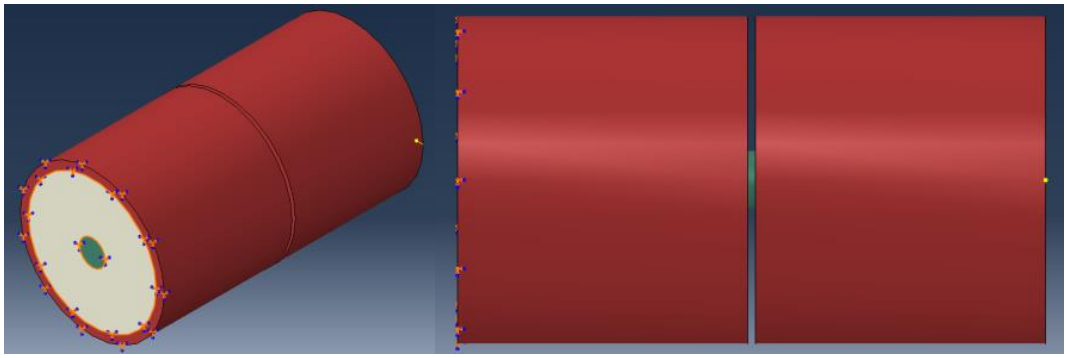

Figure 9.1 The simple cylinder model used to investigate the effect of several variables on fracture shear.

Table 9.1 Shear results from the simple cylinder model.

Case	Proximal Shear (mm)	Distal Shear (mm)	Relative Shear (mm)
Baseline	0.0358	0.0087	0.0271
Widened	0.0379	0.0053	0.0326
Widened and thinned	0.0450	0.0092	0.0359
Widened, thinned and weakened.	0.00471	0.0117	0.0354

The shear movements of the proximal fracture surface, the distal fracture surface and the proximal fracture surface relative to the distal fracture surface are given in Table 9.1. Widening the femoral diameter, and therefore the medullary canal, increased the fracture site shear movement. This was likely due to the increased distance between the stem and cortices. Thinning the cortices, while maintaining the outer femoral diameter also increased the shear, possibly due to a combination of the increased medullary canal width and the reduced support of the cortices. Weakening the cortical bone however caused a slight decrease in shear movement and this appeared to be due to increased movement of the distal fragment rather than decreased movement of the proximal fragment. This suggests that weakening the distal cortices, and therefore the distal fixation, may actually decrease shear. Given that osteoporotic bone involves a combination of a wider, thinner

cortex with lowered material properties these results would suggest that an increase in shear would be expected.

9.3 Proximally Locked Revision Stem Fixation

9.3.1 Motivation

A consistent issue with the finite element models developed and analysed in the previous chapters was a strain shielding effect on the lesser trochanter at the location of strain gauge 1. Given that strain results were only recorded on one specimen, and that the strain at gauge 1 varied the most across the area where it was measured it is possible that this reading does not represent the typical response of the experimental specimens or that additional strain readings above and below gauge 1 would show a similar pattern occurring at a slightly different height. Several sensitivity studies were performed which investigated other potential causes for this discrepancy. In Section 3.4 cases were presented where the Young's modulus of the proximal cancellous was increased from 155MPa to 2.45GPa, where the transverse movement of the femoral head was left unconstrained and where the cement-cortical bone interface was changed from a tie to an interaction ($\mu = 0.6$). Increasing the stiffness of the proximal cancellous could have increased the support for the proximal stem and resulted in increased load transfer into the proximal cortices. Removing the displacement constraints on the femoral head allowed increased bending of the femur which may have increased the proximal cortical strain. Altering the interaction properties of the cement-cortical bone interface from a tie to friction-based contact allowed the stem to subside further into the femur. Increased subsidence would move more of the load transfer to the proximal femur, particularly the increased taper at the shoulder of the stem, and therefore also may have increased proximal cortical strains.

When the results for these models were analysed however none of these modifications resulted in an increase in strain at gauge 1 that approached the experimental values.

Additionally when considering the effects of long stem revision, and hip replacement surgery in general, one of the common concerns is the proximal strain

shielding caused by the femoral stem and one of the main concerns regarding fixation failure is stem loosening. A stem design that reduced the likelihood of loosening and induced proximal strain patterns more akin to those experienced naturally could possibly therefore improve clinical outcomes.

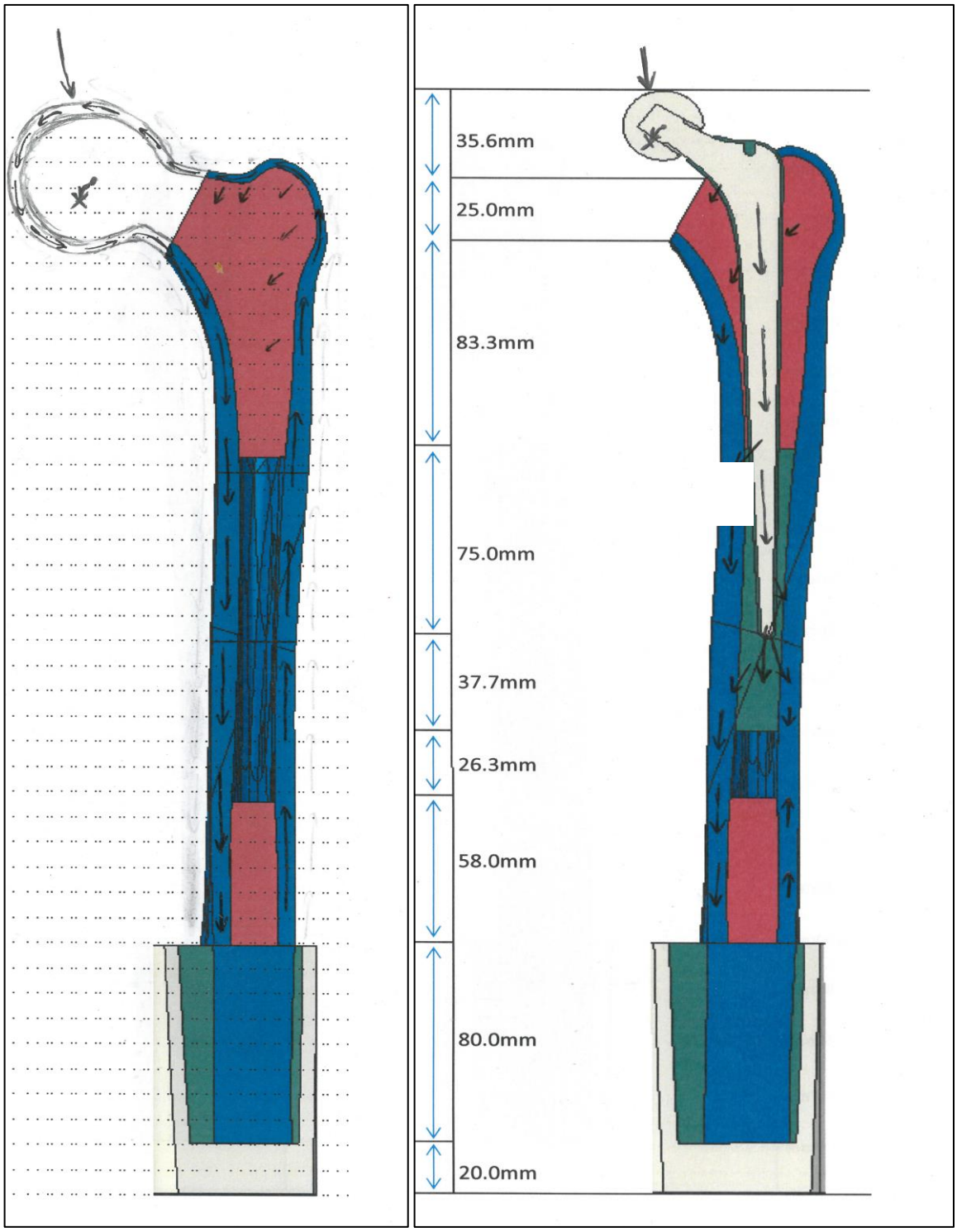

Figure 9.2 Estimation of load path changes between natural (left) and implanted (right) femurs. Under an applied load to the femoral/stem head the construct displaces so that the original centre of the head (marked by a dot) displaces distally and medially (marked by an x). Estimated key resulting load paths are then marked in arrows throughout the femurs.

In Figure 9.2 an attempt is made to estimate the changes to the load paths though the femur that occur after implantation of a femoral stem. These load paths have been simplified, magnitudes have not been calculated and the effects of muscle forces are not considered. In a natural femur the cortices transfer all of the load, compressively through the medial cortex and in tension through the lateral cortex. The cancellous bone then provides internal support and structure, maintaining the shape and integrity of the femur and smoothing out stress imbalances. In an implanted femur however proximal load transfer is very different. As the stem head moves the only load transfer comes through the compression and tension of the cancellous bone. As the distal tip of the stem is well-fixed its overall movement is small and the cancellous bone has a much lower stiffness than the other materials involved, meaning that much of this load is absorbed by the cancellous and very little is transferred to the cortices. A significant portion of the proximal load transfer between the stem and cancellous may also be a shearing force rather than a compressive/tensile force relative to the axial direction of the cortices meaning that it will not propagate distally in the same way. The first point where meaningful load transfer to the cortex occurs is approximately halfway down the stem on the medial side (point 1). The rotational stability of the stem in the mediolateral plane is coming from the stem pressing towards the medial cortex at point 1 and the lateral cortex at point 2. This applies some load to the cortices however again a significant proportion of this is a shear force rather than an axial force. Below point 1 the stem is fixed into the stiffer PMMA cement rather than the relatively soft cancellous and axial loads are more likely to be transferred across into the cortices as the stem and cement subside into the medullary canal. The majority of the total hip force applied to the femoral head is distributed from the distal tip of the stem to the cement at and below the tip of the stem. Below this point a more natural bending pattern can form as the load is distributed from the stem tip to the cement and then to the cortices however these compressive and tensile cortical strains will be focussed in a smaller section of the femur and will not propagate proximally. The reason for the majority of these differences is that in a natural femur the cortices are connected to each other and the load itself and are therefore connected to the displacements of the femoral head. In the implanted femur the cortices are disconnected from displacements of the femoral head and instead rely on receiving load transfer much more distally from the stem. This suggested that a stem design that physically links the femoral head displacements to displacements at

the proximal-most points of the medial and lateral cortices may result in improved load distribution, and therefore more natural strain values, through the proximal cortices. Distally locked stems attempted to provide improved distal fixation of the stem by attaching it in place with bicortical screws. Clinical results have been poor however as the subsidence of the stem into the medullary canal puts increased loading on these screws over time, leading to construct failures. These failures can be attributed to two factors: the distal locking screws did not prevent stem subsidence and were not sufficiently stable and structurally stiff when loaded in shear to then support the majority of the applied head forces. This study tested a design concept to lock the stem, using screw fixation, to the proximal femur rather than the distal femur in order to transfer load to the femur in a more natural fashion and prevent subsidence without inducing screw failure.

9.3.2 Proximally Locked Fixator Model Development

A model was developed where the neck of the proximal stem, where it extended out from the femur towards the hip, was altered to additionally include two plate-like structures. One extended laterally over the top of the femur and one extended medially over the femoral neck cut. Screw fixation was then modelled between these plates and the medial and lateral cortices, in effect creating a physical connection between the medial and lateral cortices and the femoral head. On the lateral cortex it appeared possible to apply these screws in such a way that they act predominantly in axial tension and compression rather than shear which may improve screw survivability, on the medial side this was more difficult and may not be practically possible. The purpose of this model was to simply test the hypothesis that a proximally locked stem could provide a more natural strain pattern in the proximal femur, without an expectation that the results could be used to produce direct clinical recommendations, and as such screw fixation was simplified to a tied contact. The proximally locked femoral stem model is shown in Figure 9.3. In order to consider these models against the experimental proximal strain results the fracture was modelled to match the experiment. A 1mm thick slice of the cortex was therefore replaced with cement which was perfectly bonded to both the proximal and distal surfaces of the fracture.

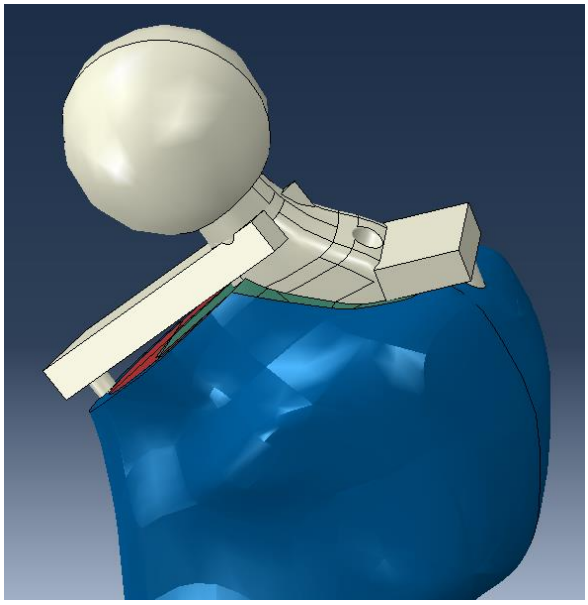

Figure 9.3 Proximally locked stem with screw fixation into the medial and lateral cortices.

9.3.2 Results

Table 9.2 Comparison of results for long stem revision PFF case with and without proximal screw fixation.

Case	Stiffness (kN/mm)	Fracture Compression (μm)	Fracture Angle (degrees)	Stem Tip Subsidence (μm)	Maximum Transverse Displacement of the Femur (mm)	Max Cement Stress (MPa)	Proximal Lateral μStrain	Proximal Medial μStrain
Baseline	4929	-0.68	0.01	24	0.14	17	92	-31
Proximal Fixator	5966	-0.66	0.01	23	0.12	37	109	-132

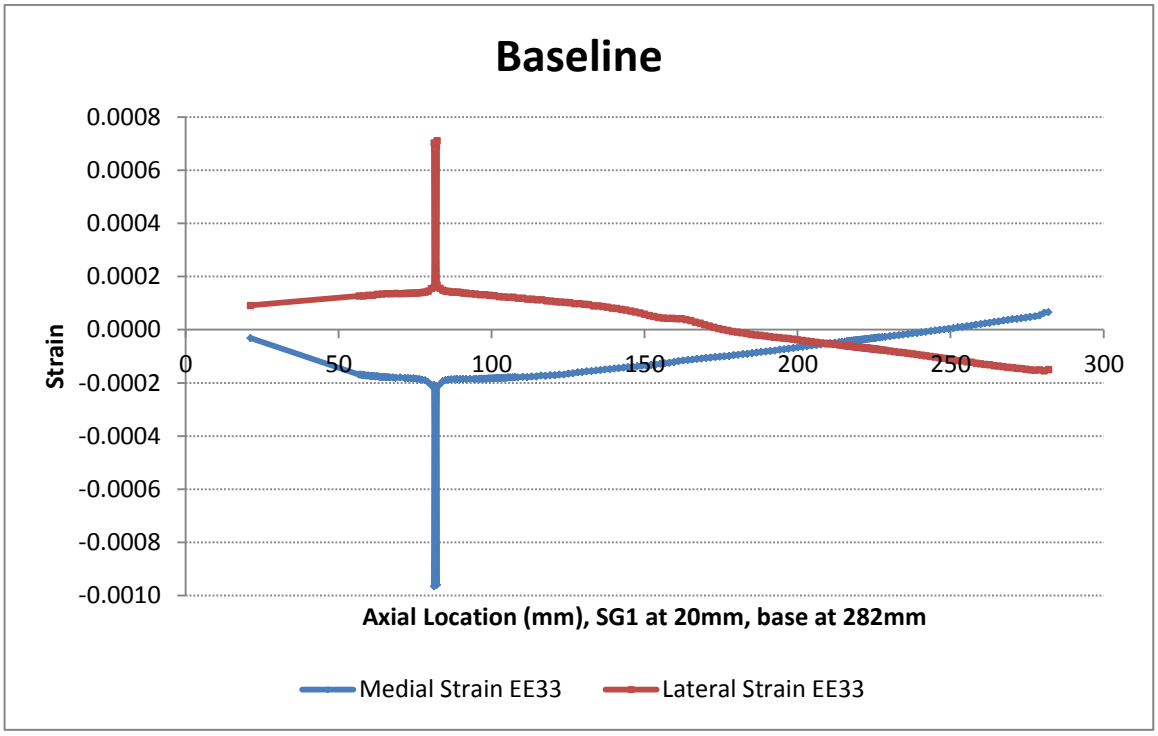

Figure 9.4 Baseline axial, longitudinal strain on the medial and lateral sides for the 10° loading angle.

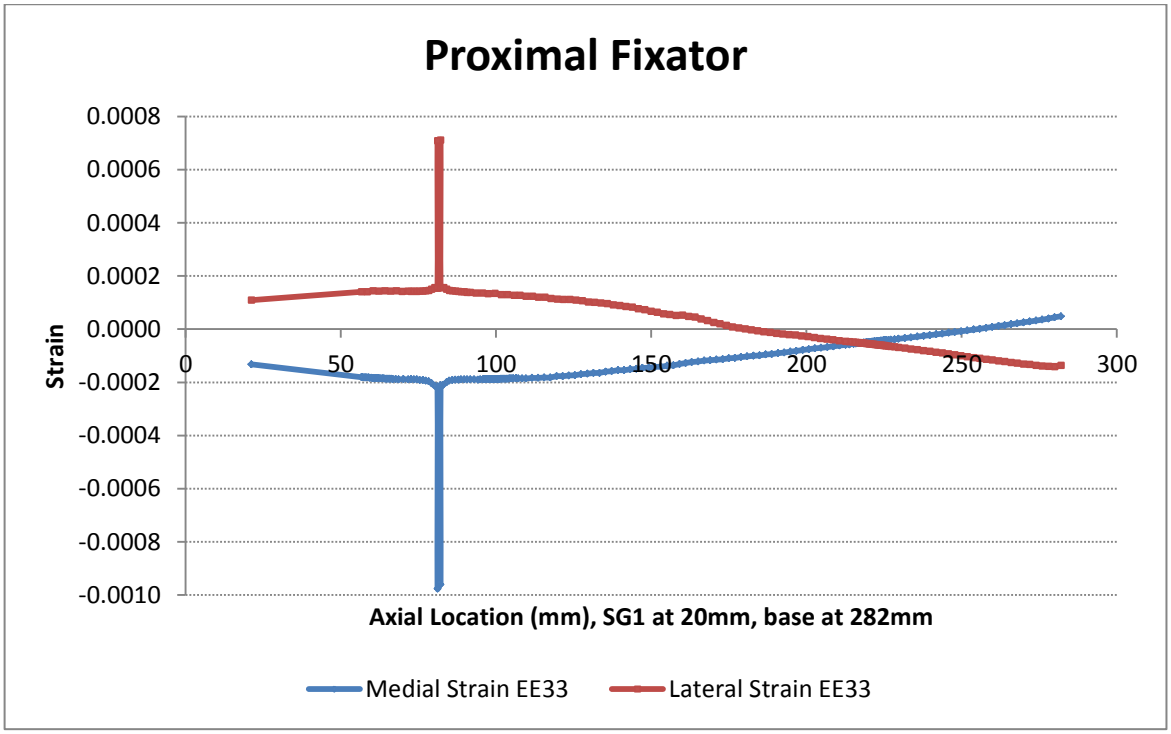

Figure 9.5 Proximally fixed long stem model axial, longitudinal strain on the medial and lateral sides for the 10° loading angle.

9.3.3 Discussion

Table 9.2 gives the results comparison of the proximally locked long stem model against the baseline long stem model. The proximally locked stem decreased the maximum transverse displacement of the femur by 15% and caused a corresponding increase in construct stiffness of 21%. It had little effect on the fracture compression, fracture angle and stem tip subsidence. Maximum cement stress at the stem tip was increased by 114% despite a decrease in stem tip subsidence. Lateral proximal strain, which was less affected by strain shielding, increased by 19% with the proximally fixed stem and medial proximal strain, which was severely affected by strain shielding in the baseline case, was increased by over 300%. Figures 9.4 and 9.5 give the overall strain patterns along the medial and lateral sides of the femur. With the proximally fixed stem the increased proximal strain on both sides of the femur can be clearly seen. Below this the strain pattern was relatively unchanged, with small increases in strain around the middle of the diaphysis and a small decrease in strain towards the distal portion of the femur. Overall the concept of physically linking the displacements of the femoral head to the proximal-most medial and lateral cortices resulted in the predicted reduction in proximal strain shielding. It also showed that higher values of proximal, medial cortical strain could be obtained in the finite element models given appropriate load transfer, suggesting that either a load transfer mechanism active in the experimental specimens is not being replicated successfully in the FE models or that the proximal experimental strain from the single instrumented specimen is not a typical response for the group. In theory a stem that includes screw fixation to the cortices would subside less than one without, as long as the screw fixation did not fail. In order to evaluate whether a design such as this could reduce subsidence over time however would require either FE modelling with a more accurate cement-cortex interface, cyclic loading and failure mechanisms for the cement and cancellous bone or experimental fatigue testing with an appropriately accurate simulation setup.